Sedimentary and geomorphological signature of the Northeast Greenland Ice Stream (NEGIS) on the continental shelf

GEORGIA EMILY JANE WARE

Sedimentary and geomorphological signature of the Northeast Greenland Ice Stream (NEGIS) on the continental shelf

Georgia Emily Jane Ware

Thesis submitted for the degree of Master of Science (by Research)

Department of Geography

Durham University

2021

Abstract

The Northeast Greenland Ice Stream (NEGIS) drains 16% of the Greenland Ice Sheet (GrIS), hence it is important to understand how the NEGIS might respond to the ongoing and future atmospheric and oceanic warming. Exploring longer term records of NEGIS dynamics during the Last Glacial Maximum (LGM) and the Holocene is one way to improve confidence in NEGIS modelling. This study uses glacial sedimentology and geomorphology to determine the characteristics and depositional origin of sediment on the northeast Greenland continental shelf, providing an insight into past NEGIS dynamics. Five gravity cores, together with sub-bottom acoustic profiles, were retrieved from the Norske and Westwind cross-shelf troughs. These have revealed the presence of massive and stratified diamictons, and laminated, stratified, and massive muds. Drumlins, mega-scale glacial lineations (MSGLs), sediment wedges and iceberg ploughmarks have also been identified.

Subglacial deformation, and possibly lodgement, produced till, drumlins, and MSGLs during the LGM advance of the NEGIS. During retreat, deposition took place at the grounding line via debris flow processes, which contributed to the formation of asymmetrical sediment wedges. Beyond the grounding line, sediment was deposited and reworked by iceberg rafting, suspension settling from meltwater plumes, mass flow activity, and iceberg keel scouring.

Sediment wedges at the shelf edge in Westwind Trough provide confirmation that the NEGIS reached the outer shelf at the LGM. Ice withdrawal from the shelf edge in Westwind Trough took place in a step-like manner and was driven by iceberg calving. Iceberg calving also drove ice recession through mid Norske Trough, and this recession was punctuated by a grounding line readvance that could have been related to Younger Dryas cooling. The NEGIS likely moved into inner Norske Trough during the early Holocene, with retreat partially generated by melting at the ice margin at this time. Different grounding line regimes (ice shelf vs grounded tidewater) may have been present in Norske and Westwind troughs during retreat.

Table of Contents

List of Figures

List of Tables

Statement of Copyright

Acknowledgements

Firstly, I thank my supervisors Professor Dave Roberts and Professor Colm Ó Cofaigh, who have given me considerable guidance and encouragement throughout this process and helped me adapt to working during the Covid-19 pandemic. I am grateful for the time they have spent reading my work, and their detailed feedback and suggestions have been invaluable. Thanks goes to the staff in the Geography labs who assisted with thin section preparation, and to Ian Chaplin for making the thin sections. I also acknowledge the guidance of Professor Emrys Phillips, who taught me a lot about using micromorphology to analyse glacial sediments.

I appreciate the support I have received from friends, particularly those from the Geography Department. Finally, my parents and sisters certainly did not expect to have me living at home with them whilst I completed this Masters but have been very patient. They have been hugely supportive through their constant words of encouragement, as well as always being willing to go for a walk with me.

1. Introduction and rationale

1.1 Recent mass loss from the Greenland Ice Sheet

During the 20th century, 9013 ± 3181 Gt of ice were lost from the Greenland Ice Sheet (GrIS), contributing to 25.0 ± 8.8 mm of global sea level rise (Kjeldsen et al., 2015). From the 1980s to the present day, mass loss from the GrIS has increased six-fold (Mouginot et al., 2019). Mass loss has been driven by a combination of increased surface runoff driven by rising atmospheric temperatures, and the acceleration and retreat of marine terminating ice streams (e.g., Dowdeswell, 2006; Rignot and Kanagaratnam, 2006; Joughin et al., 2010; Sasgen et al., 2012; Enderlin et al., 2014; Bevis et al., 2019; King et al., 2020). Between 1972 and 2018, marine terminating ice streams were responsible for ~66% of mass loss from the GrIS (Mouginot et al., 2019). This is because the high flow speeds of ice streams allows them to transport large volumes of ice from the interior of the ice sheet to the ocean, meaning that they exert significant control on the mass balance, configuration, and stability of the GrIS (Bennett, 2003; Rignot et al., 2008; McMillan et al., 2016; Rignot et al., 2019; Shepherd et al., 2020).

Moving forward, continued anthropogenic warming is predicted to have a devastating impact on the GrIS, with a global temperature increase of 0.8-3.2°C determined to be a threshold for complete loss of the ice sheet (Robinson et al., 2012), which would equate to 7 m of global sea level rise (Church et al., 2013). Consequently, there is an urgent need to understand how the GrIS might respond in the future to continued changes in ocean and atmospheric temperatures.

Given the role of marine terminating ice streams in GrIS mass loss, it is particularly important to understand how these ice streams may respond to future climate perturbations. In light of this, the Northeast Greenland Ice Stream (NEGIS) will be the subject of this investigation. The NEGIS is located in the northern sector of the GrIS and is the largest ice stream in this region (Fig. 1.1a). It splits into three marine terminating outlet glaciers, Nioghalvfjerdsfjorden Glacier (NG) (also referred to as 79°N Glacier), Zachariae Isstrøm (ZI), and Storstrømmen Glacier (SG) (Fig. 1.1a). Prior to 2003, NEGIS outlet glaciers were stable in comparison to

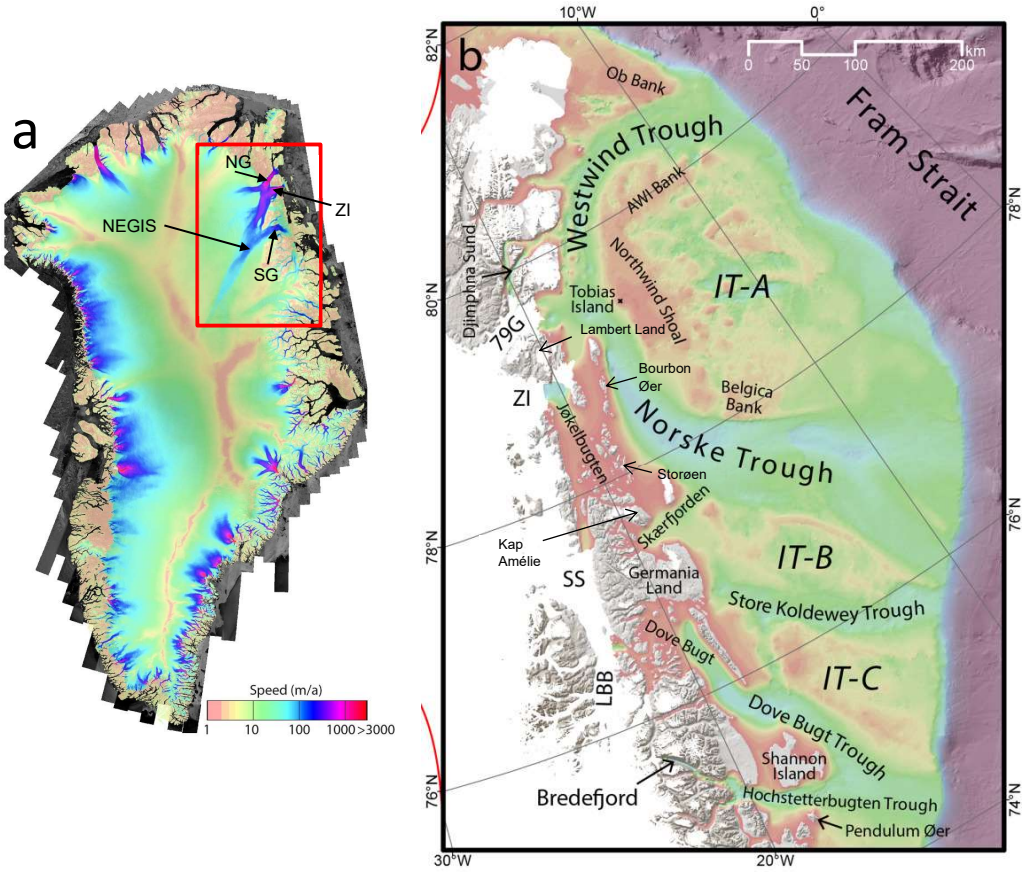

Figure 1.1 (a) Velocity mosaic of the GrIS from Joughin et al. (2018). The red box shows the location of the NEGIS and its outlet glaciers NG, ZI and SG. (b) Map showing the location of ice streams, land areas and submarine features referred to in the text between 74°N to 82°N, which includes the study area. 79G = 79°N Glacier (Nioghalvfjerdsfjorden Glacier-NG), ZI = Zachariae Isstrøm, SS = Storstrømmen Glacier (SG), LBB = L. Bistrup Bræ, and IT = inter-trough areas. The current margin of ZI and NG are shown. From Arndt et al. (2015).

other sectors of the GrIS, displaying minimal changes in surface elevation and mass balance (Rignot et al., 2001; Rignot and Kanagaratnam, 2006). However, ZI has recently undergone rapid dynamic thinning and retreat following a 95% reduction in the size of its ice shelf between 2002-2014 (Khan et al., 2014; Mouginot et al., 2015) (Fig. 1.2). Its grounding line retreated 3.5 km inland between 2011-2015 (Fig. 1.2), and the rate of ice thinning was twice as high between 2010-2014 as it was between 1999-2010 (Mouginot et al., 2015). NG was more stable than ZI during the same time period, with its grounding line remaining in a similar position between 2011-2015 (Mouginot et al., 2015). However, net mass loss from the NG ice shelf is currently the highest of the remaining ice shelves in Greenland (Wilson et al., 2017), and the ice shelf exhibited a 30% reduction in thickness between 1998-2014 (Mouginot et al., 2015). Reduction or

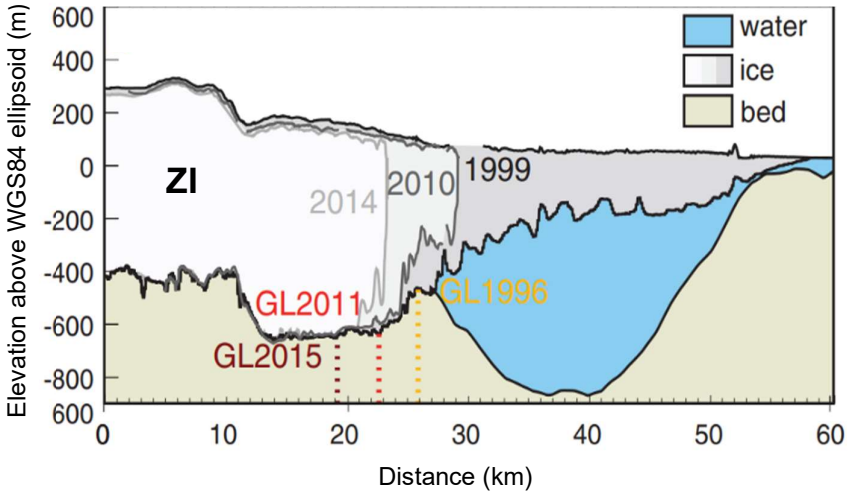

Figure 1.2 Change in ice front position (1999-2014) and grounding line position (1996-2015) of ZI. Dashed lines represent grounding line position. The loss of the ZI ice shelf is evident. From Mouginot et al. (2015).

loss of the buttressing effect of this ice shelf could trigger acceleration of NG, similar to the speed up of outlet glaciers which was observed following the collapse of the Larsen B ice shelf on the Antarctic Peninsula (Rignot et al., 2004).

These recent changes in NEGIS stability have been attributed to both ocean and atmospheric warming. The incursion of warm Atlantic Intermediate Water (AIW) to the margin of ZI led to ice removal at the grounding line and retreat (Mouginot et al., 2015; An et al., 2021). Thinning of the NG ice shelf has also been attributed to incursion and warming of AIW in the sub-ice shelf cavity, leading to bottom melting of the ice shelf (Wilson and Straneo, 2015; Mayer et al., 2018; Linderman et al., 2020; Schaffer et al., 2020). Khan et al. (2014) suggest that an increase in regional air temperature from 2003 also led to increased calving from both the ZI and NG margins. ZI has a retrograde bed which makes it susceptible to marine ice sheet instability, suggesting that its rapid retreat is likely to continue (Schoof, 2007; Khan et al., 2014; Mouginot et al., 2015; Choi et al., 2017).

The NEGIS drains 16% of the GrIS (Khan et al., 2014), and large reserves of ice are held in northern Greenland, hence there is potential for major ice discharge from the GrIS if the NEGIS outlet glaciers continue to thin and retreat (Mouginot et al., 2019). Furthermore, ZI and NG together contain 1.1 m of sea level rise equivalent (Mouginot et al., 2015), meaning loss of these glaciers would have major implications for global sea level rise. Thus, it is vital to gauge how NG and ZI might behave in the future. Previous modelling has found that ZI has already

entered a phase of unstoppable retreat and that its mass loss is set to continue, whilst NG will not undergo large changes over the next century (Choi et al., 2017). However, this model was calibrated using short term observations of outlet glacier change. Modelling future NEGIS behaviour using knowledge of long-term ice stream dynamics prior to instrumental records in order to calibrate and validate models will generate greater confidence in model outcomes. For that reason, modelling the response of NEGIS to continued ocean and atmospheric warming would be aided by a high resolution reconstruction of NEGIS dynamics and controls both during the Last Glacial Maximum (LGM), and particularly during the subsequent warming which occurred in the transition from the LGM to the Holocene.

1.2 Ice sheet reconstruction

Long-term records of changes in the extent, thickness and dynamics of ice sheets and ice streams allow palaeo-ice sheets to be reconstructed over millennial timescales (e.g., Andrews, 1982; Funder et al., 2011; Chiverrell et al., 2013; Stokes et al., 2015; 2016; Clark et al., 2018). Ice sheet extent, thickness and dynamics can be established using glacial geological records, glacio-isostatic data, and sea-level records (Stokes et al., 2015; e.g., England et al., 2006; Funder et al., 2011; Kilfeather et al., 2011; Livingstone et al., 2012; Ó Cofaigh et al., 2013a; Bentley et al., 2014; Roberts et al., 2018; 2019). Integration of these palaeo-datasets into numerical modelling allows former ice sheet evolution to be illustrated (Stokes et al., 2015; e.g., Whitehouse et al., 2012; Jamieson et al., 2014; Lecavalier et al., 2014; Peltier et al., 2015).

Glacial geomorphology and sedimentology have been widely used to obtain information about the glacial geological record of a particular region (e.g., Ó Cofaigh et al., 2002b; 2005a; 2005b; 2013a; Hogan et al., 2010; 2011; 2016; Kilfeather et al., 2011; Callard et al., 2018; 2020; Roberts et al., 2018; 2019). This is because the characteristics of sediment facies and landforms can be indicative of particular depositional processes, which has made them indispensable tools in reconstructing palaeo-ice sheets because they reveal the nature of former glacial depositional environments (Evans and Benn, 2004; Hubbard and Glasser, 2005). In recent years, sedimentology and geomorphology have been used in a wealth of studies to establish past glacial depositional environments and ice dynamics in areas of former ice sheet beds, particularly former ice stream beds, which are

currently underwater (Stokes et al., 2015). This has greatly improved knowledge of the extent and dynamics in the marginal regions of palaeo-ice sheets (Stokes et al., 2015). These studies used detailed description and interpretation of seafloor sediment cores and/or offshore acoustic or seismic profiles to reconstruct the former advance and retreat of ice streams from multiple ice sheets, including the Antarctic Ice Sheet (AIS) (e.g., Hiemstra, 2001b; Shipp et al., 2002; Evans et al., 2005; Ó Cofaigh et al., 2005a; 2005b; Kilfeather et al., 2011), the British-Irish Ice Sheet (BIIS) (e.g., Peters et al., 2015; 2016; Scourse et al., 2019; Callard et al., 2018; 2020; Roberts et al., 2019), and the Svalbard-Barents Sea Ice Sheet (SBIS) (e.g., Hogan et al., 2010; Bjarnadóttir et al., 2013; 2014; Newton and Huuse, 2017; Streuff et al., 2018).

Micromorphology is a branch of glacial sedimentology which can be used to divulge greater detail about sediment structure and texture, and therefore can be vital in making interpretations of sediment genesis (e.g., van der Meer, 1993; 1997; Carr, 2001; van der Meer et al., 2003; Menzies, 2000; Hiemstra and Rijsdijk, 2003; Hiemstra et al., 2005; Roberts and Hart, 2005; Ó Cofaigh et al., 2005a; Larsen et al., 2006; 2007; Phillips et al., 2007; 2018; Kilfeather et al., 2010; Linch and Dowdeswell, 2016; Spagnolo et al., 2016; Hart, 2017). It can also be useful in the interpretation of sediments which have a very similar macro-scale appearance but different genetic origins, particularly subglacial tills and glacimarine diamictons (e.g., Hiemstra, 1999; Kilfeather et al., 2010). Despite its value, micromorphology was not employed to describe the glacial sedimentological record investigated in most of the studies listed above. As a result, there is an opportunity to demonstrate how the use of micromorphology in the analysis of submarine glacial sediment can strengthen reconstructions of ice marginal depositional processes, and therefore reconstructions of glacial history.

1.3 The glacial history of the Greenland Ice Sheet

Submarine sedimentology and geomorphology have been used to reconstruct ice stream dynamics and palaeo-ice sheet history for multiple regions of the GrIS (e.g., Evans et al., 2002; Dowdeswell et al., 2010; 2014; Hogan et al., 2016; Streuff et al., 2017; Reilly et al., 2019). For example, description of acoustic profiles and sediment cores retrieved from Disko Bay, and the Disko, Uummannaq and Melville Bugt troughs in western Greenland have revealed the characteristics of the LGM and Holocene sediments and landforms (Desloges et al., 2002; Gilbert

et al., 2002; Ó Cofaigh et al., 2013a; Hogan et al., 2012; 2016; Sheldon et al., 2016; Slabon et al., 2016; Streuff et al., 2017; Jennings et al., 2017). This sediment-landform assemblage has been used to establish that in the central western sector of the GrIS, ice streams expanded to the shelf edge during the LGM, and that ice retreat took place at variable speeds and was separated by stillstands (Ó Cofaigh et al., 2013a; Dowdeswell et al., 2014; Hogan et al., 2016; Sheldon et al., 2016; Slabon et al., 2016; Jennings et al., 2017). These studies of the offshore glacial geological record have resulted in a much improved understanding of the former dynamics of the central western sector of the GrIS.

Some reconstructions of NEGIS dynamics during and following the LGM have been undertaken in northeast Greenland, however due to the year-round sea ice cover this sector of the GrIS has been the subject of relatively fewer studies in comparison with other regions such as the central western GrIS. Mapping of submarine landforms in Norske and Westwind troughs, on the northeast Greenland continental shelf, has revealed mega-scale glacial lineations (MSGLs), grounding zone wedges (GZWs), recessional moraines and iceberg grounding pits (Evans et al., 2009; Winkelmann et al., 2010; Arndt and Evans, 2016; Arndt et al., 2017a). Based on this landform assemblage, it has been inferred that NEGIS was fast flowing and expanded to the shelf edge at the LGM, and retreated in a spatially and temporally variable manner (Evans et al., 2009; Winkelmann et al., 2010; Arndt and Evans, 2016; Arndt et al., 2017a).

However, there is currently minimal data about the sedimentary record associated with the LGM advance and retreat of the NEGIS. Hence, there is scope for an investigation of the nature of the sediments present on the continental shelf. This would create a more in depth understanding of the offshore geological record in northeast Greenland, and allow more detail about glacigenic processes and depositional environments associated with the NEGIS to be elucidated. Determination of these depositional processes would contribute to a more developed understanding of the dynamics of both the NEGIS and the northeastern sector of the GrIS during and following the LGM.

1.4 Aims and research questions

This project aims to investigate and reconstruct the glacigenic processes associated with the LGM advance and retreat of the NEGIS across the northeast Greenland continental shelf. These new findings will be integrated with pre-

existing interpretations of NEGIS retreat dynamics based on the bathymetric and acoustic data from Norske and Westwind troughs (e.g., Winkelmann et al., 2010; Arndt et al., 2015; 2017a).

Research questions:

1. What are the macroscale, microscale and acoustic characteristics of the sedimentary facies and landforms present in the Norske and Westwind troughs?
2. Which glacigenic processes characterise (a) the advance of the NEGIS across the continental shelf, and (b) the retreat of the NEGIS across the continental shelf?
3. What implications do these landforms and sediments have for understanding of NEGIS dynamics on the northeast Greenland continental shelf?

1.5 Regional setting and study area

Northeastern Greenland (between 75°N to 81°N) is the setting for this investigation. This is the region in which the NEGIS terminates into the ocean. The NEGIS is one of the largest ice streams of the GrIS, initiating ~700 km inland close to the ice divide (Fahnestock et al., 2001), and splitting into its outlet glaciers NG, ZI and SG near the coast (Fig. 1.1a). Along the coastline between 75°N to 81°N there are a series of fjords and inlets (Fig. 1.1b). The grounding lines of NG, ZI and SG are currently stationed inside the coastline within Nioghalvfjerdsfjorden, Jøkelbugten Fjord and Borgfjorden respectively. NG is one of the few remaining outlet glaciers in Greenland fronted by an ice shelf, which covers the 20 km wide Nioghalvfjerdsfjorden, is 76 km long and 100-300 m thick, and has a grounding depth of 600 m (Mayer et al., 2000; Rathmann et al., 2017; Wilson et al., 2017). ZI has had a 30 km wide, grounded tidewater margin since its former ice shelf experienced a 95% reduction in area between 2002 and 2014 (Mouginot et al., 2015).

The northeast Greenland continental shelf is noticeably wider than other areas of the Greenland shelf (up to ~300 km in places), and is dissected by two prominent cross-shelf troughs which extend to the continental shelf edge (IBCAO v3; Jakobsson et al., 2012) (Fig. 1.1b; 1.3). The focus of this study will be Westwind Trough which dissects the shelf to the northeast, and Norske Trough which

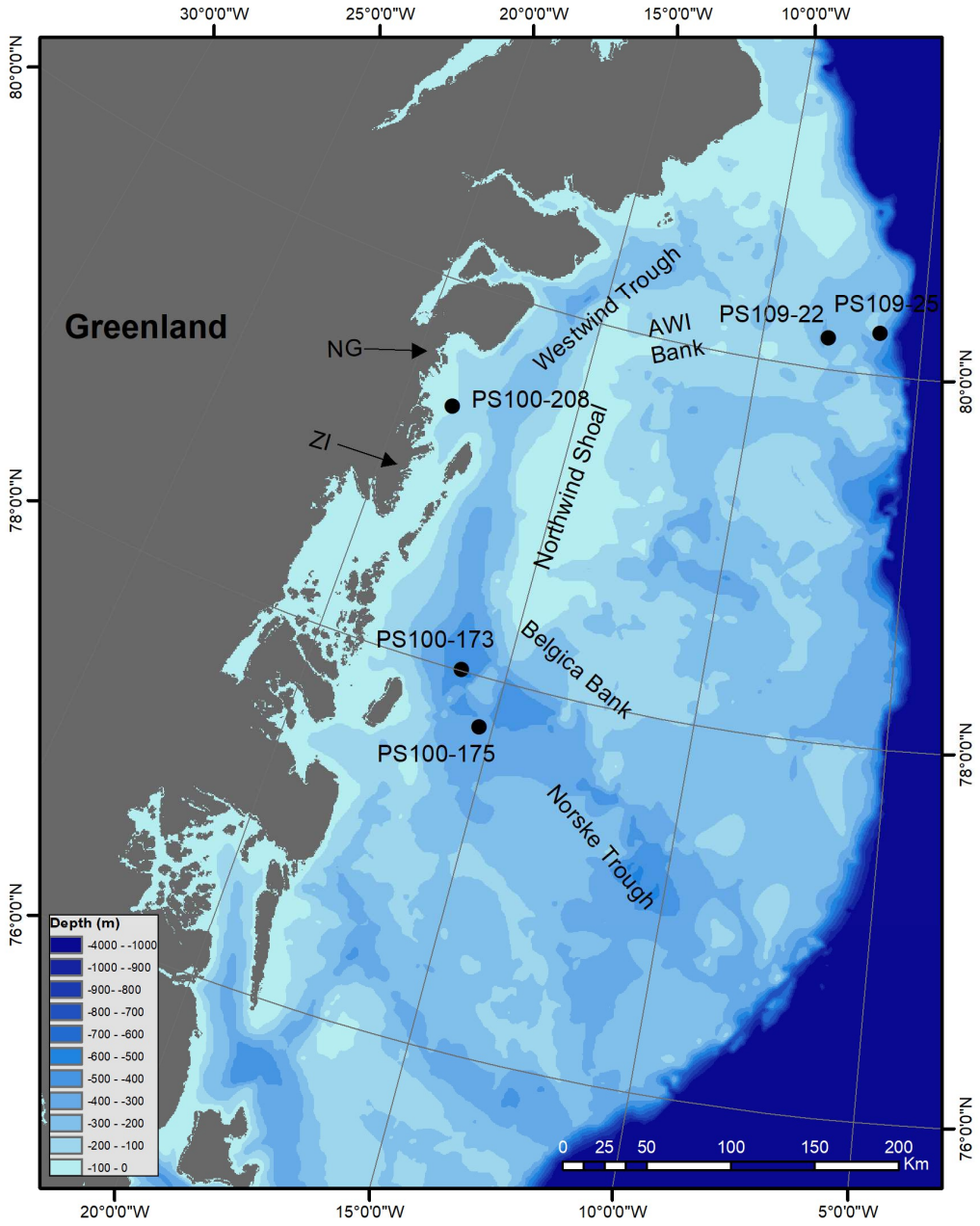

Figure 1.3 Bathymetry of the northeast Greenland continental shelf between 75°N and 81°N, including the bathymetry of Norske and Westwind troughs, and the intervening shallow banks. The location at which the five sediment cores used in this study were recovered is shown. Map produced using IBCAO v3 data (Jakobsson et al., 2012)

dissects it to the southeast (Fig. 1.1b; 1.3). Norske Trough is 350 km long, and widens progressively from 35 km on the inner shelf to 200 km at the shelf edge (Arndt et al., 2015). A large area of the trough has a depth between 300-500 m, and in places it is greater than 500 m (Fig. 1.3). A maximum water depth of 320 m on the outer shelf and 560 m on the inner shelf gives Norske Trough a reverse slope (Arndt et al., 2015). Westwind Trough is both narrower and shallower than

Norske Trough. It is 300 km long, ~40 km wide on the inner shelf, and up to ~70 km wide on the outer shelf (Fig. 1.3). It is predominantly less than 300 m deep, although parts of the inner trough reach depths of 300-500 m and it reaches a maximum depth of 900 m beneath the NG ice shelf, also giving it a reverse slope (Fig. 1.3) (Ardnt et al., 2015). Both troughs display large sills transverse to their centreline on the mid-shelf (Arndt et al., 2015).

A shallower region separates Norske and Westwind troughs. Three banks are present on this inter-trough area; AWI Bank (average depth ~100 m), Northwind Shoal (average depth 20-80 m) and Belgica Bank (average depth ~100 m) (Fig. 1.1b; 1.3) (Arndt et al., 2015).

2. Literature Review

2.1 Overview of the LGM and Holocene history of the GrIS

2.1.1 GrIS history

Palaeo-ice sheet reconstructions using onshore and offshore data have shown that during the LGM the GrIS was more extensive than at present, with ice advancing onto the continental shelf during this time (Funder et al., 2011). Based on terrestrial and nearshore evidence, which includes marine limits and ice marginal deposits, the GrIS was thought to have extended to the mouth of fjords at the LGM (e.g., Funder et al., 1994; Hubberten et al., 1995; Funder and Hansen, 1996). However, recent evidence indicates that ice largely reached the continental shelf edge across Greenland, but there was some spatial variability in the extent between different sectors of the GrIS. In southeastern and western Greenland, ice likely reached the shelf edge in Kangerlussuaq Trough (Jennings et al., 2006; Dowdeswell et al., 2010), Sermilik Fjord (Roberts et al., 2008), Nanortalik (Bennike et al., 2002), Holsteinsborg Dyb (Roberts et al., 2009), Disko and Uummannaq troughs (Roberts et al., 2013b; Ó Cofaigh et al., 2013a; 2018; Lane et al., 2014; Dowdeswell et al., 2014; Hogan et al., 2016; Sheldon et al., 2016; Jennings et al., 2017), and Melville Bugt (Slabon et al., 2016; Newton et al., 2017).

In northern Greenland, ice reached the mid to outer continental shelf in the Wandel Sea (Nørgaard-Pedersen et al., 2008), and was extensive across the shelf in the Lincoln Sea (Larsen et al., 2010). Recent geophysical data suggests that ice may also have expanded to the shelf edge in Norske, Westwind and Store Koldeway troughs in northeastern Greenland (see section 2.1.2.2 for greater detail) (Arndt et al., 2017a; Laberg et al., 2017). In eastern Greenland, ice reached at least the mid-shelf and likely the shelf edge in the Kejser Franz Joseph Fjord and Kong Oscar Fjord outlet systems (Evans et al., 2002; Ó Cofaigh et al., 2004; Arndt, 2018). In Scoresby Sund, Dowdeswell et al. (1994b) initially proposed that ice extended to the fjord mouth at the LGM based on the position of the Kap Brewster moraine ridge. However, Arndt (2018) recently suggested that the GrIS may have actually reached a mid-shelf position at the LGM. Furthermore, cosmogenic exposure dates from the Kap Brewster peninsula imply that ice advanced to the outer shelf beyond Scoresby Sund (Håkansson et al., 2007). Multiple studies have concluded that during the Younger Dryas, the ice margin

was positioned at the head of Hall Bredning in Scoresby Sund (Marienfeld, 1992; Dowdeswell et al., 1994b; Hall et al., 2008; Kelly et al., 2008). Nevertheless, Arndt (2018) proposed that the Kap Brewster moraine actually marks the Younger Dryas ice extent in Scoresby Sund. The GrIS coalesced with the Innuitian Ice Sheet (IIS) in the Nares Strait, northwest Greenland, causing the strait to become completely ice covered (England, 1999; England et al., 2006).

The initial retreat of the GrIS was asynchronous, with dates ranging from 21 ka BP to 9.5 ka BP across the ice sheet. Apart from Holsteinsborg Dyb, where ice recession may have commenced at 21 ka BP (Roberts et al., 2009), ice recession took place earliest in eastern Greenland, initiating at 18.4-18.9 ka BP in Scoresby Sund (Nam et al., 1995). In the northern, southeastern and western sectors of the GrIS, retreat started at a similar time between 17.1 ka BP and 16 ka BP (Jennings et al., 2006; Roberts et al., 2008; Larsen et al., 2010; Slabon et al., 2016; Jennings et al., 2017). Deglaciation of the Nares Strait took place substantially later than the rest of the ice sheet. Radiocarbon dates suggest between 11.8 ka BP to 10.6 ka BP at the northern end of the strait, and between 10.2 ka BP to 9.5 ka BP to the south (England, 1999). More recent onshore cosmogenic surface dates also indicate that the deglaciation of Nares Strait took place <12 ka BP (Ceperley et al., 2020).

Geophysical and lithological data recovered from fjords, cross-shelf troughs and banks on the Greenland continental shelf have provided insights into ice sheet dynamics during GrIS retreat. In central western Greenland, retreat of the ancestral Jakobshavn Isbrae in Disko Trough was rapid although punctuated by minor stillstands on the mid-shelf (Hogan et al., 2016), and retreat through Uummannaq Trough was also rapid and punctuated by stillstands (Roberts et al., 2013b; Ó Cofaigh et al., 2013a; Dowdeswell et al., 2014; Sheldon et al., 2016). In northwest Greenland, retreat was slow but continuous in northern Melville Bay Trough, and more episodic with evidence of a mid-shelf Younger Dryas stabilisation in the central and southern Melville Bay troughs (Slabon et al., 2016). An absence of recessional landforms in Kangerlussuaq Trough implies that ice retreated rapidly to the inner shelf (Dowdeswell et al., 2010). In the southeast Greenland fjords, including in Kangerlussuaq Fjord, moraines are only present in inner fjord positions, which implies that retreat also continued rapidly and continuously through the fjords (Batchelor et al., 2019).

2.1.2 NEGIS history

2.1.2.1 Pre-LGM

The behaviour of NEGIS has been reconstructed back to ~45,000 years ago using ^{14}C and cosmogenic isotope (^{10}Be) dating (Larsen et al., 2018). Radiocarbon dates in the range of 41.1 ± 0.5 to 26.3 ± 0.2 ka from Lambert Land (adjacent to ZI; see Fig. 1.1b for location), alongside radiocarbon dates of 37.0 ± 1.0 to 28.4 ± 0.3 ka from moraines adjacent to SG, suggest that the ice retreated approximately 20-40 km inland from its current position before 41 ka until 26 ka (Larsen et al., 2018). Therefore, there is evidence for a pre-LGM period when the NEGIS margin was located much further inland than present.

2.1.2.2 LGM extent and dynamics

Based on terrestrial evidence, it was thought that outlet glaciers in northeast Greenland were thin and extended to the fjord mouths or the innermost continental shelf during the LGM (Landvik, 1994; Funder and Hansen, 1996). The proximity of LGM glacial deposits to the current ice margin, such as the large outer moraines on the Germania Land peninsula (see Fig. 1.1b for location), were used to propose a LGM ice extent that was restricted to the present coastline (Landvik, 1994; Hjort, 1997). However, Bennike and Bjorck (2002) suggested that these landforms are actually pre-LGM in age, and were preserved by LGM cold-based ice which advanced onto the continental shelf.

More recent investigations of offshore sediments and landforms in Norske and Westwind troughs also indicate former ice stream presence on the northeast Greenland continental shelf. A map of submarine landforms in Norske and Westwind troughs is shown in Figure 2.1. An acoustically transparent unit underlain by a sharp basal reflector, interpreted as a soft subglacial till, has been identified in both Norske and Westwind troughs, and is thought to have been deposited during the LGM (Evans et al., 2009; Arndt et al., 2017a) (Fig. 2.2a; b). Streamlined glacial lineations and MSGLs, are developed on the surface of this acoustically transparent unit (Fig. 2.1; 2.2a; b), and are also interpreted to have formed subglacially by the ice advancing across the continental shelf (Evans et al., 2009; Arndt and Evans, 2016; Arndt et al., 2017a). The presence of elongated subglacial landforms within a cross-shelf trough have been used to show that it was streaming ice which advanced through Norske and Westwind troughs, with this fast flow likely facilitated by the soft basal till layer (Evans et al., 2009). Glacial

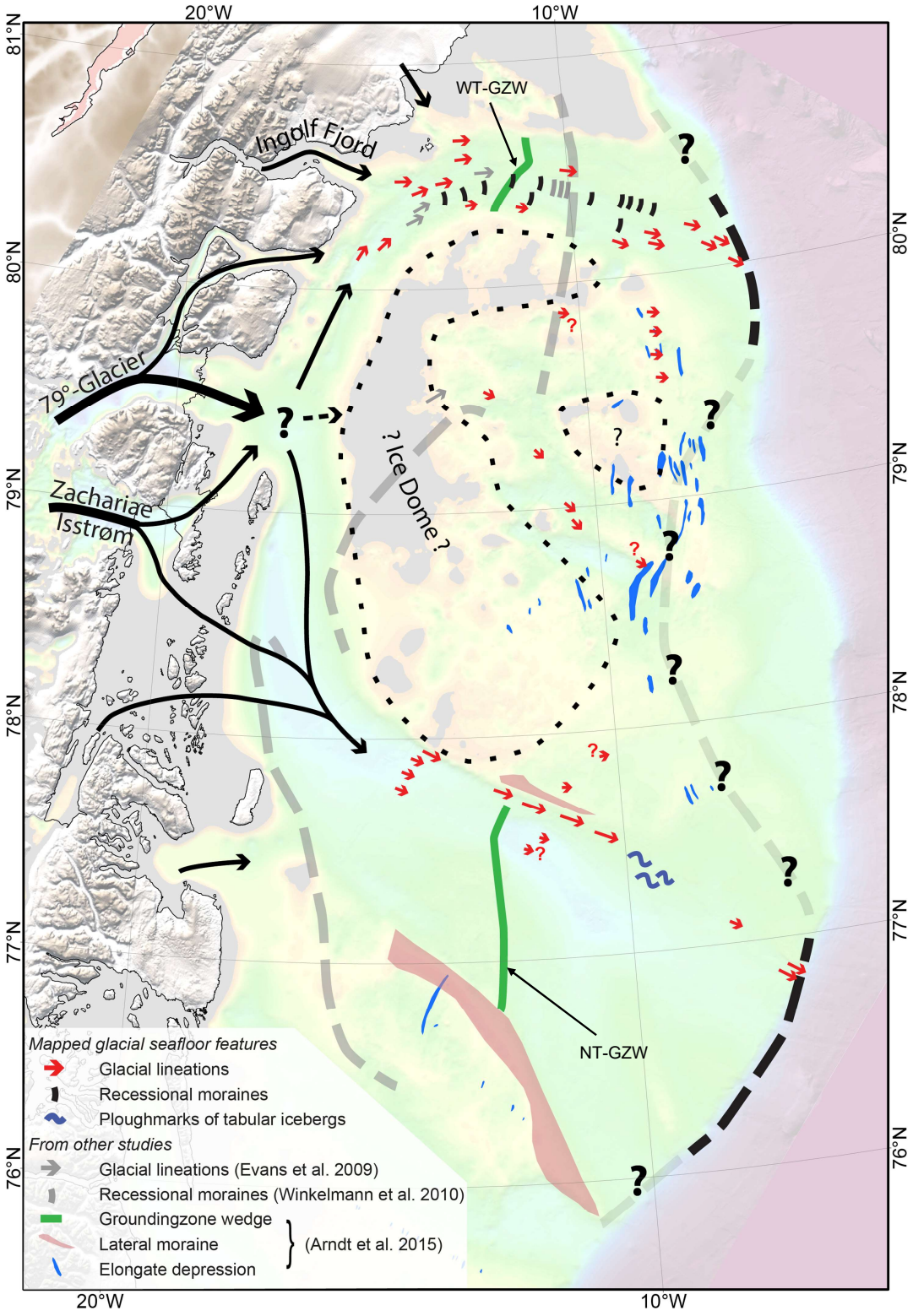

Figure 2.1 Map of submarine landforms present in Norske and Westwind troughs. Adapted from Arndt et al (2017a), including data from Evans et al. (2009), Winkelmann et al. (2010) and Arndt et al. (2015). Black dashed line represents LGM ice extent proposed by Arndt et al. (2017a), grey dashed line represents previous minimum ice extent proposed by Funder et al. (2011).

lineations have also been identified in two areas of Northwind Shoal and AWI Bank, which indicates that ice was also present in inter-stream areas (Evans et al., 2009; Arndt et al., 2017a) (Fig. 2.1). The presence of these lineations has been used to propose that a separate ice dome may have been present on Northwind Shoal, from which ice flowed in two branches through the two deeper parts of the bank (Evans et al., 2009; Arndt et al., 2017a).

Initially, a minimum mid to outer continental shelf ice extent in Norske and Westwind troughs was proposed based on the location of the mid-shelf lineations identified by Evans et al. (2009) (Fig. 2.1). However, Arndt et al. (2017a) identified glacial lineations at the shelf edge in the both troughs (Fig. 2.1), indicating that the NEGIS outlet glaciers likely extended to the shelf edge. Additionally, geophysical data revealed stacked acoustically transparent sediment lobes, interpreted as sediment gravity flow deposits, on the northeast Greenland continental slope (Evans et al., 2009). Mienert et al. (1993) also identified a tributary channel system present on the continental slope as further evidence of debris flow processes. This evidence of debris remobilisation implies that the GrIS reached an outer shelf position in this region. Collectively, this recent evidence has challenged the traditional restricted LGM ice sheet reconstruction in northeast Greenland.

2.1.2.3 Recessional landforms and deglacial retreat dynamics and timing

Geomorphological mapping has identified recessional glacial landforms in both Norske and Westwind troughs, which have been used to constrain the retreat dynamics of the NEGIS. In Westwind Trough, a series of arcuate to elongated submarine ridges (50-300 m wide, 5-25 m high), interpreted as recessional moraines, are found on the mid shelf (Fig. 2.1; 2.2c) (Winkelmann et al., 2010; Arndt and Evans, 2016; Arndt et al., 2017a). Additionally, large bathymetric sills (50-80 km long) occupy the mid-shelf of both troughs (Arndt et al., 2015) (Fig. 2.1). The bathymetric sill in Norske Trough is 80 km long, and the sill in Westwind Trough is 50 km long (Arndt et al., 2015). These have been inferred to be GZWs based on their asymmetric and wedge-shaped morphology (Arndt et al., 2015). The GZW in Westwind Trough will be hereafter referred to as WT-GZW, and the mid Norske Trough GZW will be referred to as NT-GZW (Fig. 2.1)

Two prominent ridges also occur at the northern and southern edges of outer Norske Trough, which are 50 km and 170 km long, and 30 m and 100 m high respectively (Arndt et al., 2015). These ridges are interpreted as lateral moraine

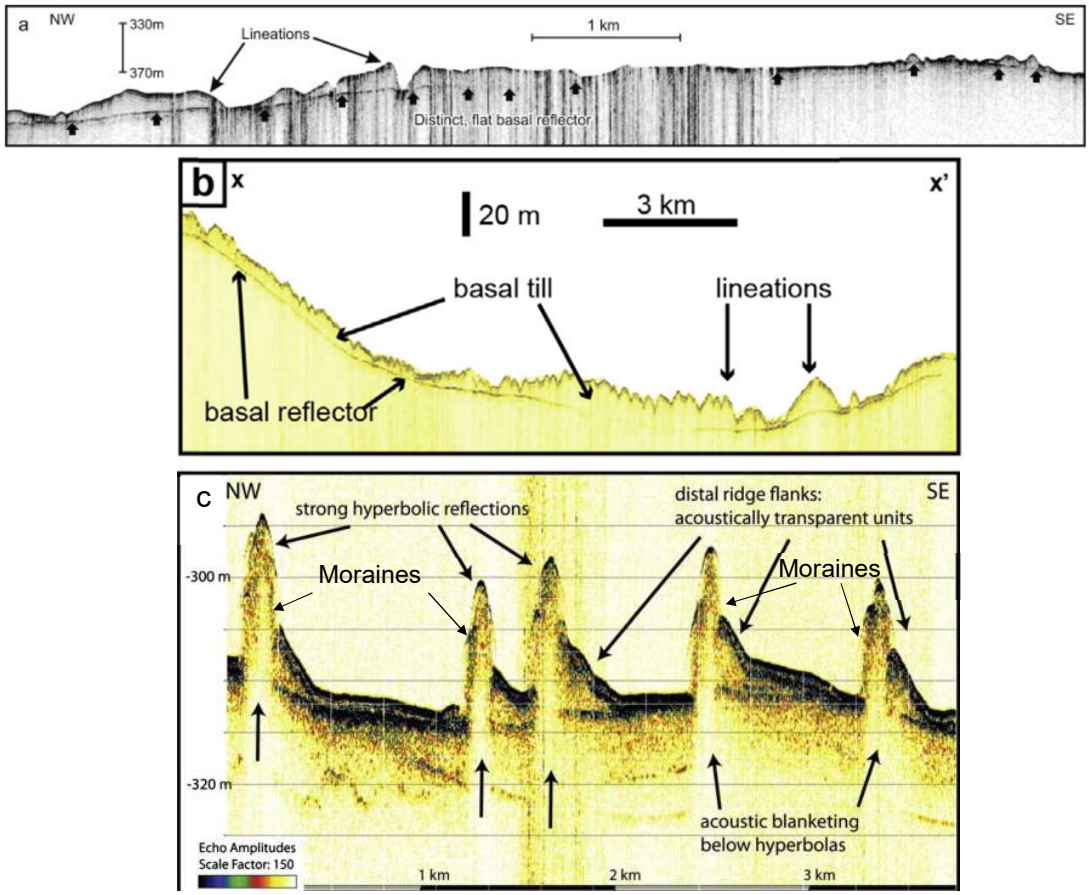

Figure 2.2 Acoustic profiles of landforms and sediments identified in Norske and Westwind troughs (a) TOPAS sub-bottom profile record from Westwind Trough showing the acoustically transparent sediment unit underlain by a basal reflector (subglacial till), with glacial lineations on its surface. From Evans et al. (2009) (b) Parasound sub-bottom profile from mid Norske Trough showing the acoustically transparent unit with a distinct basal reflector (subglacial till), which displays glacial lineations on its surface. From Arndt et al. (2017a) (c) Parasound profile of recessional moraines in mid Westwind Trough. From Winkelmann et al. (2010).

complexes (Fig. 2.1) (Arndt et al., 2015). U-shaped furrows (100 m wide, 5-10 m deep), mainly orientated NNE to SSW, are also frequent in both troughs (Arndt et al., 2017a). Some very large furrows (up to 800 m wide) with flat bases are also reported from outer Norske Trough (Arndt et al., 2017a). Both types are interpreted as iceberg ploughmarks, with the larger flatter furrows attributed to grounding of large tabular icebergs with flat bases (Arndt et al., 2017a).

The absence of ice marginal depositional features such as moraines or GZWs from the shelf edge in Norske and Westwind troughs (Fig. 2.1) suggests that initial retreat of the NEGIS was rapid in both troughs (Ó Cofaigh et al., 2008; Dowdeswell et al., 2008b; Arndt et al., 2017a). There is currently no dating to constrain the timing at which retreat from the outer shelf initiated. The presence of

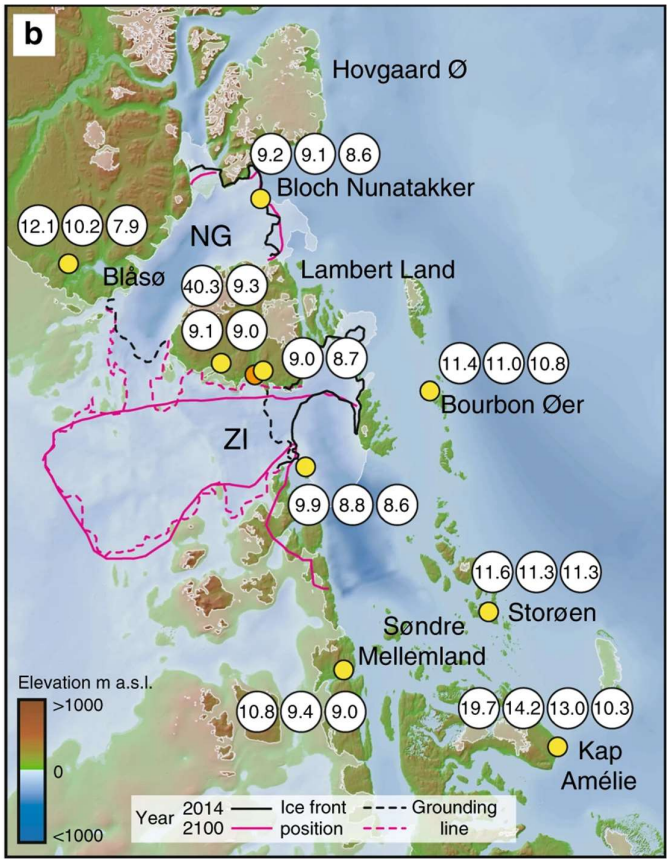

Figure 2.3 Map showing the new cosmogenic exposure dates (yellow circles) and new ^{14}C dates (orange circles) from northeast Greenland presented by Larsen et al. (2018). Dates from Bourbon Øer, Storøen and Kap Amélie indicate the timing at which the outer coastline was deglaciated by the NEGIS. Dates from Blåsø, Lambert Land, ZI, Søndre Mellemland, and Bloch Nunatakker indicate the timing of deglaciation around the present ice margin. Bed topography and bathymetric data are from Morlighem et al. (2017), and the outlines of glacier margins are based on GIMP data (Howat et al., 2014). Observed and modelled ice front predictions are from Choi et al. (2017).

recessional moraines in outer and mid Westwind Trough implies that there were periods when the ice margin halted or underwent minor readvance during retreat, and that therefore retreat was stepwise over this area (Ó Cofaigh et al., 2008; Dowdeswell et al., 2008b; Winkelmann et al., 2010; Arndt and Evans, 2016; Arndt et al., 2017a). A longer grounding line stillstand in mid Westwind Trough is indicated by the presence of WT-GZW (Ó Cofaigh et al., 2008; Dowdeswell et al., 2008b; Arndt et al., 2015). The lack of moraines on the inner shelf of Westwind Trough implies a subsequent transition to more rapid retreat (Arndt and Evans, 2016). In contrast, ice retreat through Norske Trough appears to have taken place more continuously than in Westwind Trough based on the absence of recessional moraines across the shelf (Fig. 2.1) (Dowdeswell et al., 2008b; Arndt et al., 2017a). However, there must have been at least one prolonged grounding line

stillstand during retreat through Norske Trough to allow for the formation of the NT-GZW (Ó Cofaigh et al., 2008; Arndt et al., 2015).

Based on the oldest radiocarbon date from a moraine on the outer coast, the entrance of Nioghalvfjerdsfjorden was ice free from 9.7 cal ka BP (Bennike and Weidick, 2001), suggesting that the ice had retreated from the continental shelf and into the fjords by this time. Recent cosmogenic isotope dates from Bourbon Øer, Storøen, and Kap Amélie (Fig. 2.3) reveal a mean deglaciation age for the outer coastline of 11.7 ± 0.6 ka. Deglaciation of sites close to the present ice margin had a mean age of 9.3 ± 0.4 ka, indicating that retreat from the outer coastline to the present day margin took place in ~2.4 kyr (Larsen et al., 2018). Evidence of raised marine sediments in the fjord of 79°N glacier, dated to 7.7-4.5 cal ka BP, suggests that the fjord was ice free during this part of the Holocene (Bennike and Weidick, 2001; Bennike and Bjorck, 2002). It is likely that ice build-up restarted after 4.5 cal ka BP during Neoglacial cooling over Greenland (Bennike and Weidick, 2001).

2.2 Overview of subglacial, glacimarine and sub-ice shelf processes and sediments

A wealth of studies have been dedicated to developing an understanding of subglacial, ice marginal and glacimarine processes in terrestrial, fjord and continental shelf settings. This has allowed the characteristics of the sediments produced by subglacial and glacimarine processes to be elucidated. The nature of these processes and their associated deposits will be reviewed in the following section.

2.2.1 Subglacial processes

Evans et al. (2006a) identify three end members which form in the subglacial environment: (1) subglacial traction till, (2) glacitectonite, and (3) subglacial melt-out till. Table 2.1 shows the characteristics of these three types of sediment. Subglacial traction till is usually the product of multiple subglacial processes, including deformation, ploughing, lodgement and deposition by water films, the occurrence of which change spatially and temporally across the ice-bed interface (Evans et al., 2006a; Evans, 2018). This phenomenon has been described as a mosaic of changing bed conditions (Piotrowski et al., 2004). Subglacial deformation of the underlying soft substrate can be responsible for ice motion

(Alley et al., 1986; Boulton, 1986; Boulton and Hindmarsh, 1987), and sediment from this deforming layer is deposited either by ice-bed decoupling or an increase in the yield strength of the deforming layer (Benn and Evans, 2010). Ploughing and lodgement occur when boulders protruding from the sole of the glacier are pushed through the substrate, and are deposited when resistance from the basal sediment exceeds the force exerted on the boulder by the overlying ice (Boulton, 1976; Dreimanis, 1989; Clark and Hansel, 1989). Ice motion can transition from deformation to sliding in response to spatial and temporal changes in subglacial effective pressure, which can cause the ice to decouple from the bed, and water films and/or braided canal or pipe systems to develop (Clark and Walder, 1994; Piotrowski and Kraus, 1997; Engelhardt and Kamb, 1998; Boulton and Dobbie, 1998; Piotrowski and Tulaczyk, 1999; Boulton et al., 2001).

Subglacial traction tills are generally massive or stratified diamictons, displaying a wide range of internal features indicative of deposition in a subglacial environment, including clast pavements, fissile partings, bullet-shaped striated clasts, stringer/pod structures and dyke structures (see Table 2.1 for greater detail) (e.g., Clark and Hansel, 1989; Hicock, 1991; Evans et al., 1995; 2016; 2018; Evans and Twigg, 2002; Dowdeswell et al., 2004; Larsen et al., 2004; Evans et al., 2005; Evans and Hiemstra, 2005; Ó Cofaigh et al., 2005a; 2007; Davies et al., 2009; Roberts et al., 2013a; Eyles et al., 2015). Some subglacial traction tills display a two-tiered structure, comprising a porous upper a-horizon underlain by a denser b-horizon which reflect ductile and brittle deformation respectively (Boulton and Hindmarsh, 1987; Benn, 1995; Evans and Twigg, 2002; Evans et al., 2016; 2018). Water films deposit sandy/muddy stringers (Piotrowski and Kraus, 1997; Piotrowski and Tulaczyk, 1999), whilst the development of braided canal or pipe systems are recorded by lenses of stratified sediment (Clark and Walder, 1994; Walder and Fowler, 1994; Evans et al., 1995).

A glacitectonite is defined as a sediment that has undergone deformation but retains some of the structural characteristics of its parent material (Benn and Evans, 1996; Evans, 2018). Primary sedimentation can be the product of ice marginal sedimentation (e.g., mass flows, suspension settling) (e.g., Ó Cofaigh et al., 2011), or deposition by non-glacial processes (e.g., Phillips et al., 2013b; Roberts et al., 2013a), followed by deformation as the primary deposits are overridden (subglacial to ice-marginal glacitectonism) or thrusted by advancing ice

Table 2.1 Characteristics of subglacial traction tills, subglacial and proglacial glacitectonites, and melt-out tills from a range of locations.

Deposit	Sediment characteristics	Location and study
Subglacial traction till	Massive, matrix-supported diamictons. Evidence of fissility, clast pavements, and A/B horizon development.	Southeast Iceland (Boulton and Hindmarsh, 1987; Evans and Hiemstra, 2005; Evans et al., 2018)
	Alternating massive and fissile (contains closely spaced partings) diamictons. Bullet-shaped striated clasts evident.	Western Iceland (Evans et al., 2016)
	Massive till with soft clasts and stringers, evidence of meltwater channels.	Knud Strand, Denmark (Larsen et al., 2004)
	Massive, matrix-supported diamicton. Stratified/laminated in places. Displays stringer/pod structures.	North Yorkshire, UK (Roberts et al., 2013a)
	Massive or stratified, matrix-supported diamictons. Contain lens-shaped bodies of stratified sediment, boulder pavements and smeared inclusions.	East Yorkshire, UK (Evans et al., 1995)
	Fissile, matrix-supported diamicton. Bullet shaped and striated clasts present. Rafts and pods present in lower part of the diamicton.	Saskatchewan Glacier, Canadian Rockies (Eyles et al., 2015)
	Matrix-supported diamicton containing faceted and striated clasts. Some fissility and stratification. Contains boulder pavements, dyke structures, and lenses of sand and clay with concave bases and flat tops	Whitburn, County Durham, UK (Davies et al., 2009)
	Two diamicton units: (1) 'soft' massive, matrix-supported diamicton displaying planar structures, crude clast alignment, overlying (2) 'stiff' massive, matrix-supported diamicton with a higher shear strength than the soft diamicton.	Marguerite Bay and Robertson Trough, Antarctica (Dowdeswell et al., 2004; Evans et al., 2005; Ó Cofaigh et al., 2005a; 2007)
Subglacial glacitectonite	Raft of undisturbed shale to brecciated shale to clast supported diamicton. Recumbent folds evident.	North Yorkshire, UK (Roberts et al., 2013a)
	Bedrock rich, massive to stratified, clast- to matrix-supported diamicton. It displays bedrock rafts, thrusts, clast fabric, brittle faults and folding.	Anglesey, northwest Wales (Phillips et al., 2013b)
	Stratified diamictons, displaying dropstone structures, pods of chalk and sand, chalky stringers, continuous diamictic laminae, boudins, augens, and folding in pressure shadows.	West Runton, Norfolk, UK (Roberts and Hart, 2005)
	Large hydrofracture system composed of a network of bedding parallel sills and subvertical dykes present within the bedrock. Dykes and sills contain laminated sand, silt and clay.	Meads of St John, northeast Scotland (Phillips et al., 2013a)
Proglacial glacitectonite	Thrust bound slabs of chalk and chalk rafts.	North Norfolk, UK (Burke et al., 2009; Vaughan-Hirsch et al., 2011)
Melt-out till	Structureless silt/sand, or layers of silt/sand with dispersed boulder sized clasts, and laminae and lenses of mud/sand aggregates.	Matanuska Glacier, Alaska, USA (Lawson, 1981; Larson et al., 2006)

(proglacial glacitectonism). Structures associated with subglacial glacitectonism include discontinuous laminae/stringers, pod structures, rafts, fissile partings, faults, thrusts and folds (Table 2.1) (Evans and Ó Cofaigh, 2003; Roberts and Hart, 2005; Lee and Phillips, 2008; Roberts and Hart, 2011; Ó Cofaigh et al., 2011; Roberts et al., 2013a; Phillips et al., 2013b). Proglacial glacitectonism can produce rafts, and landforms including hill-hole pairs, moraines and cupola hills (Table 2.1) (Phillips and Merritt, 2008; Burke et al., 2009; Vaughn-Hirsch et al., 2011; Phillips, 2018). Subvertical dyke structures, formed when water is pressurised by the overlying ice, can also be produced by glacitectonism (Table 2.1) (Rijsdijk et al., 1999; Evans and Ó Cofaigh, 2003; Phillips and Merritt, 2008; Ó Cofaigh et al., 2011; Phillips et al., 2013a; Evans et al., 2016).

Melt-out till describes sediment deposited by slowly moving or stagnant debris-rich ice (Evans et al., 2006a; Benn and Evans, 2010). It has been much less widely described than the other two subglacial end members, likely due to its low preservation potential (Paul and Eyles, 1990). It is characterised by massive to stratified diamictons, or pebbly silts/sands, which display lenses of mud/sand aggregates, distinct layering, and gravity induced disturbance (Table 2.1) (Lawson, 1981; Evans et al., 2006a; Larson et al., 2006).

A sequence of two subglacial tills is common to some cross-shelf troughs in both Greenland and Antarctica. Geophysical data retrieved from these cross-shelf troughs have revealed the presence of an acoustically transparent sediment unit underlain by a strong basal reflector (Shipp et al., 1999; Lowe and Anderson, 2002; Dowdeswell et al., 2004; Ó Cofaigh et al., 2002b; 2005a; 2005b; 2007; Evans et al., 2005; 2006; 2009; Mosola and Anderson, 2006; Livingstone et al., 2012; Larter et al., 2019). These acoustic units have been interpreted as a lower stiff till, overlain by a soft, porous till which often has MSGL on its upper surface (Dowdeswell et al., 2004; Ó Cofaigh et al., 2005a; 2007; Evans et al., 2005; 2006; 2009; Mosola and Anderson, 2006; Livingstone et al., 2012). Multiple explanations for this sequence have been proposed. The two tills could have been deposited during different periods of ice advance (Evans et al., 2005; 2009; Ó Cofaigh et al., 2007), or the two-tiered structure could represent the development of an A/B horizon during subglacial deformation (Ó Cofaigh et al., 2005a; 2007). Alternatively, the sequence could reflect a change in depositional process, with the lower stiff till deposited predominantly by lodgement, whilst the genesis of the soft

till above was related to either subglacial deformation, or a combination of subglacial deformation and lodgement (Wellner et al., 2001; Shipp et al., 2002; Heroy and Anderson, 2005; Ó Cofaigh et al., 2007).

Coring of subglacial tills deposited on continental shelves has revealed massive, matrix-supported diamictons containing angular to sub-rounded clasts (Wellner et al., 2001; Shipp et al., 2002; Dowdeswell et al., 2004; Evans et al., 2005; 2006; Heroy and Anderson, 2005; Hillenbrand et al., 2005; 2010; Ó Cofaigh et al., 2005a; 2007; 2013a; Graham et al., 2009; Kilfeather et al., 2011; Hogan et al., 2016; Sheldon et al., 2016). Such tills commonly display a range of deformation structures, including planar structures at macroscale, and plasmic fabrics, folding and turbate structures at microscale (Ó Cofaigh et al., 2005a, 2007, 2013a; Sheldon et al., 2016).

2.2.2 Grounded tidewater and glacimarine processes

The depositional processes that take place in glacimarine settings include suspension settling from meltwater plumes, iceberg rafting, and mass flow activity including debris flows and turbidity currents (Fig. 2.4). The characteristics of the sediment deposited by these processes is demonstrated in Table 2.2.

At the grounding line of a glacier, subglacial and englacial streams discharge sediment laden meltwater into the marine environment, which mixes with ambient seawater and forms overflow plumes due to the buoyancy forces (Cowan and Powell, 1990; Powell, 1990; Ó Cofaigh and Dowdeswell, 2001). The sediment in these plumes can be transported varying distances depending on current velocity, and sediment is deposited as single sand and coarse silt grains sink through the water column (Fig. 2.4) (Cowan et al., 1997; Dowdeswell et al., 1998). Finer clay particles join together as they settle through the water column, referred to as flocculation (Cowan and Powell, 1990). Suspension settling deposits comprise fine grained muds, silts and sands with low shear strengths (Table 2.2) (Cowan and Powell, 1990; Cowan et al., 1999; Ó Cofaigh et al., 2001; Evans et al., 2002; Desloges et al., 2002; Gilbert et al., 2002; Sheldon et al., 2016; Streuff et al., 2017). In ice proximal locations, suspension settling deposits often display alternating, millimetre scale planar coarse and fine laminae, imparted by diurnal to seasonal fluctuations in meltwater discharge or changes in the position of meltwater efflux (Mackiewicz et al., 1984; Gilbert et al., 1993; Cowan et al., 1999; Ó Cofaigh and Dowdeswell, 2001; Ó Cofaigh et al., 2001; Streuff et al., 2017).

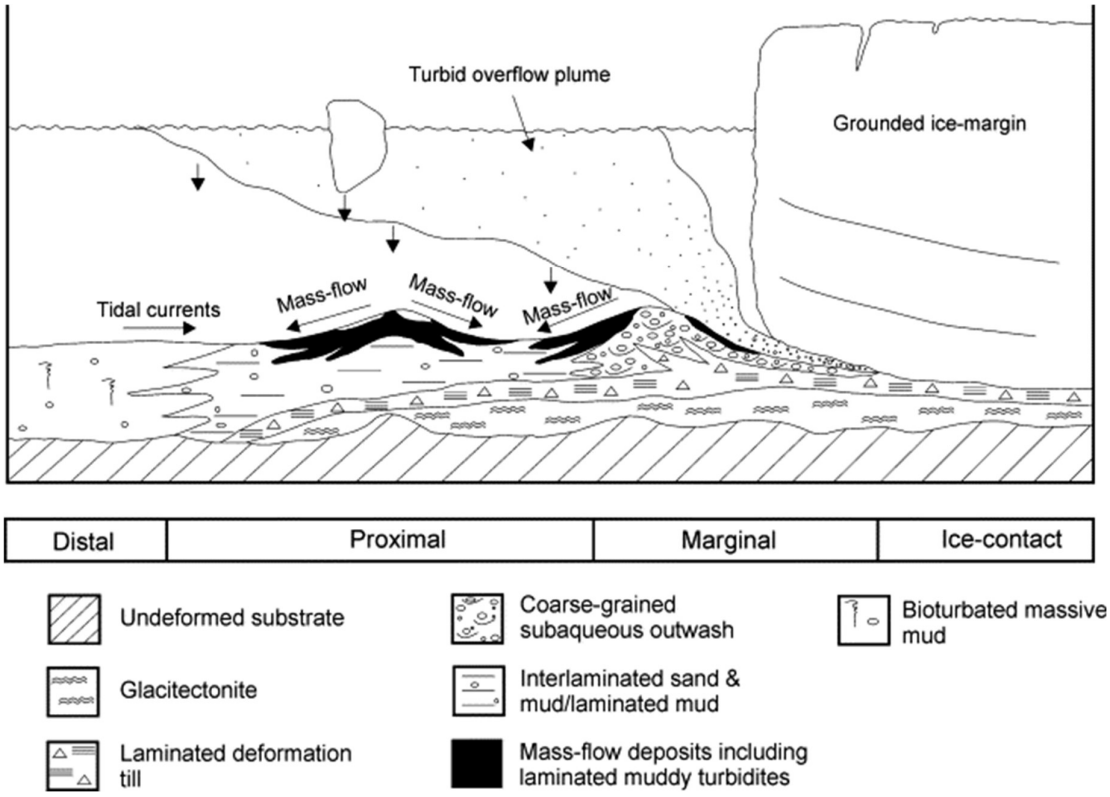

Figure 2.4 Sedimentary processes occurring at a tidewater margin. Arrows indicate release of sediment from turbid meltwater plumes and iceberg rafting. From Ó Cofaigh and Dowdeswell (2001), after Eyles and McCabe (1989) and Hart and Roberts (1994).

Often, the coarser laminae have a sharp lower contact and grade upward into the finer laminae (Mackiewicz et al., 1984; Cowan et al., 1999; Ó Cofaigh and Dowdeswell, 2001). With increased distance from the ice margin, suspension settling muds become more diffusely stratified to massive, and the grain size and thickness of laminae is reduced (Streuff et al., 2017).

Glacimarine sediment can also be deposited by turbidity currents, a type of subaqueous sediment gravity flow event in which sediment is transported by fluid turbulence (Talling et al., 2012; 2013). In a glacial setting, they can be caused by the remobilisation of sediment piles triggered by icebergs or small readvances, rapid sedimentation at the ice margin, or by meltwater flows with high sediment concentrations emerging from the ice margin and forming turbid underflows (Cowan and Powell, 1991; Gilbert et al., 1993; Ó Cofaigh and Dowdeswell, 2001). Turbidity current deposits in glacial environments comprise either sand fining upwards into mud, or ungraded muddy sand, often with convoluted planar to wispy laminae, load and flame structures, and sharp basal contacts (Table 2.2) (Gilbert et al., 1993; Ó Cofaigh et al., 2001; Desloges et al.,

Table 2.2 Examples of the sedimentary characteristics associated with different modes of glacimarine sedimentation, compiled from various locations.

Mode of deposition	Sediment characteristics	Location and study
Suspension settling from meltwater plumes	Rhythmically laminated mud and silt. Coarse and fine lamina alternate in rhythmic couplets. Laminae are planar and parallel.	Scoresby Sund, east Greenland (Ó Cofaigh et al., 2001)
	Interlaminated mud and very fine silt to sand. Sand/silt has a sharp lower contact and gradational upper contact with the mud. Laminae are mm scale.	Muir Glacier Fjord, Alaska, USA (Cowan et al., 1999)
	Laminated muds, wavy to wispy to planar, fine to crude scale. Contain a small number of distributed clasts.	Kejser Franz Josef Fjord, east Greenland (Evans et al., 2002)
	Massive to stratified mud with variable amounts of clasts. Matrix is composed of silt and clay. Stratified in the ice proximal environment, stratification is more diffuse in the ice distal setting.	Disko Bay, west Greenland (Streuff et al., 2017)
	Laminated fine muds.	Disko Bay Fjords, west Greenland (Desloges et al., 2002; Gilbert et al., 2002)
	Massive to faintly laminated fine grained mud.	Expedition Fjord, Canadian High Arctic (Gilbert et al., 1993)
	Dark grey crudely stratified grey mud. Stratification is imparted by grain size variations in the matrix.	Uummannaq Trough, west Greenland (Sheldon et al., 2016)
Turbidity current activity	Sands with sharp lower contacts that grade upwards into mud. Laminae may be convoluted and display load/flame structures. Laminae thickness can be variable and can vary from planar to wispy.	Scoresby Sund, east Greenland (Ó Cofaigh et al., 2001)
	Graded fine sand to mud.	Expedition Fjord, Canadian High Arctic (Gilbert et al., 1993)
	Contorted to massive mud, with fine sand rich units in laminae/cm thick layers.	Disko Bay, west Greenland (Streuff et al., 2017)
	Thin ungraded layers of muddy sand.	Disko Bay Fjords, west Greenland (Desloges et al., 2002; Gilbert et al., 2002)
	Sand-mud couplets consisting of a lower layer of massive to laminated silty to sandy mud, with massive to weakly laminated clayey mud above.	Kejser Franz Josef Fjord, east Greenland (Evans et al., 2002)
	Weakly graded sand beds.	Ikerasak, west Greenland (Desloges et al., 2002)
Debris flows activity	Massive diamicton with sharp basal contacts.	Scoresby Sund, east Greenland (Ó Cofaigh et al., 2001)
	Dense matrix supported diamicton, with a contorted appearance and a low shear strength. Mud strata are present within the diamicton facies.	Disko Bay, west Greenland (Streuff et al., 2017)
	Fine grained mud displaying micro-scale faults and convoluted bedding.	East Greenland fjords (Smith and Andrews, 2000)
	Massive muddy diamicton with a fine grained matrix and inclined and aligned clast fabrics.	Kejser Franz Josef Fjord, east Greenland (Evans et al., 2002)

Debris flows activity on trough mouth fans	Massive, poorly sorted matrix supported diamicton.	Bear Island Trough Mouth Fan, Barents Sea Margin (Laberg and Vorren, 1995; 2000)
	Dark grey to olive grey massive muddy diamictons. Diamictons are structureless and unsorted, and contain frequent pebble sized clasts.	Scoresby Sund Fan, east Greenland (Ó Cofaigh et al., 2002a)
	Massive, matrix supported diamicton, with occasional faint stratification.	Disko Trough Mouth Fan, west Greenland (Ó Cofaigh et al., 2018)
IRD rainout	Massive to stratified diamicts with non-erosive, gradational/conformable contacts. Clasts lack a consistent orientation, and diamicton pellets are present.	Scoresby Sund, east Greenland (Ó Cofaigh et al., 2001)
	Massive, matrix supported diamicton containing isolated lenses of gravel and coarse sand. Laminated fine silty sand and clay are also present within the diamicton.	Scoresby Sund, east Greenland (Dowdeswell et al., 1994a)
	Muddy sediment containing horizons of coarse sand grains and small pebbles.	Expedition Fjord, Canadian High Arctic (Gilbert et al., 1993)
	Massive to stratified diamicton containing abundant sub-angular to sub-rounded clasts which lack a consistent orientation.	East Greenland fjords (Smith and Andrews, 2000)
	Laminated to stratified sandy mud with scattered clasts, and stratified matrix supported diamicton.	Bear Island Trough, Barents Sea (Rüther et al., 2011)
Alternation between meltwater plume sedimentation and iceberg rafting	Laminated mud alternating with massive diamicton.	Scoresby Sund, east Greenland (Dowdeswell et al., 2000)
	Diffusely laminated mud interbedded with diamictic layers.	Disko Bay, west Greenland (Hogan et al., 2016; Streuff et al., 2017)

2002). Alternatively, discrete layers of ungraded muddy sand have been recorded as turbidity current deposits (Gilbert et al., 2002). The ideal model of turbidity current deposition is termed the 'Bouma sequence' (Fig. 2.5), however the complete sequence is rarely found, and many turbidity current deposits differ largely from this model (Bouma, 1962; Talling, 2014).

Debris flows also rework sediment in an ice proximal environment (Fig. 2.4). Sediment transport in debris flows is supported by matrix cohesion and grain-to-grain interactions, rather than by fluid turbulence (Shanmugan, 1997; Talling et al., 2012; 2013). Debris flows deposit contorted, poorly sorted massive mud-rich diamicton or mud units, with evidence of sediment reworking such as interbedded mud strata and convoluted bedding, and clast alignment (Table 2.2) (Eyles and Eyles, 2000; Smith and Andrews, 2000; Evans et al., 2002; Streuff et al., 2017). Larger scale debris flows also form Trough Mouth Fans (TMFs), which are fan-

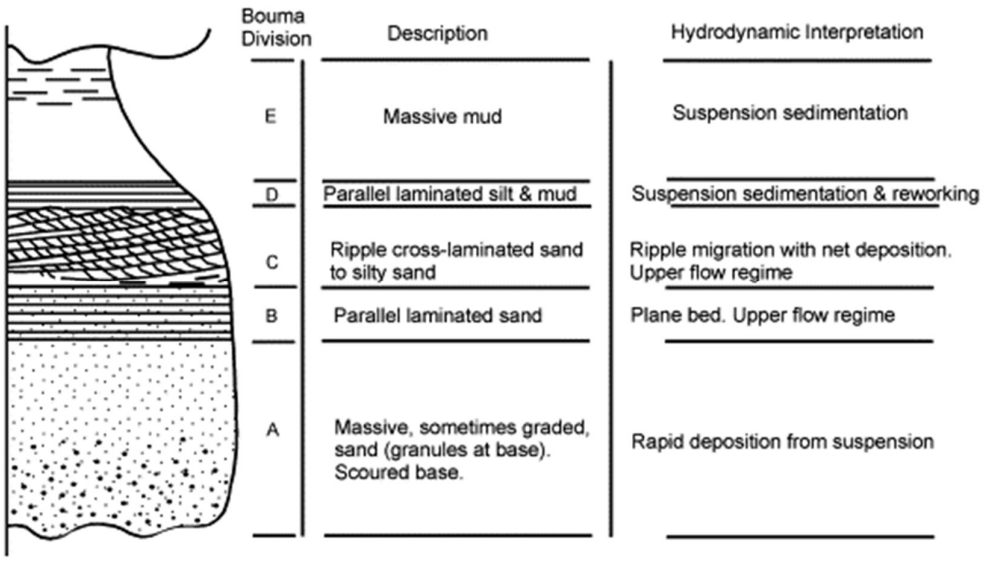

Figure 2.5 Bouma sequence model for facies deposition by turbidity currents. From Ó Cofaigh and Dowdeswell (2001) after Collinson and Thompson (1989).

shaped sediment accumulations at the mouth of glacial troughs on continental slopes (Laberg and Vorren, 1995; Dowdeswell et al., 1997; Vorren et al., 1998; Ó Cofaigh et al., 2003). During periods when ice is stationed at the shelf edge, large volumes of glacigenic sediment accumulate and are remobilised down the continental slope by debris flows to form TMFs, which comprise massive, poorly sorted, and structureless diamictons (Table 2.2) (Laberg and Vorren, 1995, 2000; Dowdeswell et al., 2002; 2008a; Ó Cofaigh et al., 2002a; 2018; Taylor et al., 2002).

It is important to note that deposition by both turbidity currents and submarine debris flows in glaciated troughs is not solely driven by sedimentation at the grounding line. Turbidity currents and debris flows can also be triggered on steep slopes within or at the sides of glacial troughs and fjords, by rapid sedimentation which eventually leads to slope failure (Syvitski and Farrow, 1989; Piper and Normark, 2009; Xu, 2011). As a result, the presence of turbidity current and/or debris flow deposits in a glacial setting are not necessarily indicative of deposition at the grounding line.

Glacimarine sediment is also deposited by the release of debris from floating icebergs calved from the ice margin, termed ice-rafted debris (IRD) (Fig. 2.4) (Dowdeswell et al., 1994a; 1998; Ó Cofaigh, 2007). Sediment deposited by iceberg rafting is characterised by massive to stratified diamictons with gradational or conformable contacts, clast clusters and a sub-vertical clast orientation or a lack

of consistent clast orientation, or alternatively muds with scattered or discrete horizons of coarser grains (Table 2.2) (Gilbert et al., 1993; Dowdeswell et al., 1994a; Smith and Andrews, 2000; Ó Cofaigh et al., 2001; Rüther et al., 2011). Iceberg rafted diamicton may also contain isolated lenses of gravel and coarse sand deposited by iceberg overturning, which dumps the sediment from the iceberg surface onto the seafloor (Dowdeswell et al., 1994a). Although they can appear macroscopically similar, Licht et al. (1999) suggested that iceberg rafted diamicton can be distinguished from subglacially deposited diamicton by a higher percentage and variation in total organic carbon, the presence of tephra layers, and greater variation in pebble abundance because flux of iceberg rafted sediment is variable through time.

In some environments these different depositional processes interact, for example the alternation of iceberg rafting and suspension settling produces laminated diamicton and fines, labelled 'glacimarine varves' (Table 2.2) (Cowan et al., 1997). Two mechanisms for the formation of 'glacimarine varves' have been proposed in different locations. Dowdeswell et al. (2000) suggest that during open water conditions in summer, the rainout of debris from calved icebergs forms massive to stratified diamictons. Subsequent increased sea ice cover in winter then supresses iceberg rafting, allowing deposition by suspension settling from turbid meltwater plumes to deposit a layer of mud (Dowdeswell et al., 2000). Alternatively, the genesis of a similar facies in west Greenland was attributed to an increase in meltwater derived fines in summer, and a subsequent reduction in winter that allowed sedimentation by iceberg rafting to become dominant (Hogan et al., 2016; Sheldon et al., 2016; Streuff et al., 2017).

2.2.3 Sub-ice shelf processes

A specific glacimarine depositional regime and facies succession has been identified for glaciers which terminate in ice shelves (Domack and Harris, 1998; Smith et al., 2019). This idealised succession is shown in Figure 2.6, and an illustration of these depositional processes is shown in Figure 2.7. Table 2.3 summarises the characteristics of sediment deposited in an ice shelf environment.

Debris flows comprised of subglacial till emanating from the grounding line often occur in the grounding zone of an ice shelf fronted glacier (Fig. 2.7) (Smith et al., 2019). Stacking of successive debris flows can lead to the formation of wedge

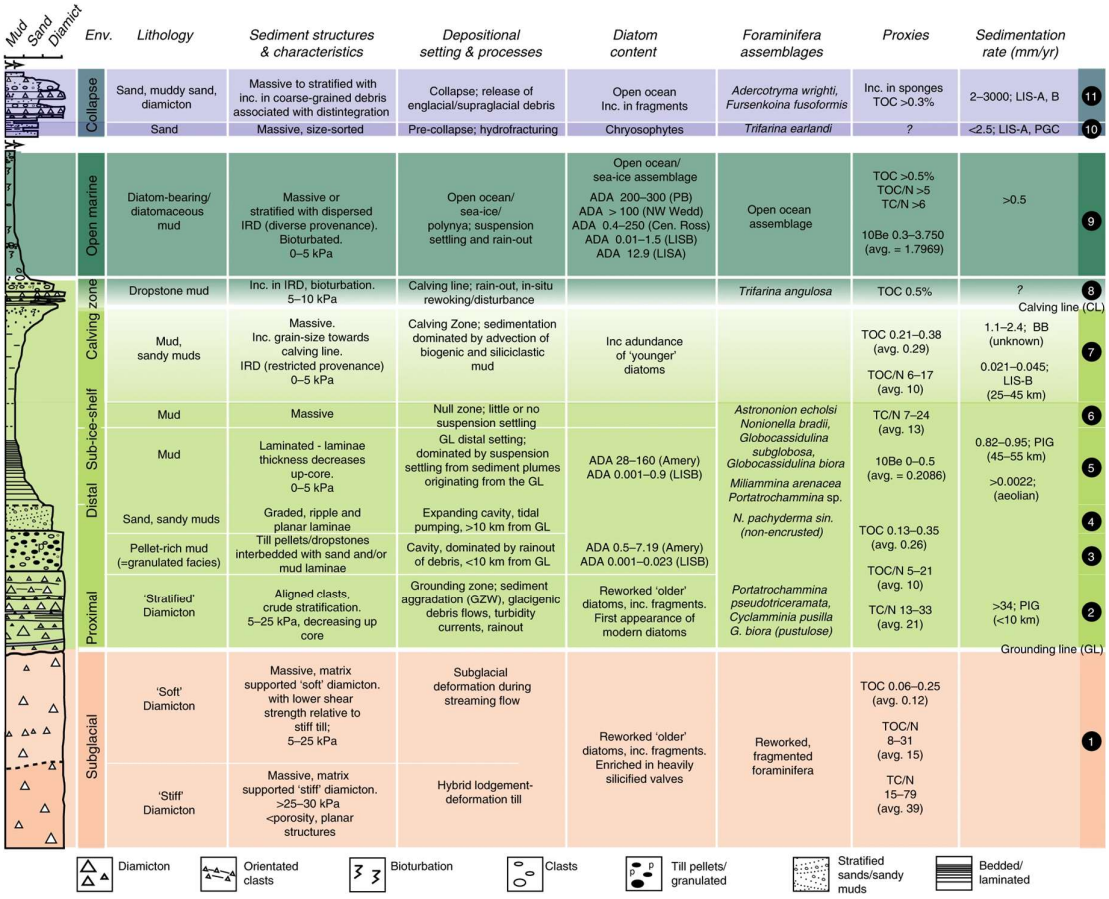

Figure 2.6 Idealised sedimentary succession in an ice shelf environment, outlining the depositional processes, diatom count, foraminifera assemblages, proxies and sedimentation rate associated with each sediment facies. From Smith et al. (2019).

shaped sediment bodies, known as GZWs (Howat and Domack, 2003; Ó Cofaigh et al., 2005b; Mosola and Anderson, 2006; Dowdeswell and Fugelli, 2012). GZWs in acoustic profile are characterised by their asymmetric and subdued shape with a steep ice distal end and gentle slope towards the grounding line, internal reflectors representing foreset beds, and acoustically transparent nature (Fig. 2.8) (e.g., Ó Cofaigh et al., 2005b; Dowdeswell and Fugelli, 2012; Batchelor and Dowdeswell, 2015; Dowdeswell et al., 2016; Evans and Hogan, 2016; Arndt et al., 2017b).

Beyond the grounding line but still proximal to the ice margin, deposition takes place by the rain-out of debris from the base of the ice shelf, which is winnowed by currents to remove the fine mud and sand (Fig. 2.6; 2.7) (Powell et al., 1996;

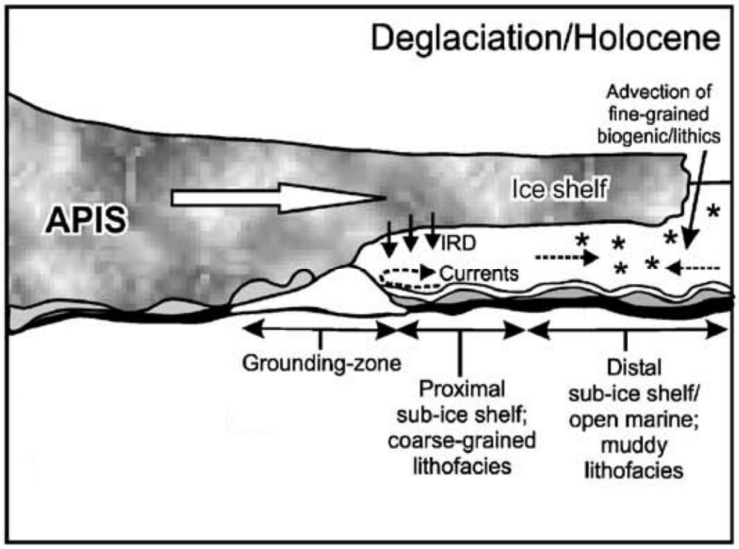

Figure 2.7 Depositional processes and sediment facies in an ice shelf setting during deglaciation. Adapted from Evans et al. (2005).

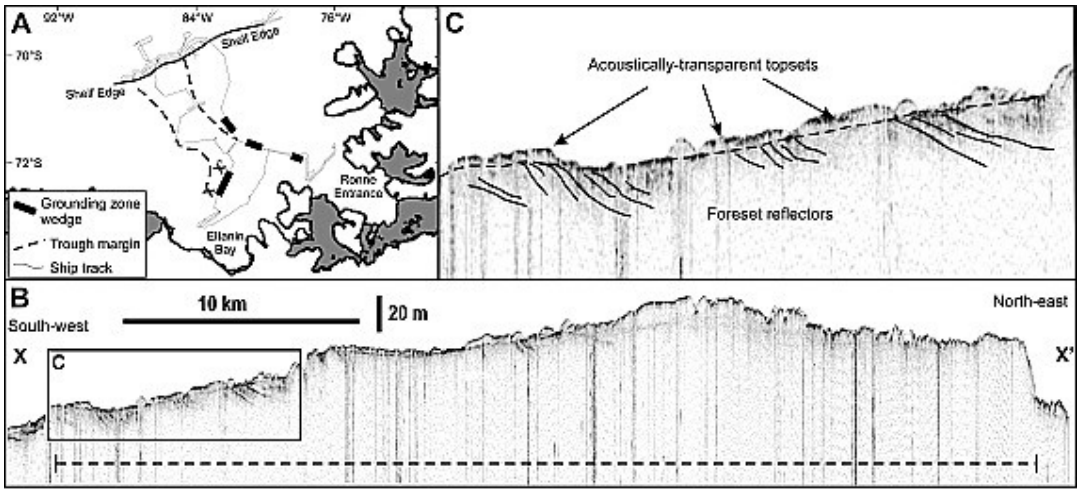

Figure 2.8 A GZW in the Bellinghausen Sea, Antarctica. (A) Location of GZWs within Bellinghausen Sea (B) Acoustic profile showing the asymmetric shape and acoustic transparency of the GZW. Dashed line marks the extent of the GZW (C) Internal reflectors showing the dipping foresets within the GZW. From Ó Cofaigh et al. (2005b).

Domack and Harris, 1998; Domack et al., 1999; Evans and Pudsey, 2002; Evans et al., 2005; Smith et al., 2019). This forms poorly sorted to stratified, sandy to gravelly mud or diamicton facies, often with dispersed dropstones and pelletised till, termed granulated diamicton or pellet-rich mud (Table 2.3) (Powell et al., 1996; Domack et al., 1999; Evans and Pudsey, 2002; Evans et al., 2005; Heroy and Anderson, 2005; Pudsey et al., 2006; Yokohama et al., 2016; Smith et al., 2017; Prothro et al., 2018). Tidal pumping, which involves alternate periods of tidal inflow and outflow of water carrying suspended sediment within the sub-ice shelf cavity, can also deposit sorted silt and sand laminae within this coarse facies (Domack, 1990; Domack et al., 1999; Evans et al., 2005). These ice proximal sub-ice shelf

Table 2.3 Characteristics of sediment deposited by ice shelf related processes from different locations in Antarctica.

Mode of deposition	Sediment characteristics	Location and study
Rain-out from the base of the ice shelf and current winnowing	Coarse grained gravelly sand to gravelly mud, laminated in places. Contains dropstones.	Larsen A and Larsen Inlet (Evans and Pudsey, 2002)
	Muddy diamicton containing pelletised till matrix, dropstone disturbed mud laminations and dispersed clasts.	Northern Larsen continental shelf (Evans et al., 2005)
	Clast rich sandy diamicton with a 'granulated' texture. Granules are composed of silty clay or diamicton.	South central Ross Sea (Domack and Harris, 1998)
	Poorly sorted 'shelfstone' sandy mud.	Mackay Glacier (Powell et al., 1996)
	Muddy gravel and coarse sand unit, displaying stratification, dropstones and till pellets.	Ross Sea (Domack et al., 1999)
	Coarse grained dark grey diamict, gravelly mud, muddy gravel and sandy gravel, overlain by olive brown to brown sandy muds and diamictons.	Northern Larsen Ice Shelf (Pudsey et al., 2006)
	Poorly sorted mud, sand, and gravel.	Ross Sea (Yokohama et al., 2016)
	Stratified to homogenous sandy and gravelly mud.	Pine Island Glacier (Smith et al., 2017)
Suspension settling of winnowed fines or from meltwater plumes	Massive terrigenous silty clay. Occasional coarse debris.	Larsen A and Larsen Inlet (Evans and Pudsey, 2002)
	Poorly sorted massive clay to silty mud. Poorly sorted angular gravel sized clasts present in both units.	Northern Larsen continental shelf (Evans et al., 2005)
	Structureless bioturbated mud.	South central Ross Sea (Domack and Harris, 1998)
	Fine grained silty clay displaying fine laminations of silt, clay and sand at the base, with massive silty clay above. Absence of coarse IRD.	Ross Sea (Domack et al., 1999)
	Structureless silty clay, sparse iceberg rafted sand.	Northern Larsen Ice Shelf (Pudsey et al., 2006)
	Massive to weakly stratified mud.	Marguerite Bay (Kilfeather et al., 2011)
	Light olive-grey homogenous silty clay overlain by olive-grey to brown, bioturbated sandy mud. Two discrete layers of coarser sediment are present within the overall unit.	Larsen B embayment (Jeong et al., 2018)
	Thin mud unit with subtle grain size sorting and minor concentrations of iceberg rafted material.	Ross Sea (Yokohama et al., 2016)
	Well sorted, laminated to homogenous muds. Lack of coarse clasts.	Pine Island Glacier (Smith et al., 2017)
Rainout from icebergs at the calving line	Brown, diatomaceous, clast rich mud.	South central Ross Sea (Domack and Harris, 1998)
	Poorly sorted sand and gravel.	Ross Sea (Domack et al., 1999)
	Massive, grey to olive grey pebbly mud. Some crude bands of pebbles and bands of matrix evident.	Marguerite Bay (Kilfeather et al., 2011)
	Horizon of gravel.	Weddell Sea (Domack et al., 2005)
	Diatomaceous sediment with a variable concentration of iceberg rafted material.	Ross Sea (Yokohama et al., 2016)

sediments can be reworked by mass flows caused by the grounding of ice shelves on sea-floor ridges (Smith et al., 2017). In some cases, deposition from meltwater plumes takes place proximal to the grounding line. For example in Marguerite Bay, Antarctica, a laminated grey mud, indicative of deposition by meltwater derived suspension settling, overlies the subglacial till rather than the granulated facies reported in other locations (Kilfeather et al., 2011).

Distal to the grounding line in sub-ice shelf settings, deposition occurs by suspension settling of fines from plumes of sediment winnowed in the proximal zone, or sediment laden meltwater plumes emerging from the grounding line (Fig. 2.6; 2.7) (Domack and Harris, 1998; Evans et al., 2005; Simkins et al., 2017; Prothro et al., 2018; Smith et al., 2019). Suspension settling forms laminated to weakly stratified to massive mud with small quantities of gravel sized clasts (Table 2.3) (Domack and Harris, 1998; Evans and Pudsey, 2002; Evans et al., 2005; Pudsey et al., 2006; Kilfeather et al., 2011; Yokohama et al., 2016; Smith et al., 2017; 2019; Jeong et al., 2018; Prothro et al., 2018). In some locations, these distal sub-ice shelf muds transition into a facies deposited during the retreat of an ice shelf calving front (Domack and Harris, 1998; Kilfeather et al., 2011; Smith et al., 2019). This facies deposited by the rainout of sediment from calved icebergs can consist of IRD rich, massive to crudely stratified clast rich muds, or alternatively horizons of poorly sorted sand and gravel (Table 2.3) (Domack and Harris, 1998; Domack et al., 1999; 2005; Kilfeather et al., 2011; Yokohama et al., 2016; Smith et al., 2019).

2.3 Microscale sediment characteristics

Micromorphology refers to the microscale analysis of sediment structure and texture, providing detail about sediment which is not visible to the naked eye (Carr, 2004). It has improved understanding of sediment deposition in a range of environments, such as volcanic, fluvial, slope, lacustrine, periglacial, and glacial settings (see references within van der Meer and Menzies, 2011). The use of micromorphology in the study of subglacial and glacimarine sediments, and the microscale characteristics of sediment from these environments, are outlined below.

2.3.1 Micromorphology of subglacially deformed sediment

Micromorphology has been widely employed in the identification and analysis of subglacially deformed sediment (e.g., van der Meer, 1993; 1997; van der Meer et al., 2003; Menzies, 2000; Phillips and Auton, 2000; Hiemstra and Rijsdijk, 2003; Roberts and Hart, 2005; Ó Cofaigh et al., 2005a; Larsen et al., 2006; 2007; Phillips et al., 2007; 2018; Spagnolo et al., 2016). Subglacial sediment is often characterised by microstructures associated with both planar and rotational deformation (e.g., van der Meer, 1993; Carr, 2001). Prominent linear features commonly developed in subglacial sediment include grain lineations, elongate zones of plasma, fractures, and masepic and unistrial plasmic fabrics (van der Meer, 1993; van der Meer and Hiemstra, 1998; Hiemstra, 1991; 2001a; Carr, 2001; Carr et al., 2006; Ó Cofaigh et al., 2005a; 2013a; Narloch et al., 2012). These form when brittle, planar deformation leads to the development of shear planes (Menzies et al., 1997; Fuller and Murray, 2002; Hiemstra and Rijsdijk, 2003; van der Meer et al., 2003; Ó Cofaigh et al., 2005a).

Features associated with rotational subglacial deformation include skeleton grain turbates, skelsepic and lattesepic plasmic fabrics, intraclasts, grain coatings, pressure shadows, folds, boudins, and microstringers (van der Meer and Laban, 1990; van der Meer, 1993; Hiemstra, 1999; Carr, 2001; Hiemstra et al., 2005; Ó Cofaigh et al., 2005a; Roberts and Hart, 2005; Reinardy et al., 2011; Lea and Palmer, 2014; Hodder et al., 2016). Skelsepic plasmic fabrics and skeleton grain turbates share a similar origin, related to the rotation of a single coarse grain or group of grains, which exerts stress on nearby smaller grains or plasma and causes them to become aligned with the surface of the larger grain (van der Meer, 1993; 1997; Hiemstra and Rijsdijk, 2003). Particle rotation during ductile shearing causes stringers and folds to be initiated (Roberts and Hart, 2005),

Micromorphology has been employed to develop more detailed polyphase histories of subglacial materials, which often display structures associated with both planar and rotational deformation (Phillips and Auton, 2000; Phillips et al., 2011). Multiple stages of sediment deformation can be identified by determining the relationship between microstructures, rather than these structures just being indicative of a particular depositional process (Phillips et al., 2011). With this in mind, Phillips et al. (2011) put forward a new ‘microstructural mapping’ methodology for thin section analysis, which involves digitally delineating grain

orientations to identify clast microfabrics across the slide. Domains with similar grain alignments can then be picked out, which correspond to different phases of deformation (Ferguson et al., 2011; Phillips et al., 2011; 2018a; 2018b; Spagnolo et al., 2016; Gehrmann et al., 2017). Determining the relationship between microstructures or groups of microstructures on thin sections (brittle and ductile deformation structures such as folds, shears, microfaults, rotations, grain lineations) allows groups of structures formed during particular stages of deformation to emerge (Phillips and Auton, 2000; van der Wateren et al., 2000; Lee and Phillips, 2008; Phillips et al., 2007; 2018a). Establishing the relationship between the identified microstructures and microfabrics allows a detailed deformation chronology for a single slide to be put together (Phillips et al., 2011; Phillips et al., 2018a; 2018b).

Multiple phases of deformation and microstructure development can be related to spatial and temporal changes in porewater pressure which alter the style of deformation (Menzies, 2000; 2012; Menzies et al., 1997; 2006; 2019; van der Meer et al., 2003; Narloch et al., 2012; 2013; Phillips et al., 2018a). During periods of lower porewater pressure planar deformation structures are formed, whilst elevated porewater pressure results in ductile deformation and rotational structures (Menzies et al., 1997). Spatial variation in the microstructures evident within subglacial tills can also be driven by clay content, with deformation in till with a low clay content dominated by linear shearing which produces lineations, boudinage and a strong microfabric (van der Meer et al., 2003; Hart, 2017). Tills with a higher clay content are dominated by rotational deformation, forming turbates, pressure shadows and weaker microfabrics (van der Meer et al., 2003; Hart, 2017).

2.3.2 Micromorphology of glacimarine sediment

As demonstrated in section 2.2, massive diamictons with similar macroscopic characteristics can be produced by multiple processes, including subglacial till deposition, sub-ice shelf rainout, debris flows, and iceberg rafting and scouring, often existing in close spatial proximity. As a result, most previous investigations of glacimarine micromorphology have focussed on diamictons, with the aim of determining microstructures indicative of particular depositional processes in order to aid genetic distinction both from subglacial tills, and between different glacimarine processes (Hiemstra, 1999; Carr, 2001; Kilfeather et al., 2010; Linch

and Dowdeswell, 2016). The following section will outline current understanding of the microstructures associated with different glacimarine depositional processes.

2.3.2.1 Suspension settling from meltwater plumes and iceberg rainout

Thin sections from ice proximal suspension settling and iceberg rafting deposits in northeast Ireland displayed sub-horizontal to steeply dipping banding of both skeleton grains and plasma, as well as sorted pockets of sediment (Kilfeather et al., 2010). The banding could be attributed to reworking by mass flows or fluctuations in meltwater discharge. Mass flows are common proximal to the grounding line because the high sedimentation rates and iceberg action can lead to sediment remobilisation (Cowan and Powell, 1991; Kilfeather et al., 2010). Alternatively, deposition by successive sediment laden plumes of meltwater could also account for the banded sediments (Mackiewicz et al., 1984; Cowan and Powell,1990; Kilfeather et al., 2010). A particularly distinct feature of these sediments deposited by ice proximal suspension settling and iceberg rafting from northeast Ireland was fine vertical lineations with dropstones at their base (‘dropstone tracks’) (Kilfeather et al., 2010). These were likely formed as a clast moved through the saturated sediment (Kilfeather et al., 2010).

In contrast, sediments deposited by ice distal suspension settling and iceberg rafting lacked evidence of post-depositional reworking. Ice distal suspension settling and either iceberg rafting or sub-ice shelf meltout in Marguerite Bay, Antarctica, produced fine grained and massive to very weakly banded sediment, with infrequent plasma intraclasts and grain lineations (Kilfeather et al., 2010). In Svalbard, sediment deposited by a combination of relatively ice distal suspension settling and iceberg rafting was coarse textured and well sorted, with bedding-parallel grain fabrics (Carr, 2001). Plasmic fabrics and deformation structures were absent (Carr, 2001).

2.3.2.2 Mass flows

Debris flow deposits have been distinguished from other glacimarine diamictons based on skeleton grain coatings, microfabrics, and rotational deformation structures. Thin sections from Greenland, Ireland and Antarctica display clay and fine silt coatings on skeleton grains, suggested to form on the surface of grains whilst they were suspended in a subaqueous environment during debris flows (Hiemstra, 2001a; Kilfeather et al., 2010). Sub-vertical orientation of skeleton

grains, linked to grains sinking through a wet matrix, and soft sediment deformation structures such as flame structures and undulating boundaries between sediments, are also characteristic of debris flow deposits formed in close proximity to the ice margin (Kilfeather et al., 2010). However, steeply dipping skeleton grains cannot be used in isolation as an indicator of debris flows because they can also be indicative of high shear stress (Kilfeather et al., 2010). The presence of solely rotational deformation structures indicative of unconfined deformation, and poorly defined intraclasts which would not be preserved under subglacial shear, provide a good mechanism for distinguishing diamicton deposited by debris flow from subglacial till (Hiemstra, 2001a).

2.3.2.3 Iceberg keel scour

Structures associated with planar shear, sediment mixing, and high porewater pressure characterise sediment that has undergone iceberg scour (Linch and Dowdeswell, 2016). Planar shear is evident in iceberg scoured diamicton from Scoresby Sund based on unistrial plasmic fabrics and skeleton grain lineations (Kilfeather et al., 2010; Linch and Dowdeswell, 2016). These failure planes form as the sediment is displaced horizontally and vertically by extension and compression as an iceberg ploughs through it (Linch et al., 2012; Linch and Dowdeswell, 2016). Type III intraclasts and stringers texturally similar to adjacent bedding, formed during reworking and incorporation of surrounding sediment during scouring, are also common in this diamicton (Kilfeather et al., 2010; Linch and Dowdeswell, 2016). Water escape structures present in iceberg-scoured sediments include bands of realigned clasts and matrix, furrows with sorted clasts and matrix either side of the channel, and matrix ‘water marks’ which have a higher birefringence than surrounding sediment (Linch and Dowdeswell, 2016). Water escape structures form when high pressure develops both beneath the iceberg keel and in the zone of high stress in front of it, and as sediment flows away from the keel in response to both scouring and gravity (Linch et al., 2012; Linch and Dowdeswell, 2016).

Although some of these micro-structures can also occur in deposits formed by other glacimarine processes, the combination of planar structures, sediment mixing, and porewater structures described above is best explained by keel scouring (Kilfeather et al., 2010; Linch and Dowdeswell, 2016). Furthermore, studies of iceberg-scoured glacilacustrine sediment display very similar

microstructural assemblages, providing further evidence that these features in association are evidence of keel scouring (Linch et al., 2012; Linch and van der Meer, 2015). Subglacial and mass wasting deposits usually display a much wider range of microstructures, for example multiple types of plasmic fabrics, more frequent rotational structures, and a wider range of porewater and sediment mixing structures (Table 2.4) (Linch and Dowdeswell, 2016).

Table 2.4 Microstructures associated with different subglacial and glacimarine depositional environments. The table highlights the more limited assemblage of structures found in iceberg scoured sediments, which is key to their identification. C = Clay, Dm = Diamicton. From Linch and Dowdeswell (2016).

Microstructure	Subglacial	Mass-wasting	Iceberg scour (C)	Iceberg scour (Dm)
ROTATION/DUCTILE				
Strain caps and shadows	Rare	Rare		
Grain turbates/rotation structures	●●●	●●		●
Clast haloes	●	●	?	?
Scavenging turbates	●●●	●●		
Symmetric pressure shadows	Rare	●		
Asymmetric pressure shadows	●	●		
Folds	●	●	●●●	●●
Sheath folds	●	●	●●	●
Comet structures	●	●		
Layering and foliation	●●●	●●●		
Tiled units	Rare	●●●		
Necking structures	●	●		
Secondary foliation	Rare	●		
Crenulation foliation	●	●		
Realigned bedding	●●	●	●●●	●●●
PLANAR/BRITTLE				
Augen-shapes	●	●	●	●
Normal faults	●	●	●●●	●
Reverse/Thrust faults	●	●	●●	
Discrete shears	●●●	●●●	●	●●●
Grain lineations	●●●	●●●		●
Grain stacks/bridges	●	●		
Kinkbands	●	Rare		
ABRASION				
Crushed quartz grains	●●	Rare		
Grain concentrations	●●●	●●		
Partially destroyed clasts	Rare	Rare	●●	
SEDIMENT MIXING				
Intraclasts I (void)	●	●		
Intraclasts II (plasmic fabric)	Rare	Rare		
Intraclasts III (sediment)	●●	●	●	●●●
Multiple domains	●	●	●●●	●●●
POREWATER				
Water escape	●	●	●●	●
Flow	Rare	●	●●	
Cutans (argillans)	●	Rare		
Sill and dyke	●	●		
Silt or clay coatings	●	●		
Silt or clay cappings	●	●		
Polygonal structures	●	Rare		
PLASMIC FABRIC				
Skelsepic	●●●	●●	?	●
Lattisepic	●	●		
Masepic (varieties)	●●●	●		
Omnisepic	●●	●		
Insepic	●●●	●		
Vosepic	Rare	Rare		
Unistrial	●	●	●●●	●●●
Kinking	●	Rare		
Bedding-parallel	Rare	●	?	?
Banded plasma	●	●		●

ADDITIONAL				
Dropstones	Rare	Rare	●●●	●●●
Structural sequences	Rare	Rare	●	
Sub-horizontal microfabric(s)	●●●	●	●●	●●

3. Methodology

3.1 Materials

The investigation will use geophysical data and sediment cores which were collected on the PS100 and PS109 cruises of the RV Polarstern to the northeast Greenland continental shelf, which took place in 2016 and 2017 respectively. Data was principally collected from Norske and Westwind troughs during these cruises. Five of the cores that were obtained have been selected for use in this investigation; PS100-173 and PS100-175 from mid Norske Trough, PS100-208 from inner Norske Trough, and PS109-22 and PS109-25 from outer Westwind Trough. The location at which they were collected, and the length of each core, are shown in Table 3.1 and Figure 1.3. These particular cores were selected because they span both Norske and Westwind troughs, as well as outer, mid and inner trough positions. This enables the glacigenic depositional processes associated with the NEGIS to be established from the outer shelf through to the inner shelf, and therefore any spatial and temporal changes in deposition style to be determined. All five cores were recovered using a gravity corer, and were subsequently divided into sections up to 1 m in length and split in half. They were logged, described, and tested for shear strength at ~10 cm intervals upon collection.

Table 3.1 Locational details of the five cores used in this study.

Core	Latitude (N)	Longitude (W)	Region	Water depth (m)	Core recovery (cm)
PS100-173	78˚ 0.556’	16˚ 10.236’	Mid Norske Trough	505	366
PS100-175	77˚ 44.264’	15˚ 20.141’	Mid Norske Trough	375	158
PS100-208	79˚ 20.613’	18˚ 33.202’	Inner Norske Trough	304	935
PS109-22	80˚ 11.018’	07˚ 26.587’	Outer Westwind Trough	329	265
PS109-25	80˚ 14.371’	05˚ 55.803’	Outer Westwind Trough	397	268

Sub-bottom profiles were also collected on the PS100 and PS109 cruises by a hull-mounted Parasound DS III-P70 system, operating at a pulse mode of 4-20 kHz and a pulse length of 0.5 ms. These Parasound sub-bottom profiles show the acoustic stratigraphy of the sub-seafloor. The sub-bottom profiles from the regions around the site of the five cores have been used in this study.

3.2 Methods

Detailed description of the characteristics of glacigenic sediments and landforms facilitates in depth interpretations about the processes by which they were formed (Evans and Benn, 2004). Therefore, to obtain information about the properties of the sediment-landform assemblage in Norske and Westwind troughs, descriptions of acoustic stratigraphy and core sedimentology (at both macro- and micro-scale), as well as multi-sensor core logger (MSCL) analysis were employed.

3.2.1 Acoustic stratigraphy

Descriptions of the acoustic characteristics of submarine sediment have been widely used to make genetic interpretations (e.g., Dowdeswell et al., 2010; Hogan et al., 2012). The acoustic characteristics of the sediment units around each core site were described to include the nature of their upper and basal reflector, their internal characteristics, and their stratigraphic relationship with surrounding units. The acoustic sequence at each core site was split into acoustic facies (AFs). Screenshots of the Parasound data from each core site were annotated in CorelDRAW to aid description and facies recognition. AFs which occurred in multiple areas were identified to allow the compilation of an overall set of 12 AFs present across all the core sites.

3.2.2 Core sedimentology

In order to gain further detail about sediment characteristics, sediment cores from some of the identified AFs were analysed (e.g., Callard et al., 2018; Streuff et al., 2017; 2018).

3.2.2.1 Macro-scale sedimentology

In order to determine the macro-scale characteristics of the sediment in each core, x-radiograph images were described in detail to include grain size, sorting, depositional structures, deformation structures, clast content, and contacts between sediment units. These descriptions were used alongside the ship-based logs and descriptions to identify a set of lithofacies (LFs) present in each core, and to determine the sedimentological properties of each of these lithofacies. Vertical profile logs of each core were also created using these lithofacies descriptions.

3.2.2.2 Micro-scale sedimentology

Micromorphology was used to supply greater detail about the characteristics of some lithofacies because it can elucidate further information about sediment

structure not visible to the naked eye (e.g., Ó Cofaigh et al., 2005a). Micromorphological analysis was undertaken using thin sections.

Thin section preparation

Six sections (6-8 cm in length) from four of the sediment cores (PS100-173, PS100-175, PS109-22 and PS109-25) were selected for thin section preparation. These were chosen by preliminary examination of the cores to pick out sediment units from which greater detail might aid their genetic interpretation. Thin section location within a lithofacies was chosen by examining the unit for sedimentary structures such as dropstone structures or bedding, or else randomly. Table 3.2 shows the location of the thin sections within the core from which they were taken. The previously halved core sections were split again to create core quarters, and blocks of sediment ~1 cm in thickness were removed from these quartered core sections to make thin sections. All six samples had a diamictic texture. As a result, their brittle nature and the frequent small clasts meant that blocks were not able to be removed by slicing. Instead, material was gradually removed around the edges of the ~1 cm block, working towards the centre of the sample until sufficient material was removed to allow a block of sediment to be prised away from the core section.

Table 3.2 Thin section names and their location within their respective cores.

Thin section name	Core	Depth in core (cm)	Lithofacies
PS100-173a	PS100-173	340-346	LF1-173
PS100-173b	PS100-173	232-240	LF2-173
PS100-175a	PS100-175	142-150	LF1-175
PS109-22a	PS109-22	120-128	LF1-22
PS109-25a	PS109-25	209-215	LF2-25
PS109-25b	PS109-25	81-88	LF3-25

Thin sections were prepared from these sediment blocks at Durham University, following the process outlined by Lee and Kemp (1992), Carr and Lee (1998), Menzies (2000), and Menzies and van der Meer (2018). The samples were firstly air dried, then impregnated with resin. Impregnation of these diamictons was challenging because of their high consolidation, lack of pore networks, and low permeability, which made it difficult for resin to spread through the sample (Carr and Lee, 1998). Following their full impregnation, the samples were mounted on glass slides and the excess sediment was removed. They were then ground and polished to a ~30 μm thickness and a cover slip was added ready for their analysis.

Thin section analysis

The following process was devised for the systematic examination of each thin section. The thin sections were scanned using a high resolution flatbed scanner, and these images were opened in a graphics package (CorelDRAW). Thin sections were examined under both a Meiji and a Leica microscope using magnifications between 1x to 10x. Using the micromorphological terminology of van der Meer (1993; 1997), Menzies (2000), and Carr (2004), sediment texture, colour, grain size, depositional structures (e.g., bedding, dropstone structures), and deformational microstructures were identified and described under plane light. Table 3.3 shows a glossary of micromorphological terminology employed in this study. Microstructures were photographed, and the location of each structure was also marked on the thin section scans in CorelDRAW to create thin section 'maps'. Examination of the slides under cross-polarised light allowed the plasma, which refers to the particles <30 μm in size, to be studied in greater detail. Plasmic fabrics, which describe the arrangement of plasma in thin sections and their relationship with skeleton grains, were identified. Their type, distribution and orientation were described and marked on the thin section 'maps'. The types of plasmic fabric that were identified in this study are defined in Table 3.3 (Brewer, 1976; Zaniewski, 2001; Menzies and van der Meer, 2018).

Table 3.3 Glossary of micromorphological terminology used in this study. Terminology is from Brewer (1976), van der Meer (1993; 1997), Menzies (2000), Zaniewski (2001) and Carr (2004).

Terminology	Definition
Skeleton grains	Grains coarser than ~30 μm (greater than the thickness of a thin section)
Plasma	Grains finer than ~30 μm. Individual grains are not visible under a microscope.
Skeleton grain turbate	A circular arrangement of grains around a larger grain (corestone), with the long axes of the smaller grains aligned with the surface of the larger grain. Sometimes circular grain arrangements lack a corestone.
Skeleton grain lineation	Skeleton grains with their long axes arranged into a line.
Intraclast	A distinct sediment pocket of different texture within the sediment body.
Grain coating	Plasma and small skeleton grains plastered in a layer around a single skeleton grain.
Plasmic fabric	The arrangement of the plasma in thin sections, best visible under cross-polarised light.
Unistrial plasmic fabric	Plasma arranged in thin, discrete and continuous lines in a single direction (appearance of discrete shears).
Masepic plasmic fabric	Plasma arranged in broader parallel bands in one direction.
Bimasepic plasmic fabric	Plasma arranged in broader bands in two directions.
Skelsepic plasmic fabric	Plasma arranged parallel to the surface of a skeleton grain.
Lattesepic plasmic fabric	Plasma arranged in two sets approximately perpendicular to eachother, resulting in a lattice-like appearance.

3.2.3 Multi-sensor core logger (MSCL) analysis

The five sediment cores underwent MSCL analysis using a GEOTEK logger at Durham University to measure their properties. Bulk density, p-wave velocity, and magnetic susceptibility collected by the MSCL analysis were plotted in C2 for use in this investigation. The cores were also photographed, and x-radiograph images of the cores were collected.

4. Results

In this chapter the acoustic stratigraphy at each core site, followed by the macro- and micro-scale sedimentology of each core, will be presented in turn. Twelve different acoustic facies (AF1-AF12) have been identified across the five sites (Table 4.1), some of which are present at multiple sites and others that are specific to one location. Acoustic data has been presented by firstly describing the acoustic facies peripheral to the core site, then describing the facies present at the core site. Some acoustic profiles were collected along a transect transverse to the cross shelf troughs, and others were collected along the long-axis of the troughs. Individual lithofacies identified in each core are described, and this is supplemented by descriptions of thin sections taken from selected lithofacies. Annotated acoustic profiles are shown in Figure 4.1, core logs and physical properties are displayed in Figure 4.2, x-radiograph images of cores are exhibited in Figure 4.3, and photographs of selected microstructures are shown in Figures 4.4-4.15. A summary of the microstructures associated with each lithofacies is shown in Figure 4.16. These descriptions will be followed by interpretation of depositional origin of each acoustic facies and lithofacies in Chapter 5.

4.1 Mid Norske Trough: PS100-173

4.1.1 Acoustic facies

Six out of the twelve acoustic facies, AF2, AF3, AF4, AF5, AF6 and AF10, are present surrounding the PS100-173 core site (Fig. 4.1b; Table 4.1). The acoustic profile in Figure 4.1b was acquired on a transect along the long-axis of Norske Trough (Fig. 4.1a). Over the majority of the area around PS100-173, only AF3 and AF6 are present (Fig. 4.1b). AF2 is present discontinuously along the profile, and is acoustically transparent with a strong upper reflector and no basal reflector. AF3 overlies AF2, and is a structureless and acoustically transparent to semi-transparent sediment unit with a strong upper reflector. AF3 displays a basal reflector where it is underlain by AF2, whilst where AF2 is absent it lacks a basal reflector. Its upper surface is slightly hummocky, and it contains occasional buried dome shaped mounds which lack lower reflectors. These buried mounds have a width of 170-210 m, and range in height from 7-11 m. In places AF3 is overlain by dome-shaped semi-transparent sediment accumulations with flat bases which comprise AF4. These domes range in width from 200 m to 750 m, and in height

Table 4.1 Characteristics and interpretation of the acoustic facies and lithofacies identified in Norske and Westwind troughs. The acoustic facies from which each lithofacies was recovered is shown.

Acoustic facies (AFs)	Description	Core sites at which these AFs occur	Interpretation	Lithofacies (LFs) recovered from each AF	Depositional origin of each LF
AF1	Acoustically impenetrable and continuous surface reflector.	PS100-208	Bedrock	-	-
AF2	Acoustically transparent to semi-transparent structureless unit with a strong upper reflector and no basal reflector. Occurs discontinuously.	PS100-173 PS100-175 PS109-22 PS109-25	Stiff till	-	-
AF3	Structureless acoustically transparent to semi-transparent unit which overlies AF2. Its upper surface is usually hummocky.	PS100-173 PS100-175	Soft till	-	-
AF4	Dome-shaped sediment mounds with strong upper and lower reflectors.	PS100-173	Drumlins	-	-
AF5	Very localised acoustically transparent/semi-transparent unit infilling small depressions on the surface of AF4 and AF3.	PS100-173	Glacimarine infill	LF1-173	Iceberg rafting and suspension settling
				LF2-173	Subglacial deformation, iceberg-rafting, and some suspension settling
AF6	Conformable, semi-transparent unit with a strong upper reflector overlying AF3/AF4/AF5. Can be discontinuous.	PS100-173 PS100-175	Glacimarine drape	LF3-173	Suspension settling
				LF4-173	Iceberg rafting and suspension settling
				LF1-175	Iceberg rafting with some suspension settling
				LF2-175	Suspension settling
AF7	Weakly acoustically stratified to structureless unit.	PS100-208	Suspension settling deposit.	-	-
AF8	Acoustically stratified unit alternating between opaque and acoustically transparent sediment. It drapes highs and infills depressions.	PS100-208	Alternating suspension settling and debris flows deposits.	-	-

Table 4.1 *Continued*

Acoustic facies (AFs)	Description	Core sites at which these AFs occur	Interpretation	Lithofacies (LFs) recovered from each AF	Depositional origin of each LF
AF9	Acoustically stratified sediment which infills depressions. Stratification ranges from very weak to well developed and undisturbed.	PS100-208	Suspension settling and/or turbidity current deposit.	LF1-208	Suspension settling with some deposition by iceberg rafting and turbidity current activity.
				LF2-208	Suspension settling with some deposition by iceberg rafting.
				LF3-208	Suspension settling and iceberg rafting
				LF4-208	Suspension settling
AF10	Acoustically transparent lenticular sediment bodies.	PS100-173 PS100-208	Small debris flow deposits.	-	-
AF11	Wedge shaped acoustically transparent unit with a strong upper reflector.	PS100-208	Large debris flow deposits.	-	-
AF12	Acoustically semi-transparent and structureless sediment unit with a discontinuous basal reflector, arranged in wedges which taper seaward. Contains some seaward dipping internal reflectors.	PS109-22 PS109-25	Sediment wedges comprised of subglacially derived debris flow deposits.	LF1-22	Iceberg rafting with some suspension settling. Some small scale grain remobilisation.
				LF2-22	Suspension settling
				LF1-25	Iceberg rafting with some suspension settling
				LF2-25	Iceberg rafting with some suspension settling. Reworking by glacitectonism or small scale remobilisation
				LF3-25	Debris flow activity

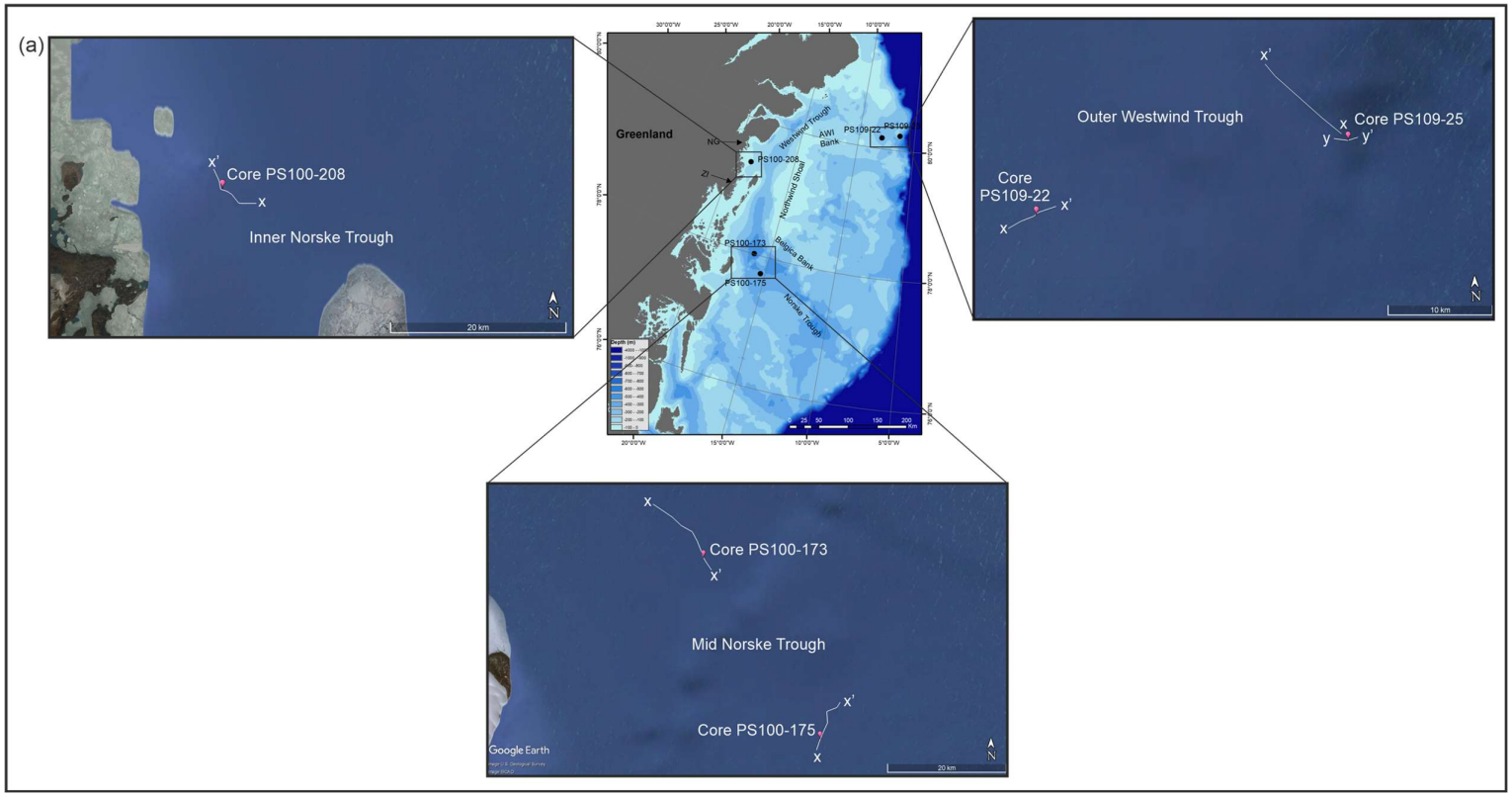

Figure 4.1 Acoustic profiles of each core site. (a) shows the ship tracklines which the acoustic profiles were collected along. The tracks correspond to the position of x/y and x'/y' marked on the acoustic profiles b-f. Images from Google Earth, US Geological Survey and IBCAO. (b-f) Parasound sub-bottom profiles of the area around each core site with acoustic facies labelled. Enlargements of the acoustic stratigraphy immediately surrounding each core site are shown, accompanied by an interpretative cartoon showing acoustic facies distribution. Core recovery locations are shown. The length of each section of Parasound screenshot has been shown instead of a horizontal scale bar because the scale of these images changes laterally. Mid Norske Trough: (b) PS100-173, (c) PS100-175. Inner Norske Trough: (d) PS100-208. Note the difference in horizontal scale of (d) with the acoustic profiles from mid Norske and outer Westwind. Outer Westwind Trough: (e) PS109-22. In (e(iii)) the dipping internal reflectors are indicated by red arrows. (f) PS109-25. Note that (f(i)) does not cover the PS109-25 core site, but the area immediately adjacent to the core site. The core site is only shown in (f(ii)), which was taken on a different track.

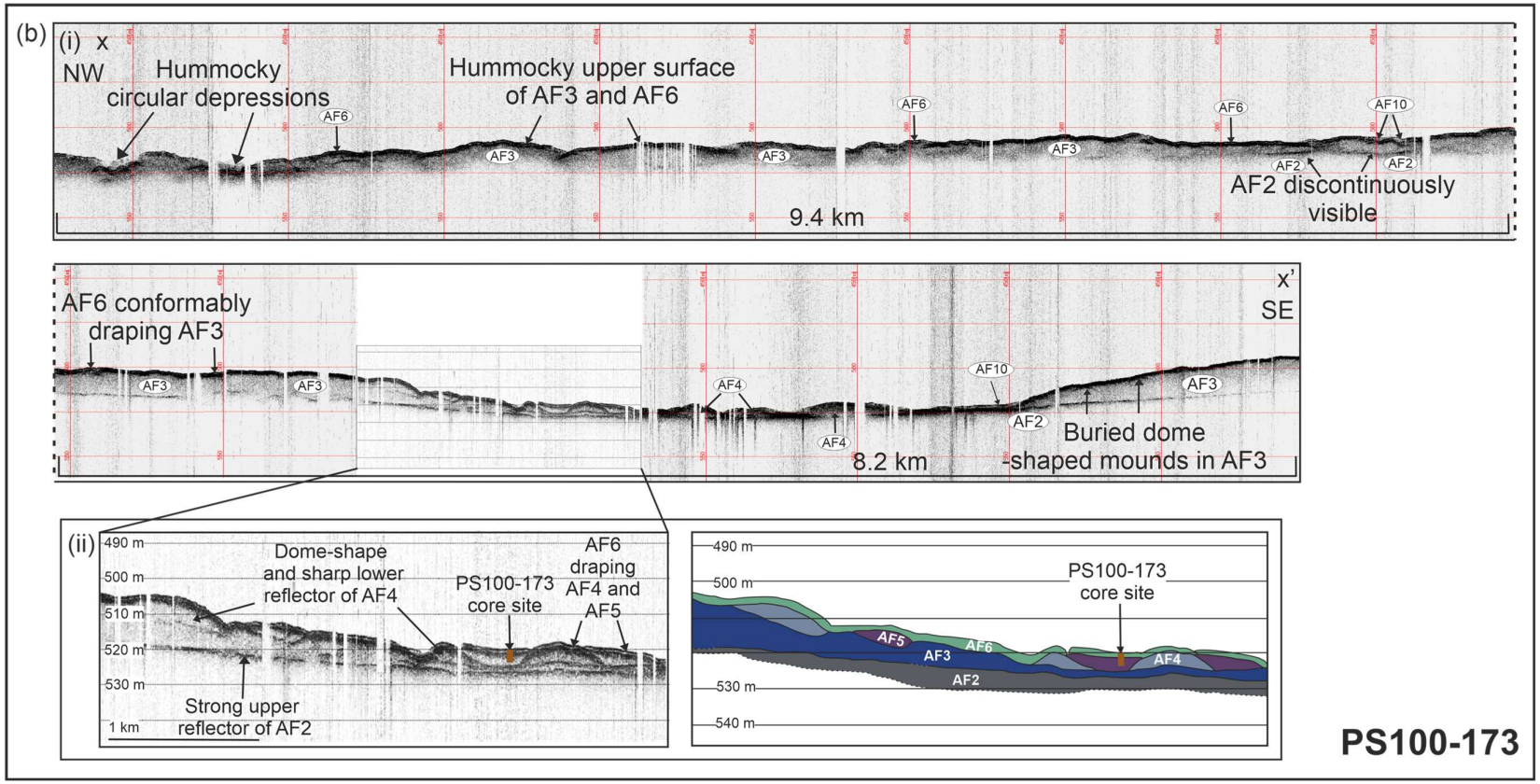

Figure 4.1 *Continued*

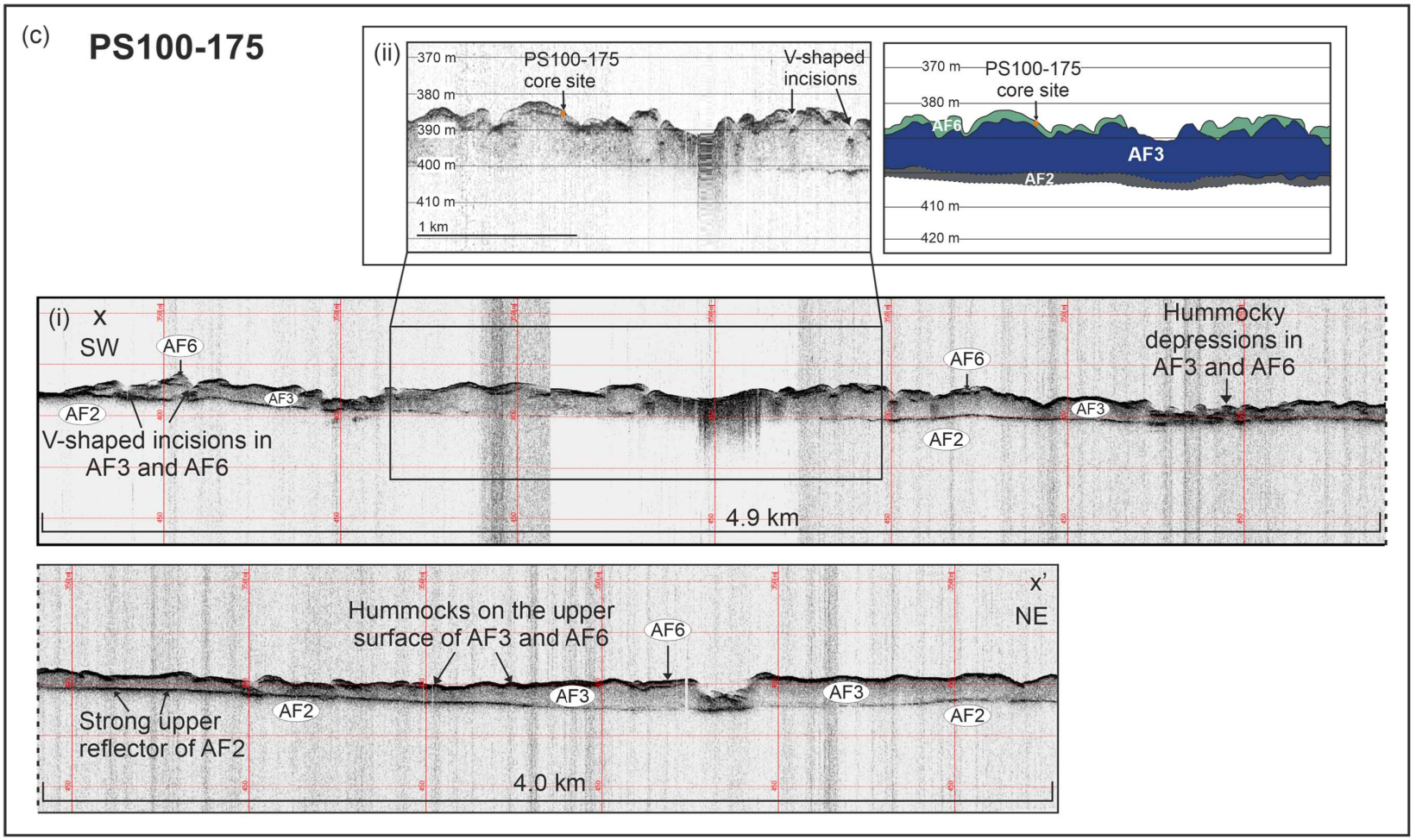

Figure 4.1 *Continued*

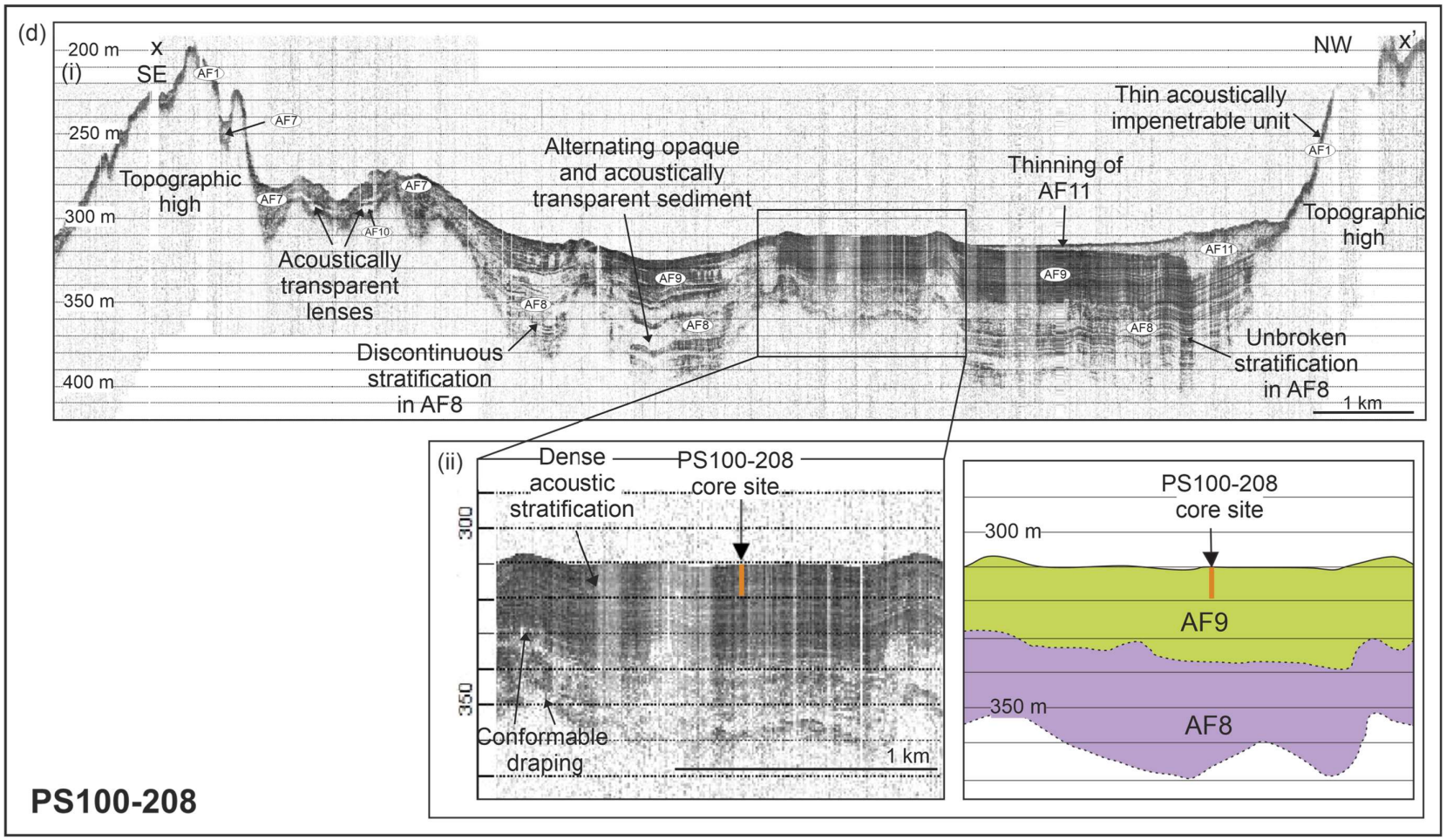

Figure 4.1 *Continued*

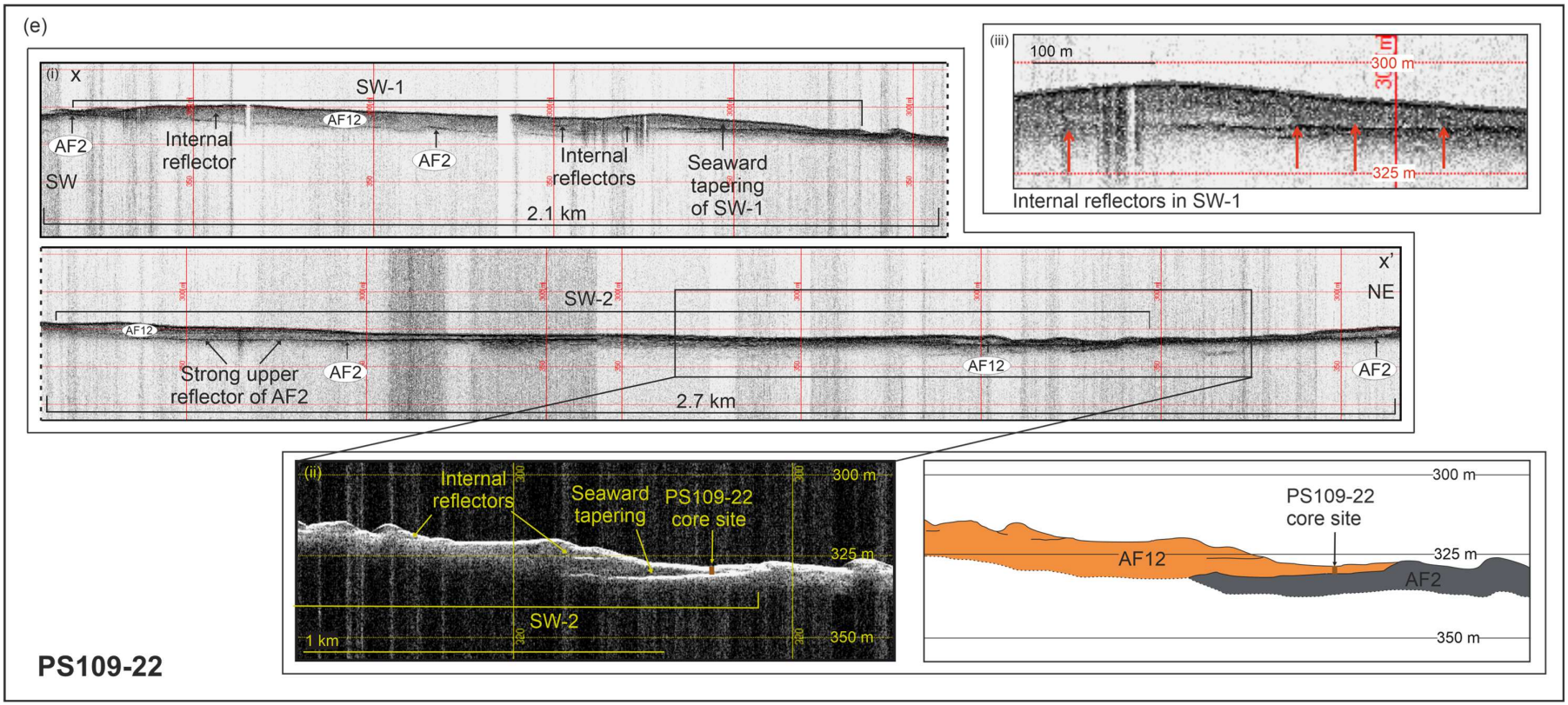

Figure 4.1 *Continued*

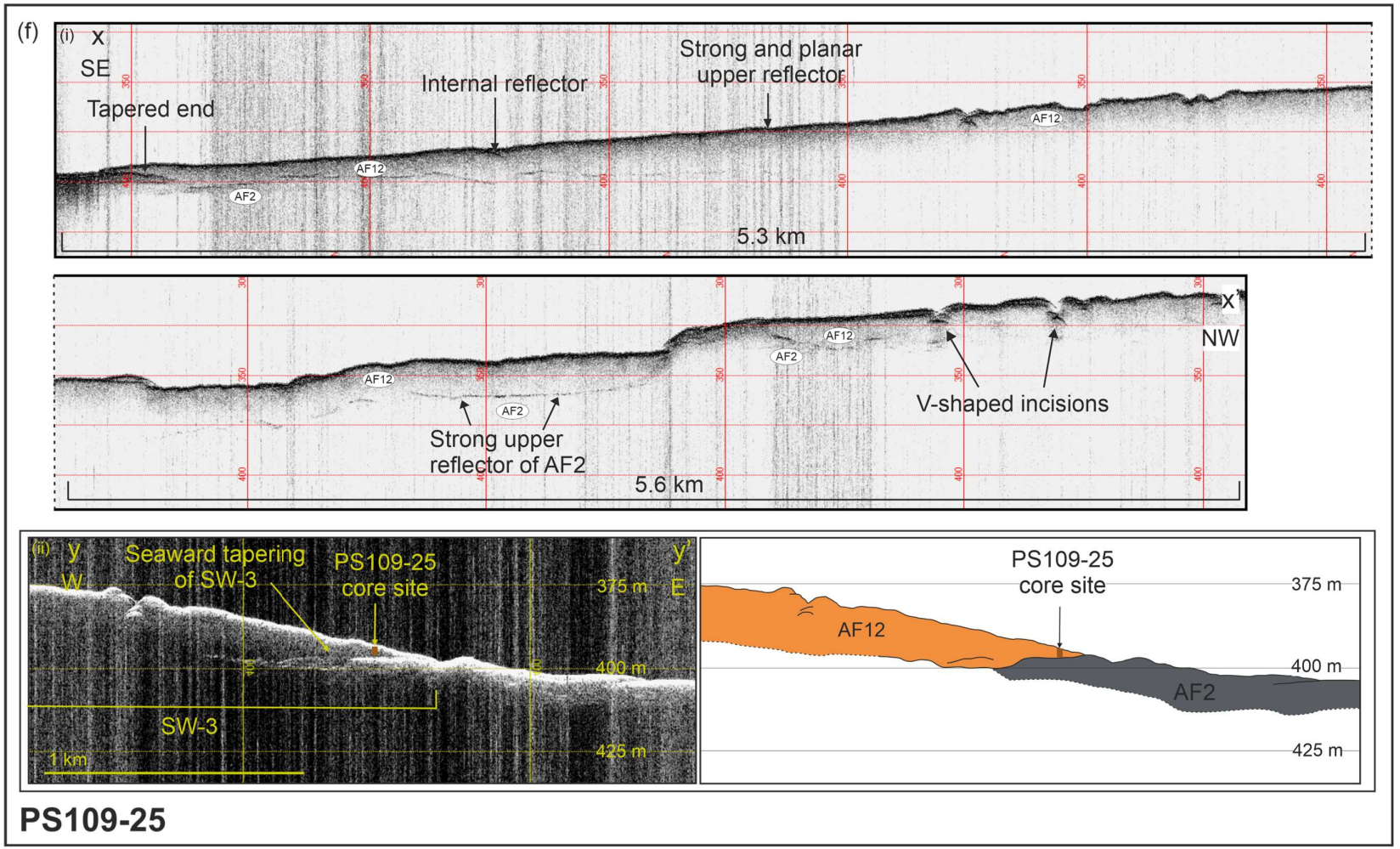

Figure 4.1 *Continued*

from 3.2 m to 4.7 m. AF4 has strong upper and lower reflectors. AF5 is very localised, and infills depressions on the surface of AF3, or the depressions between the dome-shaped mounds of AF4. AF5 is acoustically semi-transparent to transparent and has a strong upper reflector. AF6 is a semi-transparent conformable drape present on the surface of AF3, AF4 and AF5. It has a strong and continuous upper reflector, and its upper surface is hummocky. AF10 is a very localised acoustically transparent unit with a lenticular geometry on the surface of AF6. These lenticular sediment bodies are 90-100 m in width. In places the upper surface of AF3 and AF6 are locally disturbed by circular depressions which are hummocky at their bases. The width of these depressions is between 260-330 m, and their depth is 3.5-6.5 m.

AF2, AF3, AF4, AF5 and AF6 are present around the PS100-173 core site (Fig. 4.1b(ii)). AF2 and AF3 are present at the base of the sequence, overlain by AF5 which infills a depression between two dome shaped mounds of AF4. AF6 is draped over the surface of AF4 and AF5. The PS100-173 core was recovered from AF5 and AF6 (Fig. 4.1b; Table 4.1).

4.1.2 Core lithology

PS100-173 contains four lithofacies (Fig. 4.2a; 4.3a). Lithofacies 1 (LF1-173) (294-367 cm) is a dark greyish brown (5 YR 3/2) massive to crudely stratified, matrix-supported diamicton, which grades upward into a crudely stratified pink/red clay (5 YR 4/3) from 324 cm. Shear strength is 13-18 kPa (Fig. 4.2a). Magnetic susceptibility displays variability (8-733 $x10^{-5}$ SI), and bulk density is 2.06-2.61 g/cc. P-Wave velocity is 59-2743 m/s. Clasts are angular to sub-rounded and up to pebble sized (up to 20 mm a-axes), and clast frequency decreases upward through the unit. From 302-316 cm, stratification within the clay is imparted by inclined and discontinuous grey stringer-like structures (8-20 mm thick), which are diffuse to very diffuse (Fig. 4.3a). These stringers display inclined and recumbent fold structures, and are composed of silty clay with sand grains. LF1-173 has a sharp contact with the unit above.

Lithofacies 2 (LF2-173) (136.5-294 cm) is a massive to crudely stratified, matrix-supported brown diamicton (5 YR 4/2-5 YR 3/2). It has a shear strength of 5-18.8 kPa (Fig. 4.2a). Magnetic susceptibility is variable (12-724 $x10^{-5}$ SI), and bulk density is 0.62-2.9 g/cc. P-wave velocity is 57-3067 m/s. Clasts are angular to rounded, and are predominantly small pebble sized (up to 15 mm a-axes), with

occasional larger pebbles (up to 55 mm a-axes). The lower 27 cm and upper 14 cm of the facies are stratified by crude banding in the matrix of the diamicton.

Lithofacies 3 (LF3-173) (84.5-136.5 cm) is a laminated clay (5 YR 4/3) (Fig. 4.2a). Shear strength is 1-7 kPa. Magnetic susceptibility is generally low but peaks at 90 cm (MS = 73-948 x10 SI), and bulk density is 1.63-2.65 g/cc. P-Wave velocity is 1480-3773 m/s. Laminae are horizontal and undisturbed, aside from the presence of a normal fault (Fig. 4.3a). The transition from LF2-173 below is gradual, with diamicton interbedded within laminated clay comprising the lower 11 cm of LF3-173. These beds of diamicton have sharp contacts with the laminated clay.

Above the interbedded contact, LF3-173 can be divided into three different sections (Fig. 4.3a). In the lower part of the unit (LF3a-173:109-119 cm), there are repeated pairs of laminae which appear dark and light on the x-radiograph image, with the darker laminae representing clay with a slight silt component and the lighter laminae representing clay. There is a sharp contact between each individual pair of laminae. Individual pairs of laminae vary in thickness from 2.5 mm to 10 mm. The coarser lamina is generally thicker than the finer within each pair. Small clasts up to 4 mm a-axes are present within the coarser laminae between 109-117 cm. In the mid-section of lithofacies 3 (LF3b-173: 106.8-109 cm), the finer laminae become thicker than the coarser laminae. The fine laminae are 2-7 mm in thickness, and the coarser laminae are 1-2 mm. The sharp contacts between each individual laminae remain. In the upper part of lithofacies 3 (LF3c-173: 84.5-106.8 cm), laminae are more diffuse and become increasingly diffuse upwards (Fig. 4.3a). The lighter laminae are thicker and increase in thickness upwards, displaying a maximum thickness of 20 mm. The darker lamina have a maximum thickness of 3 mm. Clasts up to 8 mm a-axes appear from 92 cm to the top of the unit.

Lithofacies 4 (LF4-173) (0-84.5 cm) is a massive, matrix-supported brown diamicton (5 YR 4/2), which grades upwards into a brown clay (5 YR 4/2), then into an olive brown clay (10 YR 4/2) (Fig. 4.2a; 4.3a). Shear strength is 4-6.4 kPa. Magnetic susceptibility is uniformly low (0-139 $x10^{-5}$ SI) and bulk density is 0.70-2.68 g/cc. P-Wave velocity is 62-1925 m/s. The lower 6.5cm of the diamicton is interbedded with multiple diffuse, 2 mm thick clay laminae (Fig. 4.3a). Between 65-

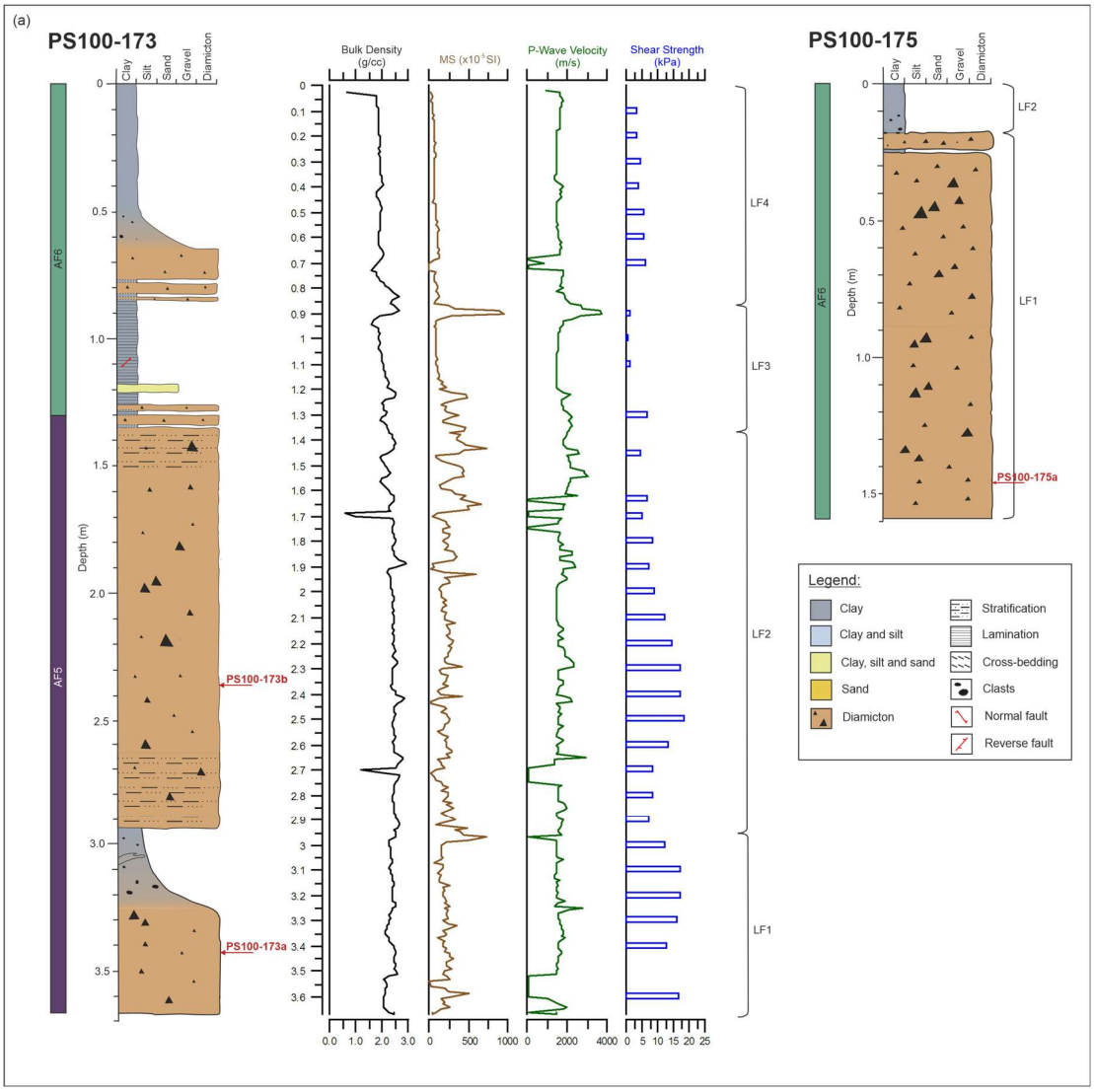

Figure 4.2 Sediment logs and physical properties (including bulk density, magnetic susceptibility, p-wave velocity and shear strength) of the cores from (a) mid Norske Trough, (b) inner Norske Trough, and (c) outer Westwind Trough. Some or all of the physical properties data is missing for certain cores. The acoustic facies from which each core was recovered are shown. The locations of the six thin section samples are also displayed against the core logs.

84.5 cm, the diamicton becomes increasingly less gritty. From 65 cm upward, the diamicton gradually fines upward into massive clay. Clast frequency gradually decreases upwards through LF4-173, with clasts becoming infrequent from 64cm and absent from the 32 cm to the top of the unit. Within the lower diamictic part of LF4-173, clasts are up to 22 mm in a-axes length. Clasts within the clay are smaller, with a-axes up to 10 mm in length.

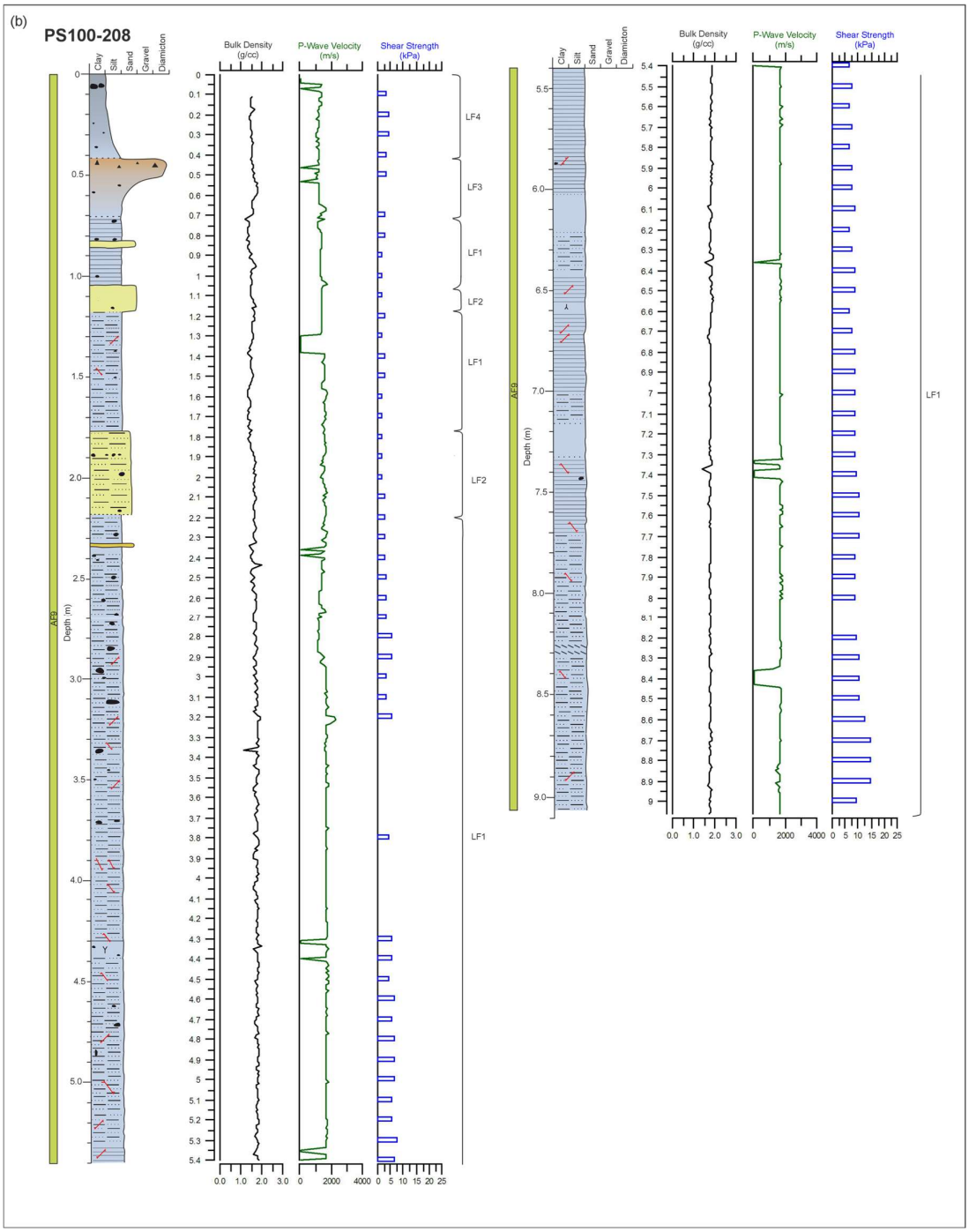

Figure 4.2 *Continued*

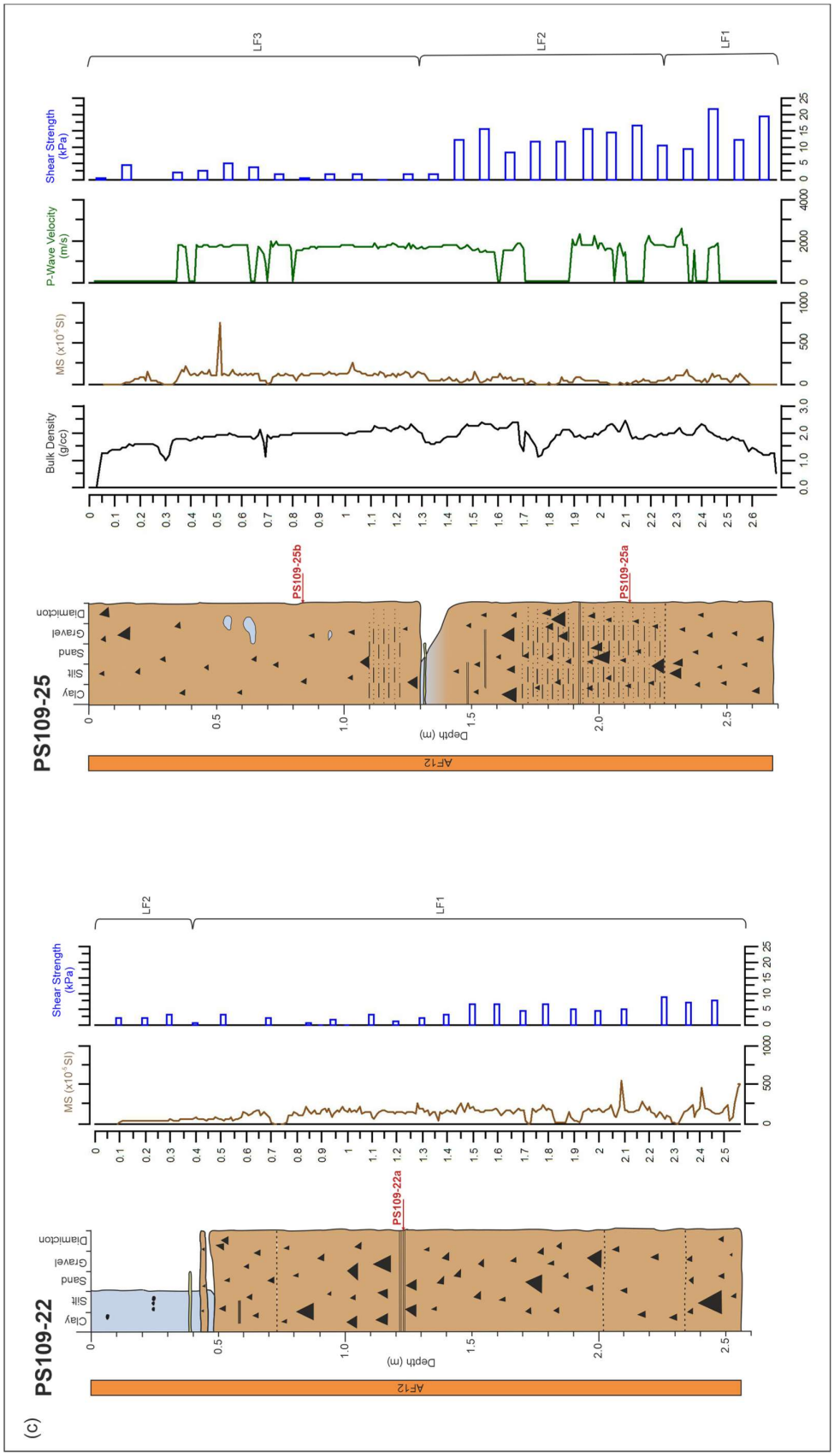

Figure 4.2 *Continued*

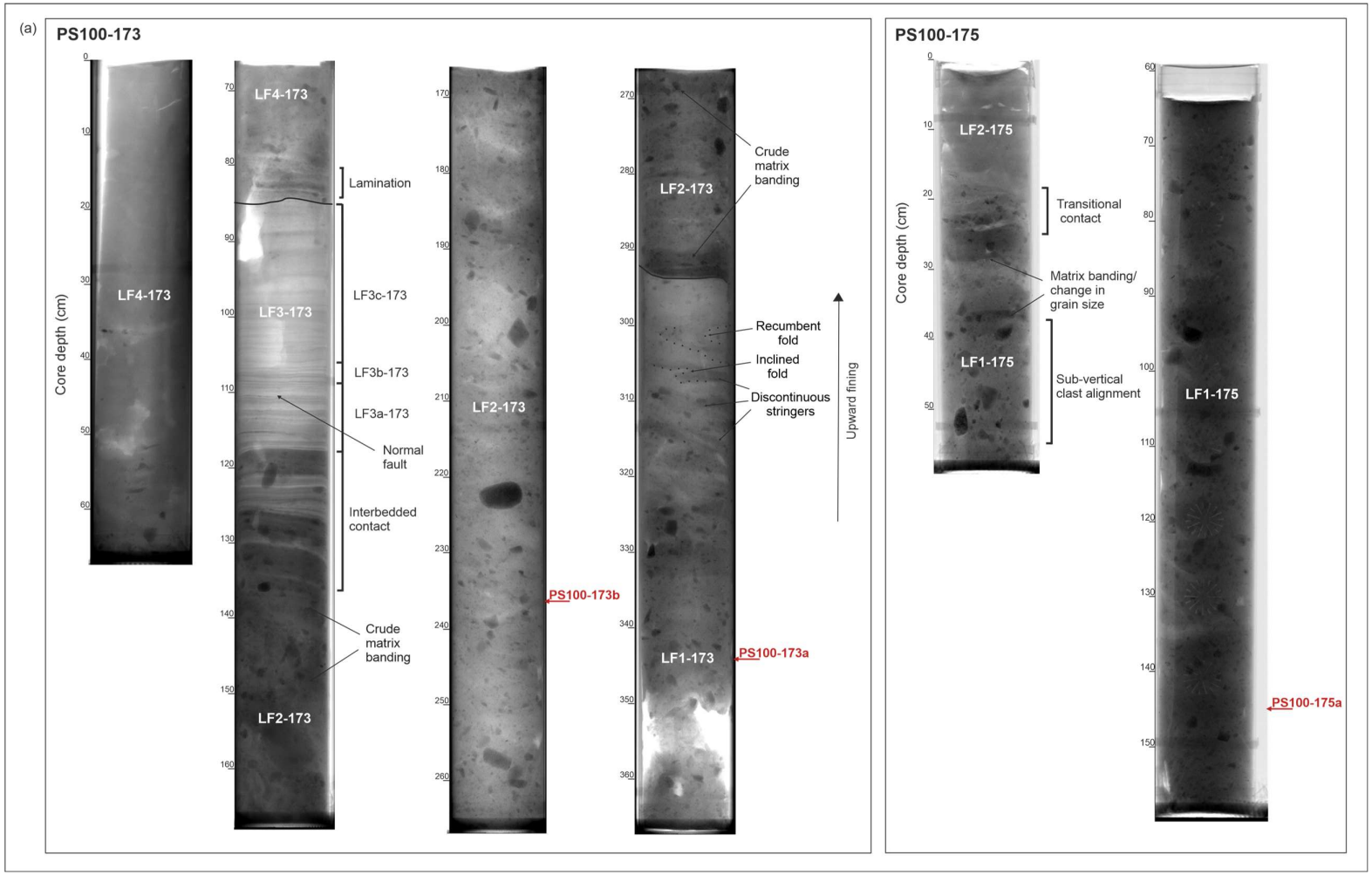

Figure 4.3 Annotated x-radiograph images of the five cores used in this study. The lithofacies in each core are labelled, and thin section locations are shown in red. (a) mid Norske Trough (b) inner Norske Trough. Due to its length, sections of the PS100-208 x-radiographs are shown rather than the entire core. (c) outer Westwind Trough.

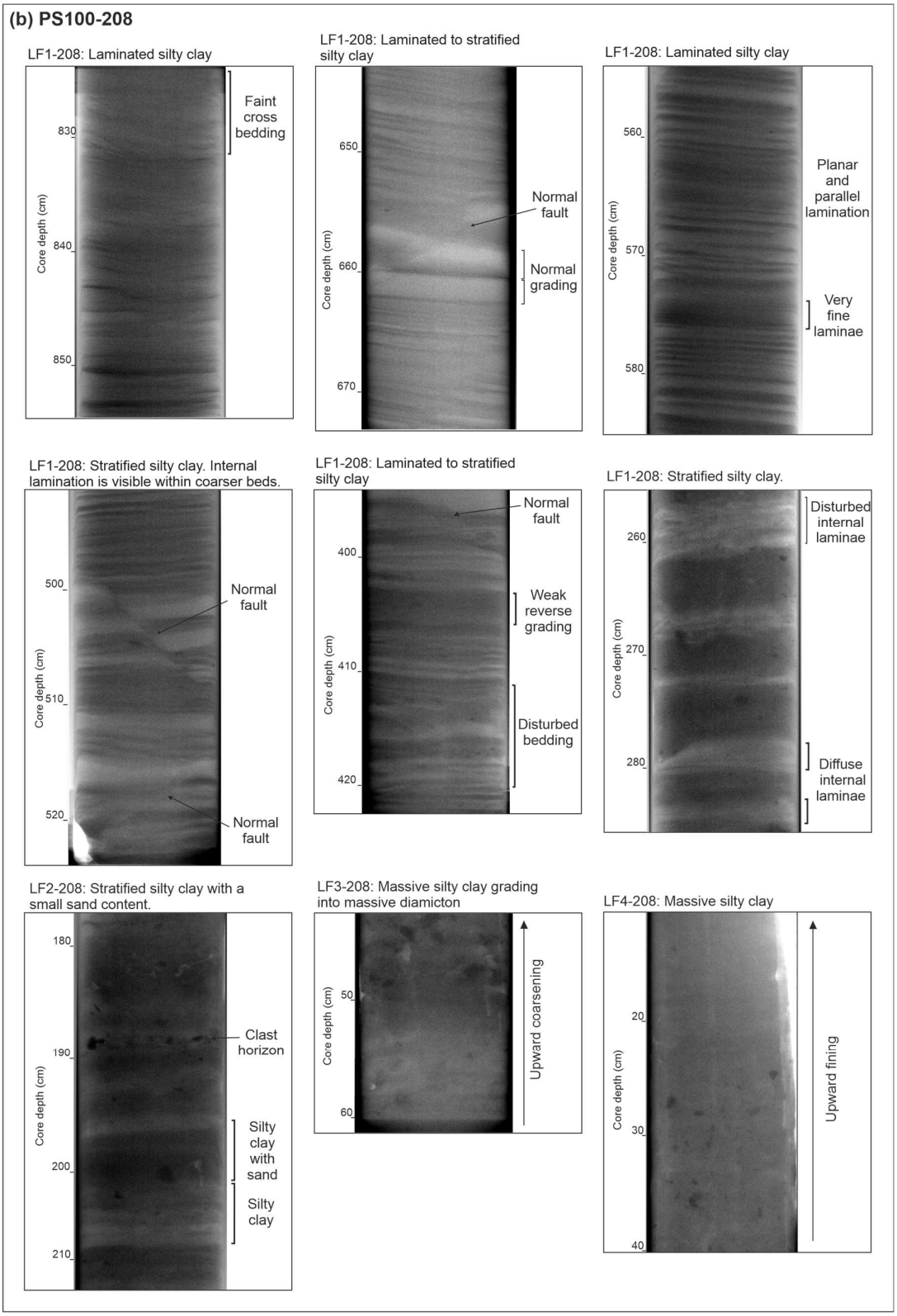

Figure 4.3 *Continued*

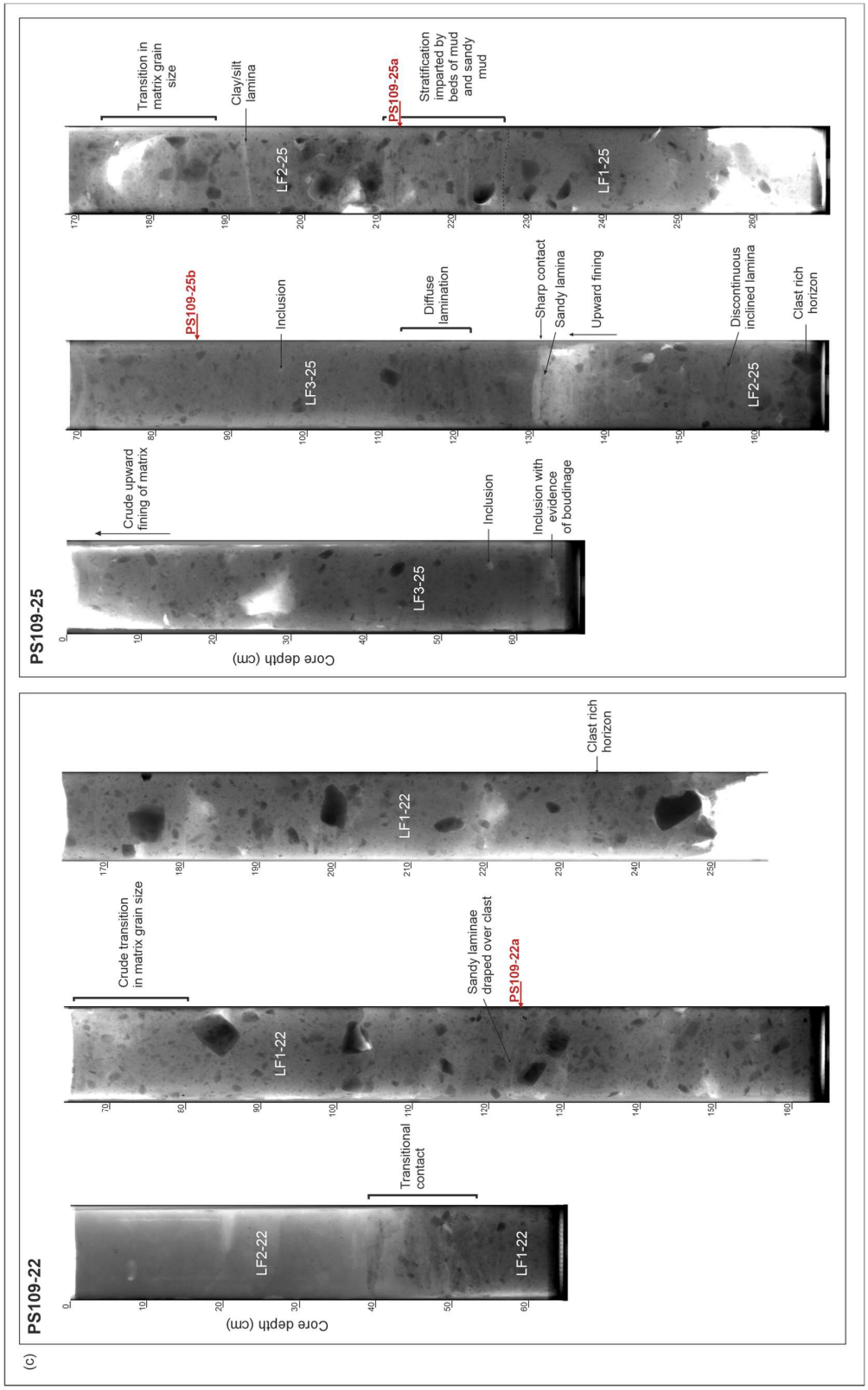

Figure 4.3 *Continued*

4.1.3 Micromorphology

Thin sections from depths of 340-346 cm (PS100-173a) and 232-240 cm (PS100-173b) from the PS100-173 core, within LF1-173 and LF2-173 respectively, are described below.

4.1.3.1 PS100-173a (340-346 cm – LF1-173)

This sample comprises a brown, matrix-supported massive diamicton. The matrix is composed of plasma. Microfossils have not been identified. The assemblage of microstructures present on the slide is shown in Figure 4.16. Turbate structures are present, and can often be found in groups of multiple adjacent turbates (Fig. 4.4a). Corestones in turbates can be single grains or clusters of multiple grains, or in some cases corestones are absent.

Both rotational and planar plasmic fabrics are well developed in the matrix of the diamicton. The distribution of these plasmic fabrics is shown in Figure 4.5. Skelsepic plasmic fabrics are developed surrounding grains with up to ~0.5 mm a-axes. In most cases birefringence is only present around part of the grain (Fig. 4.4b), however some grains are fully surrounded (Fig. 4.4c). Skelsepic fabrics can be found both in groups of multiple grains surrounded by oriented plasma (Fig. 4.4c), or in isolated grains. They have also been found adjacent to masepic plasmic fabric in multiple locations (Fig. 4.4b; 4.5).

Planar plasmic fabrics in this slide are predominantly masepic, characterised by bands (predominantly less than 1 mm in width) of pervasive short plasma domains (Fig. 4.4d; 4.4e). There are some isolated examples of discrete and more continuous unistrial plasmic fabrics present adjacent to masepic plasmic fabrics (Fig. 4.4e). Two sets of planar fabric directions have been identified: (1) a sub-horizontal set and (2) a steeply dipping sub-vertical set, visible in Figure 4.5. The second set occurs in isolated locations, with the majority of the planar plasmic fabrics within the first set.

4.1.3.2 PS100-173b (232-240 cm – LF2-173):

This sample consists of a massive, brown, matrix-supported diamicton. There are some localised areas in which the diamicton is predominantly skeletal grain supported with a limited plasma component. In parts of the slide, the matrix appears patchy due to the presence of areas of darker plasma (Fig. 4.6a).

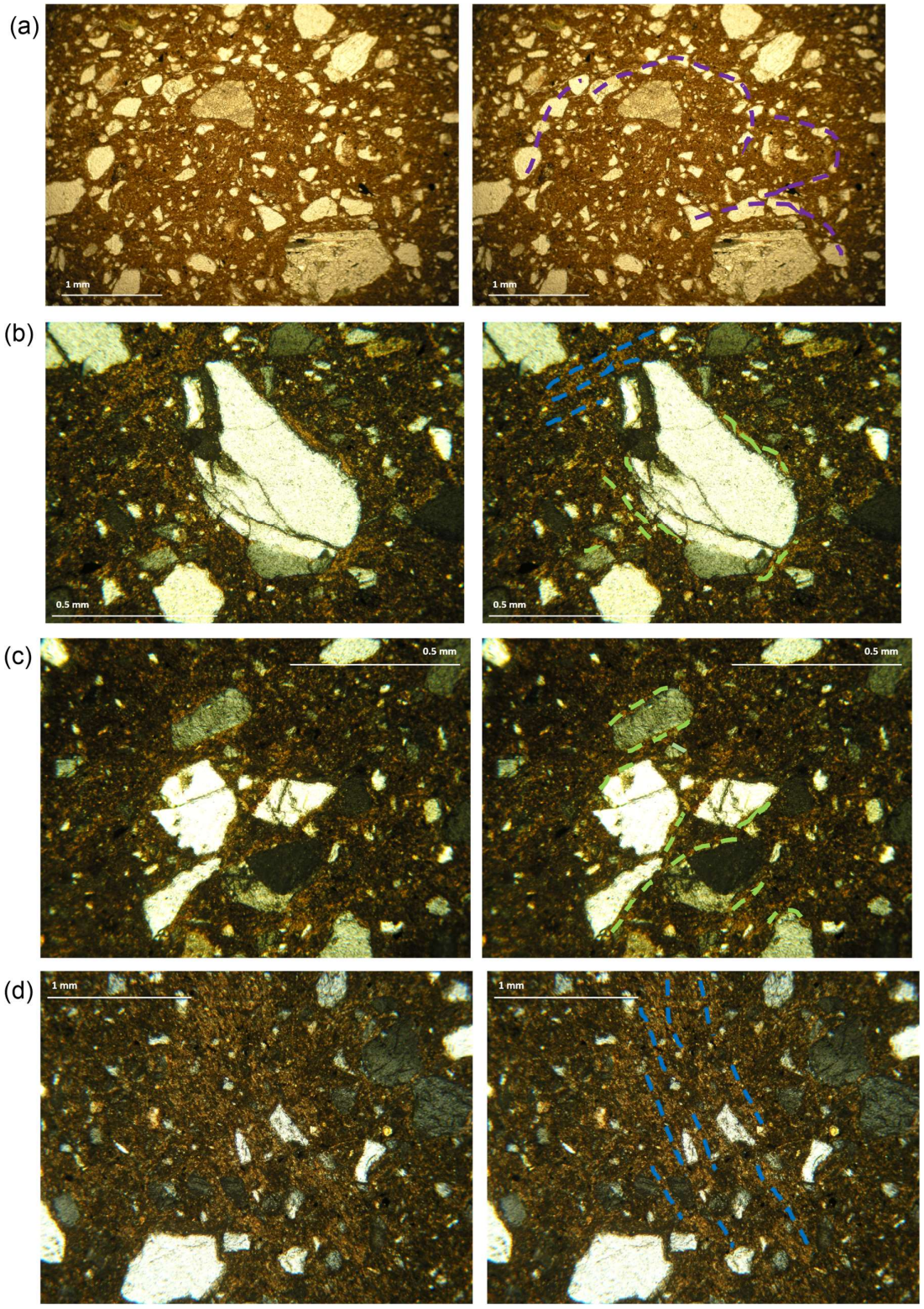

Figure 4.4 Photographs of microstructures present in PS100-173a. (a) Multiple skeleton grain turbates (b) Skelsepic plasmic fabric and adjacent masepic plasmic fabric (c) Skelsepic plasmic fabrics surrounding a cluster of skeleton grains (d) Masepic plasmic fabric (e) Masepic plasmic fabric (blue) and adjacent unistrial plasmic fabric (orange)

(e)

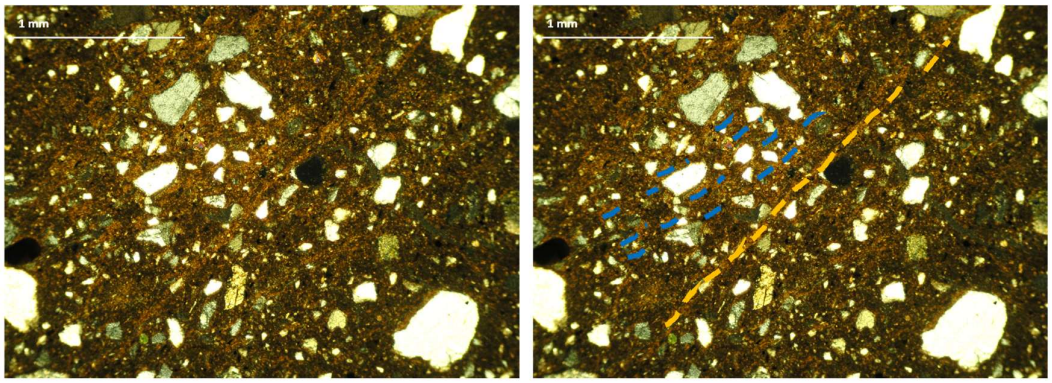

Figure 4.4 *Continued*

Microfossils are not evident. Skeleton grain turbates are present both with and without corestones. In places there are multiple turbate structures adjacent, and examples of turbates with multiple bands of grains arranged around the central grain (Fig. 4.6c).

Both planar and rotational plasmic fabrics are extensively present in the diamicton matrix (Fig. 4.7; 4.16). They are more frequent than in PS100-173a, and are larger scale (bands of masepic plasmic fabrics are predominantly greater than 1 mm in width). Masepic plasmic fabrics, which appear as well-defined bands of discontinuous plasma, are extensive and very well developed over the whole slide (Fig. 4.6d). Frequently, two adjacent bands of masepic fabric with different orientations are visible at different stages of slide rotation (bimasepic plasmic fabrics) (Fig. 4.6d). Across the slide, three possible sets of planar plasmic fabrics can be identified based on their orientation (Fig. 4.7).

Skelsepic plasmic fabrics are frequently found adjacent to and within bands of masepic fabric (Fig. 4.7), or independently (Fig. 4.6b). They usually only partially surround the skeletal grain. Localised areas of perpendicular, discontinuous plasma domains, lattesepic plasmic fabric, have also been identified (Fig. 4.6e; 4.16). In places, there are also large masses of plasmic fabric within which a dominant direction is indistinguishable.

4.2 Mid Norske Trough: PS100-175

4.2.1 Acoustic facies

AF2, AF3 and AF6 are present surrounding the PS100-175 core site (Fig. 4.1c). The acoustic profile shown in Figure 4.1c was acquired on a transect transverse to

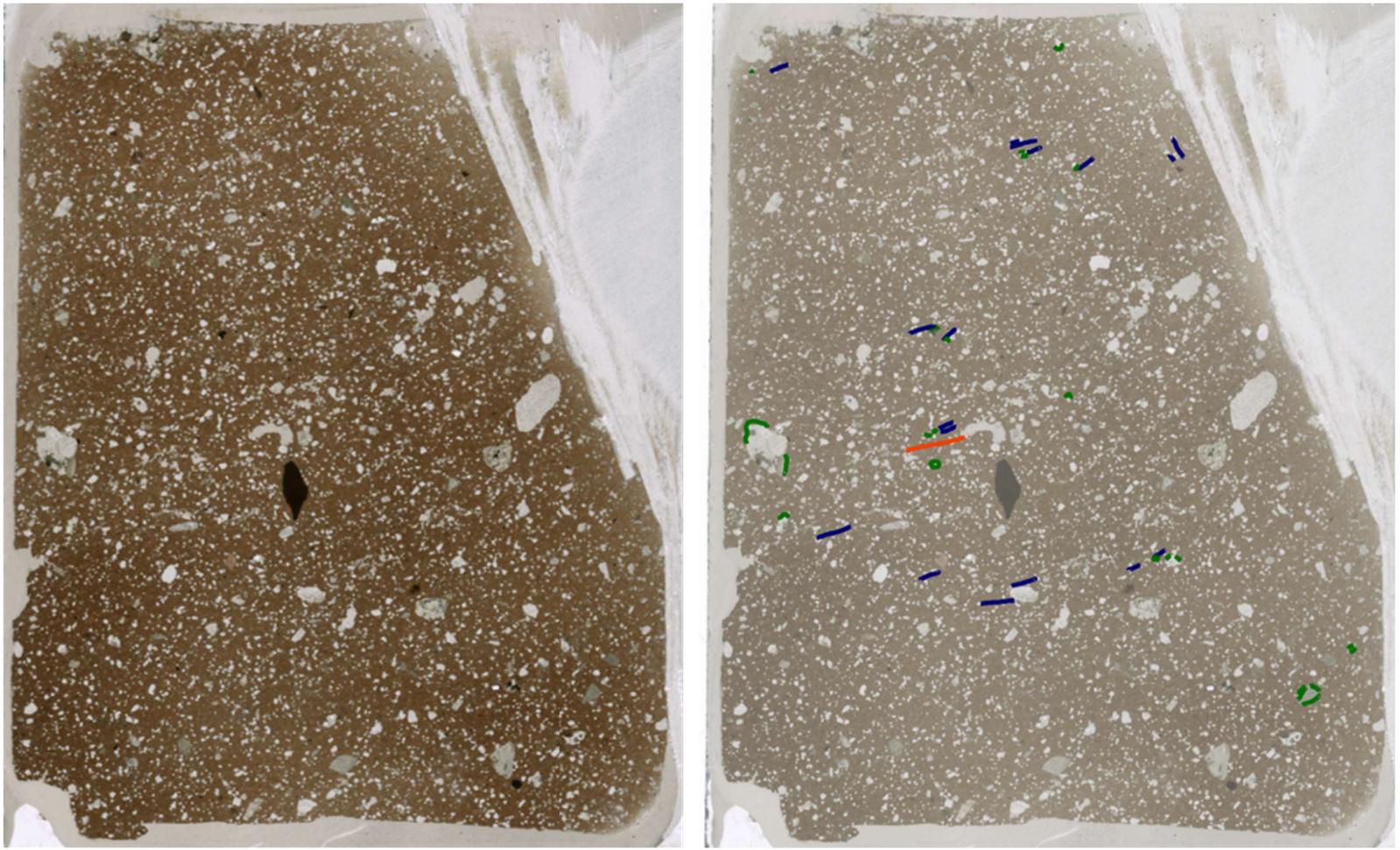

Figure 4.5 Thin section ‘map’ of PS100-173a showing the location and orientation of some plasmic fabrics. Blue = masepic, green = skelsepic, orange = unistrial.

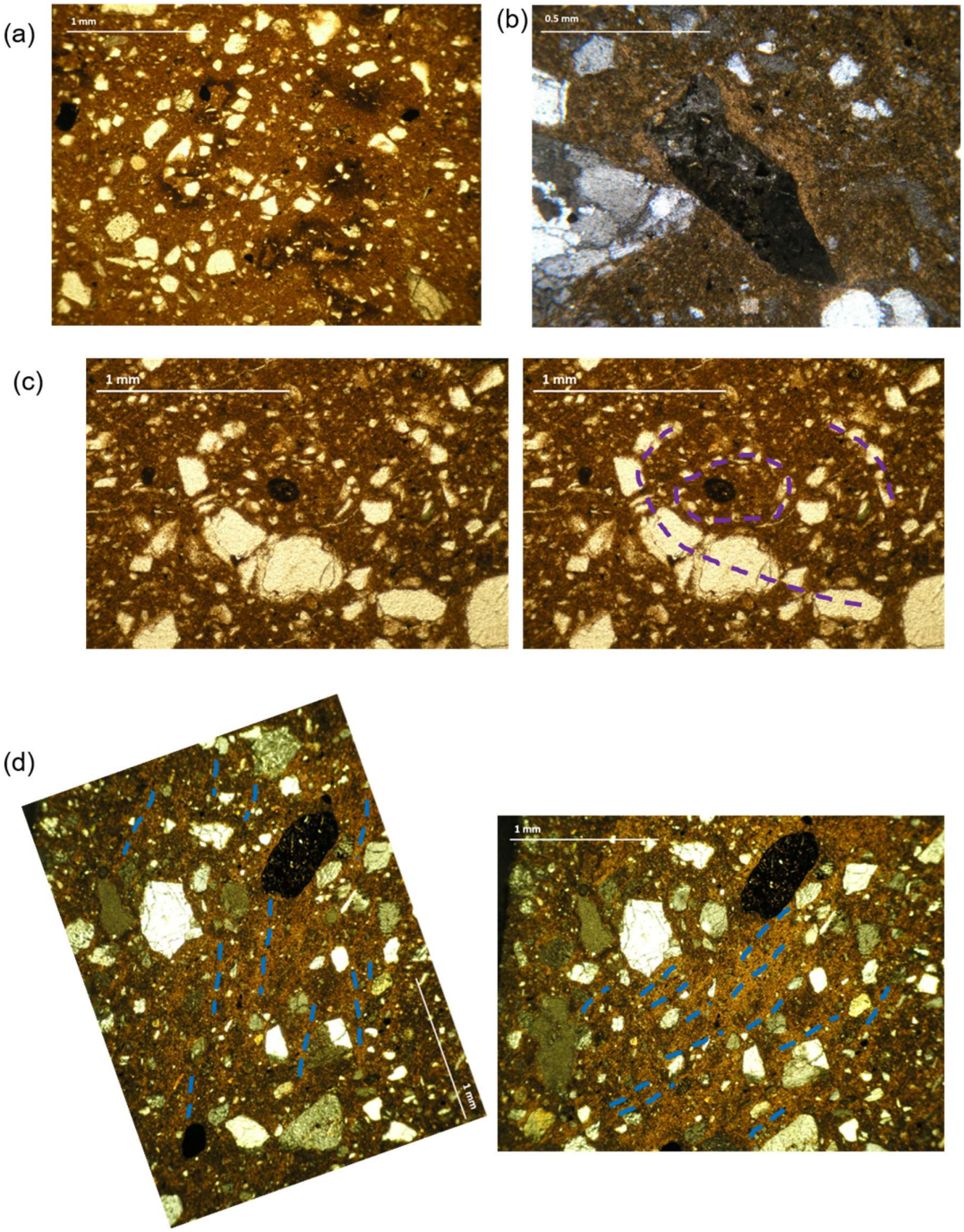

Figure 4.6 Photographs of microstructures present in PS100-173b. (a) Patchy areas of darker plasma (b) Skelsepic plasmic fabric (c) Skeleton grain turbate with two bands of clasts (d) Bimasepic plasmic fabrics, with the two photos displaying the masepic plasmic fabrics evident at different stages of rotation (e) Lattesepic plasmic fabric.

(e)

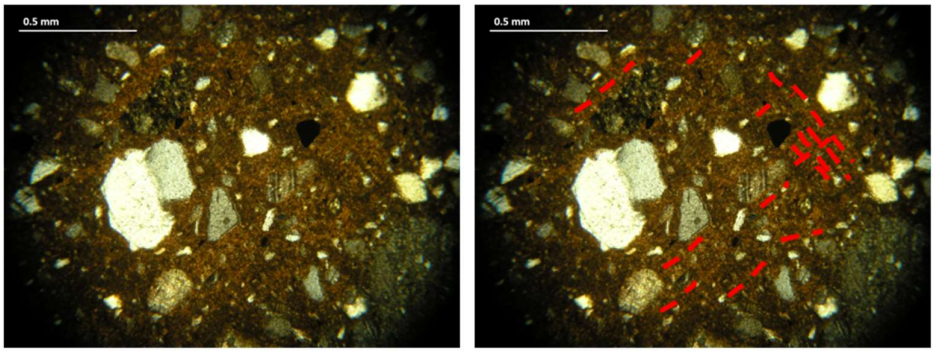

Figure 4.6 *Continued*

the long-axis of Norske trough (Fig. 4.1a). AF2 is a massive, acoustically transparent to semi-transparent sediment unit with a strong upper reflector. It is discontinuous, with frequent breaks in its upper reflector (Fig. 4.1c). AF2 is overlain by a massive, acoustically semi-transparent sediment unit (AF3) with a strong upper reflector and a hummocky, irregular upper surface. These hummocks on the surface of AF3 have a width of ~100-500 m. AF6 is conformable with the hummocky upper surface of AF3, but is only present discontinuously. It is massive and semi-transparent. The upper two facies (AF3 and AF6) have a chaotic appearance. There are multiple locations where they are heavily depressed and their upper reflectors disturbed, giving the appearance of a series of closely spaced hummocks within a depression superimposed on the hummocky surface of AF3 (Fig. 4.1c). These depressions are 320-660 m wide and 3.8-6.4 m deep. There are also frequent v-shaped incisions with reflectors at their bases which disturb the upper surface of AF3 and AF6. These incisions have a width of 50-60 m, and a depth of 2.8-3.3 m. All three acoustic facies are present at the PS100-175 core site, and the core was recovered from AF6 (Fig. 4.1c(ii)).

4.2.2 Core lithology

PS100-175 is composed of two lithofacies (Fig. 4.2a; 4.3a). Lithofacies 1 (LF1-175) (18-159 cm) is a massive, matrix-supported grey diamicton (2.5 YR 3/1). Its matrix is composed of silt and clay. Clasts are subangular to subrounded, and are up to large pebble gravel size (up to 45 mm a-axes). A sub-vertical clast alignment is identifiable (Fig. 4.3a). In places, crude stratification is imparted by bands of coarser matrix, which become more prominent upwards through the lithofacies. A discontinuous (15 mm thick, 70 mm wide) gritty bed is evident at 36 cm. From 35 cm to the top of the unit clast frequency decreases. Between 18-25 cm, lithofacies 1 starts to transition into lithofacies 2. At 23 cm, there is a discontinuous 10 mm

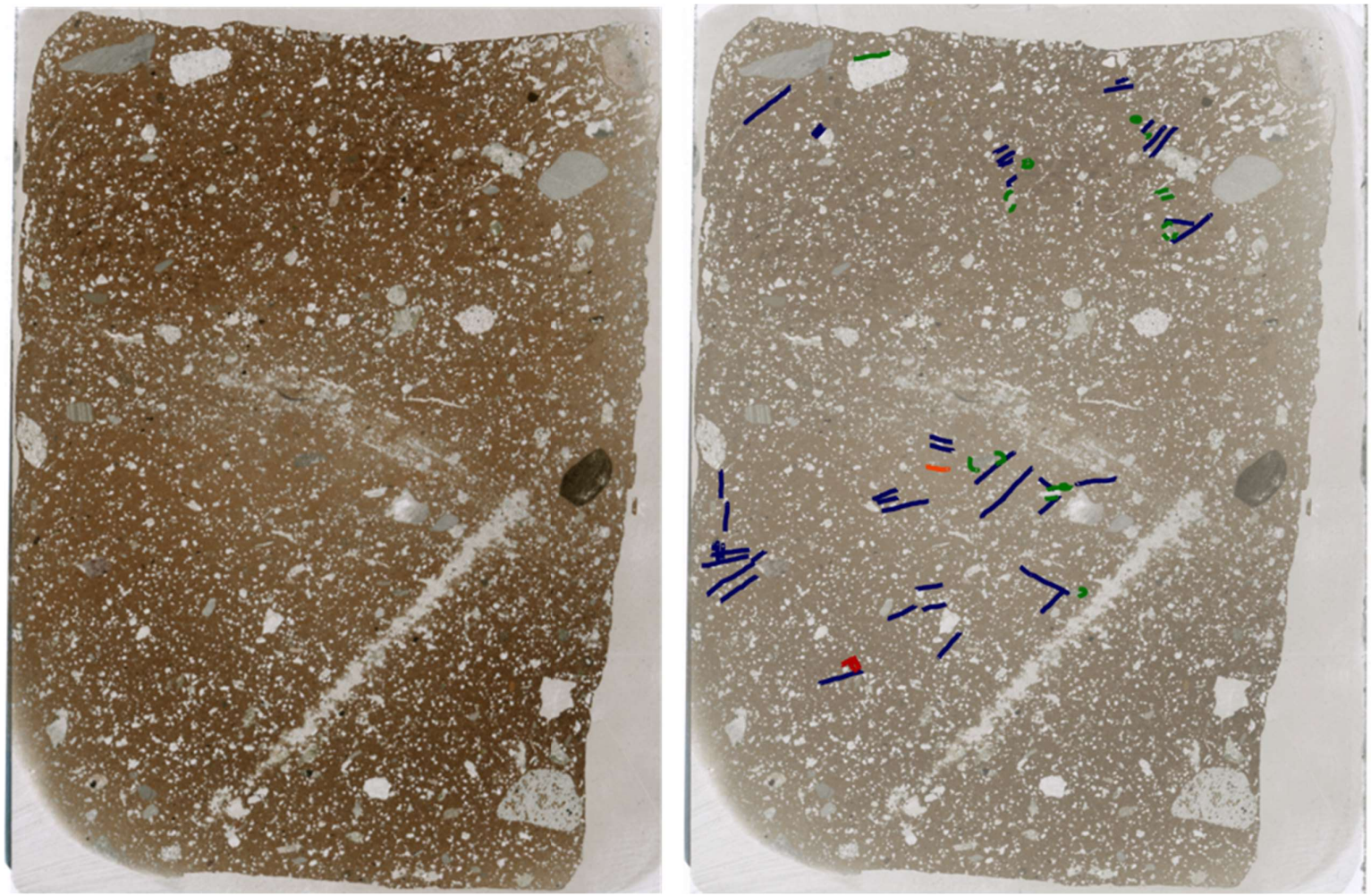

Figure 4.7 Thin section 'map' of PS100-173b showing the location and orientation of some plasmic fabrics. Blue = masepic, green = skelsepic, orange = unistrial, red = lattesepic.

thick, 70 mm wide clay rich lamina with a sharp contact with the surrounding diamicton (Fig. 4.3a). Above this (18-23 cm) the diamicton matrix fines, and clasts become much less frequent as the diamicton grades upward into clay.

Lithofacies 2 (LF2-175) (0-18cm) is a massive olive brown clay (10YR 4/2), containing occasional grey mottles (Fig. 4.2a; 4.3a). Between 10-18 cm it contains occasional small clasts with a-axes up to 3mm in length. Clasts are absent from 10 cm to the top of the unit.

4.2.3 Micromorphology

A sample from a depth of 142-150cm (PS100-175a), within LF1-175, was analysed from the PS100-175 core.

4.2.3.1 PS100-175a (142-150 cm – LF1-175)

PS100-175a comprises a dark brown, massive, matrix- to clast-supported diamicton. The matrix displays frequent patchy areas of darker plasma, which have a wispy appearance and are discontinuous (Fig. 4.8a). There are localised areas with high skeleton grain frequencies and grain clusters. Circular skeletal grain alignments have been identified, sometimes with multiple inset circles of grains (Fig. 4.8b; 4.16). These skeleton grain turbate structures more frequently lack corestones, although turbates with corestones are also present.

Localised planar and rotational plasmic fabrics have both been identified (Fig. 4.9; 4.16). Masepic plasmic fabrics, characterised by bands of discontinuous plasma domains, are present but are poorly developed and are not extensive across the slide. In some places the masepic fabric is weakly developed, and is made up of very short and thin dashes of plasma with a linear alignment, rather than bands of plasma (Fig. 4.8d). A single example of a unistrial plasmic fabric, composed of more continuous dashes of plasma is also present (Fig. 4.8c). Apart from one example, the planar plasmic fabrics share one gently dipping orientation (Fig. 4.9). Skelsepic plasmic fabrics are more common than planar plasmic fabrics but are still poorly developed, appearing as discrete short dashes of plasma adjacent skeleton grains (Fig. 4.8e), or infrequently as thicker bands of plasma domains partially or fully surrounding grains (Fig. 4.8f). In places skelsepic plasmic fabrics are adjacent to skeleton grain turbates and masepic plasmic fabrics.

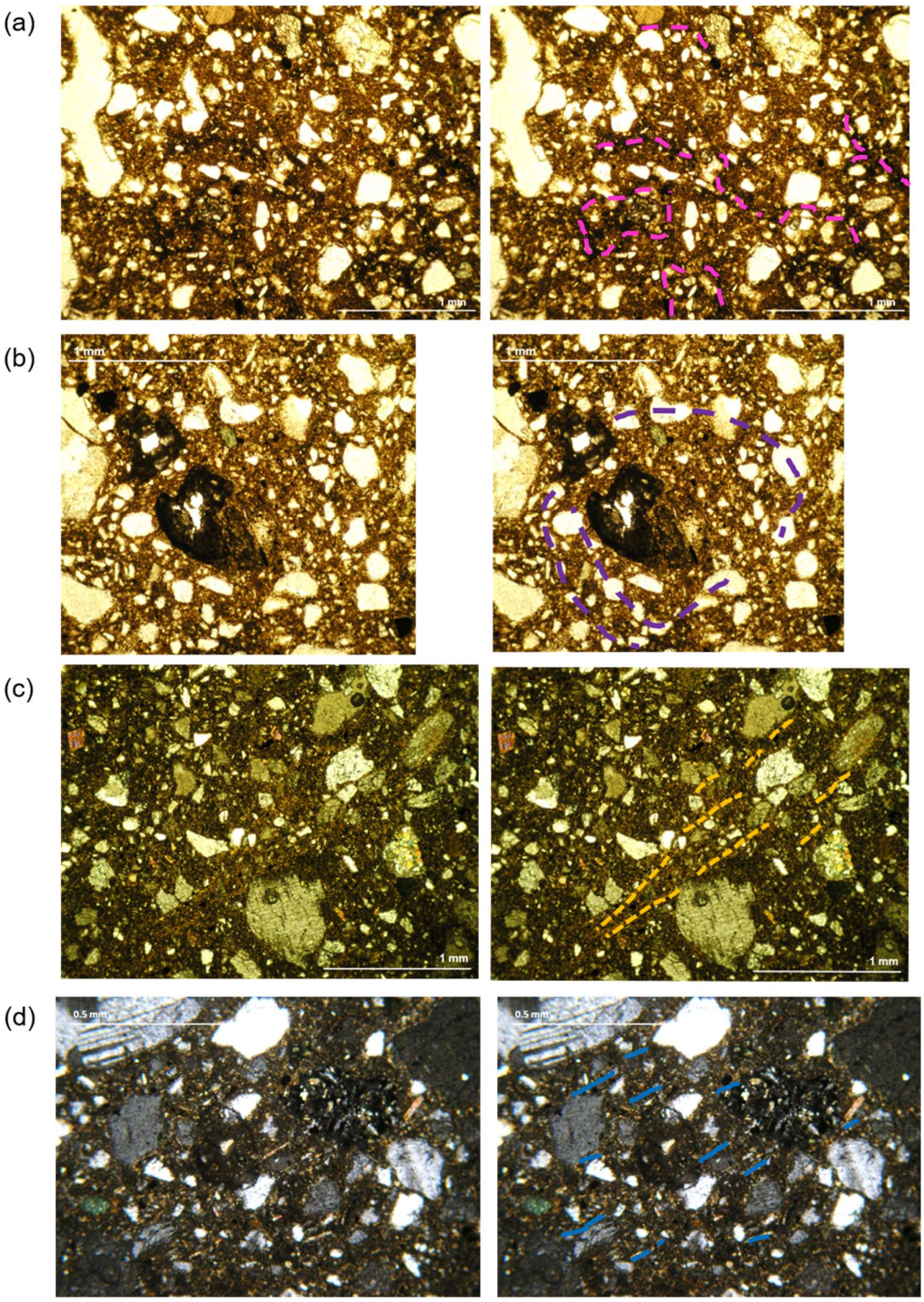

Figure 4.8 Photographs of microstructures present in PS100-175a. (a) Patchy areas of darker plasma (b) Skeleton grain turbate (c) Unistrial plasmic fabric (d) Weakly developed masepic plasmic fabrics with short dashes of plasma (e) Skelsepic plasmic fabric characterised by short dashes of plasma (f) Skelsepic plasmic fabric characterised by a band of plasma around the grain

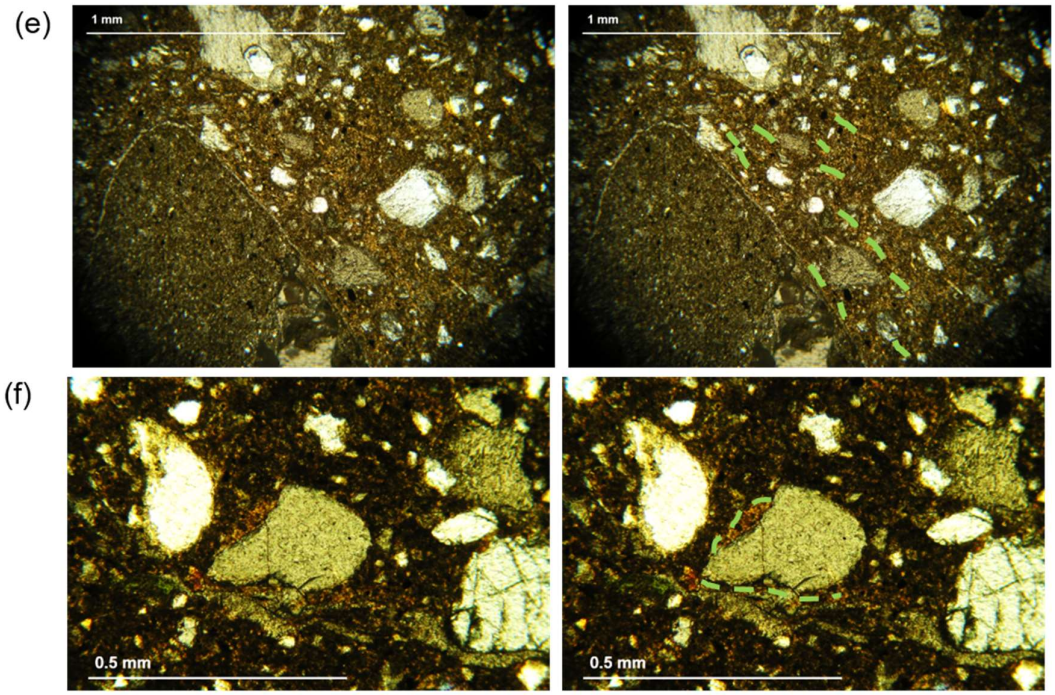

Figure 4.8 *Continued*

4.3 Inner Norske Trough: PS100-208

4.3.1 Acoustic facies

The core site of PS100-208 is located in a basin between two topographic highs (topographic highs = ~200 m water depth) (Fig. 4.1d). These topographic highs have a relief of ~200 m. The sediment pile is thick in this area, up to ~95 m. Six of the twelve acoustic facies are present, AF1, AF7, AF8, AF9, AF10 and AF11. AF1 is a thin unit with an acoustically impenetrable and continuous surface reflector present on topographic highs. AF7 drapes the more gently sloped sides of the basin and infills the depressions which occur on the topographic highs. It is very weakly acoustically stratified to structureless, and lacks a distinct basal reflector. Multiple acoustically transparent lenses (AF10) are present within AF7 on the basin slopes (Fig. 4.1d). These lenses are ~130-210 m wide.

AF8 and AF9 are present in the large depression between the two topographic highs (Fig. 4.1d). The lower unit (AF8) is acoustically stratified by alternating bands of opaque and acoustically transparent sediment. It drapes slight topographic highs and infills the depressions between. The strength of the stratification varies laterally, with the internal reflectors imparting stratification being discontinuous in some places and unbroken in others (Fig. 4.1d).

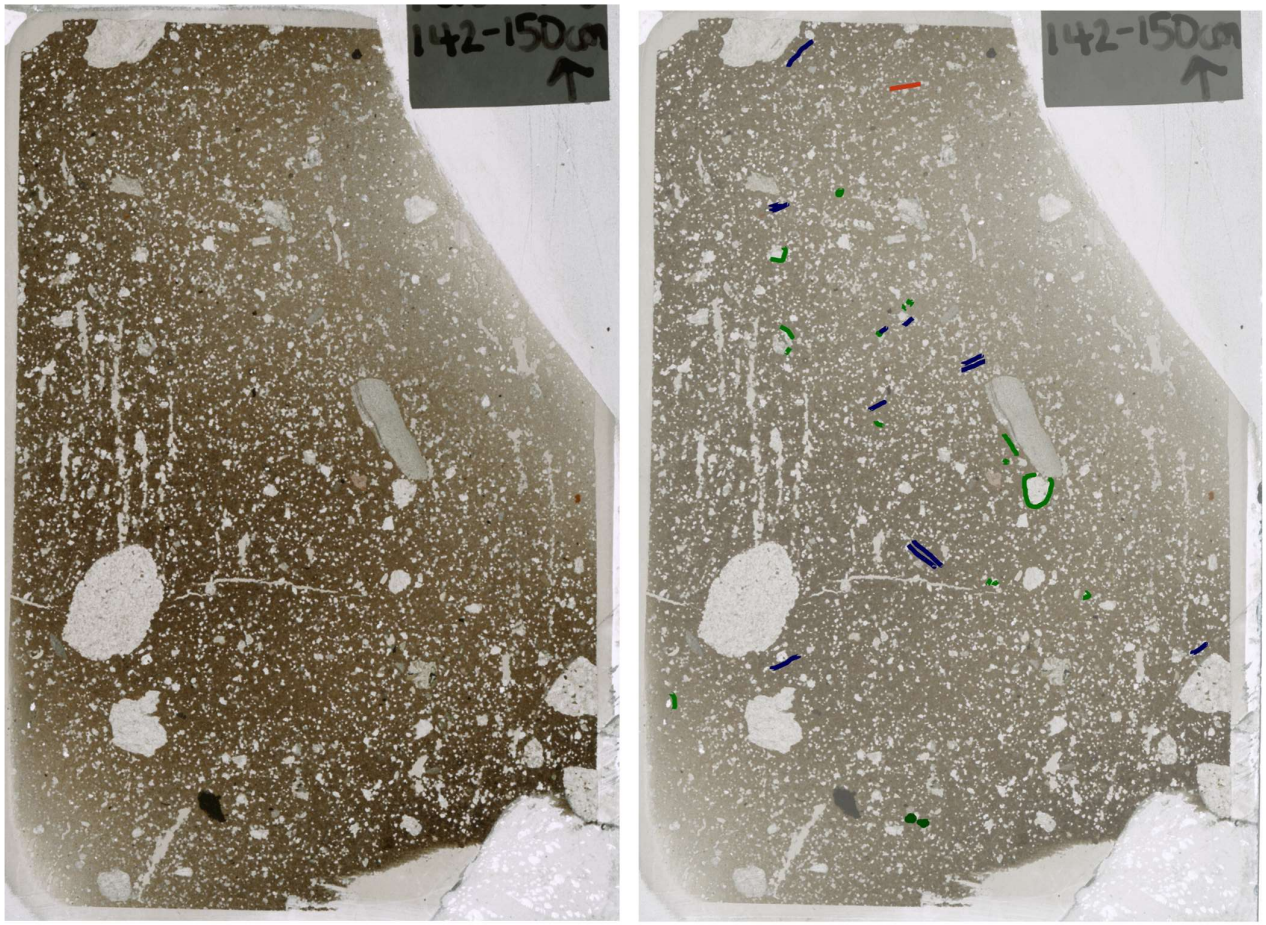

Figure 4.9 Thin section 'map' of PS100-175a showing the location and orientation of some plasmic fabrics. Blue = masepic, green = skelsepic, orange = unistrial, red = lattesepic.

Stratification within AF8 can appear disturbed over topographic highs. The base of AF8 is not smooth, and it lacks a distinct basal reflector. There is a gradual transition from AF8 into AF9 above. AF9 is an opaque and densely acoustically stratified sediment unit (Fig. 4.1d). Its internal reflectors are parallel and stratification is largely undisturbed. The unit is conformable, infilling the slight depressions on the surface of AF8. The upper reflector of AF9 is smooth and continuous. At the base of one of the topographic highs there is a further unit, AF11, which comprises massive, acoustically transparent sediment with a strong upper reflector. It infills a depression on the surface of AF9. AF11 is wedge shaped, thinning outwards towards the centre of the basin.

Both AF8 and AF9 are present at the PS100-208 core site, however the core was recovered entirely from AF9 (Fig. 4.1d(ii)). In this area, AF8 is draping the two slight bumps at the bed and infilling the depression between. Its internal stratification appears disturbed. Stratification within AF9 is undisturbed, and it is infilling a slight depression on the surface of AF8.

4.3.2 Core lithology

The PS100-208 core comprises four lithofacies (Fig. 4.2b). Lithofacies 1 (LF1-208) is made up of laminated to stratified silty clay. It occurs between 218-906 cm, 117-177 cm, and 70.5-104 cm, thus making up the majority of the PS100-208 core. Shear strength is 2-15 kPa (Fig. 4.2b). Bulk density is 1.13-2.01 g/cc, and p-wave velocity is 117-2286 m/s. Stratification in LF1-208 is imparted by laminae and beds of alternating coarser and finer silty clay, which appear as darker and lighter bands on the x-radiograph images (Fig. 4.3b). LF1-208 displays considerable internal complexity and vertical variability.

Between 534 cm to 906 cm, most individual beds of silty clay in LF1-208 are less than 10 mm thick, but in places lamination transitions to stratification where bed thickness is greater than 10 mm (Fig. 4.3b). Laminae/bed thickness is highly non-uniform, with the fine laminae being 1-50 mm thick, whilst the thickness of the coarser beds is up to 9 mm. Between 716-732 cm and 604-619 cm, bedding is not evident and the silty clay becomes massive. Clasts are extremely infrequent and small (5-8 mm a-axes) between 534-906 cm. From 534 cm up to 218 cm, the silty clay becomes predominantly stratified rather than laminated. There is also a large range in bed thickness, with fine beds being 2-40 mm thick and coarse beds being 1-60 mm thick, and occasionally greater than 60 mm thick. However, the thickness

of individual beds is predominantly greater than 10 mm between 218-534 cm. Clasts are observed from 534 cm upwards, and increase in frequency up core. They are more frequent in the coarser beds than in the finer beds. Clasts observed between 218 to 534 cm have a-axes lengths of up to 30 mm.

Throughout LF1-208, laminae and beds range from planar and parallel with relatively sharp contacts, to diffuse and at times laterally discontinuous (Fig. 4.3b). Occasionally, normal grading is evident where coarse beds grade upward into fine beds rather than being separated by a contact (e.g., between 657-663 cm; Fig. 4.3b). Inversely graded beds are also identified between 403-406 cm (Fig. 4.3b) and 390-393 cm. In multiple parts of LF1-208 (between 775-779 cm, 500-534 cm, 438-476 cm, 339-395 cm and 269-339 cm), individual beds of silty clay display internal lamination (Fig. 4.3b). This internal lamination can be in either the fine or the coarse beds. There is also a single example of faint cross bedding between 826-832 cm (Fig. 4.3b). Bedding is frequently offset by normal faults, and a single reverse fault is present at 586 cm. In some places bedding has become heavily disturbed and/or inclined.

Lithofacies 2 (LF2-208) comprises massive to stratified gritty silt and clay, and occurs between 177-218 cm and 104-117 cm (Fig. 4.2b). It is distinguished from LF1-208 based on its sand content. It has a shear strength of 2-3 kPa. Bulk density is 1.36-1.74 g/cc and p-wave velocity is 1342-1761 m/s. Dispersed pebble sized clasts are present (up to 18 mm a-axes). Between 177-218 cm, LF2-208 displays stratification imparted by alternating planar beds of silty clay and silty clay with sand (Fig. 4.3b). The coarse beds are 25-80 mm thick, whilst the fine beds are 10-60 mm thick, and beds display diffuse contacts. At 188 cm there is a horizon with a high clast concentration. Between 104-117 cm, LF2-208 is massive and displays a sharp contact with the unit above.

Lithofacies 3 (LF3-208), present between 42-70.5 cm, consists of massive silty clay which coarsens upwards into a massive, matrix-supported diamicton with a low clast frequency (Fig. 4.2b; 4.3b). Shear strength is 3-4 kPa. Bulk density is 1.50-1.80 g/cc, and p-wave velocity is 119-1701 m/s. Clasts are present from 59 cm upwards, and have a-axes lengths of up to 20 mm. LF3-208 has a gradational contact with LF4-208 above.

Lithofacies 4 (LF4-208), which spans the upper 42 cm of the core, comprises massive silty clay fining upward to massive clay (Fig. 4.3b). Shear strength is 4-5 kPa. Bulk density is 1.43-1.68 g/cc, and p-wave velocity is 118-1436 m/s. Clasts with diameters less than 10 mm are present between 23.5-42 cm, with clast frequency and size decreasing upward. Clasts are absent from 23.5 cm to the top of the unit, aside from the presence of two larger clasts (20 mm a-axes) between 6-8 cm.

4.4 Outer Westwind Trough: PS109-22

4.4.1 Acoustic facies

Two acoustic facies (AF2 and AF12) are present around the core site of PS109-22, at a seafloor depth of 300-330 m (Fig. 4.1e). The acoustic profile shown in Figure 4.1e is oriented sub-parallel to Westwind Trough (Fig. 4.1a). The lower facies (AF2) is a massive, transparent to semi-transparent unit with a sharp upper reflector and no basal reflector, which is present discontinuously along the profile (Fig. 4.1e). AF12, which is present overlying AF2, is acoustically semi-transparent and structureless, with a strong upper reflector. AF12 is arranged in multiple low amplitude wedge shaped sediment units which taper in a north-easterly direction (towards the continental shelf edge). Two discrete wedges (SW-1 and SW-2) have been identified and labelled in Figure 4.1e, and they will be referred to as sediment wedges from herein. SW-1 is ~1.9 km in length and up to 12 m thick. It contains internal reflectors which dip towards the northeast. SW-2 is present seaward of this wedge. The lower quality of the acoustic data in this area of the seafloor makes it more difficult to determine its characteristics, however SW-2 has been estimated to be ~2 km in length and ~9 m thick. It also displays some weak internal reflectors. In places the upper reflector of AF12 is disturbed by v-shaped depressions (Fig. 4.1e(ii)). The PS109-22 core was recovered from the seaward end of SW-2, wholly within AF12 (Fig. 4.1e(ii); Table 4.1). AF12 is underlain by AF2 at the core site.

4.4.2 Core lithology

PS109-22 is comprised of two lithofacies (Fig. 4.2c; 4.3c). Lithofacies 1 (LF1-22) (39-256 cm) is a massive, matrix-supported diamicton, with a matrix of silt and clay (Fig. 4.3c). Matrix colour transitions from brown (7.5 YR 4/2) (234-256 cm), to grey (7.5 YR 5/1) (202-234 cm), to brown (7.5 YR 4/2 – 10 YR 5/3) (54-202 cm), to reddish brown (5 YR 4/3) (39-54 cm). Shear strength ranges from 0 to 9.4 kPa

(Fig. 4.2c), with a general decrease in shear strength upward through the facies. Magnetic susceptibility is 0-551 x 10^{-5} SI. Contacts between transitions in matrix colour are sharp to gradational. The diamicton is clast rich, with clasts present up to pebble size and angular to subrounded. Clast frequency increases from 202 cm upward, with the lower 54 cm of the unit having a lower clast concentration than the rest of the facies. There are occasional large pebble gravel clasts (up to 60 mm a-axes), sometimes in clusters of multiple large clasts. There is a horizon of pebble gravel at 234 cm. In places clast fabric appears to be weakly sub-vertical to vertical. There is some localised stratification in the matrix of the diamicton, imparted by multiple 3-4 mm thick highly diffuse sand-rich lamina present between 122-124 cm. Lamina appear slightly inclined, and are draped over a large pebble (40 mm a-axes) (Fig. 4.3c). Discontinuous lamina 3-4 mm thick and 4-5 mm across are also present at 57-59 cm. In places, crude transitions in matrix grain size are also visible on the x-radiograph images (Fig. 4.3c).

The contact between lithofacies 1 and lithofacies 2 is transitional. Between 42.5-54 cm, streaked inclusions of grey (10 YR 4/2) mud appear within the LF1-22 diamicton, and from 42.5-48 cm the diamicton matrix begins to fine upwards. At 40-42.5 cm, there is a bed of massive silty clay, followed by a 10 mm lamina at 39-40 cm comprised of sand and small clasts (1-2 mm).

Lithofacies 2 (LF2-22) (0-39 cm) is a massive, dark greyish brown silty clay (Fig. 4.2c; 4.3c). Shear strength is 2.5-4 kPa. Magnetic susceptibility is low, 1-65 x 10^{-5} SI. It contains very infrequent small clasts (less than 8 mm a-axes). It contains some very diffuse textural boundaries between horizons with slight variations in silt content.

4.4.3 Micromorphology

From the PS109-22 core, one thin section sample from a depth of 120-128 cm (PS109-22a), within LF1-22, was analysed.

4.4.3.1 PS109-22a (120-128 cm – LF1-22)

PS109-22a consists of a stratified, matrix- to clast-supported diamicton. It has a coarse texture with frequent gravel sized grains (greater than 2 mm a-axes length). It appears chaotic due to rapid changes in matrix colour and skeleton grain frequency. Clusters of skeleton grains common. Stratification is imparted by the presence of five sub-horizontally inclined beds, some of which are

discontinuous, which vary in matrix colour and skeleton grain frequency and size. Beds are bounded by diffuse contacts, and individual beds are unsorted. These beds are shown in (Fig. 4.11), and have the following characteristics:

(1) Plasma supported diamicton. Matrix colour transitions from grey to brown to orange brown, and appears intermixed with wispy bands of different matrix colour in places (Fig. 4.10a). Boundaries between matrix colour transitions can be both well-defined and diffuse. Skeleton grains are medium silt to coarse sand with some granule and pebble gravel.
(2) Skeletal grain supported diamicton, with a higher frequency of skeleton grains than the bed above. Skeleton grains are medium silt up to granule and pebble gravel.
(3) Dark grey brown, discontinuous lamina (2-4 mm thickness) of plasma supported diamicton. Skeleton grains are coarse silt to coarse sand, with a limited number of granule gravel grains. Skeleton grain frequency is lower than the other four beds. A large skeleton grain (8 mm a-axis) is evident at its contact with bed 2, which slightly depresses the lamina (dropstone structure) (Fig. 4.11).
(4) Skeletal grain supported diamicton. Skeleton grains are medium silt to coarse sand, with larger gravel sized grains absent from this layer.
(5) Plasma supported diamicton, with similar characteristics to (1). Skeleton grains are medium silt to very coarse sand with some granule gravel.

Coated grains are frequent in all five beds around skeletal grains with a range of a-axes lengths (0.2-4 mm). Coatings are all massive, but two distinct types are evident: (1) diamictic coatings (Fig. 4.7c) and (2) coatings composed of solely fines (Fig. 4.10b). Coatings range in thickness (0.02-0.5 mm), with the diamictic coatings generally thicker than the coatings composed of fines. Coatings usually surround the entire grain, but there are some examples of partial grain coatings. The finer grain coatings appear either rounded or are conformable with the shape of the grain, whilst the edges of thicker diamictic coatings are generally rounded. Grain coatings consistently differ in colour from the surrounding diamicton matrix.

Intraclasts of orange silt/clay, and occasionally grey silt/clay, are also present in all five beds (Fig. 4.11; 4.16). They range in diameter from 0.3-2 mm, and have a triangular, to circular, to flattened circular shape. They generally contain small

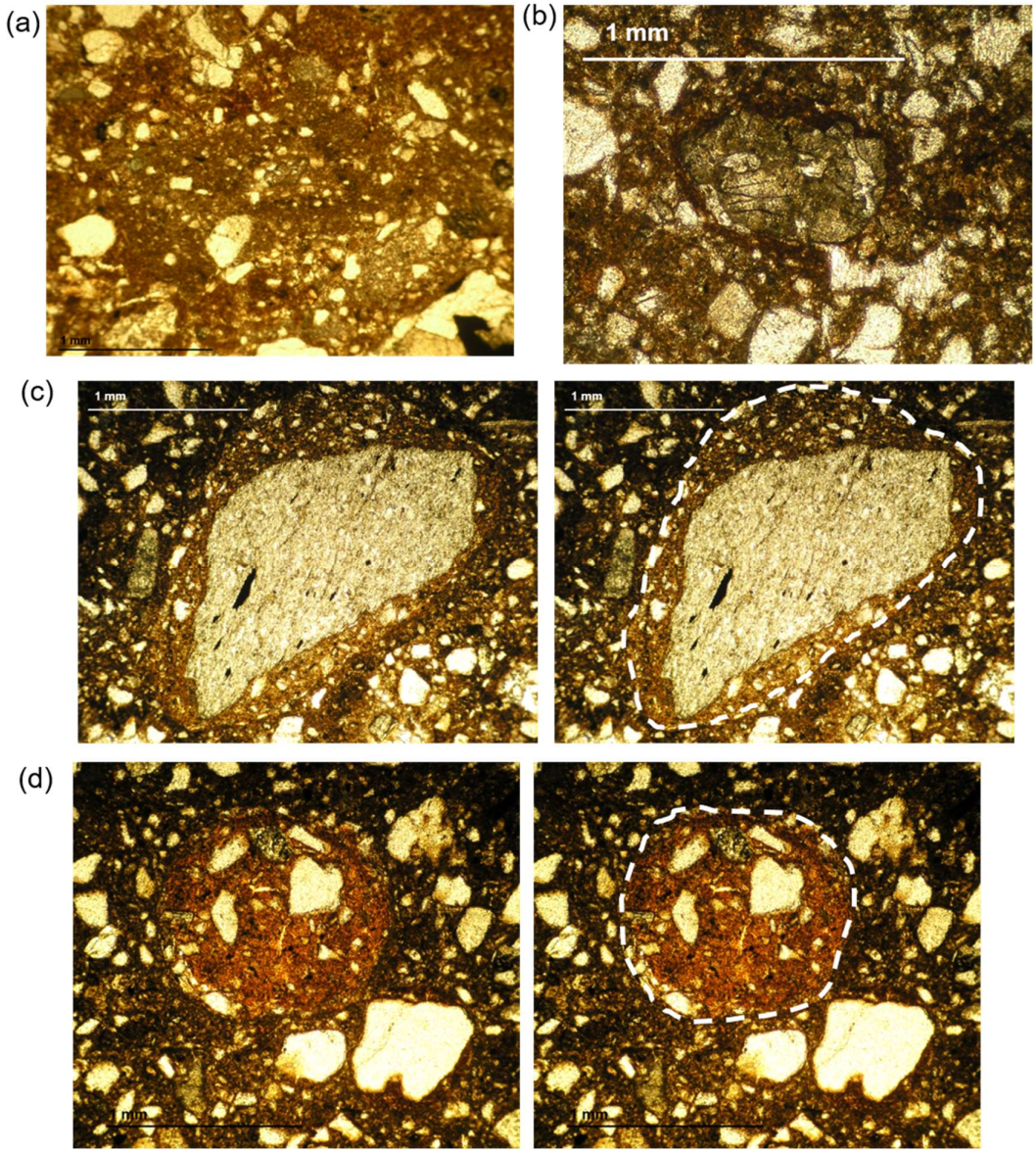

Figure 4.10 Photographs of microstructures present in PS109-22a. (a) Intermixed bands of different plasma colour (b) Skeleton grain coating composed of silt/clay (c) Diamictic skeleton grain coating (d) Circular diamictic intraclast and adjacent coated grain (e) Intraclast composed of silt/clay with no skeleton grains (f) Circular cluster of skeleton grains (g) Skelsepic plasmic fabric developed on one side of a grain.

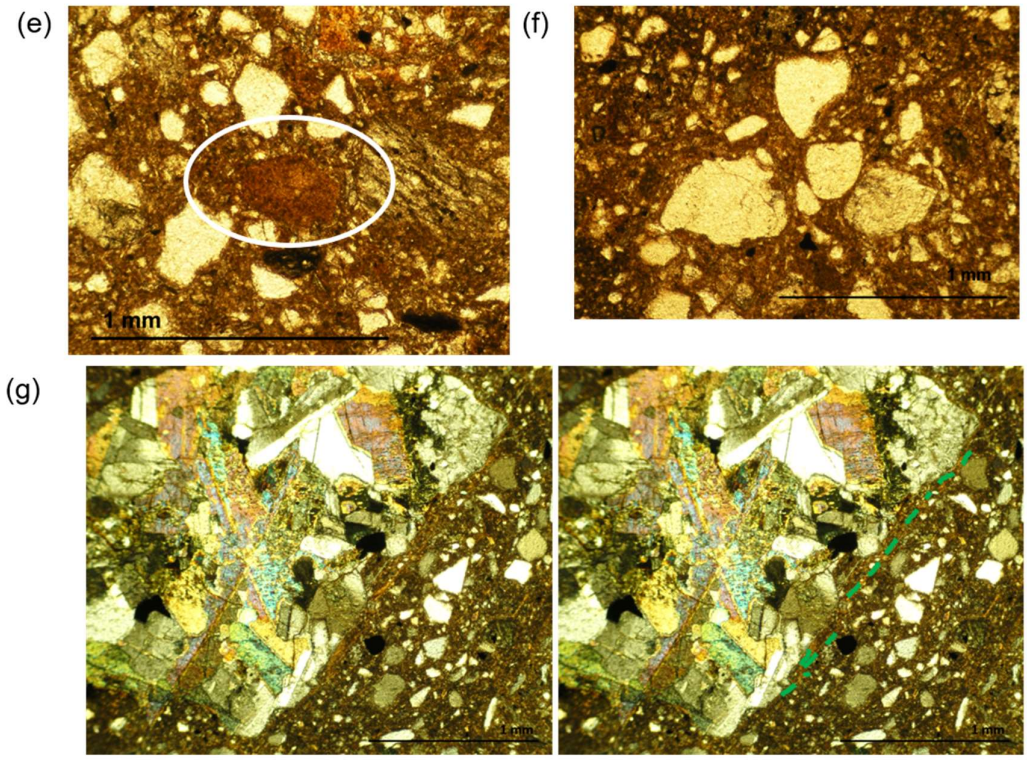

Figure 4.10 *Continued*

skeletal grains (Fig. 4.10d), however there are some examples of intraclasts in which skeletal grains are absent (Fig. 4.10e).

Skeleton grain turbate structures with single and multiple corestones, and without corestones, are present but are poorly developed (Fig. 4.11; 4.16). There are multiple examples of turbate structures with corestones displaying grain coatings. Circular clusters of 3 to 4 skeleton grains, often with fine skeleton grains surrounding the larger grains, have been identified (Fig. 4.10f). These have a similar appearance to necking structures.

A single isolated example of a skelsepic plasmic fabric is evident in the lower corner of the slide (within bed 5) (Fig. 4.10g; 4.11). Plasma is arranged in short and discrete microshears, adjacent to the flat side of the skeleton grain.

4.5 Outer Westwind Trough: PS109-25

4.5.1 Acoustic facies

AF2 and AF12 are present surrounding the core site of PS109-25 (Fig. 4.1f). It should be noted that the acoustic profile in Figure 4.1f(i) is oriented southeast to northwest across to Westwind Trough (Fig. 4.1a), whilst the Parasound screenshot Figure 4.1f(ii) is sub-parallel to the trough (oriented west to east) (Fig. 4.1a). AF2

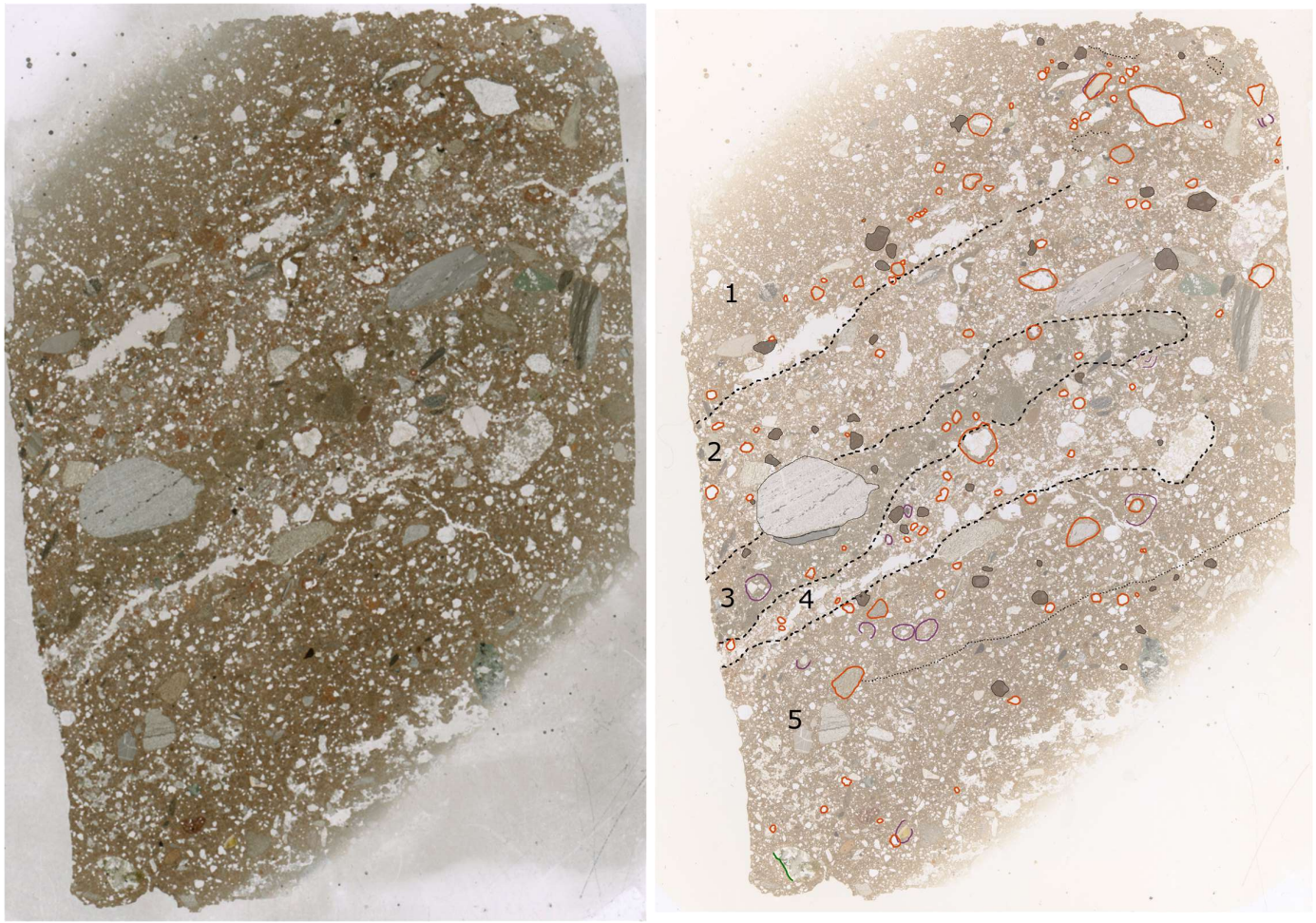

Figure 4.11 Thin section 'map' showing the distribution of features identified on the slide PS109-22a. The location of the five different beds is marked. Orange = coated grains, purple = skeleton grain turbates, grey = intraclasts, green = skelsepic plasmic fabric

has a strong upper reflector, no basal reflector, and occurs discontinuously at the base of the acoustic profile. AF12 is massive and semi-transparent, with a continuous and strong upper reflector, and some internal reflectors. Its upper reflector is generally planar, but is disturbed in places where it is incised by v-shaped incisions with reflectors at their bases (width = ~90 m, depth = 4 m) (Fig. 4.1f). The facies has a discontinuous basal reflector. AF12 overlies AF2, either infilling depressions (Fig. 4.1f(i)) or in wedge shape sediment bodies which taper at the edges (Fig. 4.1f(ii)).

Both AF2 and AF12 occur at the core site of PS109-25 (Fig. 4.1f(ii)). In this acoustic profile sub-parallel to the trough, AF12 is arranged in a massive and semi-transparent wedge-shaped unit which tapers towards the shelf edge, labelled SW-3 (Fig. 4.1f). SW-3 is underlain by AF2, and displays a v-shaped incision on its upper surface. The PS109-25 core was recovered entirely from AF12 at the seaward end of SW-3.

4.5.2 Core lithology

PS109-25 contains three lithofacies (Fig. 4.2c; 4.3c). Lithofacies 1 (LF1-25) (226.5-268cm) is a massive, matrix-supported, muddy diamicton (10 YR 4/2) (Fig. 4.3c). Shear strength is 10-20 kPa, and its bulk density is 0.5-2.3 g/cc (Fig. 4.2c). Magnetic susceptibility is 1-179 x 10^{-5} SI. The unit is clast rich, and clasts are subangular to subrounded, and up to pebble size. It lacks a sharp contact with the unit above.

Lithofacies 2 (LF2-25) (130-226.5 cm) is a stratified, matrix-supported diamicton, which fines upward into a massive silt with clay and clasts in the upper 11 cm of the lithofacies (Fig. 4.2c; 4.3c). Its colour transitions from dark greyish brown diamicton (2.5 YR 4/2) to dark brown diamicton (10 YR 4/3 – 4/2) to dark grey to dark greyish brown (2.5 YR 4/2 – 4/1) silty clay. Shear strength is 9-17 kPa and bulk density is 1.1-2.4 g/cc within the diamicton, and 2 kPa and 1.6-2.0 g/cc within the clayey silt above. Magnetic susceptibility displays variability throughout lithofacies 2 (Fig. 4.2c). It is 1-154 x 10^{-5} SI in the diamicton and 39-140 x 10^{-5} SI in the clayey silt above. LF2-25 is clast rich, and clasts are subangular to subrounded and up to pebble gravel sized (up to 4 cm a-axes). Some clasts are striated. The frequency of larger pebble size clasts decreases from 180 cm upwards. A 35 mm wide horizon with a very high clast frequency is identified (165-168.5 cm). Stratification within the diamicton is imparted by subtle changes in

grain size from clay rich to silt rich horizons of matrix. In some places, stratification is more pronounced where there are alternating beds (1 mm to few cms thick) of mud and sandy mud in the matrix of the diamicton. Discrete laminae of silt and clay up to 3 mm in thickness are present within LF2-25. These laminae lack clasts, and display both sharp and diffuse contacts with the surrounding diamicton (Fig. 4.3c). At 131 cm there is a single 2 mm sandy lamina. LF2-25 has a very sharp but non-planar contact with LF3-25 above (Fig. 4.3c).

Lithofacies 3 (LF3-25) (0-130cm) is a massive, matrix supported diamicton, with a matrix composed of silt, clay and fine sand grains (Fig. 4.3c). The upper 13 cm of the unit displays slight upward fining in the matrix. Matrix colour is brown (10 YR 4/4 - 4/3 - 4/2), with some very dark grey mottles (10 YR 3/1). Shear strength is 0.6 to 5.8 kPa and density is 1.0-2.3 g/cc (Fig. 4.2c). Magnetic susceptibility displays variability, from 1-273 x 10^{-5} SI, with a very high peak at 759 x 10^{-5} SI, but is generally higher than lithofacies 1 and 2. It has a lower clast frequency than lithofacies 1 and 2, and clasts are smaller (up to 25 mm a-axes). Clasts are subangular to rounded. LF3-25 contains multiple clay rich inclusions (Fig. 4.3c). These are 10-50 mm wide, and 3-20 mm thick, have a flattened circular shape, and have diffuse contacts with the surrounding diamicton. One of these inclusions displays evidence of boudinage. A clast (4 mm a-axis) is also present within one of these inclusions. In the lower part of the unit (112.5-122 cm) the matrix is stratified by multiple very diffuse coarser laminae (~3 mm thickness).

4.5.3 Micromorphology

Two thin sections from PS109-25 have been analysed, one from a depth of 209-215 cm (PS109-25a), within LF2-25, and another from a depth of 81-88 cm (PS109-25b), within LF3-175.

4.5.3.1 PS109-25a (209-215 cm – LF2-25)

PS109-25a consists of a brown to orange brown matrix-supported stratified diamicton. Skeleton grains are coarse silt to coarse sand (30-700 µm), and there are infrequent larger grains up to granule gravel size (up to ~3000 µm). There are some isolated areas with clusters of coarser grains (300-1500 µm). Stratification is imparted by sub-horizontal to inclined layers of diamicton, which can be distinguished based on subtle changes in plasma colour and skeleton grain frequency rather than changes in skeleton grain size (Fig. 4.13). Boundaries

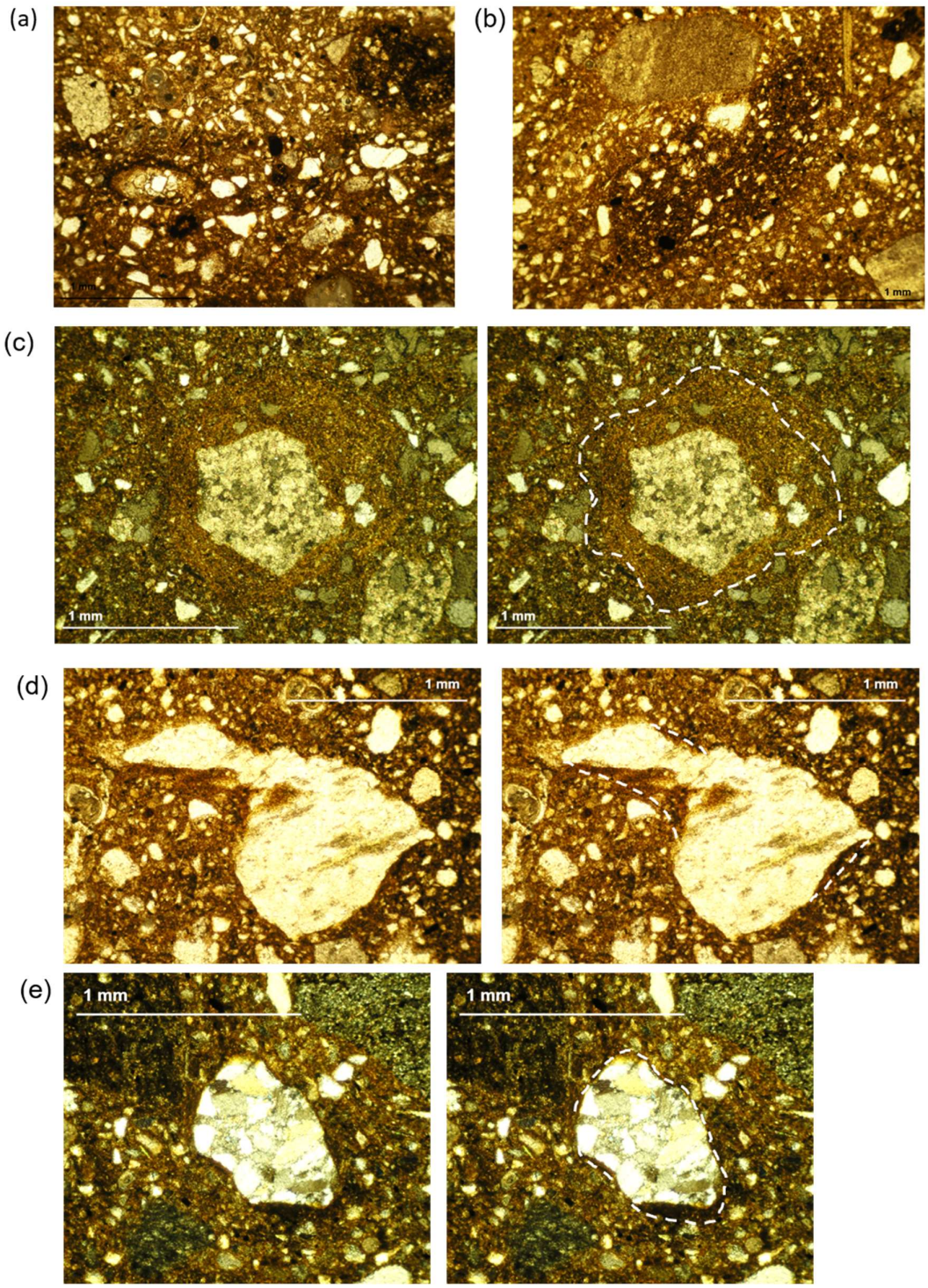

Figure 4.12 Photographs of microstructures present in PS109-25a. (a) Sharp boundary between different plasma colours (b) Pod structure (length = 2230 µm) (c) Thick grain coating (d) Grain coating infilling depressions on the grain surface (e) Grain coating which selectively thickens (f) Fine intraclasts with an example of boudinage (g) Skeleton grain turbate (h) Weakly developed augen structure (i) Vertical alignment of grains around a larger grain.

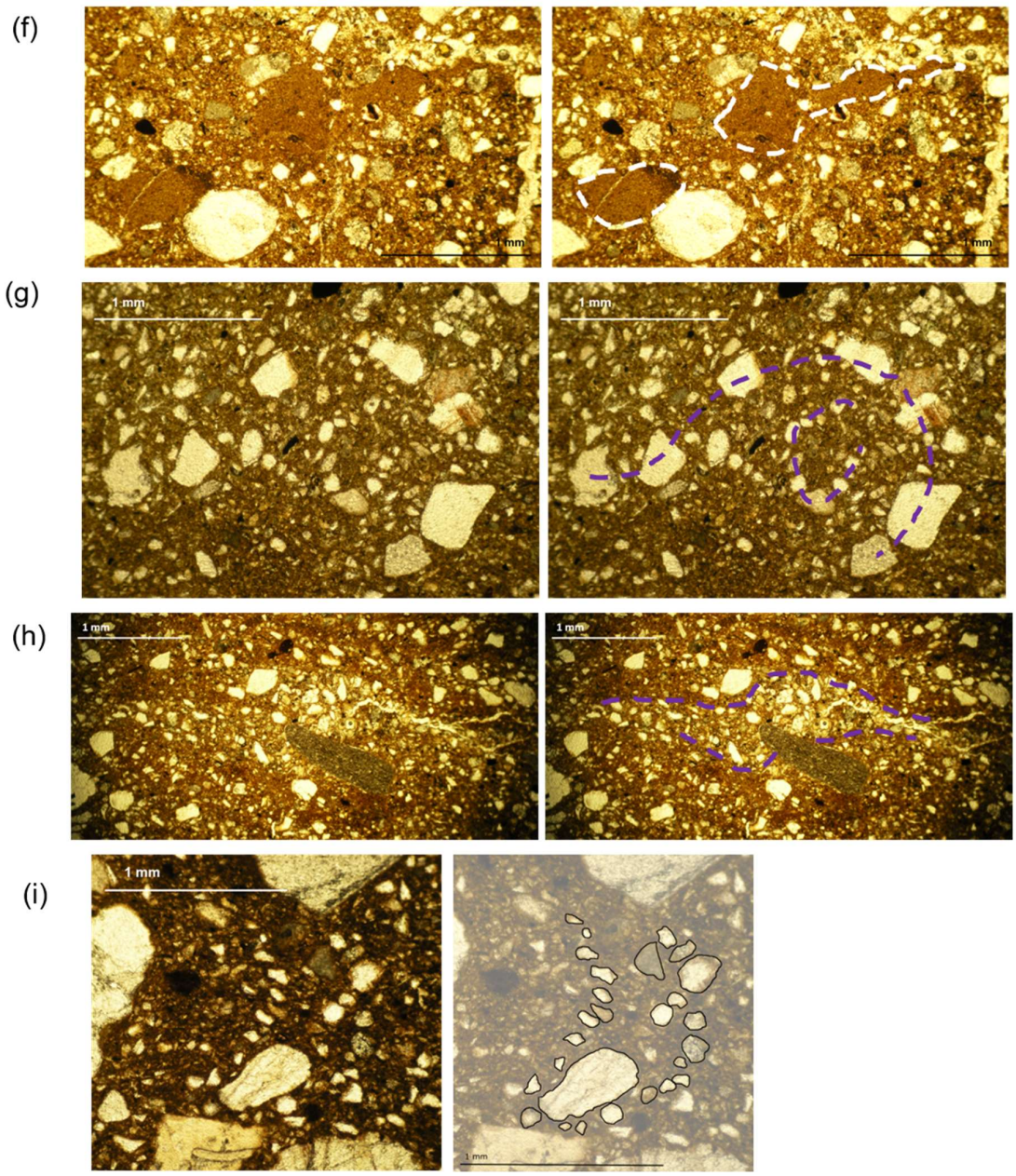

Figure 4.12 *Continued*

between bands of different plasma colour can be very diffuse to sharp, and can appear wavy (Fig. 4.12a). In places, very diffuse stringer-like bands of dark brown plasma can be seen. They range in length from 2800-4200 µm, and have the same inclination as the surrounding bedding.

Discontinuous diamictic pod structures are also present. They are identifiable by changes in matrix colour but have a similar texture to the surrounding sediment (Fig. 4.12b). These pod structures also have the same orientation as the

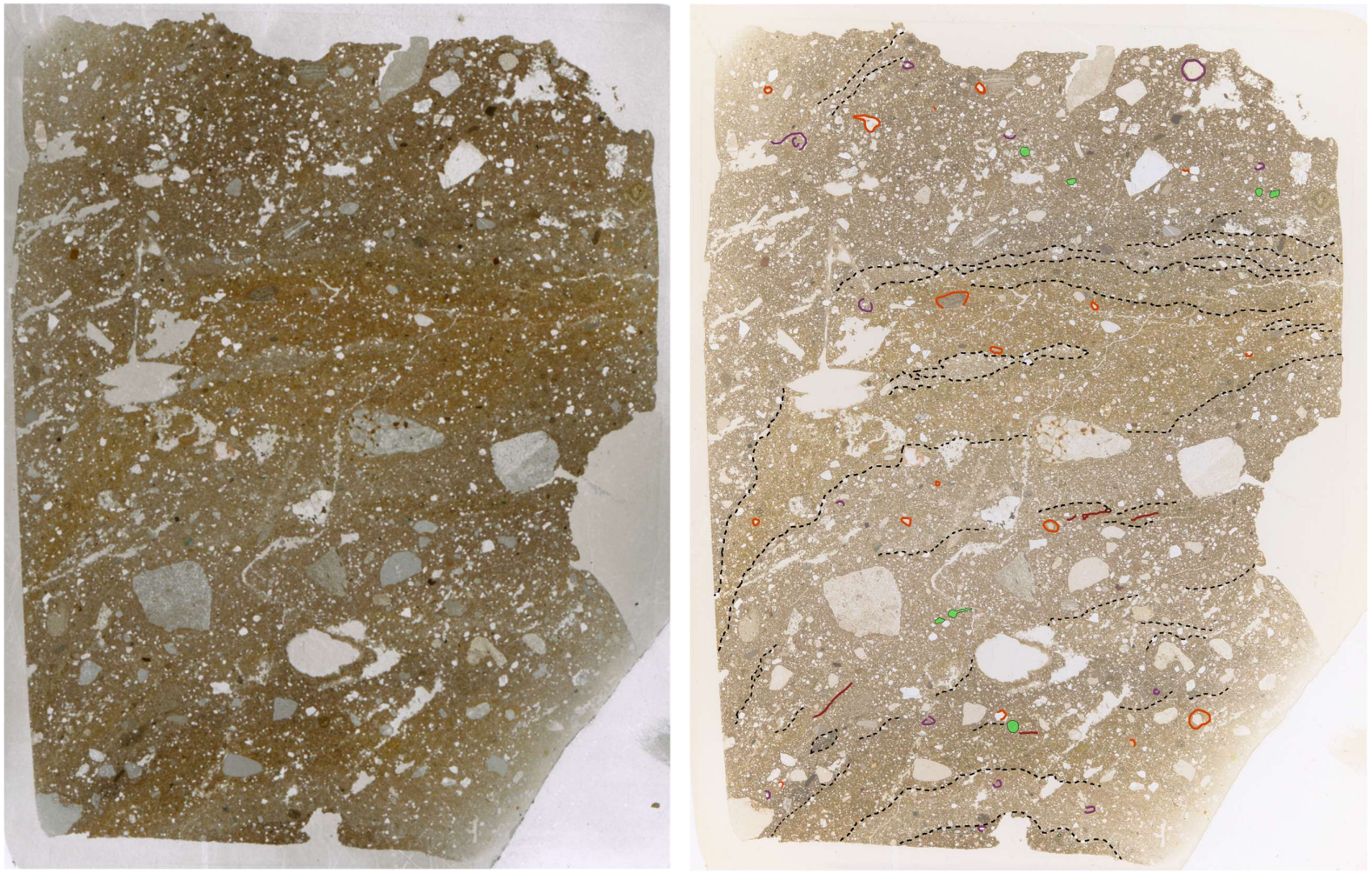

Figure 4.13 Thin section 'map' of PS109-25a showing the location of the identified microstructures. Green = intraclasts, red = stringers, purple = skeleton grain turbates/rotational structures, orange = grain coatings. Dashed black lines show bedding.

surrounding bedding. There are two large pod structures (4600 µm and 9400 µm long) with a necking structure between them in the centre of the slide (Fig. 4.13).

Coatings around skeletal grains are frequent (Fig. 4.16), with four types present: (1) grain coatings which are thick relative to the grain size and surround the entire grain (Fig. 4.12c), (2) thin coatings which surround the entire grain, (3) partial thin grain coatings (Fig. 4.12d), and (4) coatings which selectively thicken on one side of the grain (Fig. 4.12e). The thick coatings are comprised of silt and clay with some skeletal grains (diamictic), and occur less frequently than the thin coatings. Some thin coatings are made up only of clay or silt, whilst others contain some clay or silt with small skeletal grains. The partial coatings often infill depressions on the surface of the grain (Fig. 4.12d). They are both sharply and diffusely bounded. Plasmic fabrics have not been identified in any of the grain coatings.

Intraclasts also occur with moderate frequency (Fig. 4.16). Two different types are evident: (1) fine grained intraclasts composed of silt and clay (Fig. 4.12f), and (2) diamictic intraclasts. Both types have a circular to flattened circular shape. In one place there is evidence of boudinage, where a fine intraclast is deformed into an extended, stringer-like structure (Fig. 4.12f).

Multiple types of rotational features are evident. There are infrequent skeleton grain turbates, all of which are coreless (Fig. 4.12g; 4.16), and a single weakly developed augen structure comprised of skeletal grains and plasma (Fig. 4.12h; 4.16). A skeleton grain with crude evidence of rotation in the surrounding diamicton matrix is also present.

An isolated structure in which small skeletal grains aligned vertically around a larger skeletal grain is noted (Fig. 4.12i).

4.5.3.2 PS109-25b (81-88 cm – LF3-25)

PS109-25b is a massive, matrix-supported, orange brown diamicton (Fig. 4.15). There are changes in texture over the slide, imparted by poorly defined transitions in skeleton grain concentration. Some parts of the slide are skeletal grain supported with a limited plasma component (Fig. 4.14a).

Intraclasts are very frequent across the slide (Fig. 4.15; 4.16). They are composed of clay/silt, some with infrequent small skeleton grains, and have sharp boundaries with the surrounding diamicton. Intraclasts range in shape from circular, to

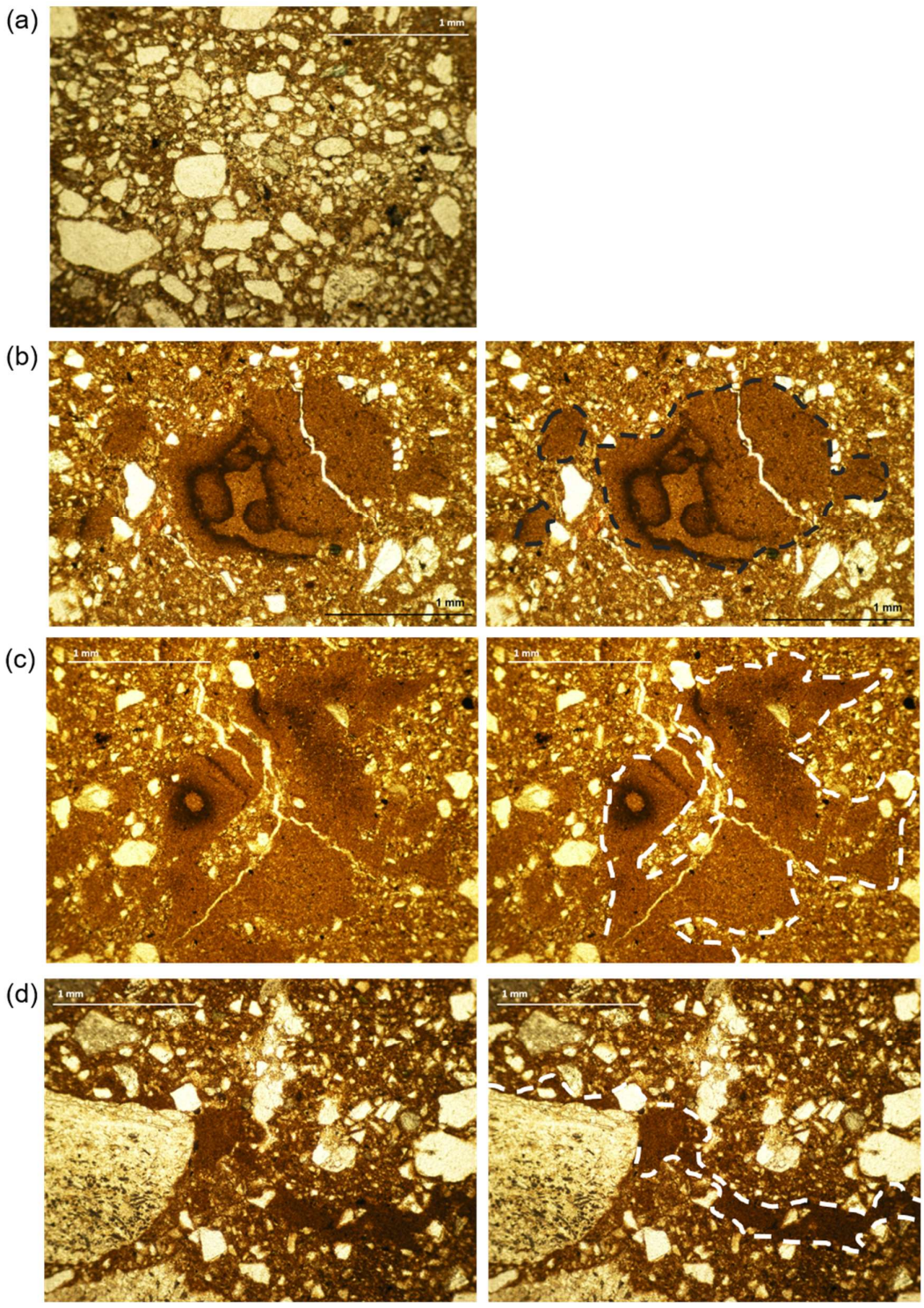

Figure 4.14 Photographs of microstructures present in slide PS109-25b (a) Skeletal grain supported diamicton (b) Circular to flattened circular intraclasts, with evidence of lateral smearing and detachment (c) Irregular shaped intraclast (d) Stringer extending from a skeletal grain with the same internal composition as the intraclasts (e) Diffuse stringer (f) Pipe structure (g) Horizontal pipe structure (h) Grain coating displaying lateral attenuation (i) Grain coatings with rounded edges

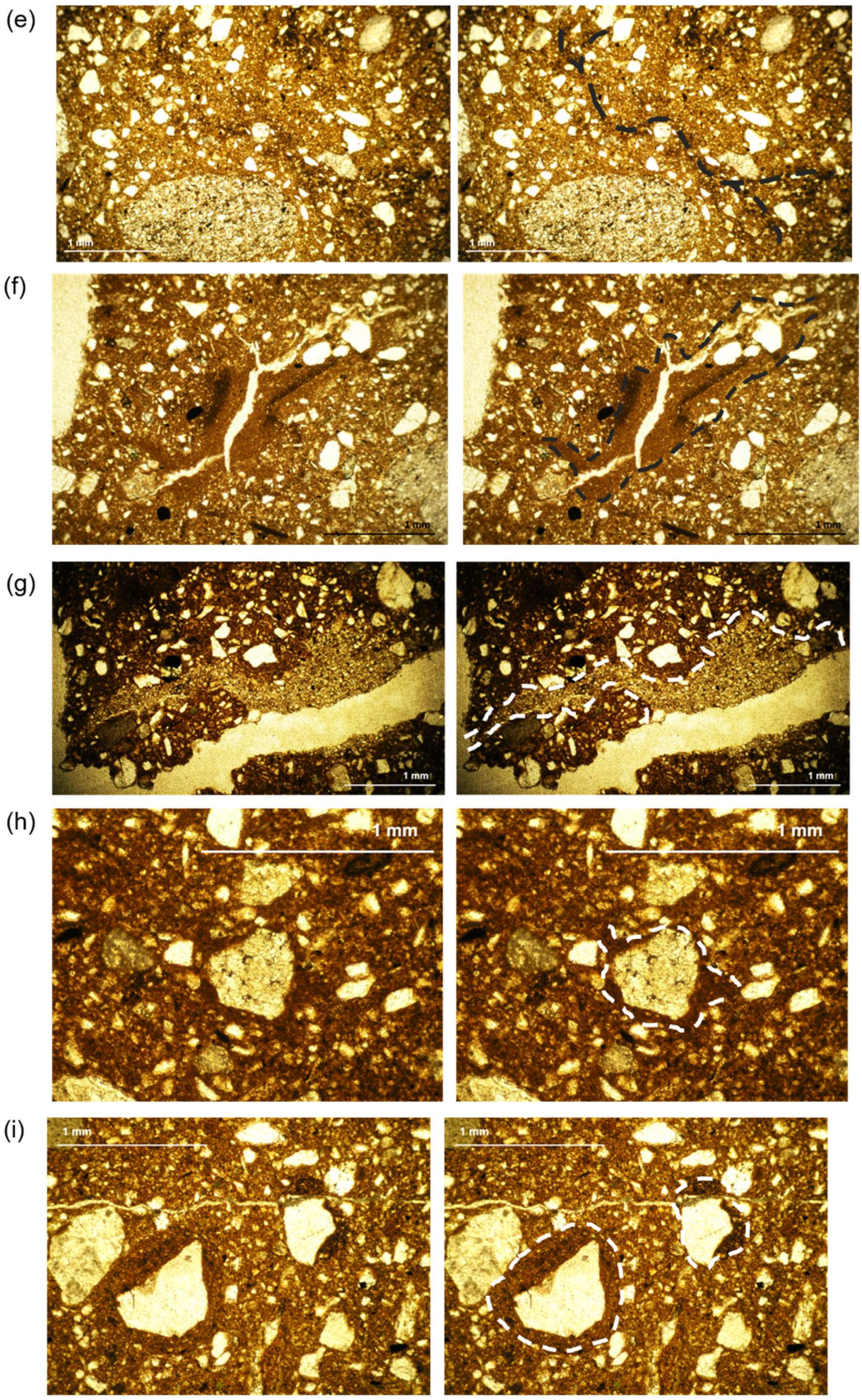

Figure 4.14 *Continued*

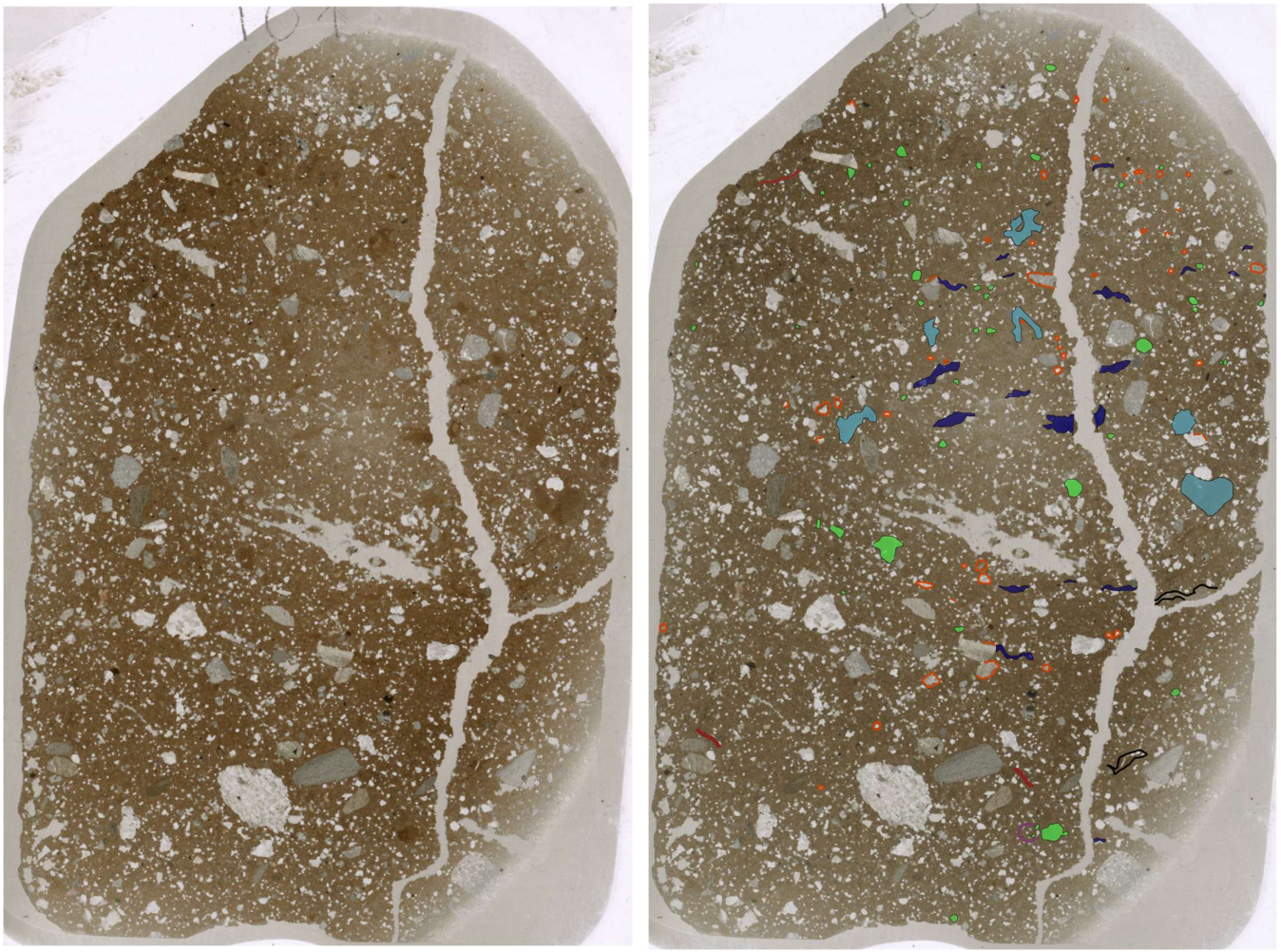

Figure 4.15 Thin section 'map' showing the location of microstructures. Green = circular intraclasts, light blue = irregular shaped intraclasts, purple = skeleton grain turbates, black = pipe structures, orange = grain coatings, dark blue = silt/clay stringers with the same composition as the intraclasts, red = diffuse stringers

flattened circular, to elongate (Fig 4.14b). There is a pair of circular diamictic intraclasts in the upper part of the slide, however diamictic intraclasts are not observed elsewhere. Many intraclasts are laterally smeared (Fig. 4.14b; 4.16), whilst some do not appear deformed. There are also some larger intraclasts with very irregular and often angular shapes (Fig. 4.14c; 4.15). Intraclasts are frequently transitional to more elongated stringer-like structures. Two types of stringer are evident (Fig. 4.15). The first type have the same composition (silt/clay) as the intraclasts, sometimes with small skeletal grains. These stringers occasionally appear to extend from large skeleton grains which are partially coated with clay/silt (Fig. 4.14d). The second type are more diffuse and thinner stringer-like structures composed of darker brown plasma and skeletal grains (Fig. 4.14e).

A sub-vertical pipe-like structure, infilled with unsorted clay, silt and small skeletal grains, is also identified (Fig. 4.14f). It has a sharp contact with the surrounding diamicton. There is also a horizontal pipe structure infilled with unsorted skeletal grains present in PS109-25b (Fig. 4.14g).

Some grains display massive coatings, 20-200 μm in thickness (Fig. 4.16). Some coatings are composed only of clay/silt, whilst others comprise clay/silt with skeletal grains. The first type of coatings composed of only clay/silt can surround the entire grain or infill depressions on the grain surface without fully covering the grain (Fig. 4.14h). They lack sharp contacts with the surrounding diamicton. The second type, which comprise clay/silt with some skeletal grains, have very rounded outer edges, and can be sharply or diffusely bounded with the surrounding diamicton (Fig. 4.14i). This second type of coating is thicker in relation to grain a-axes than the first type, with the ratio of coating thickness to grain a-axes 1:1.5-4.5, whilst for the first type the ratio is 1:10-26. Coatings composed only of clay/silt are 10-50 μm thick, whilst coatings that comprise clay/silt with skeletal grains are 75-250 μm thick. Plasmic fabrics have not been observed in the grain coatings. A grain coating displaying evidence of lateral attenuation has been identified (Fig. 4.14h).

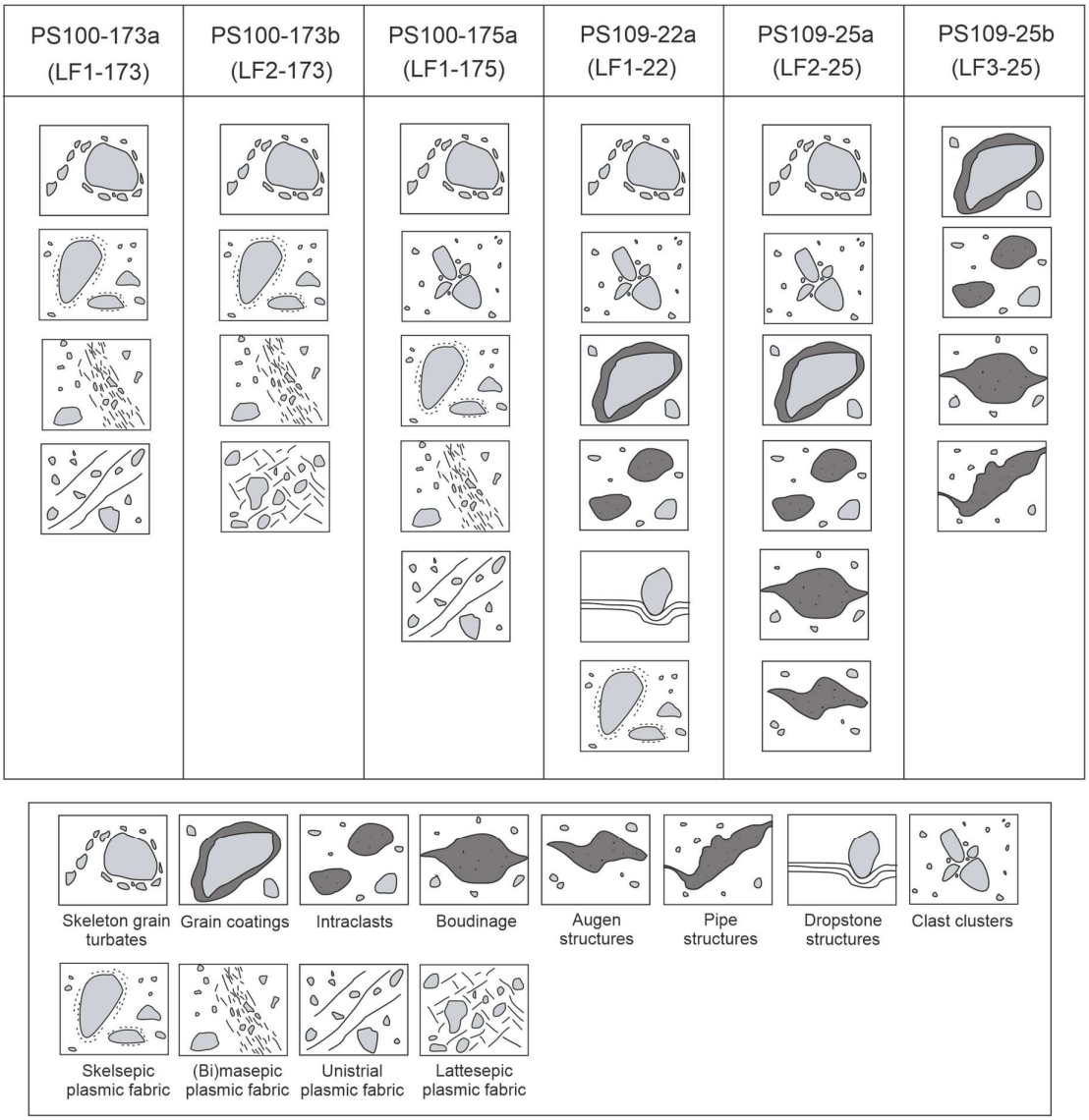

Figure 4.16 Comparison of the microstructures present on each slide, and the associated lithofacies that the thin section was from.

5. Interpretations

In this chapter, the depositional origin of the acoustic facies and sediment facies identified at and around the five core sites, which have been described above in Chapter 4, will be determined. It will be structured by outlining the formation of each acoustic facies, followed by, if applicable, the interpretation of the associated lithofacies using the available macro- and micro-scale sedimentary evidence. The lithofacies recovered from each acoustic facies, and their depositional origins, are summarised in Table 4.1.

5.1 Mid Norske: PS100-173

At the PS100-173 core site, LF1-173 and LF2-173 were recovered from AF5, and LF3-173 and LF4-173 were recovered from AF6 (Table 4.1; Fig. 4.2a).

5.1.1 AF2 and AF3

AF2 and AF3, which occur at the base of the acoustic sequence, are both interpreted as subglacial till. The structureless and acoustically transparent nature of AF3, overlying the strong upper reflector of acoustically transparent AF2, is a sequence found in other cross shelf troughs in both Greenland and Antarctica (Dowdeswell et al., 2004; Evans et al., 2005; 2006; 2009; Ó Cofaigh et al., 2005a; 2007; Mosola and Anderson, 2006; Larter et al., 2019). In these locations, the two acoustic units have been interpreted as a soft and porous till overlying a lower stiff till, the formation of which has been attributed to a combination of subglacial deformation and lodgement (Dowdeswell et al., 2004; Ó Cofaigh et al., 2005a; 2007) (Fig. 5.1). The structureless nature of AF2 and AF3 implies that the till has a massive structure (Evans et al., 2009). The buried dome-shaped mounds within AF3 are interpreted as cross-sections through buried subglacial bedforms (Evans et al., 2005; 2009).

5.1.2 AF4

AF4 is interpreted as drumlins (Fig. 4.1b; 5.2). The morphology of the dome-shaped sediment mounds comprising AF4 resembles drumlins previously reported from other contemporary and palaeo-ice sheets (e.g., Evans et al., 2005; King et al., 2007; Jakobsson et al., 2016; Ó Cofaigh et al., 2016a). Figure 4.1b was collected along a transect orientated sub-parallel to Norske Trough (see Fig. 4.1a), hence it conveys the long-axes of the drumlins in cross-section. The length of

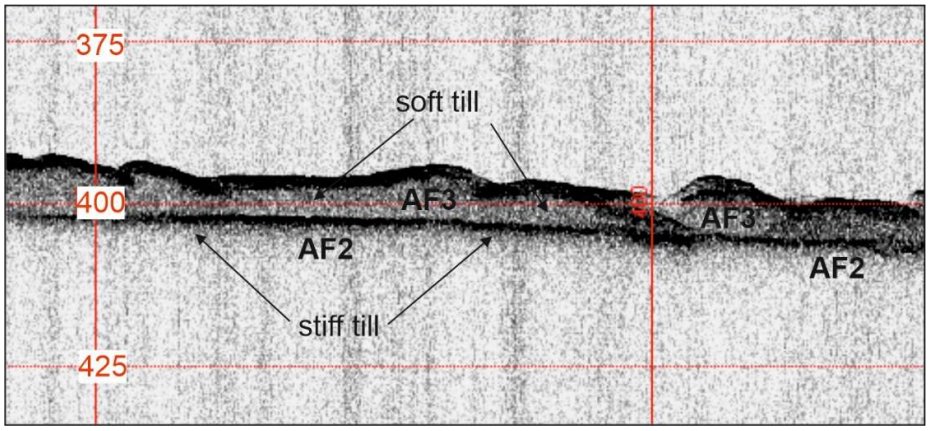

Figure 5.1 Parasound record showing the soft till and underlying stiff till. This profile is from the area adjacent to the core site of PS100-175.

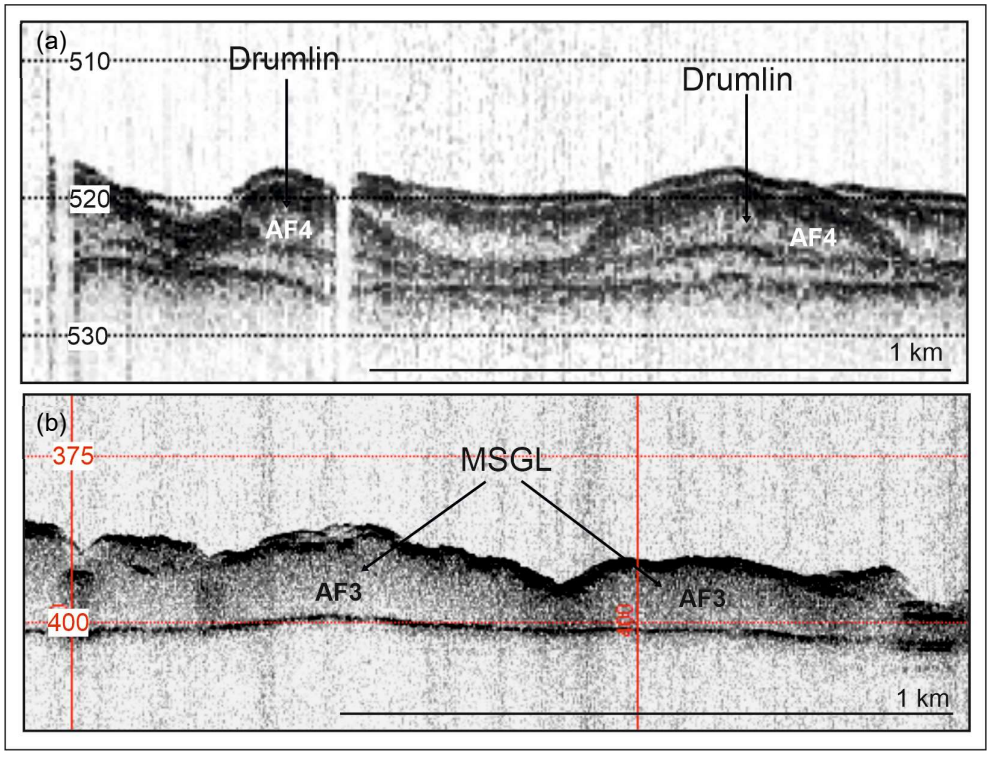

Figure 5.2 Parasound record showing (a) drumlins at the PS100-173 core site, and (b) MSGL adjacent to the core site of PS100-175.

these drumlins around the PS100-173 core site is 200-750 m, which is within the range of drumlin long-axes lengths reported by Clark et al., 2009. Their height range of 3.2-4.7 m is also consistent with heights of previously analysed drumlins (e.g., Ó Cofaigh et al., 2016a; Szuman et al., 2021). They have a similar acoustically transparent internal structure to AF2 and AF3, suggesting that they may also be composed of subglacial till.

5.1.3 AF5

AF5 is interpreted as glacimarine sediment based on its architecture, which infills depressions between AF3 and AF4 (Fig. 4.1b). LF1-173 and LF2-173 from core PS100-173 are both from AF5 (Fig. 4.2a; Table. 4.1). Glacimarine depositional processes were involved in the formation of both LF1-173 and LF2-173 (see sections 5.1.3.1 and 5.1.3.2 below), supporting a glacimarine interpretation of AF5. The slightly domed surfaces of AF5 in places (Fig. 4.1b) could suggest it was overridden and streamlined following its deposition. This is consistent with evidence of subglacial deformation and till deposition in LF1-173 and LF2-173 (see sections 5.1.3.1 and 5.1.3.2).

5.1.3.1 AF5 - Lithofacies 1 (LF1-173): Massive diamicton fining upward into clay with clasts

The massive and poorly sorted nature of the diamicton at the base of LF1-173 is characteristic of subglacial tills, and its shear strength (13-18 kPa) falls within the range for tills reported from other locations (0-40 kPa in Marguerite Bay; 0-120 kPa in Uummannaq Trough) (Ó Cofaigh et al., 2005a; 2013a; Sheldon et al., 2016). However, basal tills usually display sharp contacts with overlying glacimarine sediment due to the distinct change in depositional environment (Anderson et al., 1991; Evans et al., 2005), meaning the normal grading of the diamicton into clay is at odds with a subglacial origin for LF1-173.

A glacimarine depositional origin, followed by overriding and glacitectonism, is therefore proposed for LF1-173. Glacimarine deposition may have occurred at either a grounded tidewater margin or in a sub-ice shelf setting. In the case that LF1-173 was deposited at a grounded tidewater margin, suspension settling from iceberg rafting is suggested as the origin for the lower diamicton based on its massive and poorly sorted structure and the presence of clasts up to pebble size which lack alignment (Domack and Lawson, 1985; Dowdeswell et al., 1994a; Cowan et al., 1997; Ó Cofaigh et al., 2001). Sea ice can also transport and release sediment (Gilbert, 1990), however this sediment is predominantly fine grained (Nürnberg et al., 1994; Dowdeswell et al., 1998; Darby et al., 2009; 2011). Consequently, an iceberg rafting origin for diamicton is favoured. The upward fining of the diamicton into clay could reflect a transition to deposition dominated more by suspension settling from meltwater plumes (Gilbert et al., 1993; Hogan et

al., 2016; Sheldon et al., 2016; Streuff et al., 2017). The massive structure of this clay implies that it was deposited in an ice distal setting where only the finest sediment remained in suspension (Gilbert et al., 2002; Baeten et al., 2010; Hogan et al., 2016; Streuff et al., 2018). The continued but lower clast abundance within the upper part of LF1-173 suggests that deposition from iceberg rafting continued but decreased in dominance.

There is evidence in LF3-173 and LF4-173 from this core that deposition at this site might have taken place in a sub-ice shelf setting (see sections 5.1.4.1 and 5.1.4.2), which suggests that LF1-173 could also have been deposited in a sub-ice shelf setting, rather than at a grounded tidewater margin. In this case, the coarse grained diamicton of LF1-173 could alternatively have been deposited in a proximal sub-ice shelf environment by vertical rain-out from the base of an ice-shelf (Domack and Harris, 1998; Evans and Pudsey, 2002; Evans et al., 2005; Prothro et al., 2018; Smith et al., 2019). The upward fining of the diamicton to clay and the upward decrease in clast content could reflect a decrease in supply and rainout of coarse debris and an increase in deposition from turbid meltwater plumes in sub-ice shelf setting (Evans and Pudsey, 2002).

The presence of discontinuous and folded stringer-like structures composed of silty clay with sand grains in LF1-173 (Fig. 4.3a) suggests that it was glacitectonised within a subglacial shear zone following its deposition (Hart and Roberts, 1994; Roberts and Hart, 2005), driven by a re-advance of the ice margin. Although LF1-173 is from AF5, which has been interpreted as the product of glacimarine deposition, the slightly domed surface of some accumulations of AF5 might be evidence that it was overrun following its deposition. The discontinuous and attenuated nature of the stringers suggests that pockets of sediment with a slightly coarser texture than the surrounding clay were subject to simple shear which led to their extension, and are therefore tectonic laminae rather than a product of primary deposition (Fig. 5.3a – part A) (Hart and Boulton, 1991; Hart and Roberts, 1994; Hart, 2007). Rotation of particles has been suggested to be involved in stringer development, implying ductile deformation was taking place (Roberts and Hart, 2005). Simple shearing during ductile deformation was also responsible for the folding of these attenuated stringers (Hart and Roberts, 1994; Roberts and Hart, 2005; Hart, 2007; Phillips, 2018). The development of a

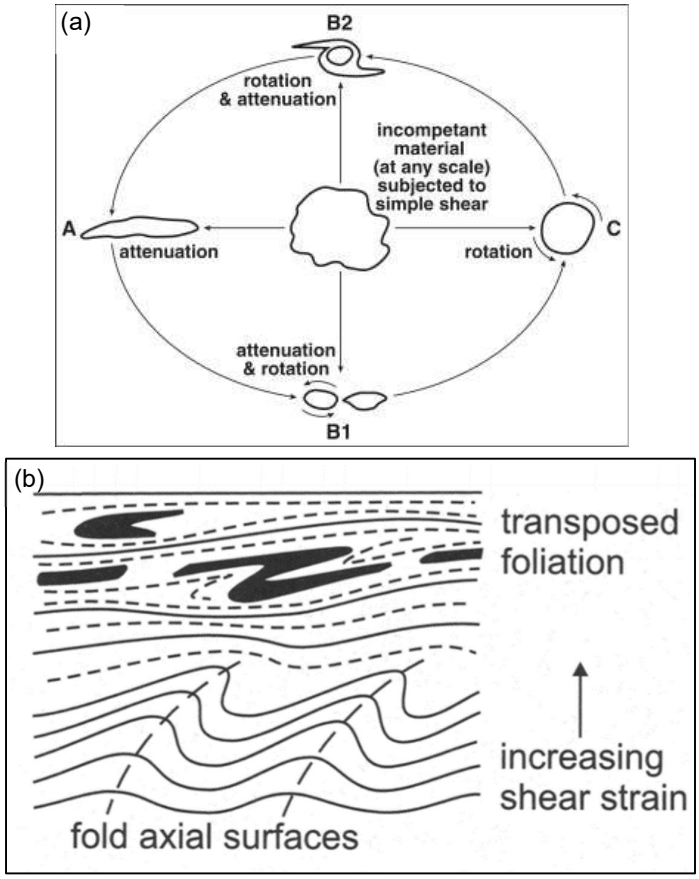

Figure 5.3 (a) Cycle of deformation for material undergoing simple shear. A = attenuation into tectonic lamination, B1 = continued deformation and boudin development, C = rotation to form circular structures, and B2 = rotation alongside attenuation leading to augen/galaxy structure development. From Hart (2007). (b) Model of fold development under compression and increasing shear strain. Folds axes become overturned and then detach as shear strain levels rise. From van der Wateren et al. (2000)

recumbent fold implies that a high level of shear strain was applied to allow the fold to become overturned (Fig. 5.3b) (van der Wateren et al., 2000).

The assemblage of microstructures observed in thin section PS100-173a, from the lower diamictic part of LF1-173, suggests that lithofacies 1 underwent subglacial deformation. Linear structures, such as the masepic and unistrial plasmic fabrics which are well developed in this sample (Fig. 4.16), are very prominent within subglacially deformed sediment from a range of localities (Table 5.1) (e.g., Hiemstra, 1999; 2001a; Carr, 2001; Hiemstra et al., 2005; Ó Cofaigh et al., 2005a; 2013a; Carr et al., 2006; Reinardy et al., 2011; Narloch et al., 2012). Circular structures, often adjacent to linear structures, are also common (Table 5.1) (e.g., van der Meer and Hiemstra, 1998; Hiemstra, 1999; 2001a; Carr, 2001; Hiemstra et al., 2005; Ó Cofaigh et al., 2005a; Narloch et al., 2012), meaning the skeleton

grain turbates and skelsepic plasmic fabrics adjacent to masepic plasmic fabrics in thin section PS100-173a also support a subglacial origin.

The assemblage of microstructures in PS100-173a indicates that both planar and rotational deformation occurred. The formation of masepic plasmic fabric is attributed to shearing along planes (Hiemstra, 1999; Carr, 1999; Ó Cofaigh et al., 2005a). Isolated development of unistrial plasmic fabrics reflects localised areas of higher strain which allowed more discrete shear planes to develop (van der Meer, 1993). Shearing along planes takes place during brittle deformation (Menzies et al., 1997; van der Meer et al., 2003), with the uniform orientation of these planar plasmic fabrics indicating they were formed during the same period of brittle deformation. The presence of skeleton grain turbates is attributed to the rotation of single coarse grains or clusters of grains undergoing shear, which exerted stress on surrounding smaller grains and caused them to become aligned with the surface of the larger grains (van der Meer, 1993; 1997; Hiemstra and Rijsdijk, 2003). Turbates without corestones can be explained by spatial changes in water content and/or sediment texture within the deforming sediment which allowed centres of rotation to form (van der Meer, 1993). Evidence of rotational structures is indicative of ductile subglacial deformation (Menzies et al., 1997), which fits with the macroscale evidence of ductile deformation from the presence of stringers and folds. Skelsepic plasmic fabrics that entirely surround grains (Fig. 4.4c) were likely formed in a similar manner, by grain rotation causing the realignment of plasma around the grain surface (Hiemstra and Rijsdijk, 2003). Skelsepic fabrics adjacent to masepic fabrics were likely formed when planar shear induced rotation in adjacent grains (Hiemstra and Rijsdijk, 2003; Ó Cofaigh et al., 2005a). It is possible that skelsepic plasmic fabrics that partially surround grains (Fig. 4.4b) were formed by clay particles being compressed against grains under stress (Hiemstra, 2001b; Hiemstra and Rijsdijk, 2003). The presence of rotational structures indicative of ductile deformation, and shears which are associated with brittle deformation, suggests that lithofacies 1 underwent polyphase deformation (Menzies et al., 1997; Menzies, 2000).

5.1.3.2 AF5 - Lithofacies 2 (LF2-173): Massive to stratified, matrix-supported diamicton

LF2-173 is interpreted as subglacial till which transitions upward into a glacimarine diamicton. The massive and poorly sorted nature of the lower part of LF2-173 is

Table 5.1 Framework used to assist interpretation of the depositional origin of the thin sections. The microscale characteristics of sediment from different depositional environments reported in other studies is shown, alongside the characteristics of the six thin sections from this study, and comparison of microstructure presence/absence between the two was useful in establishing genetic origins. (-) indicates absence.

Depositional Process	Location and study	Skeleton grain and plasma structure	Intraclasts (plasma/ diamictic)	Boudinage	Coatings on skeleton grains (plasma/ diamictic)	Skeleton grain turbates	Grain clusters	Folding	Plasmic fabrics	Dropstones	Grain lineations	Grain fabric	Planar structures
PREVIOUS STUDIES													
Subglacial deformation	**Marguerite Bay, Antarctica (Ó Cofaigh et al., 2005a)**	Massive	-	-	-	Present, often adjacent to planar structures	-	Present, rare	Present, masepic and unistrial	-	Present	Grains sometimes aligned parallel to linear features	Present, frequent - fractures, elongate zones of plasma
	McMurdo Sound, Antarctica (Hiemstra, 1999)	Massive or stratified	Present, common, plasma and diamictic	Present, common to abundant	-	Present, rare to abundant	-	Present	Present, masepic and unistrial	-	-	-	Present
	Spitsbergen (Carr, 2001)	-	Present	Present	-	Present	-	-	Present, skelsepic, omnisepic, masepic and unistrial, weakly to well developed	-	Present	Present, bimodal arrangement of grains	Present
Suspension settling and iceberg rafting	**Marguerite Bay, Antarctica (Kilfeather et al., 2010) – ice distal suspension settling**	Massive, banding	Present but rare, plasma	-	-	-	-	-	-	-	Present but rare	Present, very poorly developed	Present, rare lineations
	Cooley Point, northeast Ireland (Kilfeather et al., 2010) – suspension settling	Steeply dipping banding. Pockets/ bands of coarse grains	Present as sorted sediment pockets	-	-	-	-	-	-	Present	Present, includes dropstone track lineations	-	-
	Linns, northeast Ireland (Kilfeather et al., 2010) – suspension settling and iceberg rafting	Steeply dipping banding. Pockets/ bands of coarse grains	Present as sorted sediment pockets	-	-	-	-	-	Present, well developed, unistrial and kinking	Present	Present, rare, includes dropstone track lineations	-	-
	Spitsbergen (Carr, 2001) – ice distal suspension settling and iceberg rafting	Coarse matrix	Present, rare	-	-	Present, very infrequent	-	-	Present but rare, masepic	Present	-	Vertical grain alignment	-

Table 5.1 *Continued*

Depositional Process	Location and study	Skeleton grain and plasma structure	Intraclasts (plasma/ diamictic)	Boudinage	Coatings on skeleton grains (plasma/ diamictic)	Skeleton grain turbates	Grain clusters	Folding	Plasmic fabrics	Dropstones	Grain lineations	Grain fabric	Planar structures
Localised debris flow	**Portballintrae, Northern Ireland (Kilfeather et al., 2010)**	Banded	Present but infrequent, plasma only	-	Present but poorly developed	Present but rare	-	-	-	-	Present	Some steeply dipping grains	Only grain lineations
	Marguerite Bay, Antarctica (Hiemstra, 2001a)	Massive to stratified	Present, plasma only	-	Present, frequent	Present	Present	-	Present but poorly developed	-	-	-	Very faint planar features
	McMurdo Sound, Antarctica (Hiemstra, 1999)	Massive	Present, rare to abundant, plasma and diamictic	-	Present	Present, rare to abundant	-	-	Skelsepic only, poorly developed	-	-	-	-
Iceberg scouring	**Scoresby Sund, Greenland (Kilfeather et al., 2010)**	Massive, coarse grained	-	Present	-	Present infrequent, poorly developed	-	-	Present, silasepic only	-	Present, frequent	Present	Present – grain lineations
	Scoresby Sund, Greenland (Linch and Dowdeswell, 2016)	Massive, banded	Present, frequent	-	-	Present, infrequent	Present	Present, moderate abundance	Present, rare skelsepic, frequent unistrial	Present, frequent	Present, rare	Present, sub-horizontal alignment	Present – normal faults, discrete shears, grain lineations
THIS STUDY													
Iceberg rafting and subglacial deformation	**Mid Norske Trough – PS100-173a**	Massive	-	-	-	Present, frequent	-	-	Very frequent skelsepic and masepic, one example of unistrial	-	-	-	Masepic and unistrial plasmic fabrics
Subglacial deformation	**Mid Norske Trough – PS100-173b**	Massive, some areas of high skeleton grain frequency	-	-	-	Present, frequent	-	-	Very frequent skelsepic, masepic and bimasepic, one example of lattesepic	-	-	-	Masepic plasmic fabrics

Table 5.1 *Continued*

Depositional Process	Location and study	Skeleton grain and plasma structure	Intraclasts (plasma/ diamictic)	Boudinage	Coatings on skeleton grains (plasma/ diamictic)	Skeleton grain turbates	Grain clusters	Folding	Plasmic fabrics	Dropstones	Grain lineations	Grain fabric	Planar structures
Iceberg rafting, followed by subglacial deformation and/or iceberg scouring	**Mid Norske Trough – PS100-175a**	Massive	-	-	-	Present, frequent	Present	-	Moderately frequent and poorly developed skelsepic and masepic. Single unistrial.	-	-	-	Masepic and unistrial plasmic fabrics
Suspension settling, iceberg rafting, small scale remobilisation	**Outer Westwind Trough – PS109-22a**	Stratified, imparted by changes grain size and plasma colour	Very frequent, plasma and diamictic	-	Very frequent, both diamictic and plasma	Present but poorly developed	Present	-	Very infrequent – single skelsepic	Present, infrequent	-	-	-
Suspension settling, reworked by subglacial deformation or mass flows	**Outer Westwind Trough – PS109-25a**	Stratified, imparted by changes in skeleton grain frequency and plasma colour	Moderately frequent, plasma and diamictic	Present, very infrequent	Frequent, both diamictic and plasma	Present, infrequent	Present, infrequent	-	-	-	-	-	-
Debris flow activity	**Outer Westwind Trough – PS109-25b**	Massive, some poorly defined transitions in skeleton grain frequency	Very frequent, mostly plasma and few diamictic	Present, frequent	Moderately frequent, both plasma and diamictic	-	Present	-	-	-	-	-	-

typical of subglacial tills (Boulton, 1987), and its stratigraphic position above a glacitectonite is consistent with a subglacial depositional environment. Its shear strength is low (5-18 kPa), however weak subglacial tills have been reported from other cross-shelf troughs (0-40 kPa in Marguerite Bay, 0-120 kPa in Uummannaq Trough) (Dowdeswell et al., 2004; Ó Cofaigh et al., 2005a; Sheldon et al., 2016).

The assemblage of microstructures in PS100-173b is very similar to those in PS100-173a, as well as those reported from other subglacially deformed sediments (Fig. 4.16; Table 5.1), supporting an origin for LF2-173 by subglacial deformation. The masepic plasmic fabrics evident in PS100-173b (Fig. 4.6d) are indicative of shearing along planes, whilst the skeleton grain turbates and skelsepic plasmic fabrics suggest rotational deformation occurred, as in PS100-173a (van der Meer, 1993; Hiemstra, 1999; Carr, 1999; Hiemstra and Rijsdijk, 2003; Ó Cofaigh et al., 2005a). The presence of a lattesepic plasmic fabric is also attributed to rotational deformation (van der Meer and Laban, 1990). However, structures on this slide must be interpreted with caution due to preparation related damage visible on the slide (Fig. 4.7). As in LF1-173, the association of brittle and ductile deformation structures are suggestive of polyphase deformation within LF2-173 (Menzies et al., 1997; Menzies, 2000), with the three sets of masepic plasmic fabrics pointing to three possible phases of brittle deformation (Fig. 4.7).

The planar and undisturbed interbedded contact of LF2-173 with LF3-173, and the presence of weak stratification developed in the upper part of the unit could suggest that only part of LF2-173 underwent subglacial deformation and that the upper part of the unit was deposited in a glacimarine environment. Thin section PS100-173b, which displays evidence of subglacial deformation, is from the lower part of LF2-173. A transition from subglacial to glacimarine deposition is supported by the upward decrease in shear strength in LF2-173 (Callard et al., 2020). The upper part of LF2-173 could have been deposited by iceberg rafting from a grounded tidewater margin due to its poorly sorted nature and the presence of pebble gravel sized clasts (Dowdeswell et al., 1994; Cowan et al., 1997; Ó Cofaigh et al., 2001). Matrix banding could have been imparted by sorting of rafted sediment as it settled through the water column, traction currents winnowing fine sediment following deposition, or re-sedimentation by mass flows (Ó Cofaigh et al., 2001). Alternatively, it could have been deposited by sub-ice shelf rainout if

deposition at this site took place in a sub-ice shelf environment (Domack and Harris, 1998; Evans and Pudsey, 2002; Evans et al., 2005).

5.1.4 AF6

AF6 is interpreted as a glacimarine mud deposited during ice stream retreat, based on its draped geometry and capping position in the sedimentary sequence. Similar acoustic units have been reported in Marguerite Trough and Disko Bay, and their formation is attributed to deposition by suspension settling of fine grained sediment in an ice distal glacimarine environment (Dowdeswell et al., 2004; Ó Cofaigh et al., 2005a; Hogan et al., 2011; 2012). The circular depressions with hummocky bases (width = 260-330 m, depth = 3.5-6.5 m) which incise the upper surface of AF3 and AF6 are interpreted as cross-sections through iceberg grounding pits, which are formed by icebergs impacting and rotating on the seafloor (Barrie et al., 1992; Syvitski et al., 2001; Dowdeswell et al., 2014). Previously reported iceberg grounding pits are described as circular/semi-circular depressions several hundreds of metres in diameter and ranging in depth from 5-25 m (Syvitski et al., 2001; Gales et al., 2016; Sacchetti et al., 2016; Stewart et al., 2016). This is consistent with the morphology of the hummocky depressions which occur around the PS100-173 core site. LF3-173 and LF4-173 were recovered from AF6 at core site PS100-173.

5.1.4.1 AF6 - Lithofacies 3 (LF3-173): Laminated clay

Lithofacies 3 is interpreted as a product of suspension settling from meltwater plumes based on its fine grained and cyclical nature, and the presence of undisturbed planar and parallel laminae (Gilbert, 1983; Elverhøi et al.,1983; Cowan and Powell, 1990; Ó Cofaigh and Dowdeswell, 2001). The cyclic nature of the laminae indicates that these plumes were released periodically, and the presence of coarse and fine couplets is attributed to differential rates of settling of coarse and fine particles (Cowan and Powell, 1990; Cowan et al., 1999; Ó Cofaigh and Dowdeswell, 2001). Over the transition from LF3a-173 to LF3b-173, laminae thickness decreases, and the coarser laminae become thinner than their finer counterparts. This is interpreted to reflect a decrease in sedimentation rate driven by minor grounding line recession (Ó Cofaigh and Dowdeswell, 2001; Forwick and Vorren, 2009; Streuff et al., 2018). The upward transition to diffuse contacts between laminae and the increase in thickness of the finer laminae as the unit transitions into LF3c-173, reflects an increasingly ice-distal sediment source, from

which predominantly finer-grained sediment reaches the core site (Streuff et al., 2017; 2018).

The near complete absence of sand grains and the very low clast concentration could indicate that this unit was deposited by rain-out below an ice shelf, but distal from the grounding line (Alley et al., 1989; Evans et al., 2005). This is consistent with the transition from very low clast content at the base of the lithofacies to an absence of clasts above. Alternatively, suspension settling deposits with very low clast content can also be attributed to large volumes of meltwater masking deposition from iceberg rafting (Gilbert et al., 2002; Hogan et al., 2016; Streuff et al., 2017), so the low clast occurrence is not necessarily diagnostic of ice-shelf presence.

5.1.4.2 AF6 - Lithofacies 4 (LF4-173): Massive diamicton fining upward into massive clay

LF4-173 was deposited by iceberg rafting and suspension settling from meltwater plumes. The massive and unsorted nature and low shear strength of the diamicton indicates that it was deposited by iceberg rafting (Dowdeswell et al., 1994a; 2000; Cowan et al., 1997; Ó Cofaigh et al., 2001; Callard et al., 2020). Genesis of the fine grained laminae within the diamicton is attributed to periods of increased suspension settling relative to iceberg rafting (Jennings and Weiner, 1996). The massive, fine-grained nature and low shear strength of the clay above is characteristic of deposition by suspension settling in a more ice distal environment, with clast presence representing the occasional contribution from iceberg rafting (Batchelor et al., 2011; Hogan et al., 2016; Callard et al., 2018). The upward colour transition from brown to olive brown in the massive clay likely reflects a transition from deposition in an ice distal glacimarine environment to an open marine environment (Smith et al., 2011; Hogan et al., 2016). This is because green colouration of sediment can indicate that it is rich in diatoms, suggesting that the sediment was deposited during a period of higher biological productivity (Kilfeather et al., 2011; Smith et al., 2011). This increased productivity could have been driven by a post-glacial rise in ocean temperature (Hogan et al., 2016).

Alternatively, it is possible that LF4-173 was deposited in an ice shelf setting. The diamicton at the base of LF4-173 could have been deposited by iceberg rafting as the calving zone of an ice shelf passed over the core site (Domack and Harris,

1998; Domack et al., 1999; Kilfeather et al., 2011; Yokohama et al., 2016; Smith et al., 2019). The olive brown muds with occasional IRD above the diamicton could have been deposited by suspension settling in ice distal to an open marine environment beyond the calving line (Kilfeather et al., 2011; Smith et al., 2011; 2019). Iceberg rafted diamicton (LF4-173), overlying sediment deposited by suspension settling from meltwater plumes (LF3-173; see section 5.1.4.1), is part of the idealised facies succession associated with an ice shelf environment (Fig. 2.6) (Domack and Harris, 1998; Smith et al., 2019).

5.1.5 AF10

AF10 is interpreted as the product of localised mass flow activity based on its discontinuous and acoustically transparent nature, and lenticular geometry (Dowdeswell et al., 2010; Hogan et al., 2011; 2012; Callard et al., 2018).

5.2 Mid Norske Trough: PS100-175

Three acoustic facies (AF2, AF3 and AF6) were identified around the PS100-175 core site. LF1-175 and LF2-175 from core PS100-175 were recovered from AF6 (Table 4.1; Fig. 4.1c; 4.2a).

5.2.1 AF2 and AF3

AF2 and AF3, which have been interpreted as subglacial tills (see section 5.1.1), are also present at the base of the acoustic sequence at PS100-175 (Fig. 4.1c; 5.1). The hummocks on the upper surface of AF3 are interpreted as MSGLs based on their resemblance to MSGLs from other cross-shelf troughs, including the nearby Westwind Trough (Fig. 5.2) (Evans et al., 2005; 2009; Ó Cofaigh et al., 2005a; 2016b; Arndt and Evans, 2016). These hummocks are ~100-500 m wide, which is consistent with the width of ~350 m reported for MSGLs in Westwind Trough (Arndt and Evans, 2016), and MSGLs which have a width of 100-600 m in Marguerite Trough (Ó Cofaigh et al., 2016b). The presence of lineations on the surface of AF3, which form subglacially (Clark, 1993; Ó Cofaigh et al., 2005a; 2013b; Stokes et al., 2013b; Spagnolo et al., 2014; Piasecka et al., 2018), provides further support for an interpretation of subglacial till for AF3.

5.2.2 AF6

AF6 is discontinuously present above AF3 and is interpreted as a glacimarine drape deposited by subaqueous processes based on its draped morphology and its capping position in the acoustic sequence (see section 5.1.4). LF1-175 and

LF2-175, which were both recovered from AF6, were deposited by glacimarine processes (see sections 5.2.2.1 and 5.2.2.2), providing further support for the interpretation of AF6 as a glacimarine drape. The hummocky upper surface of AF6 at this site (Fig. 4.1c) could indicate that it was overridden and reworked subglacially following its initial deposition, with the hummocks representing glacial lineations (Evans et al., 2005; 2009).

The v-shaped incisions on the surface of AF6 (width = 50-60 m, depth = 2.8-3.3 m) are interpreted as iceberg scours formed by iceberg keels ploughing through the seafloor (Woodworth-Lynas et al., 1991; Dowdeswell et al., 1993; 2014; Evans et al., 2005). Cross sections through previously reported furrows produced by iceberg scouring in Greenland and Antarctica show a similar highly irregular, v-shaped morphology to those around the core site of PS100-175 (e.g., Syvitski et al., 2001; Evans et al., 2005; Larter et al., 2012; Gales et al., 2016). Furthermore, these furrows in Norske Trough have similar dimensions to the small furrows 50-200 m wide reported from Rockall Bank in the northeast Atlantic (Sacchetti et al., 2016). The larger depressions with hummocky bases on the upper surface of AF3 and AF6 (320-660 m wide, 3.8-6.4 m deep) are interpreted as iceberg grounding pits, formed by iceberg impact and rotation, the same as the grounding pits adjacent to the core site of PS100-173 (Barrie et al., 1992; Syvitski et al., 2001; Dowdeswell et al., 2014). Both AF3 and AF6 are incised by these furrows and pits, suggesting that these features produced by iceberg action were most likely formed following the deposition of AF6. Their frequency indicates that this region was subject to intense iceberg scouring. The seafloor is 380-400 m deep at this site, which fits with the observation of Dowdeswell et al. (1993) from Scoresby Sund and the adjacent east Greenland continental shelf that the most intense scouring takes place between 300-400 m depth.

5.2.2.1 AF6 - Lithofacies 1 (LF1-175): Massive, matrix-supported diamicton

The association of LF1-175 within AF6 suggests that it was deposited by glacimarine processes. This is supported by its massive and poorly sorted nature, and the frequent presence of clasts up to large pebble size (Fig. 4.3a) suggestive of deposition by iceberg rafting (Dowdeswell et al., 1994a; Cowan et al., 1997; Smith and Andrews, 2000; Ó Cofaigh et al., 2001). The sub-vertical clast alignment is indicative of clasts settling through the water column, a further indication that LF1-175 was deposited by iceberg rafting (Domack and Lawson,

1985). Its gradational contact with LF2-175 also supports a glacimarine origin (Ó Cofaigh et al., 2001). The decrease in clast frequency from 36 cm upwards through the facies reflects a relative decrease in the contribution from iceberg rafting. Banding and lamination in the upper part of LF1-175 could be attributed to a greater role of suspension settling in deposition, which imparts stratification by causing variation in mud supply (Powell, 1984), perhaps augmented by sediment gravity flows.

The microscale characteristics of LF1-175 also indicate a glacimarine origin. The patchy areas of plasma with a wispy appearance that are evident in thin section PS100-175a are indicative of deposition by suspension settling from different meltwater plumes (Kilfeather et al., 2010). However, PS100-175a also displays some micromorphological evidence of secondary deformation. The planar plasmic fabrics (masepic and unistrial), skelsepic plasmic fabrics and skeleton grain turbates evident in this thin section are commonly associated with subglacially deformed sediment (Table 5.1) (Hiemstra, 1999; Carr, 2001; Ó Cofaigh et al., 2005a). This suggests that the ice margin may have re-advanced over the core site following the deposition of LF1-175, and thus that LF1-175 could be a glacitectonite. This interpretation is also supported by the hummocky upper surface of AF6 in acoustic profile (Fig. 4.1c), which is consistent with streamlining following its deposition (see section 5.2.2 above).

Evidence of iceberg scouring adjacent to the core site could also suggest that the deformation of LF1-175 evident in thin section PS100-175a is related to icebergs grounding on the seafloor. Both skeleton grain turbates and skelsepic plasmic fabrics have been reported from iceberg turbated diamictons in Scoresby Sund, the formation of which is attributed to rotation driven by either downward stress from an iceberg keel or by the initial impact of the iceberg keel in the sediment (Table 5.1) (Kilfeather et al., 2010; Linch and Dowdeswell, 2016). Linch and Dowdeswell (2016) report that masepic plasmic fabrics are rarely encountered in ice-keel scoured sediment, and conclude that they cannot necessarily be attributed to scouring. Thus, a scouring origin may be inconsistent with the occurrence of masepic plasmic fabrics in PS100-175a. However, features indicative of planar shear (unistrial plasmic fabrics, augens, discrete shears and grain lineations) are also found in iceberg turbated sediments (Table 5.1) (Kilfeather et al., 2010; Linch and Dowdeswell, 2016). Planar shear leads to the

development of failure planes when sediment undergoes compression and extension as the keel advances through the sediment (Woodworth-Lynas and Guigné, 1990; Woodworth-Lynas et al., 1991; Linch et al., 2012; Linch and Dowdeswell, 2016). Consequently, masepic plasmic fabrics, which also develop under planar shear (van der Meer, 1993), could be explained by iceberg scouring. Furthermore, this is supported by the appearance of some examples of masepic plasmic fabrics in PS100-175a, which appear as very short but discrete dashes of plasma (Fig. 4.8d) rather than bands of plasma. This particular type of masepic plasmic fabric could represent weakly developed discrete failure planes, possibly an early stage of unistrial plasmic fabric development, which is consistent with the findings of Linch and Dowdeswell (2016) that iceberg scoured sediments display frequent unistrial plasmic fabrics. The combination of microscale evidence of deformation in LF1-175 with the iceberg furrows and grounding pits around the PS100-175 core site provides a compelling case for iceberg scouring having occurred in this area.

5.2.2.2 AF6 - Lithofacies 2 (LF2-175): Massive olive brown clay

The massive, fine-grained nature and olive brown colour of LF2-175 suggests that it was deposited by suspension settling in an ice distal to open marine setting (Kilfeather et al., 2011; Hogan et al., 2016), with the minimal clasts in the lower 8 cm of the unit representing a small contribution from iceberg rafting. As with LF4-173, the green colour of the sediment is indicative of deposition during a period of higher productivity, implying warmer ocean temperatures in a post-glacial open marine setting (Kilfeather et al., 2011; Smith et al., 2011; Hogan et al., 2016).

5.3 Inner Norske Trough: PS100-208

The thick sediment pile (up to ~95 m) adjacent to the core site of PS100-208, which comprises AF7-AF11, is located within a basin between two bedrock highs. The PS100-208 core was recovered from AF9 in the centre of the basin (Fig. 4.1d). This type of thick sediment accumulation is characteristic of deposition during a period of ice retreat in which ice stabilised on a bedrock high and sediment accumulated in the basin adjoining (Seramur et al., 1997; Ó Cofaigh et al., 2001; 2016c; Hogan et al., 2011; 2012). This indicates that most of these acoustic facies were likely deposited by processes in an ice proximal environment during deglaciation.

5.3.1 AF1

AF1 is interpreted as seafloor bedrock based on its thin and impenetrable nature, as is found in other Greenland cross-shelf troughs (Dowdeswell et al., 2010; 2014).

5.3.2 AF7

AF7 is interpreted as a product of glacimarine suspension settling and sediment gravity flow processes based on its infilling geometry and its stratification (Hogan et al., 2012). The contorted nature and weakness of the stratification implies reworking, most likely by sediment gravity flows or turbidity currents (Ó Cofaigh et al., 2001; Hogan et al., 2012).

5.3.3 AF8

A glacimarine origin is proposed for AF8 because of the way it infills basins and drapes topographic highs. The acoustically stratified beds are attributed to suspension settling and/or turbidity current deposition (Ó Cofaigh et al., 2001; 2016c; Ó Cofaigh and Dowdeswell, 2001; Hogan et al., 2012). The acoustically massive and transparent nature of the intervening sediment layers is indicative of a diamictic texture, the genesis of which could be related to debris flow activity (Hjelstuen et al., 2009; Lysså et al., 2010; Callard et al., 2018). This suggests that AF8 comprises interbedded suspension settling and gravity flow deposits. The hummocky bottom reflector, and the way in which the internal reflectors are discontinuous, contorted, or offset in places, is also consistent with a mass flow origin (Ó Cofaigh et al., 2001).

5.3.4 AF9

Based on its conformable nature, parallel and closely spaced undisturbed internal reflectors and its smooth upper reflector, the genesis of AF9 is attributed to glacimarine processes which produce stratified deposits, including suspension settling, turbidity currents and bottom current activity (Ó Cofaigh and Dowdeswell, 2001; Hjelstuen et al., 2009; Lysså et al., 2010). Core PS100-208 was recovered from AF9.

5.3.4.1 AF9 - Lithofacies 1 (LF1-208): Laminated silty clay

LF1-208 is interpreted as the product of suspension settling from meltwater plumes. This is based on its fine grained nature and predominantly rhythmic

bedding imparted by alternating coarse and fine laminae/beds of silty clay (Ó Cofaigh et al., 2001; Ó Cofaigh and Dowdeswell, 2001). A suspension settling origin is also supported by its low shear strength (2-15 kPa) and evidence of gradational contacts between laminae (Phillips et al., 1991; Cowan et al., 1997). The fine bedding (up to 9 mm thick coarse laminae separated by fine laminae/beds 1-50 mm thick) in the lower 372 cm of the core (between 534-906 cm) (Fig. 4.3b) is indicative of deposition in an environment in which pulsatory meltwater discharge formed overflow plumes from which packages of sediment settled in succession (Elverhøi et al., 1983; Mackiewicz et al., 1984; Cowan et al., 1997; 1999; Evans et al., 2002). Each pair of laminae most likely corresponds to an individual meltwater plume event (Mackiewicz et al., 1984). Within each plume, coarse grained material settled through the water column at a faster rate, laying down a discrete coarse laminae (Cowan and Powell, 1990; Phillips et al., 1991; Cai et al., 1997). The finer grains settled more slowly and continuously in the background, often flocculating as they settled through the water column, to form the finer laminae above (Cowan and Powell, 1990). Laminated muds related to suspension settling from meltwater plumes are usually deposited in a grounding line proximal setting (Jaeger and Nittrouer, 1999; Forwick and Vorren, 2009; Streuff et al., 2018)

From 218-534 cm the silty clay in LF1-208 becomes more thickly bedded, with individual beds measuring 1-60 mm in thickness, and generally greater than 10 mm (Fig. 4.3b). The thickness of individual beds is highly irregular but generally increases upwards through this section. The fine grained nature of the sediment, and generally planar and parallel bedding, suggests that deposition was still taking place by suspension settling from meltwater plumes. The increasing laminae/bed thickness could have been driven by the ice margin becoming more proximal in relation to the core site, because the sediment content of meltwater plumes and sedimentation rate increases with proximity to the ice margin (Lemmen, 1990; Dowdeswell et al., 1998; Jaeger and Nittrouer, 1999). This would lead to larger packages of sediment being deposited at the core site from each pulse of meltwater. The internal lamination (mm scale) present in some fine and coarse beds (Fig. 4.3b) could be related to pulsation within individual plumes which caused sorting during deposition (Phillips et al., 1991).

There is evidence that deposition by turbidity currents was also taking place alongside suspension settling from overflow plumes during the deposition of LF1-208. Turbidity currents are common in ice proximal glacimarine environments, triggered by the failure of over-steepened sediment piles or by the development of turbid underflows as meltwater with a high sediment concentration emerges from the grounding line (Cowan and Powell, 1991; Gilbert, 1992; Gilbert et al., 1993; Ó Cofaigh and Dowdeswell, 2001). This provides further evidence that the deposition of LF1-208 took place relatively proximal to the grounding line. The occurrence of faint cross lamination at 826-832 cm, consistent with Division C of the Bouma sequence (Fig. 2.4), is indicative of deposition from a dilute and fine grained turbulent flow (Talling et al., 2012). Reverse graded beds could also be related to turbidity currents (Lemmen, 1990; Phillips et al., 1991; Hein and Syvitski, 1992), deposited during accelerating turbidity current flow (Mulder and Alexander, 2001; Talling, 2014). Cross-lamination and reverse grading occur infrequently in LF1-208, implying that turbidity current activity had a more limited role in deposition in comparison with suspension settling from meltwater plumes. Although planar lamination can be the product of turbidity currents (Talling et al., 2012), the formation of the alternating coarse and fine laminae that comprise the majority of LF1-208 has been attributed to suspension settling rather than turbidity current activity because the characteristics of laminated fine grained turbidites (e.g., eroded or loaded contacts, laterally discontinuous/irregular shaped laminae, and dewatering structures; Ó Cofaigh et al., 2001) are very infrequent or absent in LF1-208.

There are two possible explanations for the almost complete absence of clasts between 534-906 cm in LF1-208. Firstly, high rates of suspension settling from meltwater plumes could have overwhelmed the rate of IRD deposition (Elverhøi et al., 1983; Cowan et al., 1997; Gilbert et al., 2002; Streuff et al., 2017). The subsequent introduction of clasts between 218-534 cm, and their gradual upward increase in frequency, could have been related to an increase in deposition by iceberg rafting (Svendsen et al., 1992; Evans et al., 2002; Kempf et al., 2013). The other possibility is that an absence of clasts could indicate the presence of an ice shelf over the core site which prevented iceberg rafting from taking place (Alley et al., 1989).

The frequent normal faults which offset the laminae/beds throughout LF1-208 could indicate that the sediment pile underwent brittle deformation following its deposition (Martín-Chivelet et al., 2011). Brittle deformation could have resulted from sliding or slumping of the sediment pile following deposition, likely driven by depositional oversteepening due to high sedimentation rates from overflow plumes (Elverhøi et al., 1983; Cowan and Powell, 1991). Alternatively, soft sediment deformation structures such as normal faults can also be produced by synsedimentary deformation (van der Meer and Warren, 1997; Hoffmann and Reicherter, 2012). A syndepositional origin for these normal faults is perhaps more likely because LF1-208 is within AF9 which occurs on the basin floor. The low gradient of the basin floor means that the sediment pile would have been less prone to oversteepening. Furthermore, the largely undisturbed stratification displayed by AF9 suggests that the facies did not undergo significant reworking by sliding or slumping.

5.3.4.2 AF9 - Lithofacies 2 (LF2-208): Massive to stratified gritty silt and clay

LF2-208 is interpreted as the product of suspension settling from meltwater plumes and iceberg rafting. The deposition of the stratified silty clay with a low sand abundance present between 177-218 cm is attributed to suspension settling from meltwater plumes based on its fine grain size, planar bedding, and low shear strength (Ó Cofaigh and Dowdeswell, 2001). The formation of alternating planar beds of silty clay and silty clay with sand is related to differential rates of settling from overflow plumes (Cowan and Powell, 1990; Phillips et al., 1991). The deposition of the massive silty clay with sand (104-117 cm) is also attributed to suspension settling (Gilbert et al., 1993; Streuff et al., 2017). LF2-208 has a slightly coarser texture than LF1-208, imparted by the introduction of sand grains. This could reflect the core site being more proximal to the grounding line than it was during the deposition of LF1-208.

The presence of clasts in LF2-208 indicates that deposition by iceberg rafting was taking place alongside suspension settling from overflow plumes (Evans et al., 2002; Kempf et al., 2013). The clast rich horizon at 188 cm could be related to a more intense period of ice rafting (Licht et al., 1999), or deposition of debris from overturning icebergs (McCabe et al., 1987; Gilbert et al., 1993).

5.3.4.3 AF9 - Lithofacies 3 (LF3-208): Massive silty clay coarsening upward into a massive diamicton

LF3-208 is interpreted as the product of suspension settling from meltwater plumes and iceberg rafting. This interpretation is supported by its low shear strength of 3-4 kPa. The deposition of silt and clay is attributed to suspension settling of fine grains settling from meltwater derived overflow plumes (Elverhøi et al., 1983; Cowan and Powell, 1990; Streuff et al., 2017). The deposition of the coarse sand grains and clasts is attributed to iceberg rafting (Cowan et al., 1997; 1999; Batchelor et al., 2011). Therefore, the upward increase in clast and sand content in LF3-208 suggests that deposition by iceberg rafting had an increasingly greater role in deposition. The release of sediment from icebergs often takes place at a greater rate in more proximal settings (Cai et al., 1997), which could suggest that the ice margin was becoming more proximal to the core site during the deposition of LF3-173.

5.3.4.4 AF9 - Lithofacies 4 (LF4-208): Massive silty clay fining upward into massive clay

The deposition of this low shear strength (4-5 kPa) mud is also attributed to suspension settling from meltwater-derived overflow plumes (Elverhøi et al., 1983; Cowan and Powell, 1990; Batchelor et al., 2011; Streuff et al., 2017). Iceberg rafting was responsible for the deposition of the clasts present in LF4-208 (Cowan et al., 1999), suggesting that the upward decrease in clast content relates to a decrease in the contribution from iceberg rafting at the core site. Consequently, it is proposed that the grounding line was becoming increasingly distal from the core site during the deposition of LF4-208, because the rate of deposition of clasts by icebergs can decrease with distance from the grounding line (Cai et al., 1997). A receding ice margin is also supported by the upcore fining of LF4-208. This facies likely represents the final recession of the ice margin from the core site.

5.3.5 AF10

AF10 occurs as transparent lenses within AF7 and is interpreted as the product of the discrete gravity flows. Their lenticular shape and acoustically transparent, homogenous nature are typical of previously reported subaqueous debris flow deposits (Damuth, 1980; Laberg and Vorren, 2000; Hjelstuen et al., 2009; Dowdeswell et al., 2010; Hogan et al., 2011; Callard et al., 2018). Their

transparency suggests a fine grain size, most likely a muddy texture (Piper et al., 1999; Hogan et al., 2012), consistent with a cohesive debris flow origin. Their presence within AF7 suggests that they were derived from localised reworking of the fine stratified sediments which comprise AF7.

5.3.6 AF11

The wedge shaped geometry of AF11 and its position adjacent to a slope points to a mass flow origin (Damuth, 1980; Hjelstuen et al., 2009; Lysså et al., 2010; Batchelor et al., 2011; Hogan et al., 2012). It lacks the acoustic transparency that is commonly associated with subaqueous debris flow deposits (e.g., Laberg and Vorren, 2000), and has a substantial thickness (up to ~25 m), suggesting it may be the product of multiple flow events which allowed the mixing of different grain sizes and therefore reduced its acoustic transparency (Hogan et al., 2012).

5.4 Outer Westwind Trough: PS109-22

AF2 and AF12 were identified around the PS109-22 core site, and the PS109-22 core was recovered entirely from AF12 (Fig. 4.1e; 4.2c).

5.4.1 AF2

AF2, which is present discontinuously around the core site of PS109-22, has been interpreted as a stiff subglacial till (see section 5.1.1).

5.4.2 AF12

Around the PS109-22 core site, AF12 is arranged in two asymmetric sediment wedges, SW-1 and SW-2 (Fig. 4.1e). The semi-transparent and structureless acoustic character of AF12 suggests that these two sediment wedges are composed of diamictic sediment (Howat and Domack, 2003). The series of dipping internal reflectors within SW-1 and SW-2 suggests that there may be some internal variation in sediment composition or layering of diamicton units, which implies multiple stages of landform development (Dowdeswell et al., 2016). Consequently, it is proposed that the genesis of SW-1 and SW-2 was related to the reworking of subglacially transported diamicton delivered to the grounding line by repeated sediment gravity flows (Howat and Domack, 2003; Ó Cofaigh et al., 2005b; Mosola and Anderson, 2006).

This suggested formation mechanism for SW-1 and SW-2 is very similar to that of GZWs. GZWs are widely understood to form by the reworking of subglacial

sediment delivered to the grounding line to form wedge-shaped deposits (Alley et al., 1989; Benn and Evans, 2010; Batchelor and Dowdeswell, 2015). The asymmetric nature of SW-1 and SW-2 is also characteristic of GZWs (Shipp et al., 1999; 2002; Dowdeswell and Fugelli, 2012; Batchelor and Dowdeswell, 2015; Callard et al., 2018). However, SW-1 and SW-2 are not interpreted as GZWs because they have a notable difference in morphological profile. Both wedges taper towards the shelf edge, with a long, flat ice distal side. This cross-sectional profile is the reverse of what is expected for GZWs, which typically have a low gradient ice proximal face and steeper ice distal face that imparts a 'ramp-scarp' profile (e.g., Dowdeswell et al., 2016; Anderson and Jakobsson, 2016).

The v-shaped depressions on the surface of AF12 adjacent to the core site are attributed to iceberg keels grounding on the seafloor, the same as those that disturb the surface of AF6 (Woodworth-Lynas et al., 1991; Dowdeswell et al., 1993; 2014; Evans et al., 2005; Larter et al., 2012; Gales et al., 2016). Iceberg scouring has been previously identified in outer Westwind Trough by Arndt et al. (2017a).

Core PS109-22 was taken from AF12 at the tapered end of SW-2.

5.4.2.1 AF12 – Lithofacies 1 (LF1-22): Massive, matrix-supported diamicton

The macroscale sedimentology of LF1-22 suggests an origin by iceberg rafting and suspension settling of material from grounding line plumes based on its predominantly massive and poorly sorted nature, the presence of angular to subrounded clasts up to pebble size, weak sub-vertical to vertical clast alignment and draped clasts, low shear strengths (0-9.4 kPa) and gradational transitions in matrix colour (Domack and Lawson, 1985; Thomas and Connell, 1985; Dowdeswell and Dowdeswell, 1989; Dowdeswell et al., 1994a; Cowan et al., 1997; Smith and Andrews, 2000; Ó Cofaigh et al., 2001; Hogan et al., 2016; Streuff et al., 2017). Laminae formation is attributed to either an increased dominance of suspension settling from meltwater plumes (Ó Cofaigh et al., 2001), or by sorting of iceberg-rafted sand and mud as it settled through the water column (Cowan et al., 1997), with the latter interpretation favoured due to the sandy texture of the laminae.

The coarse texture of thin section PS109-22a from LF1-22, and the presence of grains up to gravel size and dropstone structures, also supports deposition of LF1-

22 by a combination of iceberg rafting and suspension settling in a glacimarine environment (Carr, 2001). The intraclasts identified in thin section could be pellets of till matrix deposited by rainout of iceberg rafted debris (Menzies and van der Meer, 2018). The transitions between bands of plasma and grain-supported diamicton, and transitions in plasma colour between these bands, could be attributed to deposition from different pulses of meltwater (Powell and Molnia, 1989; Kilfeather et al., 2010). The PS109-22a thin section is from the draped sandy laminae identified in the x-radiograph images between 122-124 cm (Fig. 4.3c), which provides further evidence that these laminae were deposited by suspension settling. Although inclined banding can also be imparted by sediment remobilisation following deposition, the presence of dropstone structures at microscale and draped lamination at macroscale suggests that the banding in PS109-22a was a product of primary deposition by iceberg rafting and suspension settling.

The extensive grain coatings visible at the microscale (Fig. 4.11) suggest that some small scale remobilisation of grains did take place. Coatings which surround the entire grain have been reported from a range of depositional settings and deposits including; subaqueous and subaerial debris flow deposits, melt-out till, and gelifluction deposits, the formation of which has been associated with skeleton grain rotation within saturated sediment (van Vliet-Lanoë et al., 1984; van der Meer et al., 1992; 2010; Hiemstra, 2001b; Lachniet et al., 2001; Kilfeather et al., 2010). Therefore, the extensive presence of circular coatings which surround skeleton grains across this slide implies that a process driving grain rotation was involved in the deposition of LF1-22. Grain coatings have not been reported from deposits with an origin solely by suspension settling and iceberg rafting (Table 5.1) (Carr, 2001; Kilfeather et al., 2010). A subglacial deformation origin for rotation and grain coating formation is excluded based on limited microscale and macroscale evidence for deformation.

The presence of coated grains in thin section PS109-22a has therefore been attributed to the movement of individual grains or small clusters of grains through the water saturated sediment during deposition, or during small scale remobilisation of grains immediately following deposition. The rotation that took place as individual grains moved would have driven the adhesion of clay and silt to grain surfaces to form grain coatings (Hiemstra, 2001b; Kilfeather et al., 2010).

The colour difference between grain coatings and plasma surrounding the coated grains also implies grain movement. The colour difference indicates that coatings were derived as grains rotated within a pocket of sediment of a differing colour prior to deposition (Kilfeather et al., 2010). The presence of weakly developed skeleton grain turbate structures and the rounded shape of many intraclasts also support small scale grain rotation having taken place during or following the deposition of LF1-22 (van der Meer, 1993; 1997).

5.4.2.2 AF12 - Lithofacies 2 (LF2-22): Massive silty clay

LF2-22 is interpreted as an ice-distal suspension settling deposit based on its massive structure, fine-grained texture, and low shear strength (Kilfeather et al., 2011; Hogan et al., 2016; Streuff et al., 2017). The presence of small clasts is attributed to deposition by iceberg rafting.

5.5 Outer Westwind Trough: PS109-25

AF2 and AF12 are present around the core site of PS109-25.

5.5.1 AF2

AF2 has been interpreted as a stiff subglacial till (see section 5.1.1).

5.5.2 AF12

AF12 has been interpreted as sediment wedges composed of predominantly diamicton, which were formed by debris flows that reworked subglacially transported diamicton being delivered to the grounding line (see section 5.4.2). An acoustically structureless and semi-transparent, seaward tapering sediment wedge (SW-3) is visible around the PS109-25 core site (Fig. 4.1f(ii)). This wedge has a very similar morphology to SW-1 and SW-2, so the same formation mechanism of deposition by repeated sediment gravity flows is also envisioned for SW-3. The acoustic profile in Figure 4.1f(i) is oriented in a different direction to Figure 4.1f(ii). The upper sediment facies in Figure 4.1f(i) was categorised as AF12 given its similarity with the internal structure of SW-3, and the frequent internal reflectors that imply it was also formed by debris flows (Howat and Domack, 2003; Ó Cofaigh et al., 2005b; Mosola and Anderson, 2006). It is possible that this sediment unit also comprises part of a sediment wedge, although this interpretation remains tentative and as a result is not discussed further. The v-shaped incisions on the surface of AF12 are interpreted as iceberg scours formed by iceberg keels ploughing through the seafloor (Woodworth-Lynas et al., 1991;

Dowdeswell et al., 1993; 2014; Evans et al., 2005). Core PS109-25 was recovered from AF12 at the tapered end of SW-3 (Fig. 4.1f).

5.5.2.1 AF12 - Lithofacies 1 (LF1-25): Massive, matrix-supported diamicton

LF1-25 occurs at the base of the core and has characteristics of a subglacial till due to its massive and poorly sorted nature, and the presence of sub-angular to sub-rounded clasts (Boulton, 1987). Although the diamicton has a low shear strength (10-20 kPa), weak subglacial tills with shear strengths of 0-40 kPa have been reported from other cross-shelf troughs in Greenland and Antarctica (Dowdeswell et al., 2004; Ó Cofaigh et al., 2005a; Sheldon et al., 2016). Less consistent with a subglacial origin however is the lack of planar structures and visual evidence of clast alignment which are often associated with subglacial shear (Hiemstra and Rijsdijk, 2003; Ó Cofaigh et al., 2005a; 2013a; Hogan et al., 2016).

Alternatively, LF1-25 could be a glacimarine diamicton deposited by the rainout of IRD and/or suspension settling of subglacial sediment emanating from the grounding line. Its poorly sorted nature, muddy matrix, low shear strength, and the presence of clasts up to pebble size are all characteristic of diamictons produced by iceberg rafting and suspension settling (Domack and Lawson, 1985; Dowdeswell et al., 1994a; Cowan et al., 1997; Licht et al., 1999; Ó Cofaigh et al., 2001; Hogan et al., 2016). Furthermore, the mix of sub-angular to sub-rounded clasts is consistent with the properties of debris transported by icebergs (Dowdeswell and Dowdeswell, 1989; Smith and Andrews, 2000), and the lack of observable preferred clast orientation also supports an origin from iceberg rafting (Domack and Lawson, 1985; Jennings and Weiner, 1996; Cowan et al., 1997; Smith and Andrews, 2000). LF1-25 and LF2-25 have similar matrix textures, shear strengths and magnetic susceptibility (Fig. 4.2c), which suggests that they have the same genetic origins. LF2-25 shows strong evidence for deposition by iceberg rafting and suspension settling (see section 5.5.2.2 below), which is used to propose iceberg rafting as the most likely origin for LF1-25.

5.5.2.2 AF12 - Lithofacies 2 (LF2-25): Stratified, matrix-supported diamicton

A combination of deposition by iceberg rafting and suspension settling from meltwater plumes is proposed for LF2-25, followed by secondary deformation. Its poorly sorted and clast-rich nature, the presence of sub-angular to sub-rounded clasts, its muddy matrix, low shear strength (9-17 kPa) and lack of consistent clast

orientation are all suggestive of deposition by iceberg rafting (Domack and Lawson, 1985; Cowan et al., 1997; Ó Cofaigh et al., 2001; Hogan et al., 2016). Subtle changes in matrix grain size which impart stratification within LF2-25 could reflect sorting of sand and mud as they settled through the water column, or alternatively may record traction current winnowing of fine-grained sediments post-deposition (Cowan et al., 1997; Ó Cofaigh et al., 2001). Remobilisation of iceberg rafted sediments by mass flows is less likely to account for stratification because the transitions in matrix texture are very diffuse, rather than sharply bounded as might be expected from mass flows (Mulder and Alexander, 2001; Ó Cofaigh et al., 2001; Evans et al., 2002), although it is possible that the sediments may have undergone minor downslope resedimentation. Striated clasts in LF2-25 imply debris transport in the zone of basal traction prior to entrainment by icebergs (Dowdeswell and Dowdeswell, 1989). Horizons of high clast frequency indicate periodic winnowing of finer sediment by traction currents (Ó Cofaigh et al., 2001) or a period of increased flux of ice rafted debris (McCabe et al., 1987; Licht et al., 1999).

The clay/silt rich laminae in the matrix of LF2-25 record the operation of meltwater-related deposition when suspension settling dominated over iceberg rafting (Jennings and Weiner, 1996; Ó Cofaigh et al., 2001). The normal grading of diamicton to clayey silt with clasts at the top of LF2-25 also most likely reflects an increase in deposition by suspension settling from meltwater plumes relative to iceberg rafting (Cowan et al., 1997; Hogan et al., 2016). A decrease in iceberg rafting is also supported by the decrease in clast frequency in the upper part of LF2-25, although clasts are still present which indicates that iceberg rafting did not cease completely.

Micro-scale stratification in LF2-25 is imparted by the presence of diamicton bands in thin section PS109-25a, and their presence supports the deposition of LF2-25 by settling of sediment from pulses of meltwater and iceberg rafting. Banding can also be produced by mass flow activity (Table 5.1) (e.g., Kilfeather et al., 2010), however a suspension settling origin for stratification is favoured based on the predominantly diffuse contacts between beds. Both the diamictic and silt/clay intraclasts could be pellets of till matrix sourced from iceberg rafting (Menzies and van der Meer, 2018). The structure of skeletal grains arranged vertically around a larger grain (Fig. 4.12i) is attributed to the sinking of the larger grain through a

saturated matrix which caused the smaller grains to become reoriented, similar to the ‘dropstone tracks’ reported by Kilfeather et al. (2010). This structure also provides evidence of primary deposition by suspension settling. However, other microstructures evident in PS109-25a suggest that LF2-25 underwent secondary deformation following its deposition, which could be attributed to either: (1) subglacial deformation or (2) small scale mass flows.

Skeleton grain turbates, augens and boudinage found in PS109-25a (Fig. 4.16) are all reported from subglacially deformed sediment (Table 5.1) (Carr, 1999; 2001; Ó Cofaigh et al., 2005; 2013a; Roberts and Hart, 2005; Carr et al., 2006; Reinardy et al., 2011), which could imply that LF2-25 was glacitectonised following its deposition. Evidence of boudinage of intraclasts could record subglacial shear, and the rotation of a more competent part of the diamicton rich in skeleton grains during subglacial deformation may have formed the augen structure (Hart and Boulton, 1991; Hiemstra, 1999; Roberts and Hart, 2005). The rotation of grains, or more competent areas of matrix, under subglacial shear could have driven the adhesion of fines to grain surfaces to form grain coatings, and the alignment of skeletal grains with or without a central grain to form skeleton grain turbates (van der Meer, 1993; 1997; Hiemstra and Rijsdijk, 2003).

LF2-25 could also have been reworked by small scale mass flow activity. Skeleton grain coatings, intraclasts and skeleton grain turbates, which were identified on PS109-25a (Fig. 4.16), have all been previously reported in sediment deposited by localised mass flowage (Table 5.1) (Hiemstra, 1999; 2001a; Kilfeather et al., 2010). Grain coatings (described as ‘casing-type’ intraclasts) reported in mass flow deposits from McMurdo Sound and Marguerite Bay partially or fully coat single grains or clusters of grains and were formed by the accretion of fines as grains rotated within a water saturated debris flow (Hiemstra, 1999; 2001a). They bear similarity to partial and complete thin clay/silt rich grain coatings reported from the PS109-25a sample (Fig. 4.12d), which could indicate they were formed by the same mechanism. The mass flow deposits from McMurdo Sound were taken from a core which also contained subglacial and suspension settling deposits, and the presence of casing type intraclasts was restricted solely to the mass flow samples in that study (Hiemstra, 1999). This led to the tentative suggestion that ‘casing-type’ intraclasts (grain coatings) could be diagnostic of mass flows. The formation of skeleton grain turbates by grain rotation, rounding of intraclasts by rotation, and

extension of intraclasts can also take place within mass flows (Hiemstra, 1999; Mulder and Alexander, 2001). Therefore, it is possible that individual bands of sediment were remobilised immediately after their deposition, which allowed the rotation of individual grains and intraclasts, and very localised boudinage. Reworking would have been very localised in order to preserve the sedimentary banding evident in PS109-25a, which has been attributed to primary deposition.

Consequently, the assemblage of microstructures in PS109-25a indicates primary deposition by glacimarine processes, and also suggests that some form of secondary deformation took place. However, the assemblage of microstructures present cannot definitively confirm whether this reworking of LF2-25 was by glacitectonism or localised mass flowage.

5.5.2.3 AF12 - Lithofacies 3 (LF3-25): Massive, matrix-supported diamicton

A debris flow origin is proposed for LF3-25. This interpretation is based on its massive and poorly sorted nature, sharp lower contact, low shear strength, and lack of consistent clast orientation (Ghibaudo, 1992; Laberg and Vorren, 1995; Mulder and Alexander, 2001; Ó Cofaigh et al., 2001; Evans et al., 2002; Talling et al., 2012; Streuff et al., 2017). The sediment remobilised by the debris flow could have originated from the delivery of the subglacial deforming layer to the grounding line, or alternatively it could have originated as glacimarine sediment that underwent subsequent re-sedimentation.

Debris flows often detach rafts of underlying sediment (Ghibaudo, 1992; Domack et al., 1999), which can account for the clay rich inclusions present. These inclusions have a similar texture to the massive mud at the top of LF2-25 based on visual inspection from the x-radiographs (Fig. 4.3c), which makes it plausible they were formed by its erosion and incorporation by a debris flow. Soft intraclasts can be deformed by shearing within debris flows (Mulder and Alexander, 2001), accounting for the evidence of boudinage in LF3-25.The weak normal grading at the top of LF3-25 can be explained by the sinking of larger particles through the weak sediment (Domack et al., 1999; Benn and Evans, 2010). The shear strength of LF3-25 (0.6-5.8 kPa) overlaps with the shear strength of debris flow deposits from the Bear Island Trough Mouth Fan (3.3-16 kPa) (Laberg and Vorren, 1995). Interpretation of LF3-25 as a product of debris flow activity is consistent with the position of the PS109-25 core within SW-3, because the formation of SW-3 has

been attributed to the remobilisation by debris flows of subglacial sediment emerging at the grounding line to form beds of diamicton.

Alternatively, boudinage of one of the clay rich inclusions could also imply that LF3-25 underwent subglacial deformation post-deposition. However, the low shear strength (0.6-5.8 kPa) and preservation of weak normal grading at the top of LF3-25 makes it unlikely that the unit was glacitectonised.

The assemblage of microstructures (intraclasts, grain coatings, stringers, boudinage) in thin section PS109-25b is consistent with a debris flow origin for LF3-25. Both intraclasts and grain coatings have been reported from previous micromorphological studies of debris flow deposits (Table 5.1) (Hiemstra, 1999; Hiemstra, 2001a; Kilfeather et al., 2010). Grain coatings form in debris flows as grain rotation drives surface adhesion of fines (Hiemstra, 2001b; Kilfeather et al., 2010). Based on a debris flow origin, the intraclasts have three possible origins; (1) they were formed by the brecciation and rounding of silt/clay subglacially and delivered to the grounding line (van der Meer, 1993); (2) they are pellets of silty clay which emerged in plumes from subglacial and englacial meltwater conduits or rafted by ice, and were deposited in a glacimarine setting (Ovenshine, 1970; Menzies and van der Meer, 2018): or (3) they are rafts which were excavated from the underlying sediment by the debris flow(s). The lack of rounding in many intraclasts favours an excavational origin. Intraclasts reported from subglacial environments are rounded by rotational deformation (van der Meer, 1993), suggesting that the highly irregular shape of some of these intraclasts makes a subglacial origin unlikely. Furthermore, pellets of silt/clay carried by englacial or subglacial streams would most likely be rounded by water. Therefore, their irregular shape (Fig. 4.14c) suggests that intraclasts were excavated from the underlying sediment by the debris flow, and were only transported a short distance (Hiemstra, 1999).

The sub-vertical pipe structure comprising silty clay with some sand grains (Fig. 4.14f) is consistent with the properties of previously reported clastic dykes (van der Meer et al., 2009). Deformation within subaqueous debris flows can cause localised sediment liquefaction, leading to the upward migration of liquified silt/clay (Mulder and Alexander, 2001; Phillips, 2006), which could account for this pipe structure. It is likely the sub-horizontal pipe structure infilled with skeletal grains is also a clastic dyke. Although boudinage is not reported from other subaqueous

debris flow thin sections (Table 5.1), shearing of intraclasts in debris flows has been demonstrated (Mulder and Alexander, 2001), and boudinage is reported from subaerial debris flows (Lachniet et al., 2001; Phillips, 2006). Therefore, a debris flow origin could account for the lateral attenuation of some intraclasts and the presence of stringer-like structures on thin section PS109-25b. This boudinage would have taken place when deformation was focussed within weaker silt and clay layers as the sediment underwent shearing (Phillips, 2006).

6. Discussion

6.1 Sedimentary and geomorphological signatures of ice stream advance and retreat on the northeast Greenland continental shelf

A range of landforms and sediment facies record the former advance and retreat of the NEGIS across the northeast Greenland continental shelf. The association of drumlins, MSGL and subglacial till present in the Norske and Westwind cross-shelf troughs is characteristic of the beds of many former ice streams (Stokes and Clark, 1999; e.g., Canals et al., 2000; Wellner et al., 2001; Ó Cofaigh et al., 2002b; 2005a; 2005b; Ottesen et al., 2005; 2007; Dowdeswell et al., 2010; Sookhan et al., 2018; Hermanowski et al., 2019; van Landeghem and Chiverell, 2020), and indicates both that the NEGIS was previously present on the continental shelf and that it was fast flowing. The formation of soft till by dilatant subglacial deformation likely facilitated this fast flow, at least in part (Studinger et al., 2001; Dowdeswell et al., 2004). The timing of the advance of the NEGIS which deposited the sediments and landforms has been attributed to the most recent glaciation. This is based on previous stratigraphic and geomorphologic investigations in Norske and Westwind troughs which have concluded that they contained streaming ice at the LGM (Evans et al., 2009; Winkelmann et al., 2010; Arndt and Evans, 2016; Arndt et al., 2017a).

Twelve acoustic facies and fifteen lithofacies recording the advance and retreat of the NEGIS have been identified in Norske and Westwind troughs. Their characteristics and interpretations are summarised in Table 4.1. Three different depositional environments and associated sediment-landform assemblages have been identified: (1) subglacial processes related to NEGIS advance; (2) processes at the grounding line during NEGIS retreat; and (3) ice proximal to ice distal glacimarine processes during NEGIS retreat (Fig. 6.1). Reconstructions of the depositional environment during advance and retreat in each of the three regions of Norske and Westwind troughs are shown in Figure 6.2.

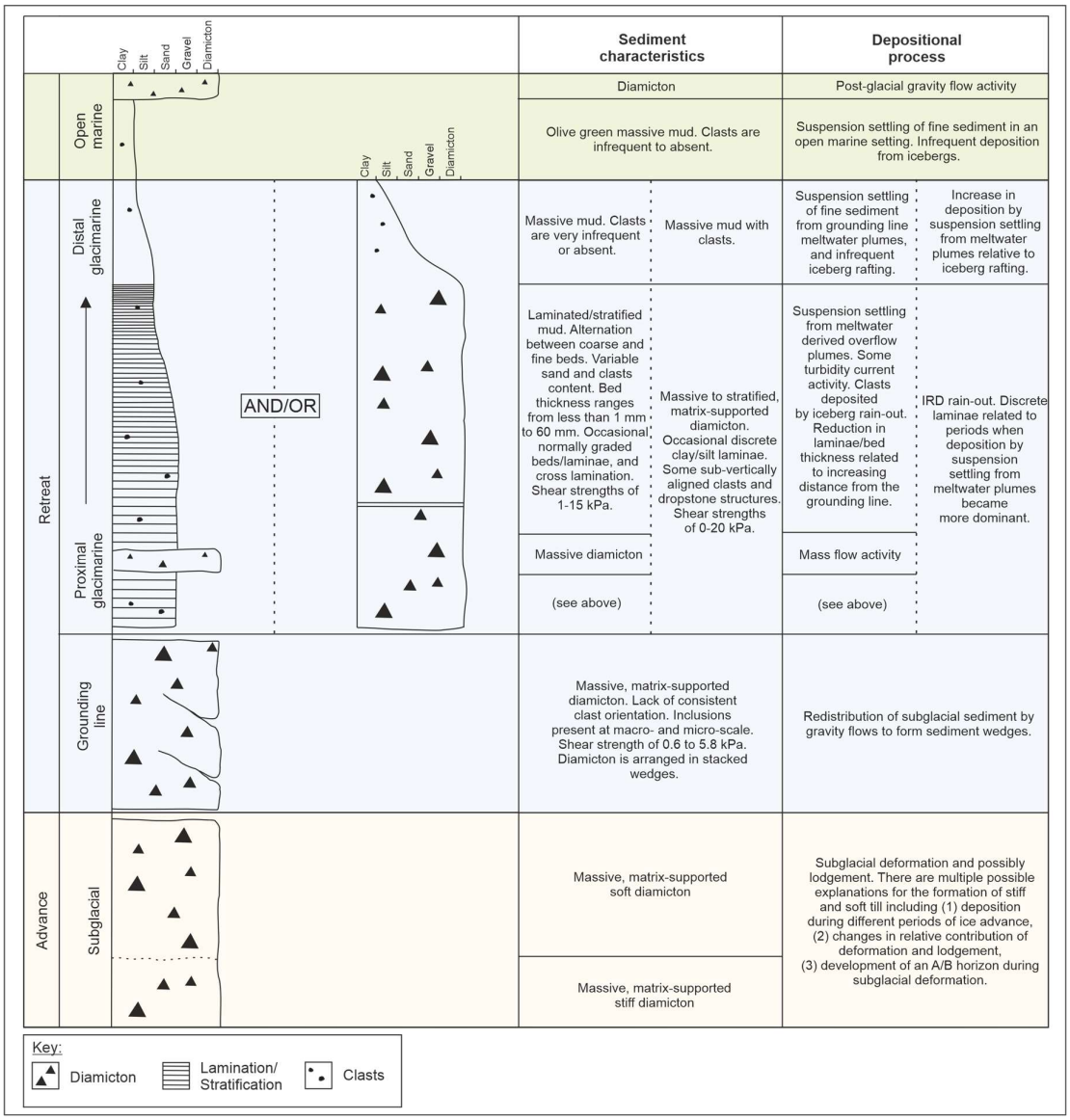

Figure 6.1 Simplified model of the sediment facies and depositional processes associated with the advance and retreat of the NEGIS across the northeast Greenland continental shelf. Two alternate types of facies have been identified in the ice proximal to distal glacimarine environment.

6.1.1 Depositional processes during NEGIS advance

Subglacial landforms and sediments record the advance of NEGIS across the continental shelf. These sediments and landforms overlie bedrock, which occurs in the acoustic record as AF1. Stiff till overlain by soft till was deposited subglacially during NEGIS advance (Fig. 6.1; 6.2b). This has been inferred from the presence of a structureless and acoustically transparent facies (AF3) overlying an acoustically transparent facies with a strong upper reflector (AF2) at core sites PS100-173 and PS100-175 in mid Norske Trough (Fig. 4.1b; 4.1c; 5.1). These acoustic characteristics are very similar to acoustic units interpreted as tills

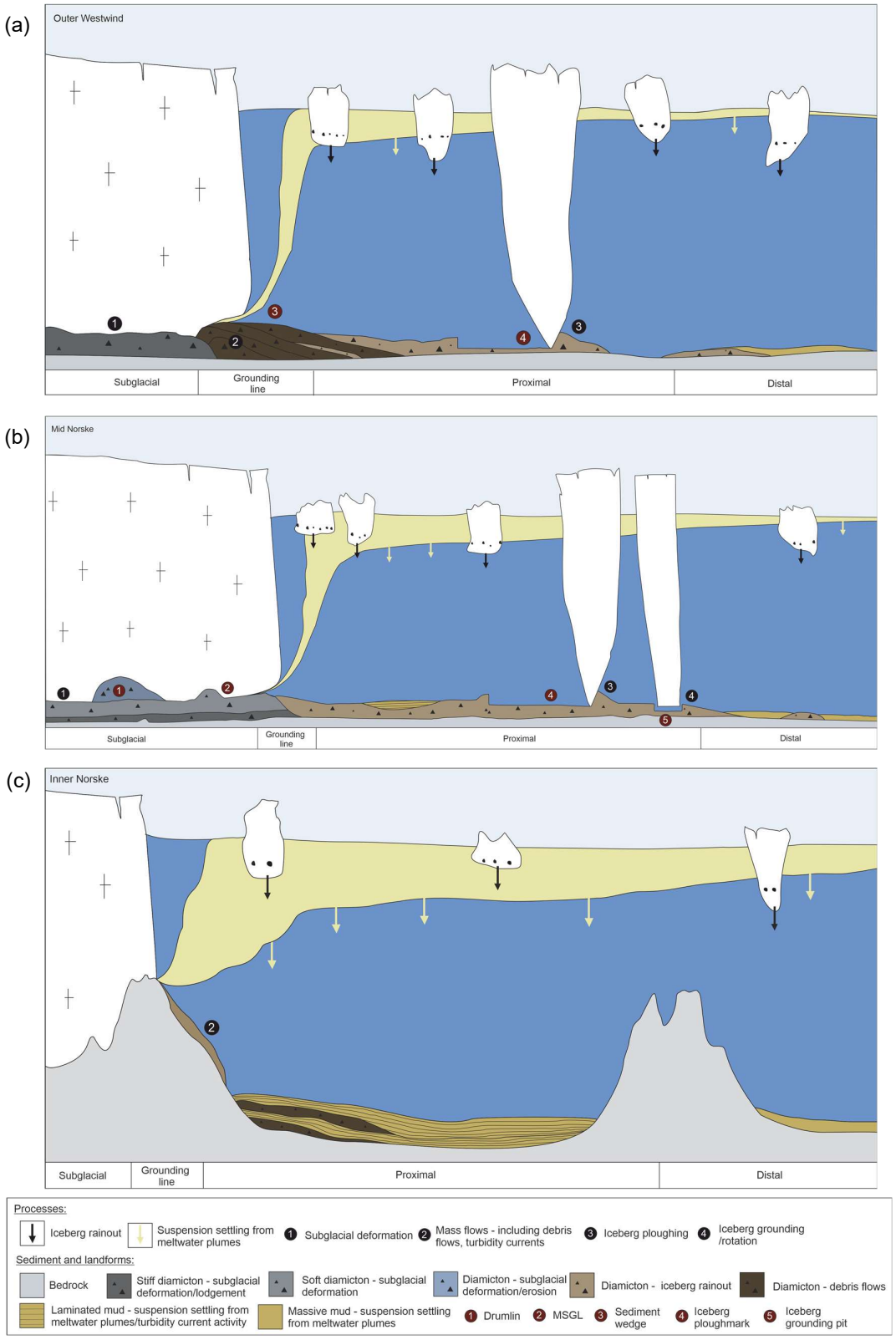

Figure 6.2 Cartoon reconstructions of the subglacial to grounding line distal depositional processes and resulting sediments and landforms present in (a) outer Westwind Trough, (b) mid Norske Trough, and (c) inner Norske Trough on the northeast Greenland continental shelf.

reported from other cross-shelf troughs on high-latitude glaciated margins (e.g., Evans et al., 2005; 2006; Ó Cofaigh et al., 2005a; 2007; Livingstone et al., 2012). Sediment cores from such acoustic facies in Marguerite Bay, Robertson Trough, and the Larsen-A shelf in Antarctica reveal a stiff, massive diamicton overlain by a soft, massive diamicton (Dowdeswell et al., 2004; Evans et al., 2005; Ó Cofaigh et al., 2005a; 2007). These diamictons have been interpreted as tills formed by subglacial deformation, or a combination of subglacial deformation and lodgement (Dowdeswell et al., 2004; Evans et al., 2005; Ó Cofaigh et al., 2005a; 2007). Ó Cofaigh et al. (2007) suggest that the formation of soft till underlain by a stiff till could be explained by three different mechanisms: (1) deposition during two different periods of ice advance, (2) a change in a till deposition mechanism from lodgement to subglacial deformation, and (3) the development of an A/B horizon structure during subglacial deformation, driven by an upward increase in dilatancy. It is likely that at least one of these processes was responsible for the genesis of the soft till underlain by stiff till in mid Norske Trough.

MSGLs were also formed in mid Norske Trough during the advance of NEGIS (Fig. 5.2b). In previous studies, subglacial deformation, ploughing of ice keels through the substrate, and subglacial meltwater rilling, have been invoked to explain the genesis of MSGLs (Clark, 1993; Tulaczyk et al., 2001; Clark et al., 2003; Ó Cofaigh et al., 2005a; 2013b; Fowler, 2010; Stokes et al., 2013b; Spagnolo et al., 2014; Piasecka et al., 2018). In this case, their incidence on the surface of AF3 (Fig. 4.1c; 5.2b), a soft till deposited by subglacial deforming bed processes, suggests their genesis is at least partially related to subglacial deformation. Therefore, it is suggested that subglacial deformation of pre-existing sediments led to the attenuation of subglacial till into lineations during grounded ice advance through the Norske Trough (Clark, 1993; Canals et al., 2000; Ó Cofaigh et al., 2013b; Stokes et al., 2013b).

NEGIS advance through Norske Trough is also recorded by the presence of drumlins formed parallel to ice flow. Multiple theories exist to explain drumlin genesis including; differential erosion (Kerr and Eyles, 2007; Eyles et al., 2016; Hermanowski et al., 2019), subglacial deformation (Piotrowski, 1987; Boulton, 1987; Rattas and Piotrowski, 2003; Jónsson et al., 2016), and instability within the deforming bed (Fowler, 2000; Stokes et al., 2013a), meaning their presence alone is not diagnostic of one particular depositional process. Drumlins in Norske Trough

occur as acoustically transparent, dome-shaped mounds (AF4), overlying the soft till (AF3) but are separated by a sharp basal reflector, indicating a transition in sediment properties (Fig. 4.1b; 5.2a). However, they are acoustically transparent like AF3 and so are most likely composed of subglacial till. Assuming that they are composed of subglacial till, they could have formed by subglacial reworking of the soft till (AF3) (Boulton, 1987).

6.1.2 Depositional processes during NEGIS retreat

Glacimarine sediments and landforms overlie the subglacial sediments and landforms in Norske and Westwind troughs. The characteristics of these glacimarine sediments and the processes by which they were deposited are shown in Figure 6.1.

6.1.2.1 Grounding line landform-sediment assemblages

Debris flow activity, the formation of sediment wedges, and secondary reworking by glacitectonism, occurred at the NEGIS grounding line during its retreat across the continental shelf (Fig. 6.1). Subglacial sediment emerging from the grounding line was remobilised as debris flows, depositing massive, matrix-supported diamicton with sharp basal contacts, attenuated intraclasts, and water escape structures (Fig. 6.1; 6.2). In outer Westwind Trough, debris flows were at least partially responsible for the genesis of three sediment wedges (SW-1, SW-2, and SW-3). The timing of their formation has been attributed to ice retreat because they are partially composed of glacimarine sediment. This is based on lithofacies interpretations of cores PS109-22 and PS109-25 which were recovered from the tapered (ice-distal) end of SW-2 and SW-3 respectively (Fig. 4.1e; 4.1f). Furthermore, the sediment wedges overlie AF2, which has been interpreted as a subglacial till (see sections 5.4.1 and 5.5.1), and there is no evidence from the cores or acoustic data to suggest that any of the sediment wedges have been over-run subsequently by ice.

The formation of these sediment wedges took place predominantly by sediment gravity flows, iceberg rainout and suspension settling from meltwater plumes (Fig. 6.2a). The dipping nature of the internal reflectors visible within SW-1 and SW-2 (Fig. 4.1e) suggests that prograding gravity flows composed of subglacial sediment emanating from the grounding line were involved in their formation (Howat and Domack, 2003; Ó Cofaigh et al., 2005b; Mosola and Anderson, 2006;

Dowdeswell and Fugelli, 2012). Therefore, it is proposed that they were formed by a backstepping grounding line from which gravity flows deposited sediment during pauses in ice retreat, forming multiple stacked sediment wedges. SW-3 lacks this same dipping internal bedding in acoustic profile, however the presence of a debris flow deposit in core PS109-25 (LF3-25) is consistent with formation, at least in part, by subglacially derived gravity flows. The low amplitude (9-15 m) of these sediment wedges could suggest that the pauses in ice retreat were brief, or that the rate of sedimentation at the grounding line was low (Callard et al., 2018). The presence of iceberg rafted diamicton in cores from SW-2 and SW-3 suggests that iceberg rain-out, with some contribution from suspension settling, deposited sediment at the seaward end of the sediment wedges (Fig. 6.2a).

Readvance of the NEGIS during overall retreat led to reworking of glacimarine sediment by glacitectonism at the grounding line. In mid Norske Trough, glacitectonism produced discontinuous stringer structures at macroscale, and planar and rotational plasmic fabrics and skeleton grain turbates at microscale, as well as depositing subglacial till (Hart and Roberts, 1994; Roberts and Hart, 2005).

6.1.2.2 Ice proximal to ice distal glacimarine landform-sediment assemblages

Beyond the grounding line, glacimarine deposition during NEGIS retreat took place by suspension settling from meltwater plumes, rain-out from icebergs, and mass flow activity (Fig. 6.1; 6.2). Glacimarine sediment was reworked by iceberg keel scouring and mass flow activity. Suspension settling of sediment from meltwater overflow plumes sourced from the grounding line deposited laminated, stratified and massive mud (Fig. 6.1). Beds/laminae range in thickness from less than 1 mm up to 60 mm. Changes in the structure of these muds have been used to infer changes in depositional setting. Proximal to the grounding line, laminated to stratified mud or sandy mud, comprising alternating coarse and fine planar laminae/beds (Fig. 6.3a), was deposited by suspension settling from meltwater plumes in both inner and mid Norske Trough (Fig. 6.2b; c) (Elverhøi et al.,1983; Ó Cofaigh and Dowdeswell, 2001; Gilbert et al., 2002; Tarlati et al., 2020). Deposition of each single lamina, or each pair of coarse and fine laminae, is attributed to suspension settling from an individual meltwater plume event (Mackiewickz et al., 1984).

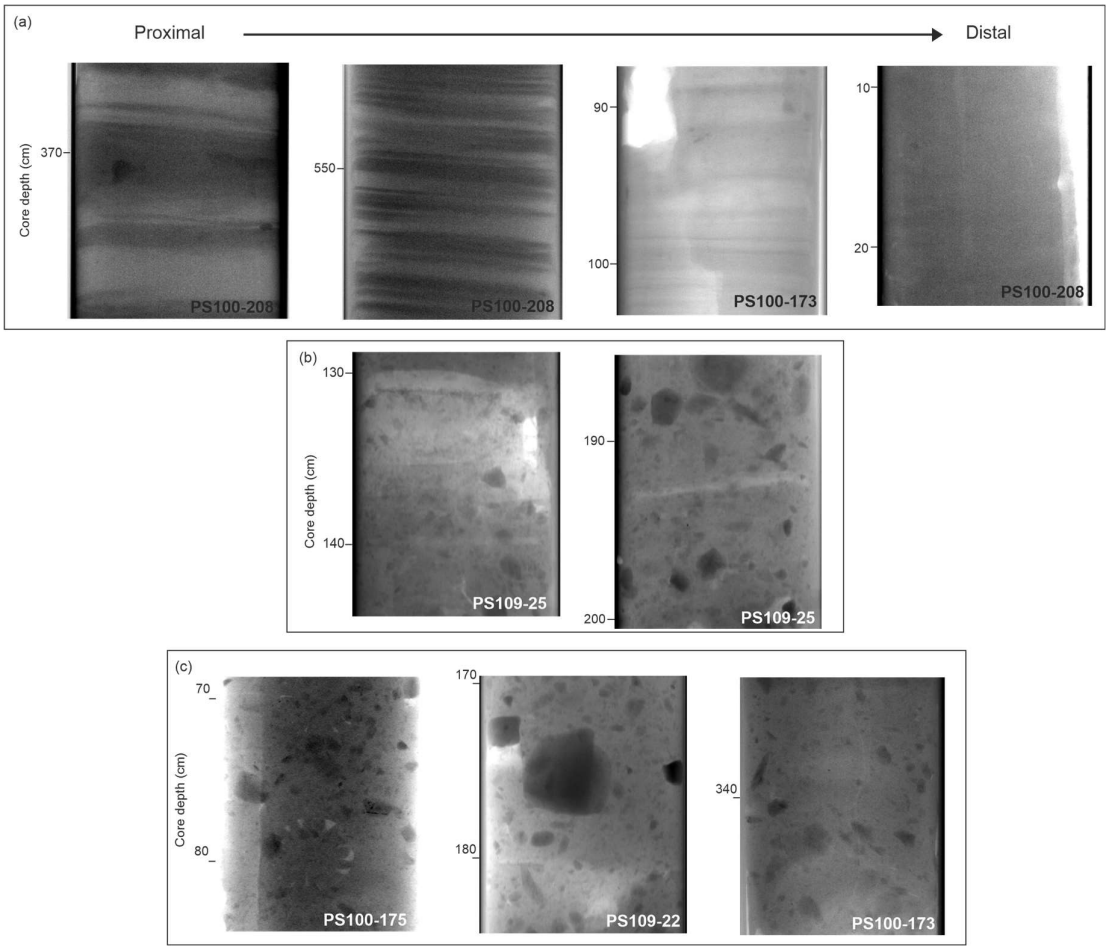

Figure 6.3 X-radiograph images of sediment facies deposited by glacimarine processes beyond the grounding line (a) laminated to massive mud deposited by suspension settling from meltwater plumes in an ice proximal to ice distal setting (b) diamicton fining upward into clay with clasts and diamicton with discrete mud laminae, both deposited by a combination of suspension settling from meltwater plumes and iceberg rafting (c) massive diamictons deposited predominantly by iceberg rainout

Cross-lamination and inverse grading were occasionally identified within this laminated mud. These could reflect deposition by turbidity currents triggered by either the failure of rapidly accumulating suspension deposits proximal to the grounding line, or the development of turbid underflow plumes (Cowan and Powell, 1991; Gilbert, 1992; Gilbert et al., 1993; Ó Cofaigh et al., 2001; Talling et al., 2012; Talling, 2014). Debris flow activity may also have taken place during suspension settling (Fig. 5.2a; 6.1), as indicated by the interbedded acoustically stratified and massive sediment units of AF9 (Hjelstuen et al., 2009; Hogan et al., 2012).

Deposition of finer mud with thinner and less well defined beds/laminae is attributed to increasing distance from the grounding line (Fig. 6.1; 6.3a), because the sediment content and quantity of coarse grains within meltwater plumes decreases with distance from source (Lemmen, 1990; Jager and Nittrouer, 1999;

Forwick and Vorren, 2009; Streuff et al., 2017; 2018). As the grounding line receded further, laminated mud transitioned into massive mud (Fig. 6.3a), deposited by suspension settling from meltwater plumes in which the only the finest sediment remained in suspension (Gilbert et al., 2002; Streuff et al., 2018) (Fig. 6.1; 6.2).

Massive to stratified diamictons with low shear strengths and pebble-sized clasts that often exhibit a weak sub-vertical alignment were deposited by iceberg rafting, likely with some input from meltwater derived suspension setting (Fig. 6.1; 6.2; 6.3c) (Dowdeswell et al., 1994a; 2000; Cowan et al., 1997; Ó Cofaigh et al., 2001; Peters et al., 2015; 2016; Callard et al., 2020). Some sediment facies display clear evidence of the competing influences of deposition by iceberg rafting and suspension settling from meltwater plumes, highlighting the interaction of these processes beyond the grounding line. Deposition of massive clay which grades up from massive diamicton, and interbedded clay/silt rich laminae within massive diamicton (Fig. 6.3b), is inferred to represent periods when meltwater deposition was dominant and exceeded the contribution from iceberg rafting (Jennings and Weiner, 1996; Ó Cofaigh et al., 2001).

The relative contribution of these different depositional processes varied between the three different regions of the continental shelf investigated in this study. In inner Norske Trough suspension settling from overflow plumes was the dominant depositional process, resulting in the accumulation of up to 95 m of acoustically stratified sediment (Fig. 4.1d). Stratified to laminated mud comprises 92% of the PS100-208 core, and individual coarse/fine beds can be up to, and occasionally greater than, 60 mm, both of which indicate high sedimentation rates and imply that large volumes of meltwater were being released from the NEGIS grounding line to allow these volumes of sediment to be deposited. In both mid Norske and outer Westwind troughs, deposition by iceberg rain-out was the dominant depositional process, although there is also a strong suspension settling signal in PS100-173 in mid Norske. Iceberg-rafted diamictons comprise ~51-85% of the outer Westwind cores, and ~43-89% of the mid Norske cores. In contrast, in inner Norske Trough IRD rainout was either lower, or was overwhelmed by suspension settling from meltwater plumes. The occurrence of distributed clasts which increase up-core in the upper 534 cm of PS100-208 indicates that intermittent

release of clasts from icebergs did take place during deposition dominated by suspension settling of fines (Tarlati et al., 2020).

Secondary reworking of glacimarine sediment took place by iceberg keel scouring and sediment gravity flow processes. In mid Norske Trough and outer Westwind Trough, iceberg grounding and rotation formed pits (260-660 m width), and iceberg ploughing formed furrows (50-90 m width) (Fig. 6.2a; b). Iceberg keel scouring may also have produced microscale deformation (planar and skelsepic plasmic fabrics) in iceberg rafted diamicton in mid Norske Trough (Kilfeather et al., 2010; Linch and Dowdeswell, 2016). Proximal to the grounding line in inner Norske Trough, faulting and inclined bedding in laminated suspension settling deposits were produced by either synsedimentary deformation (van der Meer and Warren, 1997; Hoffmann and Reicherter, 2012), or post-depositional slumping of unstable sediment piles (Cowan and Powell, 1991). Additionally, rotational structures including microscale grain coatings, rounded intraclasts and skeleton grain turbates suggest that some small scale remobilisation of individual grains or small clusters of grains took place following the deposition of iceberg rafted diamictons in outer Westwind Trough (Hiemstra, 1999).

6.1.2.3 Evidence of deposition in an ice shelf environment

Although deposition at a grounded tidewater margin can account for the deglacial sediments and landforms present in Norske and Westwind troughs, some could also have plausibly been deposited in an ice shelf setting. In mid Norske Trough, the laminated mud with a paucity of coarse grains (LF3-173), overlain by massive diamicton (LF4-173), could be indicative of deposition in an ice shelf environment. Massive and laminated mud units with variable clast content have been shown to be deposited in a distal sub-ice shelf setting by sediment plumes (Rebesco et al., 2014; Yokohama et al., 2016; Davies et al., 2017; Smith et al., 2017; Reilly et al., 2019). Furthermore, the stratigraphic succession of laminated or massive mud deposited by suspension settling, followed by pebbly mud or diamicton, has been reported from multiple other palaeo and contemporary ice shelf environments, reflecting a shift in deposition from sub-ice shelf suspension settling to iceberg rainout during ice shelf break-up (Kilfeather et al., 2011; McGlannan et al., 2017; Reilly et al., 2019; Smith et al., 2019). Laminated mud with massive diamicton above comprise facies 5 and 8 of the idealised facies succession in an ice shelf environment (Fig. 2.6; Smith et al., 2019).

The type of grounding line regime (grounded tidewater vs ice shelf) present during the formation of the sediment wedges (SW-1, SW-2, and SW-3) in outer Westwind Trough also gives an indication of whether an ice shelf was present during NEGIS retreat. The low relief of the three sediment wedges (Fig. 4.1e; 4.1f; SW-1 is up to 12 m thick, SW-2 is up to 9 m thick, and SW-3 is up to 15 m thick) is a characteristic also displayed by GZWs, which could imply that the sediment wedges were formed in a similar setting to GZWs. GZW formation is typically suggested to occur in a sub-ice shelf cavity where the low vertical accommodation space gives GZWs their low amplitude (Dowdeswell and Fugelli, 2012; Batchelor and Dowdeswell, 2015). Therefore, the low amplitude of SW-1, SW-2 and SW-3 could indicate that their formation was also constrained by an overlying ice shelf. However, the formation of these sediment wedges at a grounded tidewater margin is favoured based on multiple factors. Firstly, a sub-ice shelf cavity would most likely have a depth greater than 15 m. The cavity beneath the floating ice tongue which currently fronts the 79°N glacier has a depth up to ~500 m (Linderman et al., 2020; Schaffer et al., 2020). This suggests that the subdued shape of these sediment wedges is unlikely to be related to limited vertical accommodation space.

Furthermore, the way in which the three sediment wedges have the opposite cross-sectional profile to a typical GZW suggests that they were formed under a different grounding line regime. GZWs typically have a ‘ramp-scarp’ profile with a lower gradient ice proximal face and steeper ice distal face (e.g., Dowdeswell and Fugelli, 2012; Dowdeswell et al., 2016; Evans and Hogan, 2016). GZWs gain this shape because the low gradient ice shelf base close to the grounding line limits vertical accretion of the GZW at its proximal end (Batchelor and Dowdeswell, 2015). Sediment deposition is therefore concentrated at the seaward end of the wedge because of the upward slope of the ice shelf, forming the steeper ice distal face typical of GZWs (Batchelor and Dowdeswell, 2015; Smith et al., 2019). SW-1, SW-2, and SW-3 all lack this ‘ramp-scarp’ profile and taper towards the shelf edge. This implies that their deposition was not constrained by the geometry of an ice shelf cavity, and therefore that they were formed at a grounded tidewater margin.

Typically, moraine ridges are expected to form at tidewater margins rather than low amplitude sediment wedges because of the lack of constraining ice shelf (Batchelor and Dowdeswell, 2015). However, the mixed landform population of both GZWs and moraines identified in the Ross Sea has been used by Simkins et

al. (2018) to propose that ice shelf presence/absence may not always dictate the morphology of recessional landforms. Instead, they suggest that sediment supply and duration of grounding line stillstand exert greater control. The recessional moraines revealed in outer and mid Westwind Trough (Fig 2.1) (Winkelmann et al., 2010; Arndt and Evans, 2016) mean that Westwind Trough also possesses a mixed recessional landform population of sediment wedges and moraines. This is a further indication that the formation of subdued sediment wedges is not necessarily indicative of an overlying ice shelf. These moraines in mid Westwind Trough are 5-25 m in height and 50-250 m wide (Winkelmann et al., 2010), which is a similar height but a substantially lower width than the sediment wedges at the shelf edge in Westwind Trough. Therefore, the deposition of SW-1, SW-2 and SW-3 in outer Westwind Trough could reflect lengthier ice margin stillstands at a tidewater margin, whilst the transition to narrower recessional moraines was driven by shorter halts as the grounding line retreated onto the mid-shelf.

6.2 Implications for NEGIS dynamics

The glacigenic sediment and landforms in Norske and Westwind troughs have implications for the LGM extent and retreat dynamics of NEGIS. SW-3 is located close to the shelf edge, suggesting that it represents the maximum ice extent of the NEGIS in Westwind Trough. This confirms that the NEGIS reached a shelf edge position in Westwind Trough, as has previously been proposed by Arndt et al. (2017a) and Evans et al. (2009) based on the presence of prominent glacial lineations at the shelf edge and sediment gravity flow deposits on the continental slope respectively.

The formation of SW-1 and SW-2 inland from SW-3 in outer Westwind Trough suggests that retreat from the shelf edge was episodic (Ottesen et al., 2007; Ó Cofaigh et al., 2008; Dowdeswell et al., 2008b). Although these sediment wedges are not interpreted as GZWs *sensu stricto,* aspects of their morphology (asymmetric profile) and genetic origin (formation predominantly by sediment gravity flows) are similar to those of GZWs. This suggests that their presence may have similar implications for ice dynamics as GZWs. GZW deposition is usually associated with periods when the grounding line is stationary (Alley et al., 2007; Batchelor and Dowdeswell, 2015). Therefore, the formation of SW-1 and SW-2 inshore of the shelf edge could indicate that retreat of the NEGIS was punctuated by stillstands (c.f. Ó Cofaigh et al., 2008; Dowdeswell et al., 2008b). However,

these sediment wedges are small (maximum thickness = 15 m), and their formation has been attributed to gravity flows sourced from a backstepping margin (see section 5.1.2.1 above). Therefore, their deposition does not necessarily represent a long-term stillstand, but rather a grounding line which receded in a step-like manner. This is supported by the comparatively larger dimensions of WT-GZW in mid Westwind Trough (Fig. 2.1), which is up to ~100 m thick, the genesis of which has been previously suggested to represent a long term grounding line stabilisation (Arndt et al., 2015; Arndt et al., 2017a). In outer and mid Westwind Trough, there are numerous recessional moraines which are situated inland of SW-1, SW-2 and SW-3 (Fig. 2.1). These moraines also imply that minor halts or readvances took place during ice retreat, and hence that retreat was stepwise through outer and mid Westwind Trough (Ó Cofaigh et al., 2008; Dowdeswell et al., 2008b; Winkelmann et al., 2010; Arndt and Evans, 2016; Arndt et al., 2017a). The comparatively smaller size of these recessional moraines in relation to the sediment wedges implies stillstands may have become progressively shorter in duration as the ice sheet receded along the trough (see section 6.1.2.3).

This shortening of stillstand duration during ice retreat through Westwind Trough could have been driven by changes in trough in depth and gradient. The sediment wedges at the shelf edge occur at a depth between 300-400 m, whilst the moraines in the mid to outer trough identified by Winkelmann et al. (2010) and Arndt et al. (2017a) occur at a depth of 270-350 m. Hence, this decrease in trough depth inwards from the shelf edge implies that the positive feedback which can cause acceleration of grounding line recession on reverse bed slopes was unlikely to have been responsible for any inferred acceleration of NEGIS retreat in Westwind Trough (Schoof, 2007). Other factors can also control grounding line stability and retreat dynamics. These include changes in trough width and bed roughness, and changes in ice dynamics in response to external forcing such as rising air temperatures, precipitation changes, and sea level rise (Ó Cofaigh et al., 2008; Livingstone et al., 2012). One or more of these was most likely responsible for shortening of stillstands in Westwind Trough, however it is difficult reach a more detailed conclusion without dating the timing at which the sediment wedges and moraines were deposited.

The dominance of deposition by iceberg rainout, and the frequent iceberg grounding pits and furrows in outer Westwind and mid Norske troughs, indicate

that abundant icebergs were calved from the NEGIS margin as it retreated through these areas. This suggests that initial retreat from the shelf edge in Westwind Trough was at least partially driven by mass loss from iceberg calving, and that calving continued as the ice margin retreated across the continental shelf (Dunlop et al., 2010; Ó Cofaigh et al., 2012; Hogan et al., 2016; Peters et al., 2016).

The occurrence of sediment facies in mid Norske Trough which could have been deposited in an ice shelf environment (see section 6.1.2.3) suggests that the NEGIS might have been fronted by an ice shelf in Norske Trough during its retreat. No evidence has been revealed in this study to suggest that an ice shelf was present in Westwind Trough, making it possible that as the NEGIS retreated across the continental shelf, a grounded margin might have been present in Westwind Trough whilst a floating margin was present in Norske Trough.

Evidence of glacitectonism and possibly till deposition interrupting glacimarine sedimentation in mid Norske Trough implies that the grounding line oscillated during overall retreat (c.f. Peters et al., 2016; Callard et al., 2020). Arndt et al. (2017a) propose that NT-GZW in Norske Trough (Fig. 2.1), which is present seaward of the PS100-173 and PS100-175 core sites, could have been formed during a Younger Dryas readvance. The position of this NT-GZW is consistent with the ice margin having readvanced over the PS100-173 and PS100-175 core sites at this time, making it possible that glacitectonism in mid Norske Trough was indeed related to a Younger Dryas readvance of the NEGIS. Recent cosmogenic dating has determined that Bourbon Øer, Storøen, and Kap Amélie on the outer coastline were deglaciated between 14.20 ± 0.46 to 10.79 ± 0.39 ka (Fig. 2.3; Larsen et al., 2018). The wide range of these deglacial dates creates uncertainty about the Younger Dryas extent of the NEGIS. However, all six cosmogenic dates from Bourbon Øer and Storøen are between 10.79 ± 0.39 ka to 11.60 ± 0.85 ka (Fig. 2.3; Larsen et al., 2018), which suggests that deglaciation of Bourbon Øer and Storøen took place after the Younger Dryas termination at 11.7 ka BP. This makes it plausible that the NEGIS was positioned beyond the coastline in the cross-shelf troughs during the Younger Dryas, so it is possible that the NEGIS readvanced through mid Norske Trough during this period.

Previous investigations have demonstrated that the response of Greenland glaciers to Younger Dryas cooling was spatially variable, with evidence of both ice margin readvance and retreat during this period (Kuijpers et al., 2003; Jennings et

al., 2006; Hall et al., 2010; Funder et al., 2011; 2021; Ó Cofaigh et al., 2013a; Rinterknecht et al., 2014). Cosmogenic exposure dating of moraines in Peary Land, northern Greenland, indicate that ice margin readvance took place during the Younger Dryas (Larsen et al., 2016). This evidence of Younger Dryas readvance in other parts of northern Greenland lends indirect support for a NEGIS readvance in Norske Trough. Larsen et al. (2016) suggest that this readvance in northern Greenland is related to its distance from the Atlantic Meridional Overturning Circulation (AMOC). It has been hypothesised that in western and southern Greenland the reduction in AMOC strength that took place during the Younger Dryas caused increased temperature seasonality, as well as subsurface warming and advection of warmer water to the GrIS grounding line, which led to ice stream retreat (Denton et al., 2005; Marcott et al., 2011; Buizert et al., 2014; Rinterknecht et al., 2014; Funder et al., 2021). However, this Younger Dryas seasonality has been shown to decrease northward across Greenland (Buizert et al., 2014). Therefore, it is plausible that ice stream readvance took place in northern Greenland during the Younger Dryas, because it may not have experienced the environmental changes that drove ice stream retreat in western and southern Greenland (Larsen et al., 2016).

Glacimarine deposition in inner Norske Trough was dominated by suspension settling from meltwater plumes and gravity flow activity, a different depositional regime to outer Westwind and mid Norske where deglacial sedimentation was characterised by iceberg rainout and sediment gravity flow processes. The dominance of meltwater sedimentation in the PS100-208 core could be related to higher levels of meltwater production at the grounding line. Such increased melt would most likely have been driven by the rise in atmospheric and ocean temperatures in the early Holocene following the Younger Dryas. The NGRIP ice core records warming of 10°C in 60 years at 11.7 ka, the termination of the Younger Dryas (Steffensen et al., 2008). Furthermore, changes in ocean circulation likely influenced ocean temperatures on the northeast Greenland shelf during the early Holocene. Northward advection of warmer Atlantic Water (AW) through the Fram Strait and increased inflow across the northeast Greenland shelf into the inner shelf took place from 10.6 ka (Werner et al., 2015; Syring et al., 2020; Zehnich et al., 2020). Incursion of this warmer AW at the NEGIS grounding line would likely have led to melting and retreat (Syring et al., 2020). Therefore,

this suggests that deposition of the thick laminated muds at the PS100-208 core site on the inner shelf occurred following the Younger Dryas and during the early Holocene. This indicates that the NEGIS grounding line had retreated to the inner continental shelf by the early Holocene, and that mass loss was being driven by melting at the margin at this time.

Findings from previous investigations also make it plausible that retreat through inner Norske Trough took place during the early Holocene. Sites on the outer coast (Bourbon Øer, Storøen, and Kap Amélie; Fig. 2.3) have a mean deglaciation age of 11.7 ka (Larsen et al., 2018). The PS100-208 core site is situated inshore of these sites on the outer coastline, implying that it was deglaciated after 11.7 ka. Therefore, the cosmogenic dates retrieved by Larsen et al. (2018) also indicate that inner Norske Trough was deglaciated during the early Holocene. The upward coarsening and increase in thickness of individual beds through LF1-208 and LF2-208 may reflect occasional minor oscillations of the grounding line during this time. The PS100-270 core (79°29.83′N, 18°8.40′W), which was recovered 19 km to the north of PS100-208 in inner Norske Trough, exhibits a similar sedimentary sequence of laminated muds to PS100-208 (Syring et al., 2020). The deposition of the muds in the PS100-270 core has also been attributed to ice proximal to increasingly ice distal suspension settling from meltwater plumes as the NEGIS retreated from the inner shelf towards the inner fjords (Syring et al., 2020). Dating of these laminated muds shows that they were deposited during the early Holocene (between ~10 ka and 7.5 ka) (Syring et al., 2020). Therefore, this data recovered from the nearby PS100-270 core also suggests that NEGIS was retreating across the inner shelf during the early Holocene.

6.3 Comparison to other Greenland systems and implications for GrIS history

The interpretation that the NEGIS reached an outer shelf position in Westwind Trough is consistent with previously reported evidence that the GrIS was extensive on the continental shelf around Greenland (e.g., Ó Cofaigh et al., 2004; 2013a; 2018; Jennings et al., 2006; Nørgaard-Pedersen et al., 2008; Roberts et al., 2008; 2009; Dowdeswell et al., 2010; 2014; Newton et al., 2017; Arndt, 2018; see section 2.1.1). Collectively, this supports an extensive GrIS which extended beyond the fjord mouths and onto the continental shelf, in many cases to the shelf edge, at the LGM.

The depositional processes and landforms recording the advance and retreat of the NEGIS bear similarity to those documented from other palaeo-ice streams. A conceptual model of the landform assemblage in Norske and Westwind troughs is shown in Figure 6.4, and is consistent with fast flowing ice (Ottesen and Dowdeswell, 2009; Batchelor and Dowdeswell, 2014; Stokes, 2018). MSGLs and drumlins orientated in the former ice flow direction are widely reported from the beds of palaeo-ice streams (e.g., Shipp et al., 1999; Ó Cofaigh et al., 2002b; Ottesen et al., 2005; 2007; Livingstone et al., 2013). In Greenland, subglacial till and streamlined bedforms including drumlins and MSGLs, have been reported from Disko and Uummannaq troughs in West Greenland (Ó Cofaigh et al., 2013a; Dowdeswell et al., 2014; Hogan et al., 2016), Kangerlussuaq Trough in southeast Greenland (Dowdeswell et al., 2010), the continental shelf beyond Kejser Franz Joseph Fjord (KFJF) in east Greenland (Evans et al., 2002), and in Petermann Fjord in northwest Greenland (Jakobsson et al., 2018). These sediment-landform assemblages have been used to infer that fast flowing ice streams were present in these troughs, similar to Norske and Westwind troughs.

GZWs are widely identified transverse to former ice flow direction in glaciated cross-shelf troughs, including those on the Greenland continental shelf, where their presence is suggestive of stillstands of the grounding line during ice stream retreat (e.g., Shipp et al., 2002; Ó Cofaigh et al., 2008; Dowdeswell et al., 2008b; Dowdeswell and Fugelli, 2012; Livingstone et al., 2013; Bjarnadóttir et al., 2013; Dowdeswell et al., 2014; Batchelor and Dowdeswell, 2015; Hogan et al., 2016; Ryan et al., 2016; Sheldon et al., 2016; Newton et al., 2017; Callard et al., 2018). Therefore, the identification of sediment wedges with a long, flat ice distal side (the reverse cross-sectional profile to a GZW) in Westwind Trough, is a notable difference in recessional landform assemblage in comparison with other palaeo-ice streams. Despite the morphological differences between the Westwind Trough sediment wedges and the typical GZW, it has been suggested that their occurrence has a similar implication for former ice dynamics. Episodic ice retreat has previously been inferred from the presence of GZWs and moraines on the outer shelf of Store Koldeway Trough, which is located south of Norske Trough (see Fig. 1.1b) (Laberg et al., 2017). Therefore, the inferred stepped recession in Westwind Trough proposed in this study is consistent with previous reconstructions of episodic ice retreat in northeast Greenland. Iceberg

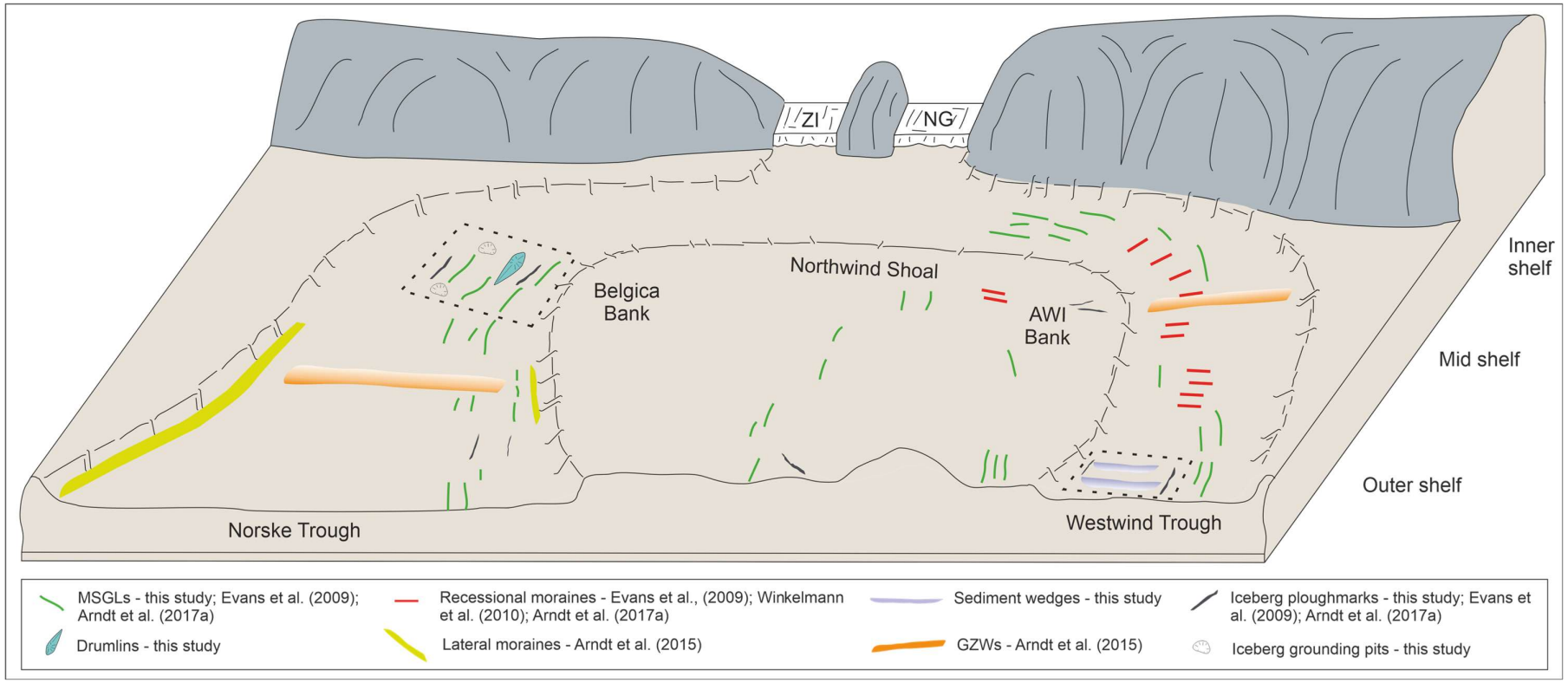

Figure 6.4 Cartoon showing the distribution of glacial landforms present in Norske and Westwind troughs, and the intervening shallow regions, produced by the advance and retreat of the NEGIS across the continental shelf. Landforms shown were identified by Evans et al. (2009), Winkelmann et al. (2010), Arndt et al. (2015), and Arndt et al. (2017a), and the dashed boxes highlight landforms from this study. Landforms are not represented to scale or in their exact position.

ploughmarks and grounding pits formed by iceberg scour have also been reported across the Greenland continental shelf (e.g., Dowdeswell et al., 1993; 1994a; Syvitski et al., 2001; Dowdeswell et al., 2014; Newton et al., 2017).

The glacimarine depositional regime during NEGIS retreat is also similar to other east and west Greenland ice streams. In general, the role of meltwater in deposition appears to increase from the outer to the inner shelf in Greenland (e.g., Evans et al., 2002; Hogan et al., 2016; Sheldon et al., 2016; Streuff et al., 2017), a pattern which is broadly reflected in the change in depositional processes from outer to mid to inner shelf in Norske and Westwind troughs. In Disko and Uummannaq troughs, west Greenland, glacimarine deposition on the outer shelf was dominated by iceberg rafting, suggesting that initial mass loss during retreat was from calving (Jennings et al., 2014; Hogan et al., 2016; Sheldon et al., 2016). On the outer shelf beyond Kejser Franz Joseph Fjord, east Greenland, massive and stratified diamictons were deposited by iceberg rafting and cohesive debris flow activity respectively (Evans et al., 2002). Sediment cores dominated by iceberg-rafted diamictons and high-intensity iceberg scours on the continental shelf adjacent to Scoresby Sund, East Greenland, also record sediment deposition and reworking by icebergs (Dowdeswell et al., 1993; 1994a). Therefore, the evidence of deposition by both iceberg rafting and gravity flows in outer Westwind Trough during the initial stage of NEGIS retreat is consistent with previous work on ice stream retreat from elsewhere around Greenland.

As ice streams retreated back to mid- and inner-shelf positions and into the fjords in both east and west Greenland, suspension settling from meltwater plumes became increasingly important. It is also notable, however, that meltwater sedimentation occurred during deglaciation of outer Westwind Trough. In Disko Tough, variations in the dominance of meltwater sedimentation vs iceberg rafting have been inferred to reflect the control of seasonality (Hogan et al., 2016), with subsequent deposition in Disko Bay itself dominated by suspension settling (Streuff et al., 2017). In inner Uummannaq Trough, deposition also occurred by a combination of suspension settling and iceberg rafting (Sheldon et al., 2016). The dominance of suspension settling recorded in core PS100-208 from inner Norske Trough, and the presence of meltwater-derived facies in core PS100-173 from the mid Norske Trough, is consistent with observations from these other Greenland ice streams. This underscores the increasing importance of meltwater delivery to

glacimarine sedimentation as retreat progresses from outer to inner shelf locations. A similar pattern has also been observed in fjords around Greenland. For example, in outer Scoresby Sund, iceberg rafted and scoured diamictons dominate the sedimentary record, whilst in the inner fjord system deposition by suspension settling from overflow plumes and turbidity currents was more influential (Dowdeswell et al., 1993; 1994a; Ó Cofaigh et al., 2001).

This study suggests the presence of an ice-shelf fronting the NEGIS during its retreat through Norske Trough. A floating ice tongue was also present on the Petermann Glacier in northwest Greenland during its Holocene retreat (Reilly et al., 2019). Cores from Petermann Fjord show that sub-ice shelf deposition was recorded by IRD-poor laminated mud (Reilly et al., 2019), similar to the possible sub-ice shelf suspension deposits in mid Norske Trough (LF3-173). However, there appears to have been limited rain-out of coarse debris in the sub-ice shelf cavity of Petermann, which contrasts with the possible sub-ice shelf diamictons in core PS100-173 from Norske Trough.

The sedimentary and geomorphological data from Norske and Westwind troughs presented in this study have allowed the reconstruction of the glacigenic depositional processes, associated depositional environments, and ice stream dynamics related to the last advance and retreat of the NEGIS across the northeast Greenland continental shelf. This contributes to the wider understanding of the glacial and glacimarine processes that took place during the advance and retreat of the GrIS during the last glaciation (c.f. Evans et al., 2002; Hogan et al., 2016; Sheldon et al., 2016; Reilly et al., 2019). Furthermore, establishing these processes has enabled preliminary inferences about the dynamics of the NEGIS to be made, which could be used to help constrain future modelling of NEGIS retreat. These include the possibility that the NEGIS may have been fronted by an ice shelf in Norske Trough, that retreat from the outer shelf in Westwind Trough was episodic, and that readvances of the grounding line may have occurred during deglaciation.

7. Conclusions

Geophysical and sedimentological data from Norske and Westwind troughs on the northeast Greenland continental shelf have provided new information about the depositional processes and landform-sediment assemblages associated with the advance and retreat of the NEGIS during, and following, the LGM. Knowledge of these processes has provided insights into the LGM extent of NEGIS, its dynamics during advance and retreat, and the associated depositional environments. The key findings are as follows:

(1) Streamlined subglacial landforms including drumlins and MSGLs as well as subglacial tills reported from Norske and Westwind troughs document the advance of streaming ice across the northeast Greenland continental shelf during the LGM. Soft and stiff tills were deposited by subglacial deformation, possibly with some contribution from lodgement, whilst the genesis of both the drumlins and MSGLs was also likely, at least in part, a product of subglacial deformation.

(2) The presence of sediment wedges at the shelf edge in Westwind Trough provides further confirmation that the GrIS reached the outer shelf offshore of northeast Greenland during the LGM, as has been previously proposed by Arndt et al. (2017a). This provides support for an extensive GrIS which advanced across the continental shelf at the LGM (e.g., Dowdeswell et al., 2010; Ó Cofaigh et al., 2013a; Hogan et al., 2016; Sheldon et al., 2016; Slabon et al., 2016; Laberg et al., 2017).

(3) As the NEGIS retreated across the continental shelf from its LGM maximum position, glacimarine and subglacial processes including iceberg rafting, suspension settling from meltwater plumes, mass flow activity (debris flows and turbidity currents), iceberg keel scouring, and glacitectonism occurred. These processes were also involved in the genesis of sediment wedges, iceberg grounding pits and iceberg ploughmarks.

    a. Low amplitude sediment wedges (9-15 m height, 1.9-2 km long) were formed in outer Westwind Trough, including at the shelf edge. They were constructed proximal to the grounding line during ice retreat, predominantly by debris flows released from a backstepping grounding line. Debris flow activity deposited massive diamicton displaying deformed inclusions at both the macro- and micro-scale.

Based on their low amplitude and lack of 'ramp-scarp' profile, it is proposed that these sediment wedges were probably formed at a tidewater margin rather than below an ice shelf. The mixed recessional landform imprint in Westwind Trough of both moraines (see Winkelmann et al., 2010; Arndt and Evans, 2016; Arndt et al., 2017a) and sediment wedges suggests that the style of recessional landform is not always dictated by ice shelf presence or absence.

b. Beyond the grounding line, suspension settling from meltwater plumes, and occasional turbidity current activity, produced laminated, stratified and massive mud across the continental shelf during retreat. Meltwater-derived facies dominate cores from inner Norske Trough, whilst on the mid and outer shelf, massive to stratified diamictons were deposited by IRD rainout, with a lesser contribution by suspension settling from meltwater plumes. Iceberg scouring also produced iceberg grounding pits, iceberg furrows, and micro-scale deformation structures on the mid and outer shelf. Therefore, it is evident that during retreat from the outer to the inner shelf, the contribution of meltwater increased whilst that from icebergs became much less dominant. Interestingly, this pattern has also been observed in glacimarine sedimentary sequences deposited by retreating ice streams elsewhere in both east and west Greenland (e.g., Evans et al., 2002; Hogan et al., 2016; Sheldon et al., 2016).

(4) Retreat of the NEGIS from the shelf edge in Westwind Trough occurred in a stepped fashion. The transition from the presence of sediment wedges in outer Westwind Trough, to smaller recessional moraines in the mid trough (Winkelmann et al., 2010; Arndt et al., 2017a), implies that stillstands became progressively shorter as the grounding line receded across the continental shelf. Mass loss by calving was dominant during ice retreat across outer Westwind and mid Norske troughs. Evidence of glacitectonism suggests that at least one period of grounding line readvance occurred whilst the ice was stationed in mid Norske Trough, which may have been driven by Younger Dryas cooling. On the inner shelf, grounding line recession was generated by melting at the ice margin and accounts for the dominance of meltwater deposits in inner Norske Trough. This melting may have been driven by the increase in atmospheric and/or ocean

temperatures which occurred during the early Holocene. This has been used to infer that the NEGIS had reached the inner shelf by the early Holocene.

(5) The NEGIS may have been fronted by an ice shelf as it retreated through Norske Trough based on the occurrence of lithofacies which share characteristics with sediment known to be deposited in an ice shelf setting. No indication of former ice shelf presence in Westwind Trough has been revealed in this study, so a tidewater margin is inferred during deglaciation. This implies that adjacent ice sheet outlets can be characterised by different grounding line regimes (ice shelf vs tidewater) during ice sheet retreat on high-latitude continental margins.

8. References

Alley, R.B., Blankenship, D.D., Bentley, C.R., Rooney, S.T. (1986) Deformation of till beneath ice stream B, West Antarctica. *Nature.* 322: 57-59.

Alley, R.B., Blankenship, D.D., Rooney, S.T., Bentley, C.R. (1989) Sedimentation beneath ice shelves – the view from ice stream B. pp101-120 in Powell, R.D., Elverhøi, A. (eds) Modern Glacimarine Environments: Glacial and Marine Controls of Modern Lithofacies and Biofacies. *Marine Geology*. 85: 101-120.

An, L., Rignot, E., Wood, M., Willis, J.K., Mouginot, J., Khan, S.A. (2021) Ocean melting of the Zachariae Isstrøm and Nioghalvfjerdsfjorden glaciers, northeast Greenland. Proceedings of the National Academy of Sciences. 118(2): e2015483118

Anderson, J.B., Jakobsson, M. (2016) Grounding-zone wedges on Antarctic continental shelves. pp 243-244 in Dowdeswell, J. A., Canals, M., Jakobsson, M., Todd, B. J., Dowdeswell, E. K. & Hogan, K. A. (eds) *Atlas of Submarine Glacial Landforms: Modern, Quaternary and Ancient.* Geological Society, London, Memoirs, 46.

Anderson, J.B., Kennedy, D.S., Smith, M.J., Domack, E.W. (1991) Sedimentary facies associated with Antarctica's floating ice masses. In Anderson, J.B., Ashley, G.M. (eds) *Glacial marine sedimentation; Paleoclimatic significance.* Geological Society of America Special Paper 261. Boulder, Colorado

Andrews, J.T. (1982) On the reconstruction of Pleistocene ice sheets: A review. *Quaternary Science Reviews*. 1: 1-30.

Arndt, J.E. (2018) Marine geomorphological record of Ice Sheet development in East Greenland since the Last Glacial Maximum. *Journal of Quaternary Science*. 33(7): 853-864.

Arndt, J.E., Evans, J. (2016) Glacial lineations and recessional moraines on the continental shelf of NE Greenland. pp 263-264 in Dowdeswell, J. A., Canals, M., Jakobsson, M., Todd, B. J., Dowdeswell, E. K., Hogan, K. A. (eds) *Atlas of Submarine Glacial Landforms: Modern, Quaternary and Ancient.* Geological Society, London, Memoirs, 46.

Arndt, J.E., Hillenbrand, C-D., Grobe, H., Kuhn, G., Wacker, L. (2017b) Evidence for a dynamic grounding line in outer Filchner Trough, Antarctica, until the early Holocene. *Geology.* 45(11): 1035-1038.

Arndt, J.E., Jokat, W., Dorschel, B. (2017a) The last glaciation and deglaciation of the Northeast Greenland continental shelf revealed by hydro-acoustic data. *Quaternary Science Reviews.* 160: 45-56.

Arndt, J.E., Jokat, W., Dorschel, B., Myklebust, R., Dowdeswell, J.A., Evans, J. (2015) A new bathymetry of the Northeast Greenland continental shelf: Constraints on glacial and other processes. *Geocehemistry, Geophysics, Geosystems.* 16(10).

Baeten, N.J., Forwick, M., Vogt, C., Vorren, T.O. (2010) Late Weichselian and Holocene sedimentary environments and glacial activity in Billefjorden, Svalbard. Pp 207-223 in Howe, J.A., Austin, W.E.N., Forwick, M., Paetzel, M. (eds) Fjord Systems and Archives. Geological Society, London, Special Publications 344.

Barrie, J.V., Lewis, C.F.M., Parott, D.R., Collins, W.T. (1992) Submersible observations of an iceberg pit and scour on the Grand Banks of Newfoundland. *GeoMarine Letters*. 12: 1-6.

Batchelor, C.I., Dowdeswell, J.A. (2015) Ice-sheet grounding-zone wedges (GZWs) on high-latitude continental margins. *Marine Geology*. 363: 65-92.

Batchelor, C.L., Dowdeswell, J.A. (2014) The physiography of High Arctic cross-shelf troughs. *Quaternary Science Reviews*. 92: 68-96.

Batchelor, C.L., Dowdeswell, J.A., Hogan, K.A. (2011) Late Quaternary ice flow and sediment delivery through Hinlopen Trough, Northern Svalbard margin: Submarine landforms and depositional fan. *Marine Geology*. 284: 13-27.

Batchelor, C.I., Dowdeswell, J.A., Rignot, E. (2019) Submarine landforms reveal varying rates and styles of deglaciation in North-West Greenland fjords. *Marine Geology*. 402: 60-80.

Benn D.I., Evans, D.J.A. (1996) The interpretation and classification of subglacially-deformed materials. *Quaternary Science Reviews*. 15(1): 23-52.

Benn, D.I. (1995) Fabric signature of subglacial till deformation, Breidamerkurjokull, Iceland. *Sedimentology.* 42: 735–747.

Benn, D.J., Evans, D.J.A (2010) *Glaciers and Glaciation*. London: Hodder Education.

Bennett, M.R. (2003) Ice streams as the arteries of an ice sheet: their mechanics, stability and significance. *Earth-Science Reviews*. 61(3-4): 309-339

Bennike, O., Bjorck, S. (2002) Chronology of the last recession of the Greenland Ice Sheet. *Journal of Quaternary Science*. 17: 211–219.

Bennike, O., Björck, S., Lambeck, K. (2002) Estimated of South Greenland late-glacial ice limits from a new relative sea level curve. *Earth and Planetary Science Letters*. 197: 171-186.

Bennike, O., Weidick, A. (2001) Late Quaternary history around Nioghalvfjerdsfjorden and Jøkelbugten, North-East Greenland. *Boreas*. 30: 205 – 227.

Bentley, M.J. et al. (The RAISED Consortium) (2014) A community-based geological reconstruction of Antarctic Ice Sheet deglaciation since the Last Glacial Maximum. *Quaternary Science Reviews.* 100: 1-9.

Bevis, M., Harig, C., Khan, S.A., Brown, A., Simons, F.J., Willis, M., Fettweis, X., van der Broeke, M.R., Madsen, F.B., Kendrick, E., Caccamise II, D.J., van Dam, T., Knudsen, P., Nylen, T. (2019) Accelerating changes in ice mass within Greenland, and the ice sheet's sensitivity to atmospheric forcing. *Proceedings of the National Academy of Sciences.* 116(6): 1934-1939.

Bjarnadóttir, L.R., Rüther, D.C., Winsborrow, M.C.M., Andreassen, K. (2013) Grounding-line dynamics during the last deglaciation of Kveithola, W Barents Sea, as revealed by seabed geomorphology and shallow seismic stratigraphy. *Boreas*. 42: 84–107.

Bjarnadóttir, L.R., Winsborrow, M.C.M., Andreassen, K. (2014) Deglaciation of the central Barents Sea. *Quaternary Science Reviews*. 92: 208-226.

Boulton, G.S. (1976) The origin glacially fluted surfaces – observations and theory. *Journal of Glaciology.* 17(76): 287-309.

Boulton, G.S. (1986) A paradigm shift in glaciology. *Nature.* 322(6074): 18.

Boulton, G.S. (1987) A theory of drumlin formation by subglacial sediment deformation. pp 25-80 in Menzies, J., Rose, J. (eds) *Drumlin Symposium*. Balkema, Rotterdam.

Boulton, G.S., Dobbie, K.E. (1998) Slow flow of granular aggregates: the deformation of sediment beneath glaciers. *Philosophical transactions of the Royal Society of London*. A365: 2713-2745.

Boulton, G.S., Dobbie, K.E., Zatsepin, S. (2001) Sediment deformation beneath glaciers and its coupling to the subglacial hydraulic system. *Quaternary International*. 86: 3-28.

Boulton, G. S., Hindmarsh, R. C. A. (1987) Sediment deformation beneath glaciers: Rheology and geological consequences. *Journal of Geophysical Research.* 92(B9): 9059–9082.

Bouma, A.H. (1962) *Sedimentology of Some Flysch Deposits*. Elsevier: Amsterdam.

Brewer, R. (1976) *Fabric and mineral analysis of soils.* Krieger: Huntington.

Buizert, C., Gkinis, V., Sveringhaus, J.P., He, F., Lecavalier, B.S., Kindler, P., Leunberger, M., Carlson, A.E., Vither, B., Masson-Delmotte, V., White, J.W.C., Liu, Z., Otto-Bliesner, B., Brook, E.J. (2014) Greenland temperature response to climate forcing during the last deglaciation. *Science.* 345(6201): 1177-1180.

Burke, H., Phillips, E., Lee, J. R., Wilkinson, I. P. (2009) Imbricate thrust stack model for the formation of glaciotectonic rafts: an example from the Middle Pleistocene of north Norfolk, UK. *Boreas.* 38: 620–637.

Cai, J., Powell, R.D., Cowan, E.A., Carlson, P.R. (1997) Lithofacies and seismic-reflection interpretation of temperate glacimarine sedimentation in Tarr Inlet, Glacier Bay, Alaska. *Marine Geology*. 143: 5-37.

Callard, S.L. , Ó Cofaigh, C., Benetti, S., Chiverrell, R.C., Van Landeghem, K.J.J., Saher, M.H., Gales, J.A., Small, D. , Clark, C.D., Livingstone, S.J., Fabel, D., Moreton, S.G. (2018) Extent and retreat history of the Barra Fan Ice Stream offshore western Scotland and northern Ireland during the last glaciation. *Quaternary Science Reviews*. 201: 280-302.

Callard, S.L., Ó Cofaigh, C., Benetti, S., Chiverrell, R.C., Van Landeghem, K.J.J., Saher, M.H., Livingstone, S.J., Clark, C.D., Small, D., Fabel, D., Moreton, S.G.

(2020) Oscillating retreat of the last British-Irish Ice Sheet on the continental shelf offshore Galway Bay, western Ireland. *Marine Geology*. 420: 106087.

Canals, M.R., Urgeles, R., Calafat, A.M. (2000) Deep sea-floor evidence of past ice streams off the Antarctic Peninsula. *Geology.* 28: 31–34.

Carr, S.J. (1999). The micromorpology of the Last Glacial Maximum sediments in the Southern North Sea. *Catena.* 35: 123-145.

Carr, S.J. (2001) Micromorphological criteria for discriminating subglacial and glacimarine sediments: evidence from a contemporary tidewater glacier, Spitsbergen. *Quaternary International.* 86: 71-79.

Carr, S.J. (2004) Micro-scale features and structures. pp 115-144 in Evans, D.J.A., Benn, D.I. (eds) *A practical guide to the study of glacial sediment*. London: Arnold.

Carr, S.J., Holmes, R., van der Meer, J.J.M., Rose, J. (2006) The Last Glacial Maximum in the North Sea Basin: micromorphological evidence of extensive glaciation. *Journal of Quaternary Science.* 21(2): 131-153.

Carr, S.J., Lee, J.A. (1998) Thin-section production of diamicts: problems and solutions. *Journal of Sedimentary Research.* 68(1): 217-220.

Ceperley, E.G., Marcott, S.A., Reusche, M.M., Barth, A.M., Mix, A.C., Brook, E.J., Caffee, M. (2020) Widespread early Holocene deglaciation, Washington Lane, northwest Greenland. *Quaternary Science Reviews*. 231: 106181.

Chiverell, R.C., Thrasher, I.M., Thomas, G.S.P., Lang, A., Scourse, J.D., Van Landeghem, K.J.J., McCarroll, D., Clark, C.D., Ó Cofaigh, C., Evans, D.J.A., Ballantyne, C. (2013) Bayesian modelling the retreat of the Irish Sea Ice Stream. *Journal of Quaternary Science*. 28(2): 200-209.

Choi, Y., Morlighem, N., Rignot, E., Mouginot, J., Wood, M (2017) Modeling the Response of Nioghalvfjerdsfjorden and Zachariae Isstrøm Glaciers, Greenland, to Ocean Forcing Over the Next Century. *Geophysical Research Letters*. 44(21): 11,0171-11,079.

Church, J.A., Clark, P.U., A. Cazenave, J.M. Gregory, S. Jevrejeva, A. Levermann, M.A. Merrifield, G.A. Milne, R.S. Nerem, P.D. Nunn, A.J. Payne, W.T. Pfeffer, D. Stammer and A.S. Unnikrishnan, 2013: Sea Level Change. In: Climate Change 2013: The Physical Science Basis. Contribution of Working Group I to the Fifth Assessment Report of the Intergovernmental Panel on Climate Change [Stocker, T.F., D. Qin, G.-K. Plattner, M. Tignor, S.K. Allen, J. Boschung, A. Nauels, Y. Xia, V. Bex and P.M. Midgley (eds.)]. Cambridge University Press, Cambridge, United Kingdom and New York, NY, USA.

Clark, C.D. (1993) Mega-scale glacial lineations and cross-cutting ice-flow landforms. *Earth Surface Processes and Landforms*. 18: 1-29.

Clark, C. D., Ely, J. C., Greenwood, S. L., Hughes, A. L. C., Meehan, R., Barr, I. D., Bateman, M. D., Bradwell, T., Doole, J., Evans, D. J. A., Jordan, C. J., Monteys, X., Pellicer, X. M., Sheehy, M. (2018) BRITICE Glacial Map, version 2: a

map and GIS database of glacial landforms of the last British–Irish Ice Sheet. Boreas. 47: 11–27.

Clark, C.D., Hughes, A.L.C., Greenwood, S.I., Spagnolo, M., Ng, F.S.I. (2009) Size and shape characteristics of drumlins, derived from a large sample, and associated scaling laws. *Quaternary Science Reviews*. 28: 677-692.

Clark, C.D., Tulaczyk, S.M., Stokes, C.R., Canals, M. (2003) A groove-ploughing theory for the production of mega-scale lineations, and implications for ice stream mechanics. *Journal of Glaciology*. 49: 240-256.

Clark, P.U., Hansel, A.K. (1989) Clast ploughing, lodgement and glacier sliding over a soft glacier bed. *Boreas*. 3: 201-207.

Clark, P.U., Walder, J.S. (1994) Subglacial drainage, eskers, and deforming beds beneath the Laurentide and Eurasian ice sheets. *Geological Society of America Bulletin.* 106: 304-314.

Collinson, J.D., Thompson, D.B. (1989) *Sedimentary Structures*. London: Chapman & Hall.

Cowan, E.A., Cai, J., Powell, R.D., Clark, J., Pitcher, J.N. (1997) Temperate glacimarine varves: An example from Disenchantment Bay, Southern Alaska. *Journal of Sedimentary Research*. 67(3): 536-549.

Cowan, E.A., Powell, R.D. (1990) Suspended sediment transport and deposition of cyclically interlaminated sediment in a temperate glacial fjord, Alaska, U.S.A. pp 75-89 in Dowdeswell, J.A., Scourse, J.D. (eds) *Glacimarine Environments: Processes and Sediments*. Geological Society Special Publication 53.

Cowan, E.A., Powell, R.D. (1991) Ice-proximal sediment accumulation rates in a temperate glacial fjord, southeastern Alaska. pp 61-73 in Anderson, J. B., and Ashley, G. M. (eds) *Glacial marine sedimentation: Paleoclimatic significance.* Boulder, Colorado: Geological Society of America Special Paper 261.

Cowan, E.A., Seramur, K.C., Cai., J., Powell, R.D. (1999) Cyclic sedimentation produced by fluctuations in meltwater discharge, tides and marine productivity in an Alaskan fjord. *Sedimentology*. 46: 1109-1126.

Damuth, J.E. (1980) Use of high-frequency (3.5--12 kHz) echograms in the study of near-bottom sedimentation processes in the deep-sea: a review*. Marine Geology.* 38: 51—75.

Darby, D.A., Myers, W.B., Jaboksson, M., Rigor, I. (2011) Modern dirty sea ice characteristics and sources: The role of anchor ice. *Journal of Geophysical Research*. 116: C09008

Darby, D.A., Ortiz, J., Polyak, L., Lund, S., Jakobsson, M., Woodgate, R.A. (2009) The role of currents and sea ice in both slowly deposited central Arctic and rapidly deposited Chuckchi-Alaskan margin sediments. *Global and Planetary Change*. 68: 58-72.

Davies, B.J., Roberts, D.H., Ó Cofaigh, C., Bridgland, D.R., Riding, J.B., Phillips, E.R., Teasdale, D.E. (2009) Interlobate ice-sheet dynamics during the Last Glacial Maximum at Whitburn Bay, County Durham, England. *Boreas*. 38: 555-578.

Davies, D., Bingham, R.G., Graham, A.C.G., Spagnolo, M., Dutrieux, P., Vaughan, D.G., Jenkins, A., Nitsche, F.O. (2017) High resolution sub-ice-shelf seafloor records of twentieth century ungrounding and retreat of Pine Island Glacier, West Antarctica. *Journal of Geophysical Research: Earth Surface*. 122: 1698-1714.

Denton, G.H., Alley, R.B., Comer, G.C., Broecker, W.S. (2005) The role of seasonality in abrupt climate change. *Quaternary Science Reviews*. 24: 1159-1182.

Desloges, J.R., Gilbert, R., Nielsen, N., Christiansen, C., Rasch, M., Øhlenschläger, R. (2002) Holocene glacimarine sedimentary environments in fjords of Disko Bugt, West Greenland. *Quaternary Science Reviews*. 21: 947-963.

Domack, E.W. (1990) Laminated terrigenous sediments from the Antarctic Peninsula: The role of subglacial and marine processes. *The Geological Society of London, Special Publications.* 53: 91–103.

Domack, E.W., Duran, D., Leventer, A., Ishman, S., Doane, S., McCallum, S., Amblas, D., Ring, J., Gilbert, R., Prentice, M. (2005) Stability of the Larsen B ice shelf on the Antarctic Peninsula during the Holocene epoch. *Nature*. 436: 681-685.

Domack, E.W., Harris, P.T. (1998) A new depositional model for ice shelves, based upon sediment cores from the Ross Sea and the MacRobertson shelf, Antarctica. *Annals of Glaciology*. 27: 281–284.

Domack, E.W., Jacobson, E.A., Shipp, S., Anderson, J.B. (1999) Late Pleistocene–Holocene retreat of the West Antarctic Ice-Sheet system in the Ross Sea: Part 2— Sedimentologic and stratigraphic signature: *Geological Society of America Bulletin*. 111: 1517–1536.

Domack, E.W., Lawson, D.E. (1985) Pebble fabric in an ice rafted diamicton. *Journal of Geology.* 93: 577–592.

Dowdeswell, J.A. (2006) The Greenland Ice Sheet and Global Sea-Level Rise. *Science.* 311(5763): 963-964.

Dowdeswell, J.A., Dowdeswell, E.K. (1989) Debris in icebergs and rates of glaci-marine sedimentation: observations from Spitsbergen and a simple model. *The Journal of Geology.* 97(2): 221-231.

Dowdeswell, J.A., Elverhøi, A., Spielhagen, R. (1998) Glacimarine sedimentary processes and facies on the Polar North Atlantic Margins. *Quaternary Science Reviews.* 17: 243-272.

Dowdeswell, J.A., Evans, J., Ó Cofaigh, C. (2010) Submarine landforms and shallow acoustic stratigraphy of a 400 km-long fjord-shelf-slope transect, Kangerlussuaq margin, East Greenland. *Quaternary Science Reviews*. 29: 3359-3369.

Dowdeswell, J.A., Fugelli, E.M.G. (2012) The seismic architecture and geometry of grounding-zone wedges formed at the marine margins of past ice sheets. *Geological Society of America Bulletin*. 124(11/12): 1750-1761.

Dowdeswell, J.A., Fugelli, E.M.G., Batchelor, C.L. (2016) Grounding-zone wedges on the West Greenland shelf imaged from multibeam and seismic data. pp 235-236 in Dowdeswell, J. A., Canals, M., Jakobsson, M., Todd, B. J., Dowdeswell, E. K., Hogan, K. A. (eds) *Atlas of Submarine Glacial Landforms: Modern, Quaternary and Ancient.* Geological Society, London, Memoirs, 46.

Dowdeswell, J.A., Hogan, K.A., Ó Cofaigh, C., Fugelli, E.M.G., Evans, J., Noormets, R. (2014) Late Quaternary ice flow in a West Greenland fjord and cross-shelf trough system: submarine landforms from Rink Isbrae to Uummannaq shelf and slope. *Quaternary Science Reviews*.

Dowdeswell, J.A., Kenyon, N.H., Laberg, J.S. (1997) The glacier influenced Scoresby Sund Fan, East Greenland continental margin: evidence from GLORIA and 3.5 kHz records. *Marine Geology*. 143: 207-221.

Dowdeswell, J.A., Ó Cofaigh, C., Noormets, R., Larter, R.D., Hillenbrand, C-D., Benetti, S., Evans, J., Pudsey, C.J. (2008a) A major trough-mouth fan on the continental margin of the Bellingshausen Sea, West Antarctica: The Belgica Fan. *Marine Geology*. 252: 129-140.

Dowdeswell, J.A., Ó Cofaigh, C., Pudsey, C.J. (2004) Thickness and extent of the subglacial till layer beneath an Antarctic paleo–ice stream. *Geology*. 32(1): 13-16

Dowdeswell, J.A., Ó Cofaigh, C., Taylor, J., Kenyon, N., Mienert, J., Wilken, M. (2002) On the architecture of high-latitude continental margins: the influence of ice-sheet and sea-ice processes in the Polar North Atlantic. p 33-54 in Dowdeswell, J. A., O'Cofaigh, C. (eds.) *Glacier-influenced Sedimentation on High-latitude Continental Margins.* London: Geological Society of London.

Dowdeswell, J.A., Ottesen, D., Evans, J., Ó Cofaigh, C., Anderson, J.B. (2008b) Submarine glacial landforms and rates of ice-stream collapse. *Geology.* 36(10): 819-822.

Dowdeswell, J.A., Uenzelmann-Neben, A., Whittington, R.J., Marienfeld, P (1994b) Late Quaternary sedimentary record in Scoresby Sund, East Greenland. *Boreas*. 23: 294-310.

Dowdeswell, J.A., Villinger, H., Whittington, R.J., Marienfeld, P. (1993) Iceberg scouring in Scoresby Sund and on the East Greenland continental shelf. *Marine Geology*. 111: 37-53.

Dowdeswell, J.A., Whittington, Jennings, A.E., Andrews, J.T. (2000) An origin for laminated glacimarine sediments through sea-ice build-up and suppressed iceberg rafting. *Sedimentology*. 47: 557-576.

Dowdeswell, J.A., Whittington, R.J., Marienfeld, P. (1994a) The origin of massive diamicton facies by iceberg rafting and scouring, Scoresby Sund, East Greenland. *Sedimentology*. 41: 21-35.

Dreimanis, A. (1989) Tills: their genetic terminology and classification. pp17-84 in Goldthwait, R.P., Matsch, C.L. (eds) *Genetic Classification of Glacigenic Deposits*. Balkema, Rotterdam.

Dunlop, P., Shannon, R., McCabe, M., Quinn, R., Doyle, E. (2010) Marine geophysical evidence for ice sheet extension and recession on the Malin Shelf: New evidence for the western limits of the British Irish Ice Sheet. *Marine Geology*. 276: 86-99.

Elverhøi, A., Lønne, Ø., Seland, R. (1983) Glaciomarine sedimentation in a modern fjord environment, Spitsbergen. *Polar Research.* 1: 127-149.

Enderlin, E.M., Howat, I.M., Jeong, S., Noh, M-J., van Angelen, J.H., van den Broeke, M.R. (2014) An improved mass budget for the Greenland ice sheet. *Geophysical Research Letters.* 41(3): 866-872.

Engelhardt, H., Kamb, B. (1998) Basal sliding of Ice Stream B, West Antarctica. *Journal of Glaciology*. 44(147): 223-230.

England, J. (1999) Coalescent Greenland and Innuitian ice during the Last Glacial Maximum: revising the Quaternary of the Canadian High Arctic. *Quaternary Science Reviews*. 18: 421-456.

England, J., Atkinson, N., Bednarski, J., Dyke, A.S., Hodgson, D.A., Ó Cofaigh, C. (2006) The Innuitian Ice Sheet: configuration, dynamics and chronology. *Quaternary Science Reviews*. 25: 689-703.

Evans, D.J.A. (2018) *Till: a glacial process sedimentology*. Chichester: Wiley Blackwell.

Evans, D.J.A., Benn, D.I. (2004) Facies description and the logging of sedimentary exposures. pp11-51 in Evans, D.J.A., Benn, D.I. (eds) *A practical guide to the study of glacial sediment*. London: Arnold.

Evans, D.J.A., Hiemstra, J.F. (2005). Till deposition by glacier submarginal, incremental thickening. *Earth Surface Processes and Landforms.* 30(13): 1633-1662.

Evans, D. J. A., Ó Cofaigh, C. (2003) Depositional evidence for marginal oscillations of the Irish Sea ice stream in southeast Ireland during the last glaciation. *Boreas.* 32: 76–101.

Evans, D.J.A., Owen, L.A., Roberts, D. (1995) Stratigraphy and sedimentology of Devensian (Dimlington Stadial) glacial deposits, east Yorkshire, England. *Journal of Quaternary Science*. 10(3): 241-265.

Evans, D.J.A., Phillips, E.R., Hiemstra, J.F., Auton, C.A. (2006a) Subglacial till: Formation, sedimentary characteristics and classification. *Earth Science Reviews*. 78(1-2): 115-176.

Evans, D.J.A., Roberts, D.H., Evans, S.C. (2016) Multiple subglacial till deposition: A modern exemplar for Quaternary palaeoglaciology. *Quaternary Science Reviews*. 145: 183-203.

Evans, D.J.A., Roberts, D.H., Hiemstra, J.F., Nye, K.M., Wright, H., Steer, A. (2018) Submarginal debris transport and till formation in active temperate glacier systems: The southeast Iceland type locality. *Quaternary Science Reviews*. 195: 72-108.

Evans, D.J.A., Twigg, D.R. (2002) The active temperate glacial landsystem: a model based on Breidamerkurjökull and Fjallsjökull, Iceland. *Quaternary Science Reviews*. 21: 2143-2177.

Evans, J., Dowdeswell, J.A., Grobe, H., Niessen, F., Stein, R., Hubberten, H., Whittington, R.J. (2002) Late Quaternary sedimentation in Kejser Franz Joseph Fjord and the continental margin of East Greenland. pp149-180 in Dowdeswell, J. A., Ó Cofaigh, C. (eds) *Glacier-influenced Sedimentation on High-latitude Continental Margins.* London: Geological Society of London.

Evans, J., Dowdeswell, J.A., Ó Cofaigh, C., Benham, T.J., Anderson, J.B. (2006) Extent and dynamics of the West Antarctic Ice Sheet on the outer continental shelf of Pine Island Bay during the last glaciation. *Marine Geology*. 230: 53-72.

Evans, J., Hogan, K.A. (2016) Grounding-zone wedges on the northern Larsen shelf, Antarctic Peninsula. pp 237-238 in in Dowdeswell, J. A., Canals, M., Jakobsson, M., Todd, B. J., Dowdeswell, E. K., Hogan, K. A. (eds) *Atlas of Submarine Glacial Landforms: Modern, Quaternary and Ancient*. Geological Society, London, Memoirs, 46.

Evans, J., Ó Cofaigh, C., Dowdeswell, J.A., Wadhams, P. (2009) Marine geophysical evidence for former expansion and flow of the Greenland Ice Sheet across the north-east Greenland continental shelf. *Journal of Quaternary Science*. 24: 279-293.

Evans, J., Pudsey, C.J. (2002) Sedimentation associated with Antarctic Peninsula ice shelves: implications for palaeoenvironmental reconstructions of glacimarine sediments. *Journal of the Geological Society*. 159: 233-237.

Evans, J., Pudsey, C.J., Ó Cofaigh, C., Morris, P., Domack, E. (2005) Late Quaternary glacial history, fl ow dynamics and sedimentation along the eastern margin of the Antarctic Peninsula Ice Sheet. *Quaternary Science Reviews.* 24(5–6): 741–774.

Eyles, C.H., Eyles, N. (2000) Subaqueous mass flow origin for Lower Permian diamictites and associated facies of the Grant Group, Barbwire Terrace, Canning Basin, Western Australia. *Sedimentology*. 47: 343-356.

Eyles, N., Boyce, J.I., Putniken, N. (2015) Neoglacial (<3000 years) till and flutes at Saskatchewan Glacier, Canadian Rocky Mountains, formed by subglacial deformation of a soft bed. *Sedimentology*. 62: 182-203.

Eyles, N., McCabe, A.M. (1989) The Late Devensian (22, 000 BP) Irish Sea Basin: the sedimentary record of a collapsed ice sheet margin. *Quaternary Science Reviews.* 8: 307-351.

Eyles, N., Putkinen, N., Sookhan, S., Arbelaez-Moreno, L. (2016) Erosional origin of drumlins and megaridges. *Sedimentary Geology.* 338: 2–23.

Fahnestock, M.A., Joughin, I., Scambos, T.A., Kwok, R., Krabill, W.B., Gogineni, S. (2001) Ice-stream-related patterns of ice flow in the interior of northeast Greenland. *Journal of Geophysical Research.* 106(D24): 34,0135-34,045.

Ferguson, A., van der Meer, J.J.M., Emrys, P. (2011) Micromorphology and microstructural analysis of polyphase deformation of tills, West Runton. pp 154-161 in Phillips, E., Lee, J.R., Evans, H.M. (eds). *Glaciotectonics: Field guide*. Quaternary Research Association: London.

Forwick, M., Vorren, T.O. (2009) Late Weichselian and Holocene sedimentary environments and ice rafting in Isfjorden, Spitsbergen. *Palaeogeography, Palaeoclimatology, Palaeoecology*. 280: 258–274.

Fowler, A.C. (2000) An instability mechanism for drumlin formation. pp 307-319 in Maltman, A., Hambrey, M.J., Hubbard, B. (eds) *Deformation of Glacial Materials. Special Publication of the Geological Society 176*. London: The Geological Society.

Fowler, A.C. (2010) The formation of subglacial streams and mega-scale glacial lineations. *Proceedings of the Royal Society of London – Series A.* 466: 3181–3201.

Fuller, S., Murray, T. (2002) Sedimentological investigations in the forefield of an Icelandic surge-type glacier: implications for the surge mechanism. *Quaternary Science Reviews*. 21: 1503-1520.

Funder, S., Kjeldsen, K.K., Kjær, K.H., Ó Cofaigh, C. (2011) The Greenland ice sheet, the last 300,000 years: a review. p. 699-713 In Ehlers, J., Gibbard, P.L., Hughes, P.D. (eds) *Quaternary Glaciations - Extent and Chronology. Part IV: A closer look. Developments in Quaternary Science 15.* Elsevier.

Funder, S., Hansen, L. (1996) The Greenland Ice Sheet: a model for its culmination and decay during and after the last glacial maximum. *Bulletin of the Geological Society of Denmark.* 42: 137–152.

Funder, S., Hjort, C., Landvik, J.Y. (1994) The last glacial cycles in East Greenland, an overview. *Boreas*. 23: 283–293.

Funder, S., Sørensen, A.H.L., Larsen, N.K., Bjørk, A.A., Briner, J.P., Olsen, J., Schomacker, A., Levy, L.B., Kjær, K. (2021) Younger Dryas ice margin retreat in Greenland: new evidence from southwestern Greenland. *Climate of the Past*. 17: 587-601.

Gales, J.A., Larter, R.D., Leat, P.T. (2016) Iceberg ploughmarks and associated sediment ridges on the southern Weddell Sea margin. pp289-290 in Dowdeswell, J. A., Canals, M., Jakobsson, M., Todd, B. J., Dowdeswell, E. K., Hogan, K. A. (eds) *Atlas of Submarine Glacial Landforms: Modern, Quaternary and Ancient*. Geological Society, London, Memoirs, 46.

Gehrmann, A., Hüneke, H., Meschede, M., Phillips, E. (2017) 3D microstructural architecture of deformed glacigenic sediments associated with large-scale glacitectonism, Jasmund Peninsula (NE Rügen), Germany. *Journal of Quaternary Science*. 32(2): 213-230.

Ghibaudo, G. (1992) subaqueous sediment gravity flow deposits: practical criteria for their field description and classification. *Sedimentology.* 39: 423-454.

Gilbert, R. (1983) Sedimentary processes of Canadian Arctic fjords. Sedimentary Geology 36, 147-175.

Gilbert, R. (1990) Rafting in glacimarine environments. pp 105-120 in Dowdeswell, J.A., Scourse, J.D. (eds*) Glacimarine Environments: Processes and Sediments*. Geological Society Special Publication No 53.

Gilbert, R. (1992) Contemporary sedimentary environments on Baffin Island, N.W.T., Canada: glaciomarine processes in fjords of eastern Cumberland Peninsula. *Arctic and Alpine Research.* 14: 1-12.

Gilbert, R., Aitken, A.E., Lemmen, D.S. (1993) The glacimarine sedimentary environment of Expedition Fiord, Canadian High Arctic. *Marine Geology*. 110: 257-273.

Gilbert, R., Nielsen, N., Moller, H., Desloges, J.R., Rasch, M. (2002) Glacimarine sedimentation in Kangerdluk (Disko Fjord), West Greenland, in response to a surging glacier. *Marine Geology*. 191: 1-18.

Graham, A.C.G., Larter, R.D., Gohl, K., Hillenbrand, C.-D., Smith, J.A., Kuhn, G. (2009) Bedform signature of a West Antarctic palaeo-ice stream reveals a multi-temporal record of flow and substrate control. *Quaternary Science Reviews*. 28: 2774-2793.

Håkannsson, L., Briner, J., Alexanderson, H., Aldahan, A., Possner, G. (2007) ^{10}Be ages from central east Greenland constrain the extent of the Greenland ice sheet during the Last Glacial Maximum. *Quaternary Science Reviews*. 26: 2316-2321.

Hall, B., Baroni, C., Denton, G. (2010) Relative sea-level changes, Schuchert Dal, East Greenland, with implications for ice extent in late-glacial and Holocene times. *Quaternary Science Reviews.* 29: 3370–3378.

Hall, B., Baroni, C., Denton, G., Kelly, M.A., Lowell, T. (2008) Relative sea-level change, Kjove Land, Scoresby Sund, East Greenland: implications for seasonality in Younger Dryas time. *Quaternary Science Reviews*. 27: 2283-2291

Hart, J.K. (2007) An investigation of subglacial shear zone processes from Weybourne, Norfolk, UK. *Quaternary Science Reviews*. 26: 2354-2374.

Hart, J.K. (2017) Subglacial till formation: Microscale processes within the subglacial shear zone. *Quaternary Science Reviews*. 170: 26-44.

Hart, J.K., Boulton. G.S. (1991) The interrelation of glaciotectonic and glaciodepositional processes within the glacial environment. *Quaternary Science Reviews*. 10: 335-350.

Hart, J.K., Roberts, D.H. (1994) Criteria to distinguish between subglacial glaciotectonic and glaciomarine sedimentation, I. Deformation styles and sedimentology. *Sedimentary Geology.* 91: 191-213.

Hein, F. J., Syvitski, J. P. (1992) Sedimentary environments and facies in an arctic basin, Itirbilung Fiord, Baffin Island, Canada. *Sedimentary Geology.* 81(1–2): 17–45.

Hermanowski, P., Piotrowski, J.A., Szuman, I. (2019) An erosional origin for drumlins of NW Poland. *Earth Surface Processes and Landforms*. 44: 2030-2050.

Heroy, D.C., Anderson, J.B. (2005) Ice-sheet extent of the Antarctic Peninsula region during the Last Glacial Maximum (LGM)—Insights from glacial geomorphology. *Geological Society of America Bulletin.* 117(11/12): 1497-1512.

Hicock, S.R. (1991) On subglacial stone pavements in till. *The Journal of Geology.* 99(4): 607-619.

Hiemstra, J. (1999). Microscopic evidence of grounded ice in the sediments of the CIROS-1 core, McMurdo Sound, Antarctica. *Terra Antartica*, *6*(4): 365-376.

Hiemstra, J.F. (2001a) Microscopic analyses of Quaternary glacigenic sediments of Marguerite Bay, Antarctic Peninsula. *Arctic Antarctic Alpine Res.* 33:258–265.

Hiemstra, J. F. (2001b) *'Dirt Pictures' Reveal the Past Extent of the Grounded Antarctic Ice Sheet*. Ph.D. dissertation, University of Amsterdam, 231 pp.

Hiemstra, J. F., Rijsdijk, K. F. (2003) Observing artificially induced strain: implications for subglacial deformation. *Journal of Quaternary Science*. 18: 373–383.

Hiemstra, J., Rijsdijk, K., Evans, D., van der Meer, J. (2005) Integrated micro- and macro-scale analyses of Last Glacial Maximum Irish Sea Diamicts from Abermawr and Traeth y Mwnt, Wales, UK. *Boreas*. *34(*1): 61-74.

Hillenbrand, C.-D., Baesler, A., Grobe, H. (2005) The sedimentary record of the last glaciation in the western Bellingshausen Sea (West Antarctica): Implications for the interpretation of diamictons in a polar-marine setting. *Marine Geology*. 216: 191-204.

Hillenbrand, C.-D., Kuhn, G., Smith, J.A., Gohl, K., Graham, A.G.C., Larter, R., Klages, J.P., Downey, R., Moreton, S.G., Forwick, M., Vaughan, D.G. (2013) Grounding-line retreat of the West Antarctic Ice Sheet from inner Pine Island Bay. *Geology*. 41(1): 35-38.

Hillenbrand, C.-D., Larter, R.D., Dowdeswell, J.A., Ehrmann, W., Ó Cofaigh, C., Benetti, S., Graham, A.G.C., Grobe, H. (2010) The sedimentary legacy of a palaeo-ice stream on the shelf of the southern Bellingshausen Sea: Clues to West Antarctic glacial history during the Late Quaternary. *Quaternary Science Reviews*. 29: 2741-2763.

Hjelstuen, B.O., Haflidason, H., Sejrup, H.P., Lysså, A. (2009) Sedimentary processes and depositional environments in glaciated fjord systems – Evidence from Nordfjord, Norway. *Marine Geology*. 258: 88-99.

Hjort, C. (1997) Glaciation, climate history, changing marine levels and the evolution of the Northeast Water polynya. *Journal of Marine Science*. 10(1-4): 23-33.

Hodder, T.J., Ross, M., Menzies, J. (2016) Sedimentary record of ice divide migration and ice streams in the Keewatin core region of the Laurentide Ice Sheet. *Sedimentary Geology*. 338: 97-114.

Hoffmann, G., Reicherter, K. (2012) Soft-sediment deformation of Late Pleistocene sediments along the southwestern coast of the Baltic Sea (NE Germany). *International Journal of Earth Science.* 101: 351-363.

Hogan, K.A., Dix, J.K., Lloyd, J.M., Long, A.J., Cotterill, C.J. (2011) Seismic stratigraphy records the deglacial history of Jakobshavn Isbrae, West Greenland. *Journal of Quaternary Science.* 26(7): 757-766.

Hogan, K.A., Dowdeswell, J.A., Noormets, R., Evans, J., Ó Cofaigh, C., Jakobsson, M. (2010) Submarine landforms and ice-sheet flow in the Kvitøya Trough, northwestern Barents Sea. *Quaternary Science Reviews*. 29: 3545-3562.

Hogan, K.A., Dowdeswell, J.A., Ó Cofaigh, C. (2012) Glacimarine sedimentary processes and depositional environments in an embayment fed by West Greenland ice streams. *Marine Geology.* 311-314: 1-16.

Hogan, K.A., Ó 'Cofaigh, C., Jennings, A.E., Dowdeswell, J.A., Hiemstra, J.F. (2016) Deglaciation of major paleo-ice stream in Disko Trough, West Greenland. *Quaternary Science Reviews*. 147: 5-26.

Howat, I.M., Domack, E.W. (2003) Reconstructions of western Ross Sea palaeo-ice-stream grounding zones from high-resolution acoustic stratigraphy. *Boreas*. 32: 56–75.

Howat, I. M., Negrete, A., Smith, B. E. (2014) The Greenland Ice Mapping Project (GIMP) land classification and surface elevation data sets. *The Cryosphere*. 8(4): 1509–1518.

Hubbard, B., Glasser, N. (2005) *Field Techniques in Glaciology and Glacial Geomorphology.* Chichester: J. Wiley & Son.

Hubberten, H.-W., Grobe, H., Jokat, W., Melles, M., Niessen, F., Stein, R. (1995) Glacial History of East Greenland Explored. *Eos*. 76(36): 353-364.

Jaeger, J.M. Nittrouer, C.A. (1999) Sediment deposition in an Alaskan Fjord: controls on the formation and preservation of sedimentary structures in Icy Bay. *Journal of Sedimentary Research.* 69(5): 1011-1026.

Jakobsson, M., Greenwood, S.L., Hell, B., Ölås, H. (2016) Drumlins the Gulf of Bothnia. pp197-198 in Dowdeswell, J. A., Canals, M., Jakobsson, M., Todd, B. J.,

Dowdeswell, E. K., Hogan, K. A. (eds) *Atlas of Submarine Glacial Landforms: Modern, Quaternary and Ancient.* Geological Society, London, Memoirs, 46.

Jakobsson, M., Hogan, K. A., Mayer, L. A., Mix, A., Jennings, A., Stoner, J., Eriksson, B., Jerram, K., Mohammad, R., Pearce, C., Reilly, B., Stranne, C. (2018) The Holocene retreat dynamics and stability of Petermann Glacier in northwest Greenland. *Nature Communications.* 9(1): 2104.

Jakobsson, M., Mayer, L.A., Coakley, B., Dowdeswell, J. A., Forbes, S., Fridman, B., Hodnesdal, H., Noormets, R., Pedersen, R., Rebesco, M., Schenke, H.-W., Zarayskaya, Y., Accettella, A.D., Armstrong, A., Anderson, R.M., Bienhoff, P., Camerlenghi, A., Church, I., Edwards, M., Gardner, J.V., Hall, J.K., Hell, B., Hestvik, O.B., Kristoffersen, Y., Marcussen, C., Mohammad, R., Mosher, D., Nghiem, S.V., Pedrosa, M.T., Travaglini, P.G., Weatherall, P. (2012) The International Bathymetric Chart of the Arctic Ocean (IBCAO) Version 3.0. *Geophysical Research Letters*. doi: 10.1029/2012GL052219.

Jamieson, S.S.R., Vieli, A., Ó Cofaigh, C., Stokes, C.R., Livingstone, S.J., Hillenbrand, C-D. (2014) Understanding controls on rapid ice-stream retreat during the last deglaciation of Marguerite Bay, Antarctica, using a numerical model. *Journal of Geophysical Research: Earth Surface.* 119(2): 247–263.

Jennings, A. E., Walton, M. E., Ó Cofaigh, C., Kilfeather, A., Andrews, J. T., Ortiz, J. D., De Vernal, A., and Dowdeswell, J. A. (2014) Paleoenvironments during Younger Dryas-Early Holocene retreat of the Greenland Ice Sheet from outer Disko Trough, central west Greenland. *Journal of Quaternary Science.* 29(1): 27–40.

Jennings, A.E., Andrews, J.T., Ó Cofaigh., St. Onge, G., Sheldon, C., Belt, S.T., Cabedo-Sanz, P., Hillaire-Marcel, C. (2017) Ocean forcing of Ice Sheet retreat in central west Greenland from LGM to the early Holocene. *Earth and Planetary Science Letters.* 472:1-13.

Jennings, A.E., Hald, M., Smith, L.M., Andrews, J.T. (2006) Freshwater forcing from the Greenland Ice Sheet during the Younger Dryas: evidence from Southeastern Greenland shelf cores. *Quaternary Science Reviews*. 25: 282–298.

Jennings, A.E., Weiner, N.J. (1996) Environmental change in eastern Greenland during the last 1300 years: evidence from foraminifera and lithofacies in Nansen Fjord, 68°N. *The Holocene*. 6(2): 179-191.

Jeong, A., Lee, J.I., Seong, Y., Balco, G., Yoo, K., Yoon, H.I., Domack, E., Rhee, H.H., Yu, B.Y. (2018) Late Quaternary deglacial history across the Larsen B embayment, Antarctica. *Quaternary Science Reviews*. 189: 134-148.

Jónsson, S.A., Benediktsson, Í.Ö., Ingólfsson, Ó., Schomacker, A., Bergsdóttir, H.L., Jacobson Jr., W.R., Linderson, H. (2016) Submarginal drumlin formation and late Holocene history of Fláajökull, southeast Iceland. Annals of Glaciology. 57(72): 128-141.

Joughin, I., Smith, B.E., Howat, I.M. (2018) A complete map of Greenland ice velocity derived from satellite data collected over 20 years. *Journal of Glaciology*. 64(243): 1-11.

Joughin, I., Smith, B.E., Howat, I.M., Scambos, T., Moon, T. (2010) Greenland flow variability from ice-sheet-wide velocity mapping. *Journal of Glaciology*. 56(197): 415–430.

Kelly, M.A., Lowell, T.V., Hall, B.L., Schaefer, J.M., Finkel, R.C., Goehring, B.M., Alley, R.B., Denton, G.H. (2008) A ^{10}Be chronology of lateglacial and Holocene mountain glaciation in the Scoresby Sund region, east Greenland: implications for seasonality during lateglacial time. *Quaternary Science Reviews*. 27: 2273-2282.

Kempf, P., Forwick, M., Laberg, J.S., Vorren, T.O. (2013) Late Weichselian and Holocene sedimentary palaeoenvironment and glacial activity in the high-arctic van Keulenfjorden, Spitsbergen. *The Holocene.* 23(11): 1607-1618.

Kerr, M., and Eyles, N. (2007) Origin of drumlins on the floor of Lake Ontario and in upper New York State. *Sedimentary Geology.* 193(1): 7–20.

Khan, S.A., Kjaer, K.H., Bevis, M., Bamber, J.L., Wahr, J., Kjeldsen, K.K., Bjork, A.A., Korsgaard, N.J., Stearns, L.A., van den Broeke, M.R., Liu, L., Larsen, N.K., Muresan, I.S. (2014) Sustained mass loss of the northeast Greenland ice sheet triggered by regional warming. *Nature Climate Change*. 4: 292-299.

Kilfeather, A.A., Ó Cofaigh, C., Dowdeswell, J.A., van der Meer, J.J.M., Evans, D.J.A. (2010) Micromorphological characteristics of glacimarine sediments: implications for distinguishing genetic processes of massive diamicts. *Geo-Mar Lett*. 30: 77–97.

Kilfeather, A.A., Ó Cofaigh, C., Lloyd, J.M., Dowdeswell, J.A., Xu, S., Moreton, S.G. (2011) Ice-stream retreat and ice-shelf history in Marguerite Trough, Antarctic Peninsula: Sedimentological and foraminiferal signatures. *GSA Bulletin*. 123(5/6): 997-1015.

King, E.C., Woodward, J., Smith, A.M. (2007) Seismic and radar observations of subglacial bedforms beneath the onset zone of Rutford Ice Stream, Antarctica. *Journal of Glaciology*. 53(183): 665-672.

King, M.D., Howat, I.M., Candela, S.G., Noh, M.J., Jeong, S., Noël, B.P.Y., van der Broeke, M.R., Wouters, B., Negrete, A. (2020) Dynamic ice loss from the Greenland Ice Sheet driven by sustained glacier retreat. *Communications Earth & Environment*. 1(1)

Kjeldsen, K.K.,Korsgaard, N.J., Bjørk, A.A., Khan, S.A., Box, J.E., Funder, S., Larsen, N.K., Bamber, J.L., Colgan, W., van den Broeke, M., Siggaard-Andersen, M-L., Nuth, C., Schomacker, A., Andresen, C.S., Willerslev, E., Kjær, K.H. (2015) Spatial and temporal distribution of mass loss from the Greenland Ice Sheet since AD 1900. *Nature*. 528: 396-400.

Kuijpers, A., Troelstra, S.R., Prins, M.A., Linthout, K., Akhmetzhanov, A., Bouryak, S., Bachmann, M.F., Lassen, S., Rasmussen, S., Jensen, J.B. (2003) Late

Quaternary sedimentary processes and ocean circulation changes at the Southeast Greenland margin. *Marine Geology*. 195: 109–129.

Laberg, J.S., Forwick, M., Husum, K. (2017) New geophysical evidence for a revised maximum position of part of the NE sector of the Greenland Ice Sheet during the last glacial maximum*. Arktos.* 3(3): https://doi.org/10.1007/s41063-017-0029-4.

Laberg, J.S., Vorren, T.O. (1995) Late Weichselian submarine debris flow deposits on the Bear Island Trough Mouth Fan. *Marine Geology*. 127(1-4): 45-72.

Laberg, J.S., Vorren, T. O. (2000) Flow behaviour of the submarine glacigenic debris flows on the Bear Island Trough Mouth Fan, western Barents Sea. *Sedimentology.* 47(6): 1105–1117.

Lachniet, M.S., Larson, G.J., Lawson, D.E., Evenson, E.B., Alley, R.B. (2001) Microstructures of sediment flow deposits and subglacial sediments: a comparison. *Boreas*. 30: 254-262.

Landvik, J.Y. (1994) The last glaciation of Germania land and adjacent areas, northeast Greenland. *Journal of Quaternary Science.* 9: 81-92.

Lane, T.P., Roberts, D.H., Rea, B.R., Ó Cofaigh, C., Vieli, A., Rodés, A. (2014) Controls upon the Last Glacial Maximum deglaciation of the northern Uummannaq Ice Stream System, West Greenland. *Quaternary Science Reviews*. 92: 324-344.

Larsen, N.K., Funder, S., Linge, H., Möller, P., Schomacker, A., Fabel, D., Xu, S., Kjær, K.H. (2016) A Younger Dryas re-advance of local glacier in north Greenland. *Quaternary Science Reviews.* 147: 47-58.

Larsen, N.K., Kjær, K.H., Funder, S., Möller, P., van der Meer, J.J.M., Schomacker, A., Linge, H., Darby, D.A. (2010) Late Quaternary glaciation history of northernmost Greenland – Evidence of shelf-based ice. *Quaternary Science Reviews.* 29: 3399-3414.

Larsen, N.K., Levy, L.B., Carlson, A.E., Buizert, C., Olsen, J., Strunk, A., Bjork, A.A., Skov, D.S. (2018) Instability of the Northeast Greenland Ice Stream over the last 45,000 years. *Nature Communications*. 9(1872).

Larsen, N.K., Piotrowski, J.A., Christiansen, F. (2006) Microstructures and microshears as proxy for strain in subglacial diamicts: Implications for basal till formation. *Geological Society of America*. 34(10): 889-892.

Larsen, N.K., Piotrowski, J.A., Kronborg, C. (2004) A multiproxy study of basal till: a time-transgressive accretion and deformation hypothesis. *Journal of Quaternary Science*. 19(1): 9-21.

Larsen, N.K., Piotrowski, J.A., Menzies, J. (2007) Microstructural evidence of low-strain, time-transgressive subglacial deformation. *Journal of Quaternary Science*. 22(6): 593-608.

Larson, G.J., Lawson, D.E., Evenson, E.B., Alley, R.B., Knudsen, Ó, Lachniet, M.S., Goetz, S.L. (2006) Glaciohydraulic supercooling in former ice sheets? *Geomorphology*. 75: 20-32.

Larter, R. D., Graham, A. G. C., Hillenbrand, C.-D., Smith, J. A., Gales, J. A. (2012) Late Quaternary grounded ice extent in the Filchner Trough, Weddell Sea, Antarctica: new marine geophysical evidence. *Quaternary Science Reviews.* 53: 111–122.

Larter, R.D., Hogan, K.A., Hillenbrand, C.-D., Smith, J.A., Batchelor, C.L., Cartigny, M., Tate, A.J., Kirkham, J.D., Roseby, Z.A., Kuhn, G., Graham, A.G.C., Dowdeswell, J.A. (2019) Subglacial hydrological control on flow of an Antarctic Peninsula palaeo-ice stream. *The Cryosphere.* 13: 1583-1596.

Lawson, D.E. (1981) Distinguishing characteristics of diamictons at the margin of the Matanuska glacier, Alaska. *Annals of Glaciology*. 2: 78-84.

Lea, J., Palmer, A. (2014) Quantification of turbate microstructures through a subglacial till: dimensions and characteristics. *Boreas*. 43(4): 869-881.

Lecavalier, B.S., Milne, G.A., Simpson, M.J.R., Wake, L., Huybrechts, P., Tarasov, L., Kjeldsen, K.K., Funder, S., Long, A.J., Woodroffe, S., Dyke. A.S., Larsen, N.K. (2014) A model of Greenland ice sheet deglaciation constrained by observations of relative sea level and ice extent. *Quaternary Science Reviews*. 105: 54-84.

Lee, J.A., Kemp, R.A. (1992) *Thin Sections of Unconsolidated Sediments: A Recipe.* CEAM report #2. Royal Holloway, University of London.

Lee, J.R., Phillips, E.R. (2008) Progressive soft sediment deformation within a subglacial shear zone – a hybrid mosaic-pervasive deformation model for Middle Pleistocene glaciotectonised sediments from Eastern England. *Quaternary Science Reviews*. 27: 1350-1362.

Lemmen, D.S. (1990) Glaciomarine sedimentation in Disraeli Fjord, High Arctic Canada. *Marine Geology*. 94: 9-22.

Licht, K.J., Dubar, N.W., Andrews, J.T., Jennings, A.E. (1999) Distinguishing subglacial till and glacial marine diamictons in the western Ross Sea, Antarctica: Implications for a last glacial maximum grounding line. *Geological Society of America Bulletin*. 111(1): 91-103.

Linch, L.D., Dowdeswell, J.A. (2016) Micromorphology of diamicton affected by iceberg-keel scouring, Scoresby Sund, East Greenland. *Quaternary Science Reviews*. 152: 169-196.

Linch, L.D., van der Meer, J.J.M. (2015) Micromorphology of ice keel scour in pebbly sandy mud and fine-grained sands: Scarborough Bluffs, Ontario, Canada. *Sedimentology*. 62: 110-129.

Linch, L.D., van der Meer, J.J.M., Menzies, J. (2012) Micromorphology of iceberg scour in clays: Glacial Lake Agassiz, Manitoba, Canada. *Quaternary Science Reviews*. 55: 125-144.

Linderman, M.R., Straneo, F., Wilson, N.J., Toole, J.M., Krishfield, R.A., Beaird, N.L., Kaznow, T., Schaffer, J. (2020) Ocean circulation and variability beneath Nioghalvfjerdsbræ (79 North Glacier) ice tongue. *Journal of Geophysical Research*: *Oceans.* 125(8): e2020JC016091.

Livingstone, S.J., Ó Cofaigh, C., Stokes, C.R., Hillenbrand, C-D., Vieli, A., Jamieson, S.S.R. (2012) Antarctic palaeo-ice streams. *Earth Science Reviews*. 111: 90-128.

Livingstone, S.J., Ó Cofaigh, C., Stokes, C.R., Hillenbrand, C-D., Vieli, A., Jamieson, S.S.R. (2013) Glacial geomorphology of Marguerite Bay Palaeo-Ice stream, western Antarctic Peninsula. *Journal of Maps*. 9(4): 558-572.

Lowe, A.L., Anderson, J.B. (2002) Reconstruction of the West Antarctic ice sheet in Pine Island Bay during the Last Glacial Maximum and its subsequent retreat history. *Quaternary Science Reviews*. 21: 1879-1897.

Lysså, A., Hjelstuen, B. O. & Larsen, E. (2010) Fjord infill in a high-relief area: Rapid deposition influenced by deglaciation dynamics, glacio-isostatic rebound and gravitational activity. *Boreas.* 39: 39–55.

Mackiewicz, N.E., Powell, R.D., Carlson, P.R., Molnia, B.F. (1984) Interlaminated ice-proximal glacimarine sediments in Muir Inlet, Alaska. *Marine Geology*. 57: 113-147.

Marcott, S.A., Clark, P.U., Padman, L., Klinkhammer, G.P., Springer, S.R., Zhengyu, L., Otto-Bliesner, B., Carlson, A., Ungerer, A., Padman, J., He, F., Cheng, J., Schmittner, A. (2011) Ice shelf collapse from subsurface warming as a trigger for Heinrich events. *Proceedings of the National Academy of Sciences.* 108(33): 13415-13419.

Marienfeld, P. (1992) Postglacial sedimentary history of Scoresby Sund, East Greenland. *Polarforschung*. 60(3): 181-195.

Martín-Chivelet, J., Palma, R.M., López-Gómez, J., Kietzmann, D.A. (2011) Earthquake-induced soft-sediment deformation structures in Upper Jurassic open-marine microbialites (Neuquén Basin, Argentina). *Sedimentary Geology*. 235(3-4): 210-221.

Mayer, C., Reeh, N., Jung-Rothenhäusler, F., Huybrechts, P., Oerter, H. (2000) The subglacial cavity and implied dynamics under Nioghalvfjerdsfjorden Glacier, NE-Greenland. *Geophysical Research Letters*. 27(15): 2289-2292.

Mayer, C., Schaffer, J., Hattermann, T., Floricioiu, D., Krieger, L., Dodd, P.A., Kaznow, T., Licciulli, C., Schannwell, C. (2018) Large ice loss variability of Nioghalvfjerdsfjorden Glacier, Northeast-Greenland. *Nature Communications*. 9: 2768.

McCabe, A.M., Dardis, G.F., Hanvey, P.M. (1987) Sedimentation at the margins of a Late Pleistocene ice-lobe terminating in shallow marine environments, Dundalk Bay, Eastern Ireland. *Sedimentology*. 34:473–49

McGlannan, A.J., Bart, P.J., Chow, J.M., DeCesare, M. (2017) On the influence of post-LGM ice shelf loss and grounding zone sedimentation on West Antarctic ice sheet stability. *Marine Geology*. 392: 151-169.

McMillan, M., Leeson, A., Shepherd, A., Briggs, K., Armitage, T.W.K., Hogg, A., Kuipers Munneke, P., van der Broeke, M., Noël, B., van der Berg, W.J., Ligtenberg, S., Horwath, M., Groh, A., Muir, A., Gilbert, L. (2016) A high-resolution record of Greenland mass balance. *Geophysical Research Letters*. 43: 7002–7010

Menzies, J. (2000) Micromorphological analyses of microfabrics and microstructures indicative of deformation processes in glacial settings. pp 245-257 in Maltman, A.J., Hambrey, M.J., Hubbard, B. (eds) *Deformation of Glacial Materials.* Geological Society, London, Special Publications 176.

Menzies, J. (2012) Strain pathways, till internal architecture and microstructures - perspectives on a general kinematic model - a 'blueprint' for till development. *Quaternary Science Reviews*. 50: 105-124.

Menzies, J., Paulen, R.C., Rice, J.M., McClenaghan, M.B., Oviatt, N.M., Dhillon, N. (2019) Deformation 'boundary front' movements in subglacial tills—A microsedimentological perspective from till sequences near Pine Point, NWT, Canada. *The Depositional Record*. 5(2): 230-246.

Menzies, J., van der Meer, J.J.M. (2018) Micromorphology and microsedimentology of glacial sediments. pp753-808 in Menzies, J., van der Meer, J.J.M (eds). *Past Glacial Environments*. Amsterdam: Elsevier.

Menzies, J., van der Meer, J.J.M., Rose, J. (2006) Till—as a glacial 'tectomict', its internal architecture, and the development of a 'typing' method for till differentiation. *Geomorphology*. 75: 172-200.

Menzies, J., Zaniewski, K., Dreger, D. (1997) Evidence, from microstructures, of deformable bed conditions within drumlins, Chimney Bluffs, New York State. *Sedimentary Geology*. 111: 161-175.

Mienert, J., Kenyon, N.H., Theide, J., Hollender, F.J. (1993) Polar continental margins: studies off East Greenland. *EOS*. 74: 225-236.

Morlighem, M., Williams, C.N., Rignot, E., An, L., Arndt, J.E., Bamber, J.L., Catania, G., Chauché, N., Dowdeswell, J.A., Dorschel, B., Fenty, I., Hogan, K., Howat, I., Hubbard, A., Jakobsson, M., Jordan, T.M., Kjeldsen, K.K., Millan, R., Mayer, L., Mouginot, J., Noël, B.Y.P., Ó Cofaigh, C., Palmer, S., Rysgaard, S., Seroussi, H., Siegert, M.J., Slabon, P., Straneo, F., van den Broeke, M.R., Weinrebe, W., Wood, M., Zinglersen, K.B. (2017) BedMachinev3: complete bed topography and ocean bathymetry mapping of Greenland from multibeam echo sounding combined with mass conservation. *Geophysical Research Letters.* 44(21): 11051–11061.

Mosola, A.B., Anderson, J.B. (2006) Expansion and rapid retreat of the West Antarctic Ice Sheet in eastern Ross Sea: possible consequence of over-extended ice streams? *Quaternary Science Reviews*. 25: 2177–2196.

Mouginot, J., Rignot, E., Bjørk, A.A., van der Broeke, M., Millan, R., Morlighem, M., Noël, B., Scheuchl, B., Wood, M. (2019) Forty-six years of Greenland Ice Sheet mass balance from 1972 to 2018. *Proceedings of the National Academy of Sciences*. 116(19): 9239-9244.

Mouginot, J., Rignot, E., Scheuchl, B., Fenty, I., Khazendar, A., Morlighem, M., Buzzi, A., Paden, J. (2015) Fast retreat of Zachariæ Isstrøm, northeast Greenland. *Science*. 350(6266): 1357-1361

Mulder, T., Alexander, J. (2001) The physical character of subaqueous sedimentary density flows and their deposits. *Sedimentology*. 48: 269–299.

Nam, S., Stein, R., Grobe, H., Hubberten, H. (1995) Late Quaternary glacial-interglacial changes in sediment composition at the East Greenland continental margin and their paleoceanographic implications. *Marine Geology. 122*(3): 243-262.

Narloch, W., Piotrowski, J.A., Wysota, W., Larsen, N.K., Menzies, J. (2012) The signature of strain magnitude in tills associated with the Vistula Ice Stream of the Scandinavian Ice Sheet, central Poland. *Quaternary Science Reviews.* 57: 105-120.

Narloch, W., Wysota, W., Piotrowski, J.A. (2013) Sedimentological record of subglacial conditions and ice sheet dynamics of the Vistula Ice Stream (north-central Poland) during the Last Glaciation. *Sedimentary Geology*. 293: 30-44.

Newton, A.M.W., Huuse, M. (2017) Glacial geomorphology of the central Barents Sea: Implications for the dynamic deglaciation of the Barents Sea Ice Sheet. *Marine Geology*. 387: 114-131.

Newton, A.M.W., Knutz, P.C., Huuse, M., Gannon, P., Brocklehurst, S.H., Clausen, O.R., Gong, Y. (2017) Ice stream reorganization and glacial retreat on the northwest Greenland shelf. *Geophysical Research Letters*. 44: 7826-7835.

Nørgaard-Pedersen, N., Mikkelsen, N., Kristoffersen, Y. (2008) Late glacial and Holocene marine records from the Independence Fjord and Wandel Sea regions, North Greenland. *Polar Research*. 27(2): 209–221.

Nürnberg, D., Wollenburg, I., Dethleff, D., Eicken, H., Kassens, H., Letzig, T., Reimnitz, E., Theide, J. (1994) Sediments in Arctic sea ice: Implications for entrainment, transport and release. *Marine Geology*. 119: 185-214.

Ó Cofaigh, C. (2007) Glacimarine sediment and ice-rafted debris. p 932-945 Elias, S. (ed) *Encyclopedia of Quaternary Science*. Amsterdam: Elsevier.

Ó Cofaigh, C., Dowdeswell, J.A. (2001) Laminated sediments in glacimarine environments: diagnostic criteria for their interpretation. *Quaternary Science Reviews*. 20: 1411-1436.

Ó Cofaigh, C., Dowdeswell, J.A., Allen, C.S.A., Hiemstra, J., Pudsey, C.J., Evans, J., Evans, D.J.A. (2005a) Flow dynamics and till genesis associated with a marine-based Antarctic palaeo-ice stream. *Quaternary Science Reviews*. 24(5-6): 709-740.

Ó Cofaigh, C., Dowdeswell, J.A., Evans, J., Kenyon, N.H., Taylor, J., Mienert, J., Wilken, M. (2004) Timing and significance of glacially influenced mass-wasting in the submarine channels of the Greenland Basin. *Marine Geology*. 207: 39-54.

Ó Cofaigh, C., Dowdeswell, J.A., Evans, J., Larter, R.D. (2008) Geological constraints on Antarctic palaeo-ice-stream retreat. *Earth Surface and Processes and Landforms*. 33: 513-525.

Ó Cofaigh, C., Dowdeswell, J.A., Grobe, H. (2001) Holocene glacimarine sedimentation, inner Scoresby Sund, East Greenland: the influence of fast-flowing ice sheet outlet glaciers. *Marine Geology*. 175: 103-129.

Ó Cofaigh, C., Dowdeswell, J.A., Jennings, A.E., Hogan, K.A., Kilfeather, A.A., Hiemstra, J.F., Noormets, R., Evans, J., McCarthy, D.J., Andrews, J.T., Lloyd, J.M., Moros, M. (2013a) An extensive and dynamic ice sheet on the West Greenland shelf during the last glacial cycle. *Geology*. 41(2): 219-222.

Ó Cofaigh, C., Dunlop, P., Benetti, S. (2012) Marine geophysical evidence for Late Pleistocene ice sheet extent and recession on the continental shelf off north-west Ireland. *Quaternary Science Reviews.* 44: 147-159.

Ó Cofaigh, C., Dunlop, P., Benetti, S. (2016a) Submarine drumlins on the continental shelf offshore of NW Ireland. pp 195-196 in Dowdeswell, J. A., Canals, M., Jakobsson, M., Todd, B. J., Dowdeswell, E. K. & Hogan, K. A. (eds) *Atlas of Submarine Glacial Landforms: Modern, Quaternary and Ancient.* Geological Society, London, Memoirs, 46.

Ó Cofaigh, C., Evans, D. J. A., Hiemstra, J. F. (2011) Formation of a stratified subglacial 'till' assemblage by ice-marginal thrusting and glacier overriding. *Boreas*. 40: 1–14.

Ó Cofaigh, C., Evans, J., Dowdeswell, J.A., Larter, R.D. (2007) Till characteristics, genesis and transport beneath Antarctic paleo-ice streams. *Journal of Geophysical Research*. 112

Ó Cofaigh, C., Hogan, K.A., Dowdeswell, J.A., Streuff, K. (2016c) Stratified glacimarine basin-fills in West Greenland fjords. pp 99-100 in Dowdeswell, J. A., Canals, M., Jakobsson, M., Todd, B. J., Dowdeswell, E. K. & Hogan, K. A. (eds) *Atlas of Submarine Glacial Landforms: Modern, Quaternary and Ancient.* Geological Society, London, Memoirs, 46.

Ó Cofaigh, C., Hogan, K.A., Jennings, J.E., Callard, S.L., Dowdeswell, J.A., Noormets, R., Evans, J. (2018) The role of meltwater in high-latitude trough-mouth fan development: The Disko Trough-Mouth Fan, West Greenland. *Marine Geology*. 402: 17-32.

Ó Cofaigh, C., Larter, R.D., Dowdeswell, J.A., Hillenbrand, C.-D., Pudsey, C.J., Evans, J., Morris, P. (2005b) Flow of the West Antarctic Ice Sheet on the continental margin of the Bellingshausen Sea at the Last Glacial Maximum. *Journal of Geophysical Research.* 110(B11): B11103.

Ó Cofaigh, C., Livingstone, S.J., Dowdeswell, J.A. (2016b) Mega-scale glacial lineations in Marguerite Trough, Antarctic Peninsula. pp175-176 in Dowdeswell, J. A., Canals, M., Jakobsson, M., Todd, B. J., Dowdeswell, E. K. & Hogan, K. A. (eds) *Atlas of Submarine Glacial Landforms: Modern, Quaternary and Ancient.* Geological Society, London, Memoirs, 46.

Ó Cofaigh, C., Pudsey, C.J., Dowdeswell, J.A., Morris, P. (2002b) Evolution of subglacial bedforms along a paleo-ice stream, Antarctic Peninsula continental shelf. *Geophysical Research Letters*. 29(8): 1199.

Ó Cofaigh, C., Stokes, C.R., Lian, O.B., Clark, C.D., Tulaczyk, S. (2013b) Formation of mega-scale glacial lineations on the Dubawnt Lake Ice Stream bed: 2. Sedimentology and stratigraphy. *Quaternary Science Reviews.* 77: 210-227.

Ó Cofaigh, C., Taylor, J., Dowdeswell, J. A., Pudsey, C. J. (2003) Palaeo-ice streams, trough mouth fans and high-latitude continental slope sedimentation. *Boreas*. 32: 37–55.

Ó Cofaigh, C., Taylor, J., Dowdeswell, J. A., Rosell-Melé, A., Kenyon, N. H., Evans, J., Mienert, J. (2002a) Sediment reworking on high-latitude continental margins and its implications for palaeoceanography: insights from the Norwegian–Greenland Sea. pp 325-348 in Dowdeswell, J. A., Ó Cofaigh, C. (eds) *Glacier-influenced Sedimentation on High-latitude Continental Margins.* London: Geological Society of London.

Ottesen, D., Dowdeswell, J.A. (2009) An inter-ice-stream glaciated margin: Submarine landforms and a geomorphic model based on marine-geophysical data from Svalbard. *Geological Society of America Bulletin*. 121(11/12): 1647-1665.

Ottesen, D., Dowdeswell, J.A., Landvik, J., Mienert, J. (2007) Dynamics and retreat of the Late Weichselian ice sheet on Svalbard inferred from high-resolution sea-floor morphology. *Boreas*. 36: 286–306.

Ottesen, D., Dowdeswell, J.A., Rise, L. (2005) Submarine landforms and the reconstruction of fast flowing ice streams within a large Quaternary ice sheet: The 2500-km-long Norwegian-Svalbard margin (57°–80°N). *Geological Society of America Bulletin*. 117: 1033–1050.

Ovenshine, A.T. (1970) Observations of iceberg rafting in Glacier Bay, Alaska, and the identification of ancient ice-rafted deposits. *Geological Society of America Bulletin*. 81: 891–894.

Paul, M.A., Eyles, N. (1990) Constraints on the preservation of diamict facies (melt-out tills) at the margin of stagnant glaciers. *Quaternary Science Reviews*. 9: 51-69.

Peltier, W.R., Argus, D.F., Drummond, R. (2015) Space geodesy constrains ice age terminal deglaciation: The global ICE-6G_C (VM5a) model. *Journal of Geophysical Research: Solid Earth*. 120: 450-487.

Peters, J.L., Benetti, S., Dunlop, P., Ó Cofaigh, C. (2015) Maximum extent and dynamic behaviour of the last British-Irish Ice Sheet west of Ireland. *Quaternary Science Reviews.* 128: 48-68.

Peters, J.L., Benetti, S., Dunlop, P., Ó Cofaigh, C., Moreton, S.G., Wheeler, A.J., Clark, C.D. (2016) Sedimentology and chronology of the advance and retreat of the last British-Irish Ice Sheet on the continental shelf west of Ireland. *Quaternary Science Reviews*. 140: 101-124.

Phillips, A.C., Smith, N.D., Powell, R.D. (1991) Laminated sediments in prodeltaic deposits, Glacier Bay, Alaska. pp51-60 In Anderson, J.B., Ashley, G.M. (eds) *Glacial marine sedimentation; Paleoclimatic significance.* Geological Society of America Special Paper 261. Boulder, Colorado.

Phillips, E.R. (2006) Micromorphology of a debris flow deposit: evidence of basal shearing, hydrofracturing, liquefaction and rotational deformation during emplacement. *Quaternary Science Reviews*. 25: 720-738.

Phillips, E.R. (2018) Glacitectonics. pp 467-502 in Menzies, J., van der Meer, J.J.M. (eds) *Past Glacial Environments*. Amsterdam: Elsevier.

Phillips, E.R., Auton, C.A. (2000) Micromorphological evidence for polyphase deformation of glaciolacustrine sediments from Strathspey, Scotland. pp 279-292 in Maltman, A.J., Hambrey, M.J., Hubbard, B. (eds) *Deformation of Glacial Materials.* Geological Society, London, Special Publications 176.

Phillips, E.R., Evans, D.J.A., van der Meer, J.J.M., Lee, J.R. (2018a) Microscale evidence of liquefaction and its potential triggers during soft-bed deformation within subglacial traction tills. *Quaternary Science Reviews*. 181: 123-143

Phillips, E.R., Everest, J., Reeves, H. (2013a) Micromorphological evidence for subglacial multiphase sedimentation and deformation during overpressurized fluid flow associated with hydrofracturing. *Boreas*. 42: 395–427.

Phillips, E., Lee, J.R., Riding, J.B., Kendall, R., Hughes, L. (2013b) Periglacial disruption and subsequent glacitectonic deformation of bedrock: an example from Anglesey, North Wales, UK. *Proceedings of the Geologists' Association*. 124(5): 802-817.

Phillips, E., Meritt, J. (2008) Evidence for multiphase water-escape during rafting of shelly marine sediments at Clava, Inverness-shire, NE Scotland. *Quaternary Science Reviews*. 27: 988-1011.

Phillips, E., Merritt, J., Auton, C., Golledge., N. (2007) Microstructures in subglacial and proglacial sediments: understanding faults, folds and fabrics, and the influence of water on the style of deformation. *Quaternary Science Reviews*. 26: 1499-1528.

Phillips, E., Spagnolo, M., Pilmer, A.C.J., Rea, B., Piotrowski, J.A., Ely, J.C., Carr, S. (2018b) Progressive ductile shearing during till accretion within the deforming bed of a palaeo-ice stream. *Quaternary Science Reviews.* 193: 1-23.

Phillips, E., van der Meer, J.J.M., Ferguson, A. (2011) A new 'microstructural mapping' methodology for the identification, analysis and interpretation of polyphase deformation within subglacial sediments. *Quaternary Science Reviews*. 30: 2570-2596.

Piasecka, E.D., Stokes, C.R., Winsborrow, M.C.M., Andreassen, K. (2018) Relationship between mega-scale glacial lineations and iceberg ploughmarks on the Bjørnøyrenna Palaeo-Ice Stream bed, Barents Sea. *Marine Geology.* 402: 153-164.

Piotrowski, J. A. (1987) Genesis of the Woodstock drumlin field, southern Ontario, Canada. *Boreas* 16(3): 249–265.

Piotrowski, J.A., Kraus, A.M. (1997) Response of sediment to ice-sheet loading in northwestern Germany: effective stresses and glacier-bed stability. *Journal of Glaciology*. 43(145): 495-502.

Piotrowski, J.A., Larsen, N.K., Junge, F.W. (2004) Reflections on soft subglacial beds as a mosaic of deforming and stable spots. *Quaternary Science Reviews*. 23: 993-1000.

Piotrowski, J.A., Tulaczyk, S. (1999) Subglacial conditions under the last ice sheet in northwest Germany: ice-bed separation and enhanced basal sliding? *Quaternary Science Reviews.* 18: 737-751.

Piper, D.J.W., Hiscott, R.N., Normark, W.R. (1999) Outcrop-scale acoustic facies analysis and latest Quaternary development of Hueneme and Dume submarine fans, offshore California. *Sedimentology*. 46: 47-78.

Piper, D.J.W., Normark, W.R. (2009) Processes than initiate turbidity currents and their influence on turbidites: a marine geology perspective. *Journal of Sedimentary Research.* 79: 347-362.

Porter, P.R., Murray, T. (2001) Mechanical and hydraulic properties of till beneath Bakaninbreen, Svalbard. *Journal of Glaciology*. 47(157): 167-175.

Powell, R.D. (1984) Glacimarine processes and inductive lithofacies modelling of ice shelf and tidewater glacier sediments based on Quaternary examples. *Marine Geology.* 57: 1-52.Ó

Powell, R.D. (1990) Glacimarine processes at grounding-line fans and their growth to ice-contact deltas. In: Dowdeswell, J.A. and Scourse, J.D. (eds.), Glacimarine Environments: Processes and Sediments, Geological Society Special Publication, 53, 53-73.

Powell, R.D., Dawber, M., McInnes, J.N., and Pyne, A.R., (1996) Observations of the grounding-line area at a floating glacier terminus. *Annals of Glaciology*. 22: 217–223.

Powell, R.D., Molnia, B.F. (1989) Glacimarine sedimentary processes, facies and morphology of the south-southeast Alaska shelf and fjords. *Marine Geology*. 85: 359–390

Prothro, L.O., Simkins, L.M., Majewski, W., Anderson, J.B. (2018) Glacial retreat patterns and processes determined from integrated sedimentology and geomorphology records. *Marine Geology*. 395: 104-119.

Pudsey, C.L., Murray, J.W., Appleby, P., Evans, J. (2006) Ice shelf history from petrographic and foraminiferal evidence, Northeast Antarctic Peninsula. *Quaternary Science Reviews*. 25: 2357-2379.

Rathmann, N.M., Hvidberg, C.S., Solgaard, A.M., Grinsted, A., Gudmundsson, G.H., Langen, P.L., Nielsen, K.P., Kusk, A. (2017) Highly temporally resolved response to seasonal surface melt of the Zachariae and 79N outlet glaciers in northeast Greenland. *Geophysical Research Letters*. 44(19): 9805-9814.

Rattas, M., Piotrowski, J. A. (2003) Influence of bedrock permeability and till grain size on the formation of the Saadjärve drumlin field, Estonia, under an east-Baltic Weichselian ice stream. *Boreas.* 32(1): 167–177.

Rebesco, M., Domack, E., Zgur, F., Lavoie, C., Leventer, A., Brachfeld, S., Willmott, V., Halverson, G., Truffer, M., Scambos, T., Smith, J., Pettit, E. (2014) Boundary condition of grounding lines prior to collapse, Larsen-B Ice Shelf, Antarctica. *Science*. 354(6202): 1354-1358.

Reilly, B. T., Stoner, J. S., Mix, A. C., Walczak, M. H., Jennings, A., Jakobsson, M., Dyke, L., Glueder, A., Nicholls, K., Hogan, K. A., Mayer, L. A., Hatfield, R. G., Albert, S., Marcott, S., Fallon, S., Cheseby, M. (2019) Holocene break-up and reestablishment of the Petermann Ice Tongue, Northwest Greenland. *Quaternary Science Reviews.* 218: 322–342.

Reinardy, B.T.I., Hiemstra, J.F., Murray, T., Hillenbrand, C.-D., Larter, R.D. (2011) Till genesis at the bed of an Antarctic Peninsula palaeo-ice stream as indicated by micromorphological analysis. *Boreas*. 40: 498-517.

Rignot, E., Box, J.E., Burgess, E., Hanna, E. (2008) Mass balance of the Greenland ice sheet from 1958 to 2007. *Geophysical Research Letters*. 35: 1–5.

Rignot, E., Casassa, G., Gogineni, P., Krabill, W., Rivera, A., Thomas, R. (2004) Accelerated ice discharge from the Antarctic Peninsula following the collapse of Larsen B ice shelf. *The Cryosphere.* 31(18): L18401.

Rignot, E., Gogineni, S., Joughin, I., Krabill, W. (2001) Contribution to the glaciology of northern Greenland from satellite radar interferometry. *Journal of Geophysical Research*. 106(D24): 34,007-34,019.

Rignot, E., Kanagaratnam, P. (2006) Changes in the velocity structure of the Greenland Ice Sheet. *Science.* 311: 986-990.

Rignot, E., Mouginot, J., Scheuchl, B., van der Broeke, M., van Wessem, M.J., Morlighem, M. (2019) Four decades of Antarctic Ice Sheet mass balance from 1979–2017. *Proceedings of the National Academy of Sciences.* 116(4): 1095-1103.

Rijsdijk, K. F., Owen, G., Warren, W. P., McCarroll, D., van der Meer, J. J. M. (1999) Clastic dykes in over-consolidated tills: evidence for subglacial hydrofracturing at Killiney Bay, eastern Ireland. *Sedimentary Geology.* 129: 111–126.

Rinterknecht, V., Jomelli, V., Brunstein, D., Favier, V., Masson-Delmotte, V. Bourlés, D., Leanni, L., Schläppy, R. (2014) Unstable ice stream in Greenland during the Younger Dryas cold event. *Geology*. 42(9): 759-762.

Roberts, D.H., Evans, D.J.A., Callard, S.L., Clark, C.D., Bateman, M.D., Medialdea, A., Dove, D., Cotterill, C.J., Saher, M., Ó Cofaigh, C., Chiverrell, R.C., Moreton, S.G., Fabel, D., Bradwell, T. (2018) Ice marginal dynamics of the last British-Irish Ice Sheet in the southern North Sea: Ice limits, timing and the influence of the Dogger Bank*. Quaternary Science Reviews*. 198: 181-207.

Roberts, D.H., Evans, D.J.A., Lodwick, J., Cox, N.J. (2013a) The subglacial and ice-marginal signature of the North Sea Lobe of the British–Irish Ice Sheet during the Last Glacial Maximum at Upgang, North Yorkshire, UK. *Proceedings of the Geologists' Association*. 124: 503-519.

Roberts, D.H., Grimoldi, E., Callard, L., Evans, D.J.A., Clark, C.D., Stewart, H.A., Dove, D., Saher, M., Ó Cofaigh, C., Chiverrell, R.C., Bateman, M.D., Moreton, S.G., Bradwell, T., Fabel, D., Medialdea, A. (2019) The mixed-bed glacial landform imprint of the North Sea Lobe in the western North Sea. *Earth Surface Processes and Landforms*. 44: 1233-1258.

Roberts, D.H., Hart, J.K. (2005) The deforming bed characteristics of a stratified till assemblage in north East Anglia, UK: investigating controls on sediment rheology and strain signatures. *Quaternary Science Reviews*. 24: 123-140.

Roberts, D.H., Hart, J.K. (2011) Macro- and microstructural evidence for the deforming glacier bed model: East Runton to West Runton. pp 143-153 in Phillips, E., Lee, J.R., Evans, H.M. (eds). *Glaciotectonics Field guide*. Quaternary Research Association: London.

Roberts, D.H., Long, A.J., Schnabel, C., Davies, B.J., Xu, S., Simpson, M.J.R., Huybrechts, P. (2009) Ice sheet extent and early deglacial history of the southwestern sector of the Greenland Ice Sheet. *Quaternary Science Reviews*. 28: 2760-2773.

Roberts, D.H., Long, A.J., Schnabel, C., Freeman, S., Simpson, M.J.R. (2008) The deglacial history of southeast sector of the Greenland Ice Sheet during the Last Glacial Maximum. *Quaternary Science Reviews.* 27: 1505-1516.

Roberts, D.H., Rea, B.R., Lane, T.P., Schnabel, C., Rodés, A. (2013b) New constraints on Greenland ice sheet dynamics during the last glacial cycle: Evidence from the Uummannaq ice stream system. *Journal of Geophysical Research*. 118: 519-541.

Robinson, A., Calov, R., Ganolpolski, A. (2012) Multistability and critical thresholds of the Greenland ice sheet. *Nature Climate Change*. 2: 429-432.

Rüther, D.C., Mattingsdal, R., Andreassen, K., Foriwck, M., Husum, K. (2011) Seismic architecture and sedimentology of a major grounding zone system deposited by the Bjørnøyrenna Ice Stream during Late Weichselian deglaciation. *Quaternary Science Reviews.* 30: 2776-2792.

Ryan, J.C., Dowdeswell, J.A., Hogan, K.A. (2016) Three cross-shelf troughs on the continental shelf of SW Greenland from Olex data. pp 67-168 in in Dowdeswell, J. A., Canals, M., Jakobsson, M., Todd, B. J., Dowdeswell, E. K., Hogan, K. A. (eds) *Atlas of Submarine Glacial Landforms: Modern, Quaternary and Ancient*. Geological Society, London, Memoirs, 46.

Sacchetti, F., Ó Cofaigh, C., Benetti, S. (2016) Iceberg ploughmarks on Rockall Bank, NE Atlantic. pp277-278 in Dowdeswell, J. A., Canals, M., Jakobsson, M., Todd, B. J., Dowdeswell, E. K., Hogan, K. A. (eds) *Atlas of Submarine Glacial Landforms: Modern, Quaternary and Ancient*. Geological Society, London, Memoirs, 46.

Sasgen, I., van den Broeke, M., Bamber, J.L., Rignot, E., Sørensen, L.S., Wouters, B., Martinec, Z., Velicogna, I., Simonsen, S.B. (2012) Timing and origin of recent regional ice-mass loss in Greenland. *Earth and Planetary Science Letters*. 333–334: 293–303.

Schaffer, J., Kanzow, T., von Appen, W-J., von Albedyll, L., Arndt, J.E., Roberts, D.H. (2020) Bathymetry constrains ocean heat supply to Greenland's largest glacier tongue. *Nature Geoscience*. 13: 227-231.

Schoof, C. (2007) Ice sheet grounding line dynamics: Steady states, stability, and hysteresis. *Journal of Geophysical. Research.* 112(F3).

Scourse, J., Saher, M., Van Landeghem, K.J.J., Lockhart, E., Purcell, C., Callard, L., Roseby, Z., Allinson, B., Pienowski, A.J., O'Cofaigh, C., Praeg, D., Chiverrell, R., Moreton, S., Fabel, D., Clark, C.D. (2019) Advance and retreat of the marine-terminating Irish Sea Ice Stream into the Celtic Sea during the Last Glacial: Timing and maximum extent. *Marine Geology*. 412: 58-68.

Seramur, K.C., Powell. R.D., Carlson, P.R. (1997) Evaluation of conditions along the grounding line of temperate marine glaciers: an example from Muir Inlet, Glacier Bay, Alaska. *Marine Geology*. 140: 307-327.

Shanmugan, C. (1997) The Bouma sequence and the turbidite mindset. *Earth Science Reviews*. 42: 201-229.

Sheldon, C., Jennings, A., Andrews, J.T., Ó Cofaigh, C., Hogan, K., Dowdeswell, J.A., Seidenkratz, M. (2016) Ice stream retreat following the LGM and onset of the west Greenland current in Uummannaq Trough, west Greenland. *Quaternary Science Reviews.* 147: 27-46.

Shepherd, A. et al. (IMBIE TEAM) (2020) Mass balance of the Greenland Ice Sheet from 1992 to 2018. *Nature*. 579: 233-239.

Shipp, S., Anderson, J., Domack, E. (1999) Late Pleistocene-Holocene retreat of the West Antarctic Ice-Sheet system in the Ross Sea: Part 1 - Geophysical results. *Geological Society of America Bulletin*. 111(10): 1486-1516.

Shipp, S.S., Wellner, J.S., Anderson, J.B. (2002) Retreat signature of a polar ice stream: sub-glacial geomorphic features and sediments from the Ross Sea, Antarctica. pp 277-304 in Dowdeswell, J. A., Ó Cofaigh, C. (eds) *Glacier-influenced Sedimentation on High-latitude Continental Margins.* London: Geological Society of London.

Simkins, L.M., Anderson, J.B., Greenwood, S.L., Gonnermann, H.M., Prothro, L.O., Halberstadt, A.R.W., Stearns, L.A., Pollard, D., DeConto, R.M. (2017) Anatomy of a meltwater drainage system beneath the ancestral East Antarctic ice sheet. *Nature Geoscience*. 10: 691-697.

Simkins, L.M., Greenwood, S.L., Anderson, J.B. (2018) Diagnosing ice sheet grounding line stability from landform morphology. *The Cryosphere*. 12: 2707-2726.

Slabon, P., Dorschel, B., Jokat, W., Myklebust, R., Hebbeln, D., Gebhardt, C. (2016) Greenland ice sheet retreat history in the northeast Baffin Bay based on high-resolution bathymetry. *Quaternary Science Reviews*. 154: 182-198.

Smith, J.A., Andersen, T., Shortt, M., Gaffney, M., Truffer, M., Stanton, T.P., Bindschandler, R., Dutrieux, P., Jenkins, A., Hillenbrand, C.-D., Ehrmann, W., Corr, H.J.F., Farley, N., Crowhurst, S., Vaughan, D.G. (2017) Sub-ice-shelf sediments record history of twentieth-century retreat of Pine Island Glacier. *Nature.* 541: 77–80.

Smith, J.A., Graham, A.G.C., Post, A.L., Hillenband, C-D., Bart, P.J., Powell, R.D. (2019) The marine geological imprint of Antarctic ice shelves. *Nature Communications*. 10(5635).

Smith, J.A., Hillenbrand, C.-D., Kuhn, G., Larter, G., Graham, A.G.C., Ehrmann, W., Moreton, S.G., Forwick, M. (2011) Deglacial history of the West Antarctic Ice Sheet in the western Amundsen Sea Embayment. *Quaternary Science Reviews*. 30: 488-505.

Smith, L.M., Andrews, J.T. (2000) Sediment characteristics in iceberg dominated fjords, Kangerlussuaq region, East Greenland. *Sedimentary Geology*. 130: 11-25.

Sookhan, S., Eyles, N., Putniken, N. (2018) LiDAR-based mapping of paleo-ice streams in the eastern Great Lakes sector of the Laurentide Ice Sheet and a model for the evolution of drumlins and MSGLs. *GFF*. 140(2): 202-228.

Spagnolo, M., Clark, C.D., Ely, J.C., Stokes, C.R., Anderson, J.B., Andreassen, K., Graham, A.G.C., King, E.C. (2014) Size, shape and spatial arrangement of mega-scale glacial lineations from a large and diverse dataset. *Earth Surface Processes and Landforms*. 39: 1432-1448.

Spagnolo, M., Phillips, E., Piotrowski, J.A., Rea, B.R., Clark, C.D., Stokes, C.R., Carr, S.J., Ely, J.C., Ribolini, A., Wysota, W., Szuman, I. (2016) Ice stream motion

facilitated by a shallow-deforming and accreting bed. *Nature Communications*. 7: 10723.

Steffensen, J.P., Andersen, K.K., Bigler, M., Clausen, H.B., Dahl-Jensen, D., Fischer, H., Goto-Azuma, K., Hansson, M., Johnsen, S.J., Jouzel, J., Masson-Delmotte, V., Popp, T., Rasmussen, S.O., Röthlisberger, R., Ruth, U., Stauffer, B., Siggaard-Andesen, M-L., Sveinbjörnsdóttir, Á.E., Svensson, A., White, J.W.C. (2008) High-resolution Greenland ice core data show abrupt climate change happens in few years. *Science*. 321: 680-684.

Stewart, T.J., Stagpoole, V.M., Wood, R.A., Carter, L. (2016) Ploughmarks and pits on the Chatham Rise: a record of deep-keeled Antarctic icebergs at 43° 200' S. pp275-276 in Dowdeswell, J. A., Canals, M., Jakobsson, M., Todd, B. J., Dowdeswell, E. K., Hogan, K. A. (eds) *Atlas of Submarine Glacial Landforms: Modern, Quaternary and Ancient*. Geological Society, London, Memoirs, 46.

Stokes, C.R. (2018) Geomorphology under ice streams: Moving from form to process. *Earth Surface Processes and Landforms.* 43: 85-123.

Stokes, C.R., Clark, C.D. (1999) Geomorphological criteria for identifying Pleistocene ice streams. *Annals of Glaciology*. 28: 67-74.

Stokes, C. R., Fowler, A. C., Clark, C. D., Hindmarsh, R. C. A., Spagnolo, M. (2013a) The instability theory of drumlin formation and its explanation of their varied composition and internal structure. *Quaternary Science Reviews.* 62: 77–96.

Stokes, C.R., Margold, M., Clark, C.D., Tarasov, L. (2016) Ice stream activity scaled to ice sheet volume during Laurentide Ice Sheet deglaciation. *Nature.* 530: 322-326.

Stokes, C.R., Spagnolo, M., Clark, C.D., Ó Cofaigh, C., Lian, O.B., Dunstone, R.B. (2013b) Formation of mega-scale glacial lineations on the Dubawnt Lake Ice Stream bed: 1. size, shape and spacing from a large remote sensing dataset. *Quaternary Science Reviews*. 77: 190-209.

Stokes, C.R., Tarasov, L., Blomdin, R., Cronin, T.M., Fisher, T.G., Gyllencreutz, R., Hättestrand, C., Heyman, J., Hindmarsh, R.C.A., Hughes, A.L.C., Jakobsson, M., Kirchner, N., Livingstone, S.J., Margold, M., Murton, J.B., Noormets, R., Peltier, W.R., Peteet, D.M., Piper, D.J.W., Preusser, F., Renssen, H., Roberts, D.H., Roche, D.M., Saint-Ange, F., Stroeven, A.P., Teller, J.T. (2015) On the reconstruction of palaeo-ice sheets: Recent advances and future challenges. *Quaternary Science Reviews*. 125: 15-49.

Streuff, K., Ó Cofaigh, C., Hogan, K., Jennings, A., Lloyd, J.M., Noormets, R., Nielsen, T., Kuijpers, A., Dowdeswell, J.A., Weinrebe, W. (2017) Seafloor geomorphology and glacimarine sedimentation associated with fast-flowing ice sheet outlet glaciers in Disko Bay, West Greenland. *Quaternary Science Reviews*. 169: 206-230.

Streuff, K., Ó Cofaigh, C., Noormets, R., Lloyd, J. (2018) Submarine landform assemblages and sedimentary processes in front of Spitsbergen tidewater glaciers. *Marine Geology*. 402: 209-227.

Studinger, M., Bell, R. E., Blankenship, D. D., Finn, C. A., Arko, R. A., Morse, D. L., Joughin, I. (2001) Subglacial sediments: A regional geological template for ice flow in West Antarctica. *Geophysical Research Letters.* 28(18): 3493–3496.

Svendsen, J.I., Mangerud, J., Elverhøi, A., Solheim, A., Schüttenhelm, R.T.E. (1992) The Late Weichselian glacial maximum on western Spitsbergen inferred from offshore sediment cores. *Marine Geology.* 104: 1-17.

Syring N., Lloyd, J.M., Stein, R., Fahl, K., Roberts, D.H., Callard, L., Ó Cofaigh, C. (2020) Holocene interactions between glacier retreat, sea ice formation, and Atlantic water advection at the inner Northeast Greenland continental shelf. *Paleoceanography and Paleoclimatology.* 35: 10.1029/2020PA004019

Syvitski, J.M.P., Farrow, G.E. (1989) Fjord sedimentation as an analogue for small hydrocarbon-bearing fan deltas. Pp21-43 in Whately, M.K., Pickering, K.T. (eds) *Deltas: Sites and Traps for Fossil Fuels*. Geological Society Special Publication, no. 41.

Syvitski, J. P. M., Stein, A. B., Andrews, J. T., Milliman, J. D. (2001) Icebergs and the Sea Floor of the East Greenland (Kangerlussuaq) Continental Margin. *Arctic, Antarctic, and Alpine Research.* 33(1): 52–61.

Szuman, I., Kalita, J.Z., Ewertowski, M.W., Clark, C.D., Livingstone, S.J. (2021) Dynamics of the last Scandinavian Ice Sheet's southernmost sector revealed by the pattern of ice streams. Boreas. https://doi.org/10.1111/bor.12512.

Talling, P.J. (2014) On the triggers, resulting flow types and frequencies of subaqueous sediment density flows in different settings. *Marine Geology*. 532: 155-182.

Talling, P.J., Masson, D.G., Sumner, E.J., Melgesini, G. (2012) Subaqeous sediment density flows: depositional processes and deposit types. *Sedimentology.* 59: 1937-2003.

Talling, P.J., Paull, C.K., Piper, D.J.W. (2013) How are subaqeous sediment density flows triggered, what is their internal structure and how does it evolve? Direct observations from monitoring of active flows. *Earth Science Reviews*. 125: 244-287.

Tarlati, S., Benetti, S., Callard, S.L., Ó Cofaigh, C., Dunlop, P., Georgiopoulou, A., Edwards, R., van Landeghem, K., Saher, M., Chiverrell, R., Fabel, D., Moreton, S., Morgan, S., Clark, C.D. (2020) Final deglaciation of the Malin Sea through meltwater release and calving events. *Scottish Journal of Geology*. 56: 117-133.

Taylor, J., Dowdeswell, J. A., Kenyon, N. H., O'Cofaigh, C. (2002) Late Quaternary compositional architecture of trough mouth fans: debris flows and suspended sediments on the Norwegian Sea margin. p 55-71 In Dowdeswell, J. A., O'Cofaigh,

C. (eds.) *Glacier-influenced Sedimentation on High-latitude Continental Margins.* London: Geological Society of London.

Thomas, G.S.P., Connell, R.J. (1985) Iceberg drop, dump and grounding structures from Pleistocene glacilacustrine sediments, Scotland. *Journal of Sedimentary Petrology*. 55: 243-249.

Tulaczyk, S.M., Scherer, R.P., Clark, C.D. (2001) A ploughing model for the origin of weak tills beneath ice streams: a qualitative treatment. *Quaternary International*. 86: 59-70.

van der Meer, J.J.M. (1993) Microscopic evidence of subglacial deformation. *Quaternary Science Reviews.* 12: 553-587.

van der Meer, J.J.M. (1997) Particle and aggregate mobility in till: Microscopic evidence of subglacial processes. *Quaternary Science Reviews*. 16: 827-831.

van der Meer, J.J.M., Carr, S.J., Kjær, K.H. (2010) Myrdalsjökull's forefields under the microscope. The micromorphology of meltout and subglacial tills. pp159-180 in Schomacker, A., Krüger, J., Kjær, K.H. (eds) The Myrdalsjökull Ice Cap, Iceland. Glacial Processes, Sediments and Landforms on an Active Volcano. Elsevier, Amsterdam, Developments in Quaternary Science, 13.

van der Meer, J., Hiemstra, J., (1998) Micromorphology of Miocene diamicts, indications of grounded ice. *Terra Antartica*, *5*(3): 363-366.

van der Meer, J.J.M., Kjær, K.H., Krüger, J., Rabassa, J., Kilfeather, A.A. (2009) Under pressure: clastic dykes in glacial settings. *Quaternary Science Reviews*. 28: 708-720.

van der Meer, J.J.M., Laban, C. (1990) Micromorphology of some North Sea till samples, a pilot study. *Journal of Quaternary Science.* 5(2): 95-101.

van der Meer, J.J.M., Menzies, J. (2011) The micromorphology of unconsolidated sediments. *Sedimentary Geology*. 238: 213-232.

van der Meer, J.J.M., Menzies, J., Rose, J. (2003) Subglacial till: the deforming glacier bed. *Quaternary Science Reviews*. 22: 1659-1658.

van der Meer, J.J.M., Mücher, H.J., Höfle, H.C. (1992) Micromorphological observations on till samples from the Shackleton Range and North Victoria Land, Antarctica. *Polarforschung*. 62(1): 57-65.

van der Meer, J.J.M., Warren, W.P. (1997) Sedimentology of late glacial clays in lacustrine basins, central Ireland. *Quaternary Science Reviews*. 16: 779-791.

van der Wateren, F.M., Kluiving, S.J., Bartek, L.R. (2000) Kinematic indicators of subglacial shearing. pp 259-278 in in Maltman, A.J., Hambrey, M.J., Hubbard, B. (eds) *Deformation of Glacial Materials.* Geological Society, London, Special Publications 176.

Van Landeghem, K.J.J., Chiverrell, R.C. (2020) Bed erosion during fast ice streaming regulated the retreat dynamics of the Irish Sea Ice Stream. *Quaternary Science Reviews.* 245: 106526.

Van Vliet-Lanoë, B., Coutard, J-P., Pissart, A. (1984) Structures caused by repeated freezing and thawing in various loamy sediments: A comparison of active, fossil and experimental data. *Earth Surface Processes and Landforms*. 9: 553-565.

Vaughan-Hirsh, D., Phillips, E., Lee, J.R., Burke, H.F., Hart, J.K. (2011) Glaciotectonic rafting of chalk bedrock: Overstrand. pp 198-217 in Phillips, E., Lee, J.R., Evans, H.M. (eds). *Glaciotectonics Field guide*. Quaternary Research Association: London

Vorren, T.O., Laberg, J.S., Blaume, F., Dowdeswell, J.A., Kenyon, N.H., Mienert, J., Rumohr, J., Werner, F. (1998) The Norwegian-Greenland Sea continental margins: morphology and late Quaternary sedimentary processes and environment. *Quaternary Science Reviews.* 17: 273-302.

Walder, J.S., Fowler, A. (1994) Channelized subglacial drainage over a deformable bed. *Journal of Glaciology*. 40: 3-15.

Weidick, A., Andreasen, C., Oerter, H., Reeh, N. (1996) Neoglacial glacier changes around Storstrømmen, North-East Greenland. Polarforschung 64, 95 – 108.

Wellner, J. S., Lowe, A. L., Shipp, S. S., Anderson, J. B. (2001) Distribution of glacial geomorphic features on the Antarctic continental shelf and correlation with substrate: implications for ice behaviour. *Journal of Glaciology* 47(158): 397–411.

Werner, K., Müller, J., Husum, K., Spielhagen, R.F., Kandiano,, E.S., Polyak, L. (2015) Holocene sea subsurface and surface water masses in the Fram Strait – Comparisons of temperature and sea-ice reconstructions. *Quaternary Science Reviews*. 147: 194-209.

Whitehouse, P.L., Bentley, Le Brocq, A.M. (2012) A deglacial model for Antarctica: geological constraints and glaciological modelling as a basis for a new model of Antarctic glacial isostatic adjustment. *Quaternary Science Reviews*. 32: 1-24.

Wilson, N., Straneo, F., Heimbach, P. (2017) Satellite-derived submarine melt rates and mass balance (2011-2015) for Greenland's largest remaining ice tongues. *The Cryosphere*. 11: 2773-2782.

Wilson, N.J., Straneo, F. (2015) Water exchange between the continental shelf and the cavity beneath Nioghalvfjerdsbræ (79 North Glacier). Geophysical Research Letters. *Geophysical Research Letters.* 42: 7648-7654.

Winkelmann, D., Jokat, W., Jensen, L., Schenke, H. (2010) Submarine end moraines on the continental shelf off NE Greenland – Implications for Lateglacial dynamics. *Quaternary Science Reviews*. 29: 1069-1077.

Woodworth-Lynas, C.M.T., Guigné, J.Y. (1990) Iceberg scours in the geological record: examples from Glacial Lake Agassiz. pp217-223 in Dowdeswell, J.A., Scourse, J.D. (eds) *Glacimarine Environments: Processes and Sediments*. Geological Society, vol. 53. Special Publication. London.

Woodworth-Lynas, C.M.T., Josenhans, H.W., Barrie, J.V., Lewis, C.M.F., Parrott, D.R. (1991) The physical process of seabed disturbance during iceberg grounding and scouring. *Continental Shelf Research*. 11(8-10): 939-961.

Xu, J.P. (2011) Measuring currents in submarine canyons: Technological and scientific progress in the past 30 years. *Geosphere.* 7(4): 868-876.

Yokohama, Y., Anderson, J.B., Yamane, M., Simkins, L.M., Miyairi, Y., Yamazaki, T., Koizumi, M., Suga, H., Kusahara, K., Prothro, L., Hasumi, H., Southon, R., Ohkouchi, N. (2016) Widespread collapse of the Ross Ice Shelf during the late Holocene. *PNAS*. 113(9): 2354-2359.

Zaniewski, K. (2001) Plasmic Fabric Analysis of Glacial Sediments Using Quantitative Image Analysis Methods and GIS Techniques. PhD. Thesis University of Amsterdam, The Netherlands.

Zehnich, M., Spielhagen, R.F., Buach, H.A., Forwick, M., Hass, H.C., Palme, T., Stein, R., Syring, N. (2020) Environmental variability off NE Greenland (western Fram Strait) during the past 10,600 years. *The Holocene*. 30(12): 1752-1766.